

DEVELOPMENT OF AN IMPROVED *IN VIVO* TOOL COMPOUND, VU6001221, FOR
NON-COMPETITIVE INHIBITION OF CHT, DISCOVERY AND DEVELOPMENT OF M₁
PAMS: BENZOMORPHOLINE AND TETRAHYDROQUINOLINE SERIES, AND
DEVELOPMENT OF NOVEL, BRAIN-PENETRANT PAR4 ANTAGONISTS

By

Jeanette L. Bertron

Dissertation

Submitted to the Faculty of the
Graduate School of Vanderbilt University
in partial fulfillment of the requirements
for the degree of

DOCTOR of PHILOSOPHY

In

Chemistry

May 31, 2020

Nashville, Tennessee

Approved:

Craig W. Lindsley, Ph.D., Chair

Gary A. Sulikowski, Ph.D.

Steven D. Townsend, Ph.D.

Matthew T. Duvernay, Ph.D.

To my family and loving husband, Bryan

ACKNOWLEDGMENTS

The research described herein was supported by the NIH division of mental health, the William K. Warren, Jr. Chair in Medicine, and the Vanderbilt Institute of Chemical Biology fellowship. I would like to thank these wonderful organizations, whom without their generosity and commitment to the advancement of science for the improvement of societal health, this work would not have been possible.

In addition, I'd like to thank my advisor, Dr. Craig Lindsley, for his unwavering support and guidance throughout my graduate career. I'm extremely grateful to him for giving me the opportunity to learn from him and grow as a scientist over the last six years. He also granted me the freedom to guide my own research, take ownership of my projects, and establish my own collaborations and connections, all of which were invaluable skillsets in my growth as a chemist. Dr. Lindsley was not only an advisor to me, but also a role model. He is as kind as he is successful and I strive to lead and motivate young scientists as he does someday. Additionally, I'd like to thank my undergraduate advisor, Dr. David Ball, for not only allowing me to do research with him, but also for connecting me with Dr. Lindsley. I can honestly say I wouldn't be where I am today had these two not invested their time and effort into me and my education. For that, I owe them my undying gratitude. I'd also like to thank Dr. Gary Sulikowski, Dr. Steven Townsend, and Dr. Matthew Duvernay for graciously serving on my dissertation committee. They each played a special role in rounding out my scientific abilities and constantly challenged me in their own ways to be a better scientist. I am so utterly grateful to them for that.

I'd also like to thank all the Lindsley lab members, past and present, campus and Cool Springs. In particular, Dr. James 'Chris' Tarr, Dr. Bruce Melancon, Dr. Andrew Felts, and Dr. Darren Engers were all instrumental in training me during my first two years with the VCNDD prior to graduate school. I cannot thank them enough for preparing me so well for graduate school. Furthermore, Dr. Annie Blobaum and Dr. Tom Bridges taught me everything I know about drug metabolism and pharmacokinetics. I want to thank them for not only providing my projects with DMPK data, but also for taking time out of their days to allow me to pick their brains about anything and everything relating to DMPK. The knowledge I've accumulated from them over the years has been invaluable in my development as a medicinal chemist. Nathan Kett has also been an integral part of my graduate career. I would not have been able to accomplish all this work without Nate's expertise in maintaining and repairing the lab instrumentation and equipment. I am so appreciative of his time and effort, ensuring everything was in working order so that we could conduct our research in a timely and efficient manner. The Lindsley lab and VCNDD as a whole have become my family away from home and I am so grateful for all their love, support, and camaraderie throughout my time here.

While graduate school presented with challenges and hardships, it also provided me with lifelong friends. My labmates Dr. Carson Reed, Dr. Mark Fulton, Caitlin Kent, and Jacob Kalbfleisch deserve a special thanks for their patience, understanding, and guidance, but most importantly for their friendship. Thank you for literally being there every single day to help me through the rough times and to celebrate the good times. I also want to thank Dr. Dr. Rachel Crouch and Matt Mulder, who began as colleagues

and became some of my closest friends. I appreciate all your love, encouragement, support, happy hours, and fun throughout my time in graduate school.

Additionally, I would like to thank all my friends and family who have been my cheerleaders throughout my undergraduate and graduate career. I couldn't have gotten this far without them in my life. Thank you for being so understanding and never making me feel bad or guilty for missing holidays, birthdays, graduations, and more. Last but not least, I would like to acknowledge my husband, Bryan Downey, for making countless sacrifices over the years, including uprooting his life to move to Nashville to be with me and support me through graduate school. Thank you for ensuring I had nothing but graduate school to worry about, allowing me to dedicate my full focus towards my research. I appreciate your confidence in me more than you know. Thank you for never letting me give up when things got tough and stressful. I wouldn't have gotten through this program without you by my side.

TABLE OF CONTENTS

	Page
DEDICATION.....	ii
ACKNOWLEDGEMENTS.....	iii
TABLE OF CONTENTS.....	vi
LIST OF TABLES.....	vii
LIST OF FIGURES.....	viii
LIST OF SCHEMES.....	xi
LIST OF ABBREVIATIONS.....	xii
Chapter	
1. Development of an Improved <i>in vivo</i> Tool Compound, VU6001221, for Non-competitive Inhibition of CHT	
Background and introduction.....	1
Choline uptake transporter (CHT) structure and function.....	1
Acetylcholine and CHT: known physiological roles.....	3
Potential therapeutic avenue for CHT inhibitors.....	5
CHT tool compounds: CHT inhibitors.....	8
Conclusions.....	9
Materials and methods.....	10
General synthetic methods and instrumentation.....	10
Reagents and cells.....	12
Choline-Induced Membrane Potential Assay.....	12
Hemicholinium-3 (HC-3) radioligand binding assays.....	13

Off-target screen.....	14
Animal care and husbandry.....	14
Metabolism and disposition methods.....	15
Plasma protein binding.....	16
Pharmacokinetics and brain tissue distribution studies in Sprague-Dawley rats.....	16
Liquid chromatography/mass spectrometry analysis.....	18
Behavioral pharmacology: animals.....	18
Behavioral pharmacology: novel object recognition task.....	19
Development of an Improved <i>in vivo</i> Tool Compound, VU6001221, for Non- competitive Inhibition of CHT.....	20
Optimization plan for ML352.....	20
Initial SAR of northern aliphatic ring.....	21
SAR of the eastern amide moiety.....	24
Tuning the electronics of the central core.....	30
SAR around fluoro, chloro, and des-methoxy congeners of ML352.....	32
Assessment of VU6001221 as a viable tool compound.....	36
Behavioral pharmacology of VU6001221 in models of cognition.....	40
Conclusions.....	42
Experimental Methods.....	42
General synthetic methods and instrumentation.....	42

References for chapter I.....	50
Appendix A.....	52
2. Discovery and Development of M ₁ PAMs: Benzomorpholine and Tetrahydroquinoline Series	
Background and introduction.....	61
G-protein-coupled receptors: muscarinic acetylcholine receptors.....	61
Muscarinic acetylcholine receptor 1 (M ₁) and its therapeutic relevance.....	63
Xanomeline as an M ₁ tool compound.....	64
Considering an orthosteric vs. allosteric approach.....	65
M ₁ tool compounds: positive allosteric modulators (PAMs).....	68
Conclusions.....	70
Materials and methods.....	71
General synthetic methods and instrumentation.....	71
Cell lines.....	73
Calcium mobilization assay.....	73
Radioligand binding assay.....	74
Drug metabolism methods: <i>in vitro</i>	75
Drug metabolism methods: <i>in vivo</i>	77
Mouse plasma-brain exposure.....	80
Electrophysiology.....	80

Eurofins lead profiling data.....	82
Behavioral pharmacology studies.....	83
Modified Irwin toxicology battery.....	84
The discovery and development of M ₁ PAMs: benzomorpholine and tetrahydroquinoline series.....	85
Scaffold hopping: quinolone to benzomorpholine core.....	85
SAR and synthesis of benzomorpholine series.....	86
Benzomorpholine core modifications.....	88
SAR around the southern biaryl rings.....	91
Resolving and evaluating single diastereomers.....	93
Assessment of VU0486846 as a viable <i>in vivo</i> tool compound.....	96
Behavioral pharmacology of VU0486846.....	105
Challenging the intramolecular hydrogen bond theory.....	107
Conclusions.....	120
Experimental methods.....	121
General synthetic methods and instrumentation.....	121
References for chapter II.....	142
Appendix B.....	145

3. Development of Novel, Brain-penetrant, Human and Mouse PAR4 Antagonists

Background and introduction.....	165
G-protein coupled receptors: protease activated	

receptors.....	165
PAR1 and PAR4 dual receptor system.....	167
PAR4 and its therapeutic relevance.....	170
PAR4 tool compounds: antagonists.....	174
Competitive vs. non-competitive PAR4 antagonists.....	176
PAR4 pharmacogeomics – single nucleotide polymorphisms.....	178
Conclusions.....	179
Materials and methods.....	180
General synthetic methods and instrumentation.....	180
Blood collection and platelet isolation.....	181
Flow cytometry.....	182
Schild analysis competition binding assay.....	183
Drug metabolism methods: <i>in vitro</i>	183
LC/MS/MS bioanalysis of samples from plasma protein binding and intrinsic clearance assays.....	185
Animal care and use.....	185
Computational modeling.....	186
Development of Novel, Brain-penetrant, Human and Mouse PAR4 Antagonists.....	187
High-throughput screening (HTS) campaign: identification of VU0543156.....	189
Initial SAR of alternate ethers.....	190

SAR around core pyrazole moiety.....	200
SAR around amide moiety.....	201
Evaluating the mode of inhibition.....	207
γ -thrombin activity screen.....	209
Human-mouse PAR4 cross-over studies.....	213
DMPK profiles of lead mouse PAR4 antagonists.....	215
Addressing the potential metabolic liabilities.....	218
Future directions and conclusions.....	222
Experimental methods.....	224
General synthetic methods and instrumentation.....	224
References for chapter III.....	247
Appendix C.....	251

LIST OF TABLES

Table	Page
1.1 SAR around the northern cycloalkylamine.....	22
1.2 SAR around the amide moiety: 2° amides.....	25
1.3 SAR around the amide moiety: 3° amides.....	29
1.4 SAR around central core.....	31
1.5 SAR around the northern cycloalkylamine with new central cores.....	32
1.6 SAR around amide moiety with new central cores.....	33
1.7 <i>In vitro</i> and <i>in vivo</i> DMPK profiles of ML352 and VU6001221.....	36
1.8 Eurofins lead profile panel for VU6001221.....	38
2.1 Solvent and base screen to generate azabenzomorpholine core.....	91
2.2 SAR around the southern biaryl rings.....	93
2.3 Structures and activities of single diastereomers: benzomorpholines.....	98
2.4 Eurofins lead profile panel for VU486846.....	98
2.5 <i>In vitro</i> and <i>in vivo</i> DMPK profile for human, rat, and cynomolgus.....	101
2.6 Modified toxicology battery test in mice.....	105
2.7 SAR around southern biaryl system with cyclohexanol amide.....	111
2.8 SAR around biaryl system with tetrahydropyranol amide.....	112
2.9 Structures and activities of single diastereomers: tetrahydroquinolines.....	114
2.10 DMPK data for single diastereomers.....	118
2.11 CNS exposure of VU6024717 in mouse.....	118
3.1 Initial SAR of southern benzyl moiety.....	192

3.2	SAR of 2-substituted benzylpyridines.....	195
3.3	SAR of methyl cycloalkyl ethers.....	198
3.4	SAR around pyrazole moiety.....	201
3.5	SAR around amide motif.....	203
3.6	SAR around eastern phenyl ring.....	205
3.7	Congeners with activity against γ -thrombin induced platelet aggregation.....	211
3.8	Lead PAR4 antagonists in mouse platelet assay.....	215
3.9	Pharmacokinetic data of mPAR4 lead compounds.....	216
3.10	CNS exposure of mPAR4 lead compounds.....	217
3.11	Mouse pharmacokinetic and CNS exposure data of VU6015744.....	217
3.12	SAR around northern methoxy substituent.....	219
3.13	SAR around the 1,4-dimethoxy phenyl motif.....	221

LIST OF FIGURES

Figure	Page
1.1 Biosynthetic pathway of acetylcholine.....	3
1.2 Commonly prescribed therapeutics for the treatment of dystonia.....	6
1.3 Known CHT antagonists.....	8
1.4 Structure of ML352 and proposed SAR strategies.....	20
1.5 Cognitive behavioral assay of VU6001221.....	41
2.1 Generic representation of the M ₁ receptor and heterotrimeric protein.....	63
2.2 Orthosteric and putitive allosteric binding sites for M ₁ receptors.....	68
2.3 Known M ₁ ago-PAMs disclosed in the literature.....	69
2.4 Previous M ₁ PAMs developed in the Lindsley lab.....	70
2.5 Scaffold hopping from BQCA to benzomorpholine core.....	86
2.6 SAR strategy around benzomorpholine core.....	87
2.7 Structure and <i>in vitro</i> DMPK profile of VU0486846.....	89
2.8 Fluorine ‘walk’ around benzomorpholine core.....	90
2.9 Predominant mechanism by which VU0486846 is metabolized.....	92
2.10 Analogs separated and assayed as single diastereomers.....	95
2.11 Structure and x-ray crystal structure of VU0486846.....	97
2.12 <i>In vitro</i> human and rat selectivity screen.....	98
2.13 Competition binding assay and electrophysiology data.....	103
2.14 Racine scale data.....	104
2.15 Rodent novel object recognition paradigm using VU0486846.....	107

2.16	scaffold hopping from benzomorpholine to tetrahydroquinoline core.....	108
2.17	Structure and x-ray crystal structure of VU6029431.....	119
2.18	Computational modeling of VU6029430 and VU6029431.....	120
3.1	Cleavage and activation of PAR1 by thrombin.....	165
3.2	PAR1 and PAR4 cleavage sites.....	167
3.3	Structure of Vorapaxar and himbacine.....	168
3.4	Thrombin induced PAR4 signaling pathways.....	171
3.5	Known PAR4 antagonists.....	175
3.6	Structures of PAR4 antagonists VU0652925 and VU0661224.....	176
3.7	In silico docking studies of VU0652925 in PAR4 homology model.....	177
3.8	Structure of HTS hit VU0543156 and proposed SAR strategy.....	190
3.9	Structures of analogs VU6014723 and VU6014232.....	191
3.10	Structure of VU6019097 docked in our PAR4 homology model.....	198
3.11	Structure and activities of analogs in PAR1 antagonists.....	202
3.12	Schild analysis progressive fold shift using VU06019097.....	207
3.13	BMS-986120 overlaid with VU6015741 in PAR4 homology model.....	208
3.14	Pharmacogenomic differences between GG and AA alleles.....	212
3.15	Single point assay with all active compounds to date in mouse platelets.....	213
3.16	Congener VU6015744 docked in hPAR4 homology model.....	215
3.17	Potential metabolic liabilities within the scaffold.....	218

LIST OF SCHEMES

Scheme	Page
1.1 Synthetic route to access northern cycloalkylamine analogs.....	21
1.2 Synthetic route to access amide analogs.....	24
1.3 Synthetic route to access core replacement analogs.....	30
2.1 Synthetic route to access benzomorpholine analogs.....	88
2.2 Synthetic route to access tetrahydroquinoline analogs.....	109
3.1 Synthetic route to access ether analogs.....	190
3.2 Synthetic route to access triazolopyridazine analogs.....	201
3.3 Synthetic route to access VU6024875.....	209
3.4 Diverging routes from general Scheme 3.1 to access analogs 3.111-3.114.....	220
3.5 Future synthetic route to access alkyl ether analogs.....	223

LIST OF ABBREVIATIONS

%F	Bioavailability
°C	Degrees Celcius
5-HT	5-hydroxytryptophan
7-TM	Seven transmembrane domain
ABT	1-aminobenzotriazole
Acetyl-CoA	Acetyl coenzyme A
ACh	Acetylcholine
AChE	Acetylcholine esterase
AD	Alzheimer's Disease
ADHD	Attention-deficit/hyperactivity disorder
AE	Adverse effects
ALS	Amyotrophic lateral sclerosis
Ar	Aryl
ATP	Adenosine triphosphate
BBB	Blood brain barrier
BHB	Brain homogenant binding
Boc	<i>tert</i> -Butyloxycarbonyl
BoNT	Botulinum toxin
cAMP	Cyclic adenylyl monophosphate
CBZ	benzyloxycarbonyl
ChAT	Choline acetyltransferase

CHT	Choline uptake transporter
CL _{HEP}	Hepatic clearance
CL _{INT}	Intrinsic clearance
CMB	Cerebral microbleed
CNS	Central nervous system
CRC	Concentration response curve
Cyno	Cynomolgus monkey
CYP	Cytochrome P
DAG	Diacyl glycerol
DCE	Dichloroethane
DCM	Dichloromethane
DIEA	<i>N,N</i> -Diisopropylethylamine
DMF	<i>N,N</i> -Dimethylformamide
DMPK	Drug metabolism and pharmacokinetics
DMSO	Dimethylsulfoxide
DtBAD	Di- <i>tert</i> -butyl azodicarboxylate
EC ₅₀	Concentration required for 20% of maximal receptor activation
EtOAc	Ethyl acetate
EtOH	Ethanol
FDA	Food and drug administration
fEPSPs	Field excitatory post synaptic potentials
f _u	Fraction unbound

GABA	Gamma aminobutyric acid
GPCR	G-protein coupled receptor
HATU	1-[Bis(dimethylamino)methylene]-1H-1,2,3-triazolo[4,5-b]pyridinium 3-oxid hexafluorophosphate
HC-3	Hemicholinium-3
HCl	Hydrochloric acid
HIS	Histidine
hPAR4	Human PAR4
HPLC	High-performance liquid chromatography
HRMS	High-resolution mass spectrometry
HTS	High-throughput screen
I.P.	Intraperitoneal
IC ₅₀	Concentration required for 50% inhibition of maximal receptor response
IMHB	Intramolecular hydrogen bond
IP3	Inositol triphosphate
IV	Intravenous
IVIVC	<i>in vitro:in vivo</i> correlation
KO	Knockout
K _p	Partition coefficient between plasma and brain
K _{p,uu}	Partition coefficient of drug unbound between plasma and brain
LCMS	Liquid-chromatography mass-spectrometry

L-Dopa	Levodopa
LTD	Long-term depression
M	Muscarinic
mAChR	Muscarinic acetylcholine receptor
MAPK	Mitogen-activated protein kinase
MeCN	Acetonitrile
MeOH	Methanol
MOE	Molecular operating environment
mPAR44	Mouse PAR4
MPO	Multiparameter optimization
MW	Molecular weight
n.p.	No product
N/A	Not applicable
nAChR	Nicotinic acetylcholine receptor
NAM	Negative allosteric modulator
NH ₄ OH	Ammonium hydroxide
NMR	Nuclear magnetic resonance
NOR	Novel object recognition
PAM	Negative allosteric modulator
PAR	Protease activated receptor
PAR4-AP	Protease activated receptor 4 activating peptide
PBL	Plasma/brain level
PD	Parkinson's disease

PFC	Prefrontal cortex
PIP ₂	phosphatidylinositol 4,5-bisphosphate
PK	Pharmacokinetics
PLC	Phospholipase C
PO	Oral administration
PPB	Plasma protein binding
PPh ₃	Triphenylphosphine
RT	Room temperature
SAR	Structure-activity relationship
SEM	Standard error of the mean
SFC	Super-critical fluid
SLC5	Solute carrier 5
SNP	Single nucleotide polymorphism
t _{1/2}	Half-life
tBuOH	<i>tert</i> -butyl hydroxide
TEA	Triethylamine
TFA	Trifluoroacetic acid
THF	Tetrahydrofuran
TPSA	Total polar surface area
TYR	Tyrosine
VACHT	Vesicular acetylcholine transporter
V _{ss}	Volume of distribution at steady state
VU	Vanderbilt University

CHAPTER I

DEVELOPMENT OF AN IMPROVED *IN VIVO* TOOL COMPOUND, VU6001221, FOR NON-COMPETITIVE INHIBITION OF CHT

Background and Introduction

Choline Uptake Transporter Structure and Function

Choline uptake transporters (CHT) belong to the solute carrier 5 (SLC5) family of solute transporters, which utilize an electrochemical sodium gradient to drive co-transportation of their substrates.^{1,2} Expression cloning and amino acid sequencing analysis predicted the SLC5 transporters to contain a 13 transmembrane (TM) domain with an extracellular N-terminus and an intracellular C-terminus. Cysteine cross-linking studies performed by Okuda and co-workers provided experimental evidence of a model of CHT as a 13 TM protein.³ In addition, the solved crystal structure of the *Vibrio parahemolyticus* Na⁺ /galactose cotransporter, a member of the SLC5 family, further supports the notion of a common 13 TM domain core.⁴

Two kinetically distinct CHT systems have been observed. The first system is a Na⁺-dependent, high-affinity, low-capacity process known as the high-affinity CHT. High-affinity CHTs are primarily localized to synaptic vesicles or endosomes and are expressed exclusively in cholinergic neurons.⁵ The high-affinity CHT is the rate limiting step for the synthesis of the neurotransmitter acetylcholine (ACh), which acts as a neuromodulator on numerous physiological and behavioral functions including

movement, cardiovascular activity, gut motility, arousal, attention, mood, and memory.⁶⁻

¹⁰ The second system is a Na⁺-independent, low-affinity, high-capacity process known as the low-affinity CHT. The low-affinity system, however, does not appear to be associated with significant formation of ACh. Rather, it is thought to be ubiquitously expressed in all cells and is necessary for the synthesis of phosphatidylcholine, a lecithin component.³ Due to the crucial involvement in the synthesis of a vital neurotransmitter, the high-affinity CHT will be the focus of this chapter.

The high-affinity CHT is localized to presynaptic terminals and is predominantly found within the cytoplasm where they exist in an inactive state. CHTs become active when they are bound to the cellular plasma membrane.^{11,12} The choline transport rates are directly related to the number of active CHTs at the cell surface.⁷ Blakely and co-workers have shown that depolarization of cholinergic terminals increase the density of active CHT bound to the cell membrane. Therefore, it has been suggested that cellular CHT trafficking from the cytoplasmic compartments to the plasma membrane may contribute to the regulation of ACh production. However, the exact mechanism of CHT trafficking is largely unknown.¹²

Binding of CHT to the plasma membrane is of utmost importance when synthesizing ACh as its precursor choline cannot diffuse across cell membranes due to a charged quaternary ammonium moiety.¹³ Membrane-bound CHT utilizes transmembrane electrochemical gradients to transport choline from extracellular space into the presynaptic terminal where it can then be converted to ACh (**Figure 1.1**).^{14,15} Following the transportation of choline into the cell, choline acetyltransferase (ChAT)

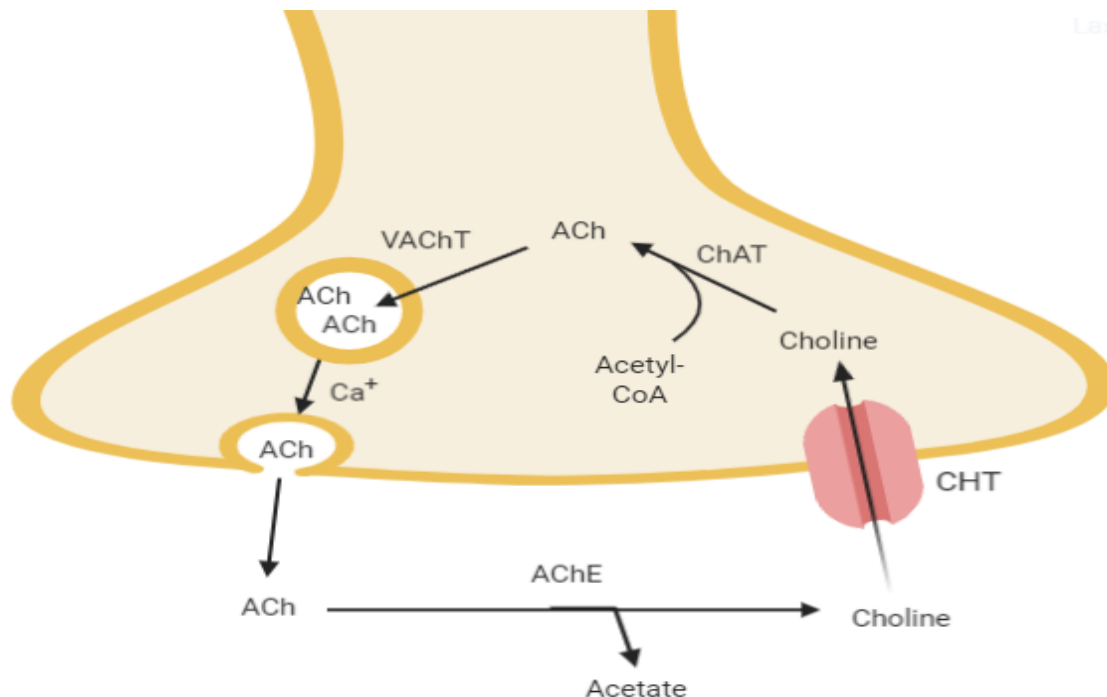


Figure 1.1 Biosynthetic pathway of acetylcholine.

synthesizes ACh from choline and acetyl coenzyme A. The ACh neurotransmitters are then transferred to synaptic vesicles by the vesicular ACh transporter (VACHT). Once packaged into vesicles, an increase in cytoplasmic Ca⁺ concentration drives the synaptic vesicles to migrate towards the presynaptic terminal and fuse with the plasma membrane. ACh is then released into the synapse where it is rapidly hydrolyzed by acetylcholine esterase (AChE) into choline and acetate, allowing choline to be recycled back through the system.^{16,17}

ACh and CHT: Known Physiological Roles

The cholinergic system has been studied extensively since the discovery of acetylcholine in 1913.^{11,18} The neurotransmitter ACh binds and activates muscarinic and nicotinic receptors, which modulate a variety of physiological and behavioral functions in both the central and peripheral nervous system, primarily having effects on the

autonomic and enteric nervous systems.^{7,11} Due to its wide distribution, ACh modulates several processes, including movement, cardiovascular activity, gut motility, arousal, attention, mood, and memory.^{19,20} Disruptions in cholinergic signaling has been implicated in an array of disorders such as atherosclerosis,⁸ myasthenia gravis,⁶ attention-deficit/hyperactivity disorder (ADHD)⁹, schizophrenia,²¹ depression,⁹ Alzheimer's disease,^{16,22} and dystonia.²³ Drug therapy has been focused predominantly around muscarinic and/or nicotinic acetylcholine receptor agonist/antagonists and acetylcholinesterase inhibitors as therapeutic strategies for altering or modulating cholinergic signaling. Unfortunately, due to the ubiquitous nature of the ACh receptors throughout the nervous system, alterations in the function of these targets have resulted in significant off-target and on-target activity, resulting in dose-limiting side effects.⁷ An important protein for altering or modulating cholinergic signaling that has been grossly over-looked is the presynaptic, high-affinity CHT. It is possible that by targeting the CHT may provide greater selectivity and reduction in off-target activity.

Genetic modifications in CHT have been implicated in increased risk of developing multiple different disorders. CHT variant ile89val, where isoleucine residue at position 89 has been switched out with amino acid valine, has been associated with major depressive disorder as well as ADHD.⁹ In addition, a single nucleotide polymorphism (SNP) from a guanine to a thiamine located in the 3' untranslated region of CHT has been implicated in carotid atherosclerosis. Studies have shown that allelic variation at this site can predict cardiac autonomic function in healthy adults, further substantiating CHTs role in cardiac function.⁸ Another perturbation in a critical coding region of CHT gene SLC5A7 is the single base deletion of c.1497delG. This deletion is

believed to result in a detrimental frameshift mutation, which causes a premature stop codon. The premature halting of transcription results in the elimination of the final 82 amino acids in the coding sequence, which deletes the intracellular c-terminus almost completely. The c-terminus has been known to play a critical role in regulating surface trafficking of proteins. Therefore, in the case of CHT, it would elicit a reduction in the synthesis of ACh. This disruption in the transcription of CHT has been linked to hereditary motor neuropathy.^{6,24} To explore the impact of these perturbations and their roles in specific disease states, a viable *in vivo* tool compound is required.

Potential Therapeutic Avenue for CHT Inhibitors

According to the Association of Neurological Surgeons, as many as 250,000 Americans are living with dystonia, making it the third most common movement disorder.²⁵ Dystonia is a highly complex neurological movement disorder that is characterized by excessive, involuntary muscle contractions, resulting in abnormal muscle movement. Dystonia's can affect any part of the body and its presentation can vary from person to person. In addition to atypical body movements, anxiety and depression are typical non-motor symptoms of dystonia.²⁶ The cause of idiopathic dystonia's is largely unknown. However, it is believed to involve the dysregulation of cholinergic, GABAergic, and dopaminergic systems.²³ The classically used treatments for dystonia's are GABAergic agents such as baclofen (1.1) and clonazepam (1.2), anticholinergics such as trihexyphenidyl (1.3) and botulinum toxin injections, and dopaminergic medications such as L-DOPA (1.4) (Figure 1.2).²⁷ Unfortunately, each of these therapies comes with their own pitfalls.

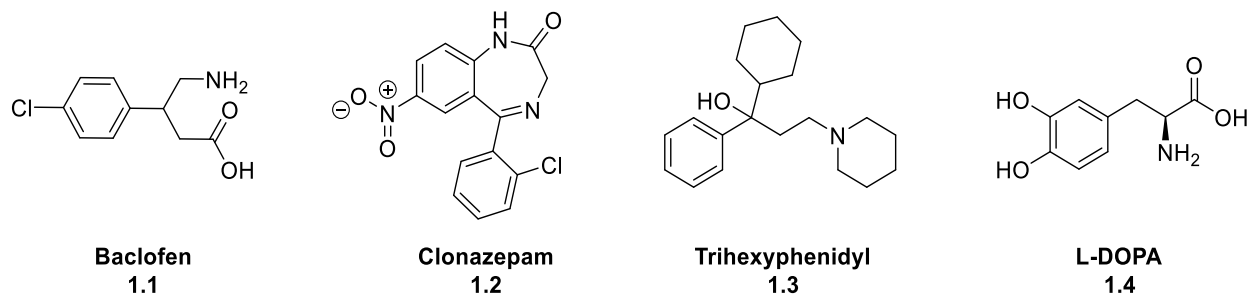


Figure 1.2 Commonly prescribed therapeutics for the treatment of dystonia **1.1-1.4**.

There are roughly 20 different types of dystonia.²⁸ The primary therapeutic for treating dystonia and spasticity is a GABA B agonist called baclofen (**1.1**).²⁹ While **1.1** can be successful in treating spasticity and dystonia in situations such as spinal cord injury, cerebral palsy, stroke, amyotrophic lateral sclerosis, and multiple sclerosis, the treatment comes with a large caveat. **1.1** has been generally referred to as a “high gain/high risk” method for managing spasticity and dystonia due to its mode of administration. **1.1** can be taken orally, albeit in large doses to elicit a therapeutic effect due to its low brain penetration. Furthermore, taking **1.1** orally has the potential to cause hepatotoxicity and thus strict monitoring of liver function is required.³⁰ Therefore, the main form of administration is through an intrathecal pump, which is a device that is implanted into the abdomen with a catheter that carries the medication directly to the spinal fluid. Unfortunately, pump failure can lead to overdose, resulting in respiratory depression and coma, or withdrawal, resulting in hyperthermia, rhabdomyolysis, and disseminated intravascular coagulation.^{30,31} In addition, improper placement of the device can cause infection and cerebrospinal fluid leakage. With such a high risk of severe side effects, **1.1** is a less-than-ideal therapeutic agent.^{31,32} Another common GABAergic medication used to treat dystonias is clonazepam (**1.2**), a benzodiazepine.³³

However, studies show that **1.2**, along with other benzodiazepines are only beneficial in about 16-23% of patients with generalized and focal dystonias.³³ In addition to its subpar clinical efficacy in treating dystonias, it also causes sedation, confusion, impaired coordination, and depression.³³ Furthermore, **1.2**, like most benzodiazepines, bears the potential for physical dependence and addiction.³⁴ The severity of the side effects and associated liabilities of these treatments indicate that GABAergic therapies may not be viable options for dystonia treatment.

Another popular course of treatment for dystonias is the administration of L-DOPA (**1.4**), a dopaminergic agent. A group of movement disorders that respond to the medication **1.4** has been classified as DOPA-Responsive Dystonia (DRD).²⁸ The underlying mechanism of this type of dystonia has been well explored and elucidated through genetic studies. The underlying cause of DRD is a perturbation in the production of dopamine by a mutation which affects the rate-limiting step of synthesis.³⁵ Therefore, **1.4** would be a feasible form of treatment for this particular type of dystonia. However, there are several other forms of dystonia for which dopaminergic medications are ineffective and therefore other therapeutic strategies must be pursued.

Excitingly, anticholinergics like trihexyphenidyl (**1.3**) and Botulinum toxin (BoNT) therapy have been known to be beneficial in all types of dystonias.³³ **1.3** has been one of few oral drugs tested for the treatment of dystonia in a double-blind, placebo-controlled trial where 71% of participants reported clinically meaningful improvement. Although **1.3** shows promising effects, most patients experience on-target, dose-limiting side effects such as drowsiness, confusion, and memory difficulty, therefore limiting its therapeutic utility.³³ In the 1980's BoNT therapy became a popular avenue for treating

dystonias and became the preferred treatment over small molecule anticholinergics. BoNT therapy utilizes a toxic protein produced by the bacterium *Clostridium botulinum*, which acts as an anticholinergic by inhibiting the release of ACh into the neuromuscular junction. The onset of the full effect is typically within the first two weeks of injection and can last for 3-4 months. The biggest downfall of BoNT therapy is antibodies can develop with repeated use, which reduces the desired therapeutic effects.^{27,29,36} The promise anticholinergics hold for treating dystonic disorders lead us to pursue an alternative, underexplored target within the cholinergic system, the CHT.

CHT tool compounds: CHT inhibitors

To date, only two small molecules are available that target CHT, hemicholinium-3 (HC-3) and ML352 (**Figure 1.3**). Unfortunately, HC-3 is a less than ideal tool molecule due to its high toxicity from off-target activity, poor CNS penetration due to its bis-quaternary ammonium salt moiety, and its competitive nature, which requires high concentrations *in vivo* to outcompete the extracellular choline concentrations.¹⁵ Because of these detrimental characteristics of HC-3, the development of a non-competitive tool molecule that inhibits CHT is necessary to further explore its physiological role in cholinergic signaling.

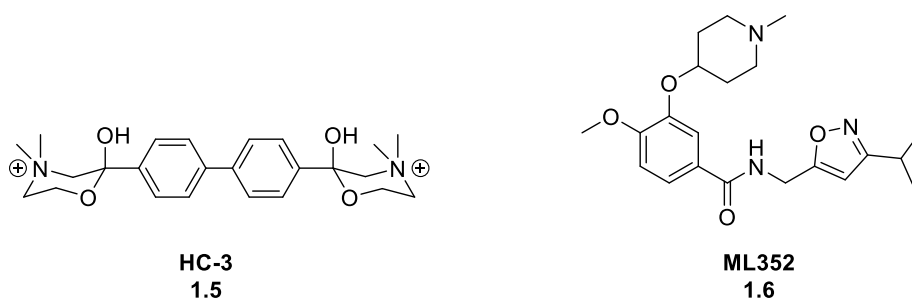


Figure 1.3 Known CHT antagonists in the literature.

Previously reported by our lab, a CHT high-throughput screen (HTS) was conducted, followed by probe optimization that provided ML352 as a non-competitive inhibitor of CHT. A membrane depolarization assay developed by the Blakely lab at Vanderbilt University was utilized in the CHT HTS to identify small molecule inhibitors of CHT. Over 300,000 compounds were screened in this assay from the NIH Molecular Library Small Molecule Repository compound collection. Compounds were screened in triplicate against a human CHT LVAA cell line using a triple add protocol. Compound or vehicle was added in the presence of no choline, an EC₂₀ concentration of choline, and an EC₈₀ concentration of choline to measure agonist, potentiation, and antagonist activity, respectively. The screen identified a 4-methoxybenzamide series and, with probe optimization efforts, resulted in ML352 (**1.2**). Unfortunately, **1.2** suffered from modest clearance ($K_p = 0.28$), supra-hepatic *in vivo* clearance in rat ($CL_p = 107$ mL/min/kg), and as a result a short elimination half-life ($t_{1/2} = 33$ min).^{13,37} While the development of **1.2** was a large advancement in the field, further optimization efforts are required to improve CNS penetration and pharmacokinetics for *in vivo* behavioral testing.

Conclusions

Beginning from ML352, we will conduct an optimization campaign through traditional medicinal chemistry approaches to improve upon its pharmacokinetic profile, while maintaining its potency and non-competitive nature to develop an acceptable tool molecule for behavioral testing. The non-competitive mode of inhibition indicates that the compounds in our series are binding to a distinctly different site than the native ligand binding site. This phenomenon is known as allosteric modulation. We believe that

a non-competitive mode of inhibition could be a potentially useful feature, as it has been reported that extracellular choline is at near saturating levels. Because of this, the competitive inhibitor would be outcompeted by choline, thus limiting its therapeutic utility. Structure-activity relationships (SAR) and drug metabolism and pharmacokinetic (DMPK) studies will guide our medicinal chemistry approaches, as there is no known crystal structure for the CHT. By attenuating the electronics and further probing chemical space, we hope to achieve the necessary DMPK parameters for *in vivo* behavioral studies. The following chapter will summarize our efforts that led to the discovery of VU6001221, a potent and selective *in vivo* tool compound.

Materials and Methods

General Synthetic Methods and Instrumentation

All NMR spectra were recorded on a 400 MHz AMX Bruker NMR spectrometer. ^1H and ^{13}C chemical shifts are reported in δ values in ppm downfield with the deuterated solvent as the internal standard. Data are reported as follows: chemical shift, multiplicity (s = singlet, d = doublet, t = triplet, q = quartet, b = broad, m = multiplet), integration, coupling constant (Hz). Low resolution mass spectra were obtained on an Agilent 6120 or 6150 with ESI source. MS parameters were as follows: fragmentor: 70, capillary voltage: 3000 V, nebulizer pressure: 30 psig, drying gas flow: 13 L/min, drying gas temperature: 350 °C. Samples were introduced via an Agilent 1290 UHPLC comprised of a G4220A binary pump, G4226A ALS, G1316C TCC, and G4212A DAD with ULD flow cell. UV absorption was generally observed at 215 nm and 254 nm with a 4 nm

bandwidth. Column: Waters Acquity BEH C18, 1.0 x 50 mm, 1.7 μm . Gradient conditions: 5% to 95% CH_3CN in H_2O (0.1% TFA) over 1.4 min, hold at 95% CH_3CN for 0.1 min, 0.5 mL/min, 55 $^\circ\text{C}$. High resolution mass spectra were obtained on an Agilent 6540 UHD Q-TOF with ESI source. MS parameters were as follows: fragmentor: 150, capillary voltage: 3500 V, nebulizer pressure: 60 psig, drying gas flow: 13 L/min, drying gas temperature: 275 $^\circ\text{C}$. Samples were introduced via an Agilent 1200 UHPLC comprised of a G4220A binary pump, G4226A ALS, G1316C TCC, and G4212A DAD with ULD flow cell. UV absorption was observed at 215 nm and 254 nm with a 4 nm bandwidth. Column: Agilent Zorbax Extend C18, 1.8 μm , 2.1 x 50 mm. Gradient conditions: 5% to 95% CH_3CN in H_2O (0.1% formic acid) over 1 min, hold at 95% CH_3CN for 0.1 min, 0.5 mL/min, 40 $^\circ\text{C}$. For compounds that were purified on a Gilson preparative reversed-phase HPLC, the system comprised of a 333 aqueous pump with solvent-selection valve, 334 organic pump, GX-271 or GX-281 liquid handler, two column switching valves, and a 155 UV detector. UV wavelength for fraction collection was user-defined, with absorbance at 254 nm always monitored. Method 1: Phenomenex Axia-packed Luna C18, 30 x 50 mm, 5 μm column. Mobile phase: CH_3CN in H_2O (0.1% TFA). Gradient conditions: 0.75 min equilibration, followed by user defined gradient (starting organic percentage, ending organic percentage, duration), hold at 95% CH_3CN in H_2O (0.1% TFA) for 1 min, 50 mL/min, 23 $^\circ\text{C}$. Method 2: Phenomenex Axia-packed Gemini C18, 50 x 250 mm, 10 μm column. Mobile phase: CH_3CN in H_2O (0.1% TFA). Gradient conditions: 7 min equilibration, followed by user defined gradient (starting organic percentage, ending organic percentage, duration), hold at 95% CH_3CN in H_2O (0.1% TFA) for 7 min, 120 mL/min, 23 $^\circ\text{C}$. All reagents were purchased from

Aldrich Chemical Co. and were used without purification. All final compounds were >98% pure by LCMS (254 nm, 214 nM and ELSD). Following these purification protocols, final compounds were transferred to a barcode vial and diluted to a concentration of 10 μ M using molecular biology grade dimethylsulfoxide (DMSO). These compounds were registered into Dotmatics and assigned a VU identification number before being tested in the primary screening assay.

Reagents and Cells

All biochemical reagents were of research grade and, unless stated otherwise, obtained from Sigma-Aldrich (St. Louis, MO, USA). Commercially available replicates and derivatives of molecules identified as hits in our HTS screen were obtained from Ambinter (Orleans, France) as dry powders. HEK 293 and HEK 293 cells stably transfected with either the human CHT (hCHT) or mutant hCHT LV-AA (L531A, V532A) were described previously⁴¹ and maintained according to American Type Culture Collection (ATCC, Manassas, VA, USA) guidelines using MEM Earles media containing 1 \times fetal bovine serum, 2 mM glutamine, 100 IU penicillin, and 100 μ g/mL streptomycin (Fisher Scientific, Pittsburgh, PA, USA). All studies used cells cultured at 70–100% confluence.

Choline-Induced Membrane Potential Assay (96-Well FlexStation Format)

HEK 293T cells stably expressing hCHT LV-AA. Control cells were assessed for choline-induced membrane depolarization as previously described.⁴¹ Briefly, cells were plated into 96-well, black walled, clear bottom poly-D-lysine coated plates (BioCoat BD Biosciences). Cells were plated in 50 μ L/well at 45 000 cells/well and allowed to grow for 48 h. Cells were preincubated in HBSS/HEPES 1 \times dye (60 μ L of blue membrane

potential dye, R8042 at 1.67 µg/mL, Molecular Devices, Sunnyvale, CA, USA) for 30 min at 37 °C in an atmosphere of 95% air/5% CO₂. Tested compounds were added at this preincubation step. Membrane potential-associated fluorescence was detected using a FlexStation (Molecular Devices) microplate fluorimeter, recording baseline (1 min) and following automated addition of choline (20 µL) to achieve 100 nM and 10 µM final concentrations in HBSS/HEPES 1× dye. Fluorescence was recorded for 2–4 min with sampling every 1.5 s. Data were analyzed by SoftMax Pro (Molecular Devices) and exported to Microsoft Excel for further evaluation.

Hemicholinium-3 (HC-3) Radioligand Binding Assays

HEK 293 cells stably expressing CHT were plated on 150 mm sterile tissue culture dish and allowed to grow to confluence. Cells were harvested from the plates with 50 mM Tris-HCl buffer (pH 7.5) and homogenized using a Polytron (Wheaton Instruments, Millville, NJ, USA) at a speed setting of 4. Homogenates were centrifuged for 15 min at 15 000g. Pellets were resuspended in 10 mL of 50 mM Tris-HCl buffer (pH 7.5) and centrifuged again for 15 min at 15 000g. The resulting pellets were resuspended in 2 mL of Tris base buffer. Protein concentrations were determined using the BCA protein assay (Pierce, Rockford, IL, USA). Hemicholinium-3 diacetate salt, [methyl-³H]-HC-3 (PerkinElmer, Waltham, MA, 120 Ci/mmol) binding assays were conducted in 50 mM TRIS-HCl buffer, 200 mM NaCl, pH 7.5, at 37 °C for 45 min. For saturation assays, serial dilutions from a 1% mix of radiolabeled and unlabeled antagonist was used to maintain specific activity. For ML352 competition binding assays, 100 µg of membranes was incubated for designated times in 10 nM [³H]-HC-3 ± varying drug concentrations. Nonspecific binding in competition assays was defined in

parallel incubations with 20 μ M unlabeled HC-3 and subtracted from total counts to define specific HC-3 binding. Nonspecific binding in saturation binding assays was defined using membranes from nontransfected HEK 293 cells. Radioactively labeled membranes were harvested on glass fiber filters (Whatman GF/B, Brandel, Gaithersburg, MD, USA) that were pretreated with 0.3% polyethylenimine and 0.2% BSA and rinsed 4x with assay buffer (50 mM Tris-HCl, 200 mM NaCl, pH 7.5). Filters were solubilized in EcoScint H (National Diagnostics, Atlanta, GA) and allowed to shake overnight, and bound radiolabel was quantified by liquid scintillation counting (TriCarb 2900TR, PerkinElmer). HC-3 binding capacity (B_{max}) and affinity (K_d) and ML352 K_i values were determined using nonlinear curve fit to a singesite inhibition model using Prism 5.

Off-Target Screen

VU221 was tested in the Lead Profiling Screen (Eurofin, Luxembourg), a binding assay panel of 68 G-protein coupled receptors, ion channels, and transporters, at 10 μ M. The Lead Profiling Screen consists of 68 primary molecular targets, including several CNS targets recommended by the European Medicines Agency (EMA) to evaluate drug dependence potential. For full assay details, see www.eurofinspanlabs.com.

Animal Care and Husbandry

All procedures with mice (C57BL/6J mice, Jackson Laboratories, Bar Harbor, ME, USA) and rats (Sprague–Dawley, Harlan, Indianapolis, IN, USA) were performed with animals at 10–20 weeks of age under an approved protocol that is reviewed annually by the Vanderbilt Institutional Animal Care and Use Committee (IACUC).

Animals were housed prior to use on a 12:12 light–dark cycle with food and water provided *ad libitum*.

Metabolism and Disposition Methods

The metabolism of ML352 was investigated *in vitro* in rat hepatic microsomes (BD Biosciences, Billerica, MA, USA) using substrate depletion methodology (% test article remaining). A potassium phosphate-buffered reaction mixture (0.1 M, pH 7.4) of test article (1 μ M) and microsomes (0.5 mg/ mL) was preincubated (5 min) at 37 °C prior to the addition of NADPH (1 mM). The incubations, performed in 96-well plates, were continued at 37 °C under ambient oxygenation, and aliquots (80 μ L) were removed at selected time intervals (0, 3, 7, 15, 25, and 45 min). Protein was precipitated by the addition of chilled acetonitrile (160 μ L), containing carbamazepine as an internal standard (50 ng/mL), and centrifuged at 3000 rpm (4 °C) for 10 min. Resulting supernatants were transferred to new 96-well plates in preparation for LC/MS/MS analysis. The *in vitro* half-life ($t_{1/2}$, min, eq 1), intrinsic clearance (CL_{int} , mL/min/kg, eq 2), and subsequent predicted hepatic clearance (CL_{hep} , mL/min/kg, eq 3) were determined employing the following equations:

$$(1) \quad T_{1/2} = \frac{\text{Ln}(2)}{k}$$

where k represents the slope from linear regression analysis of the natural log percent remaining of test compound as a function of incubation time.

$$(2) \quad CL_{int} = \frac{0.693}{in\ vitro\ T_{1/2}} \times \frac{mL\ incubation}{mg\ microsomes} \times \frac{45\ mg\ microsomes}{gram\ liver} \times \frac{45^a\ gram\ liver}{kg\ body\ wt}$$

^ascale-up factors of 20 (human) and 45 (rat)

$$(3) \quad CL_{hep} = \frac{Q_h \cdot CL_{int}}{Q_h + CL_{int}}$$

Plasma Protein Binding

Protein binding of ML352 was determined in rat plasma via equilibrium dialysis employing single-use RED plates with inserts (ThermoFisher Scientific, Rochester, NY, USA). Briefly, commercially available rat plasma (220 μ L) was added to the 96-well plate containing test article (5 μ L) and mixed thoroughly. Subsequently, 200 μ L of the plasma-test article mixture was transferred to the cischamber (red) of the RED plate, with an accompanying 350 μ L of phosphate buffer (25 mM, pH 7.4) in the trans chamber. The RED plate was sealed and incubated for 4 h at 37 °C with shaking. At completion, 50 μ L aliquots from each chamber were diluted 1:1 (50 μ L) with either plasma (cis) or buffer (trans) and transferred to a new 96-well plate, at which time ice-cold acetonitrile (2 volumes), containing carbamazepine as internal standard (50 ng/mL), was added to extract the matrices. The plate was centrifuged (3000 rpm, 10 min), and supernatants were transferred to a new 96-well plate. The sealed plate was stored at -20 °C until LC/MS/MS analysis.

Pharmacokinetics and Brain Tissue Distribution Studies in Sprague-Dawley Rats

VU221 was formulated in 10% EtOH/50% PEG400/40% saline, as well as 0.5% methylcellulose/0.1% Tween 80, in preparation from intravenous (IV) and oral (PO)

dosing, respectively. The IV dose was administered via the jugular vein to 4 dual-cannulated (carotid artery and jugular vein) adult male Sprague–Dawley rats, each weighing between 250 and 350 g (Harlan, Indianapolis, IN, USA), for a final dose of 1 mg/kg VU221; the PO dose was administered via oral gavage to 4 dual-cannulated (carotid artery and jugular vein) adult male Sprague–Dawley rats, each weighing between 250 and 350 g, for a final dose of 2.3 mg/kg dose of VU221. Whole blood collections from the IV study via the carotid artery were performed at 0.033, 0.117, 0.25, 0.5, 1, 2, 4, 7, and 24 h postdose; the PO sampling times were 0.25, 0.5, 1, 2, 3, 4, 6, 8, and 24 h postdose. Following the 24 h sample collection, rats were redosed with VU221 (1 mg/kg) followed by isoflurane treatment (0.75 min) 15 min post second dose in order to obtain blood and CNS tissue for the K_p, brain determinations. The samples for pharmacokinetic analysis were collected into chilled, EDTA-fortified tubes and centrifuged for 10 min (3000 rcf, 4 °C), with the resulting separated plasma stored at –80 °C until LC/MS/MS bioanalysis. The samples for brain tissue distribution analysis were collected at the time of euthanization, with the whole brain being removed and thoroughly rinsed with cold phosphate-buffered saline prior to freezing on dry ice. Whole brains were weighed and diluted (3 mL) with 70:30 isopropanol/ water (v/v). The mixture was subjected to mechanical homogenation employing a mini-beadbeater and 1.0 mm Zirconia/Silica Beads (BioSpec Products Inc., Bartlesville, OK, USA) followed by centrifugation (3500 rcf, 20 °C, 5 min). The liquid extraction of plasma (40 µL) and brain homogenate supernatant diluted (4×) in plasma (40 µL) was performed by conventional protein precipitation using three volumes of ice-cold acetonitrile containing an internal standard (50 nM carbamazepine). The samples were centrifuged (3500 rcf, 20 °C, 5

min), and the supernatants diluted (1:1; v/v) via transfer into a fresh 96-well plate containing deionized water for LC/MS/MS bioanalysis (vide infra).

Liquid Chromatography/Mass Spectrometry Analysis

Compounds were analyzed via electrospray ionization (ESI) on an AB Sciex API-5500 (Foster City, CA, USA) triple-quadrupole linear ion trap instrument that was coupled with Shimadzu LC-20AD pumps (Columbia, MD, USA) and a Leap Technologies CTC PAL autosampler (Carrboro, NC, USA). Analytes were separated by gradient elution using a Fortis C18 2.1 × 50 mm, 3.5 µm column (Fortis Technologies Ltd., Cheshire, UK) thermostated at 40 °C. HPLC mobile phase A was 0.1% NH₄OH (pH unadjusted), and mobile phase B was acetonitrile. The gradient started at 30% B after a 0.2 min hold and was linearly increased to 90% B over 0.8 min, held at 90% B for 0.5 min, and returned to 30% B in 0.1 min followed by a re-equilibration (0.9 min). The total run time was 2.5 min, and the HPLC flow rate was 0.5 mL/min. The source temperature was set at 500 °C, and mass spectral analyses were performed using multiple reaction monitoring (MRM) utilizing a turbo-ion-spray source in positive ionization mode (5.0 kV spray voltage). LC/MS/MS analysis was performed employing a TSQ QuantumULTRA that was coupled to a ThermoSurveyor LC system (Thermoelectron Corp., San Jose, CA, USA) and a Leap Technologies CTC PAL autosampler (Carrboro, NC, USA). Chromatographic separation of analytes was achieved with an Acquity BEH C18 2.1 × 50 mm, 1.7 µm column (Waters, Taunton, MA, USA).

Behavioral Pharmacology: Animals

In vivo studies utilized either 7–8 week old male C57Bl/6 mice (Jackson Laboratory, Sacramento, CA) or male Sprague–Dawley rats weighing 275–300 g

(Envigo, Indianapolis, IN). The animals were cared for in accordance with the National Institutes of Health Guide for the Care and Use of Laboratory Animals. All experimental procedures were approved by the Vanderbilt University Animal Care and Use Committee. All mice were grouped housed on a 12:12 light–dark cycle with lights on at 0600. All experiments were conducted during the light phase. Food and water were available ad libitum.

Behavioral Pharmacology: Novel Object Recognition Task

Novel object recognition memory was assessed as previously described.²⁶ Briefly, rats were habituated to an empty novel object recognition (NOR) arena. On test day, rats were administered vehicle (10% tween 80) or VU0486846 (1–10 mg/ kg, intraperitoneally (i.p.), 1 mL/kg, n = 12) and returned to their home cage for 30 min. Rats were then placed in the NOR arena containing 2 identical objects for 10 min. Following the exposure period, rats were placed back into their home cages for 24 h. The rats were then returned to the arena in which one of the previously exposed (familiar) objects was replaced by a novel object and exploration behavior was assessed for 3 min. Time spent exploring each object was scored by an observer blinded to the experimental conditions and the recognition index was calculated as [(time spent exploring novel object) – (time spent exploring familiar object)]/total time exploring objects.

Development of an Improved *In Vivo* Tool Compound, VU6001221, for Non-Competitive Inhibition of the Choline Transporter

The Optimization Plan for ML352

The previous optimization campaign did not explore the northern piperidine region nor the eastern amide region very thoroughly. The optimization plan for ML352 is depicted in **Figure 1.4**. We plan to expand upon the SAR at the northern portion of the molecule by employing alternate alkyl moieties at the R₃ position as well as surveying various nitrogen-containing ring sizes in place of the piperidine. We also plan to diversify the eastern region by incorporating alternative amides and heterocyclic moieties. In addition, we'd like to attenuate the electron rich phenyl core by replacing the methoxy group with electron withdrawing moieties, as this is likely the cause of the supra-hepatic clearance of ML352. Iterative parallel synthesis will be employed to diversify the three regions of the molecule. Optimization efforts described in the following chapter were a collaboration between myself and James "Chris" Tarr.

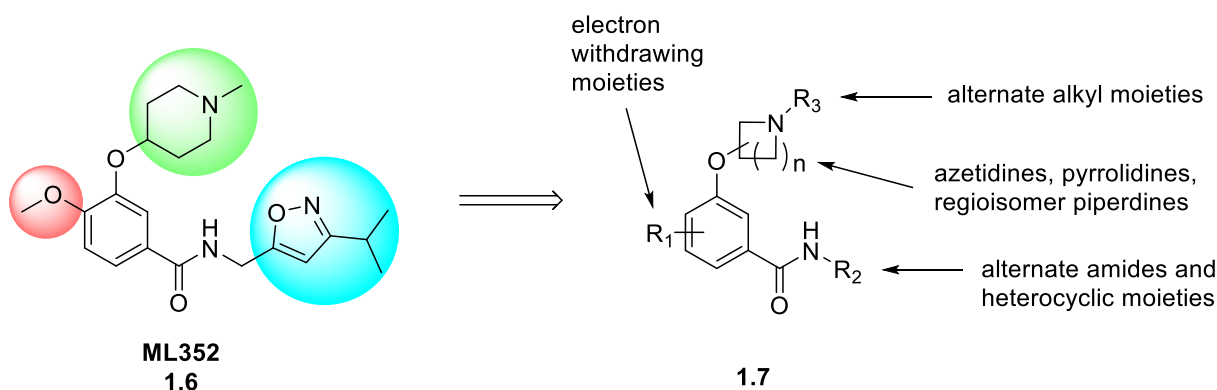
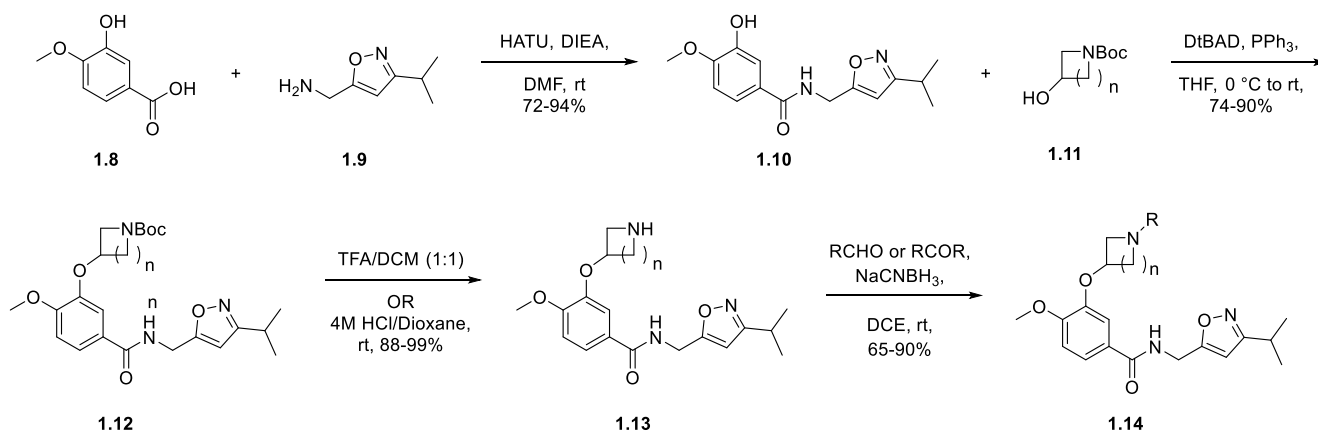


Figure 1.4 Structure of ML352 (1.6) and proposed SAR strategies.

Initial SAR of Northern Aliphatic Ring: Analogs **1.15-1.26**

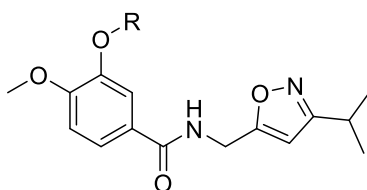
Initial SAR efforts were focused on the northern cycloalkyl ring of **1.6** to fill in SAR gaps, as previous optimization campaign solely focused on five and six membered nitrogen containing aliphatic rings. We wanted to explore alternative N-alkyl moieties and varying the nitrogen-containing saturated ring size to probe chemical space further. Analogs of this nature were rapidly synthesized from readily available starting materials in a four-step sequence outlined in **Scheme 1.1**. Commercial 4-methoxy 3-hydroxy



Scheme 1.1 Synthetic route to access northern cycloalkylamine analogs **1.15-1.26**.

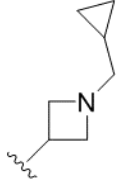
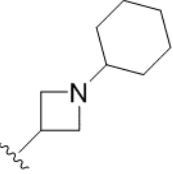
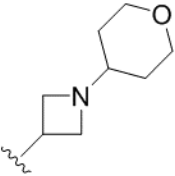
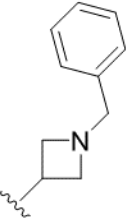
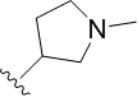
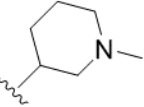
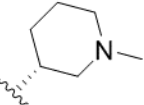
benzoic acid **1.8** was coupled with primary amine **1.9** through a HATU mediated amide coupling to generate amide **1.10**. Mitsunobu reaction conditions were then utilized to couple hydroxyl cycloalkyl amines **1.11** to **1.10**, followed by a Boc deprotection using acidic conditions to provide **1.13** in good yields. Lastly, reductive amination conditions using either aldehydes or ketones were utilized to access analogs **1.15-1.26**. To triage compounds prior to running full concentration-response curves (CRCs), a single point screen was conducted with 100 nM choline and 5 μ M compound treatment. Active compounds were considered to be those that inhibited choline uptake by 50% or

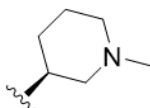
greater. As can be seen in **Table 1.1**, compound **1.24** was the only active compound from this set of compounds. The enantiomers for this compound were then separated via super-critical fluid chiral (SFC) chromatography to provide single enantiomers (of unknown absolute stereochemistry) **1.25** and **1.26**.



1.15 - 1.26

R	Compound Number	VOID	CHT % activity remaining	CHT IC ₅₀ (μM)
	1.15	VU6031558	Inactive	N/A
	1.16	VU6031559	Inactive	N/A
	1.17	VU6031560	Inactive	N/A
	1.18	VU6031561	Inactive	N/A

	1.19	VU6001215	Inactive	N/A
	1.20	VU6001212	Inactive	N/A
	1.21	VU6001213	Inactive	N/A
	1.22	VU6001216	Inactive	N/A
	1.23	VU6001557	Inactive	N/A
	1.24	VU0476326	51.7	0.36
	1.25	VU6003140	N/A	2.90



1.26

VU6005262

N/A

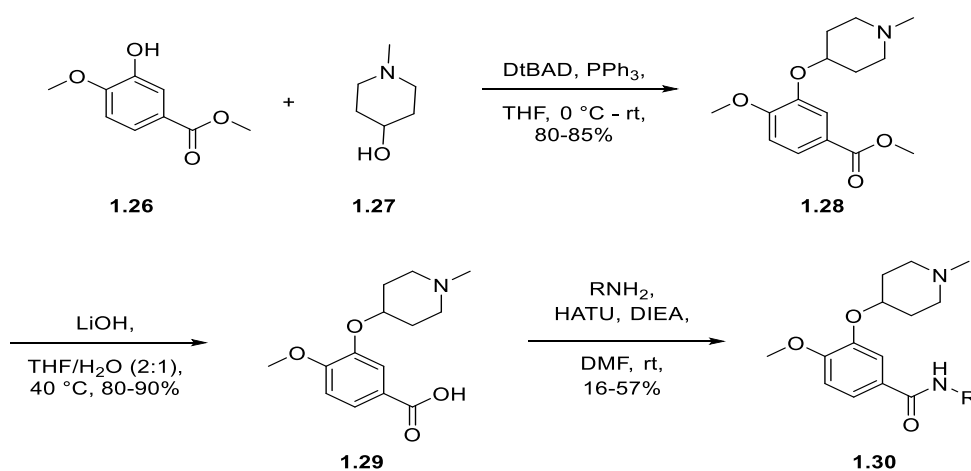
2.90

Table 1.1 SAR around the northern cycloalkylamine – analogs **1.15-1.26**.

Unfortunately, these data were a bit perplexing, as we predicted that one enantiomer would be more potent than the racemate while the other would be less potent. Here we see that both enantiomers are equipotent to each other and less potent than the racemate. Because of this, we elected to move forward without further pursuing these compounds. Having surveyed various different nitrogen containing ring sizes at this position, it was clear that the methyl piperidine moiety is essential for activity. Therefore, we shifted our focus towards exploring different sections of the molecule.

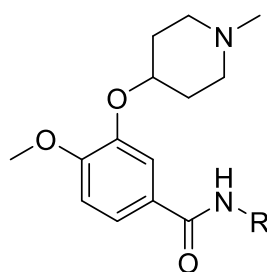
SAR of the Eastern Amide moiety: Analogs 1.33-1.64

We next wanted to probe chemical space at the eastern part of the molecule by incorporating alternative amines of various chain lengths and steric bulk. The synthesis of these analogs is depicted in **Scheme 1.2**, where this time the methyl piperidine ether



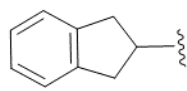
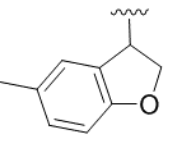
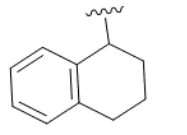
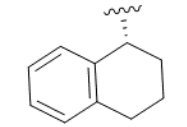
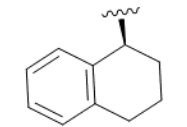
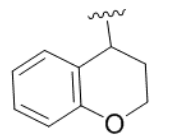
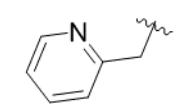
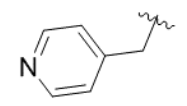
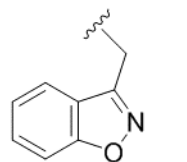
Scheme 1.2 Synthetic route to access amide analogs **1.33-1.64**.

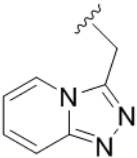
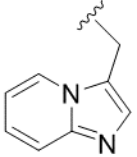
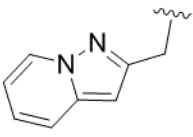
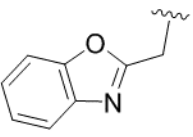
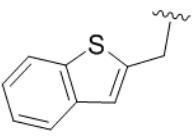
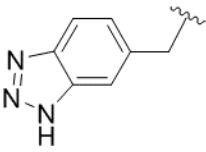
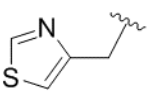
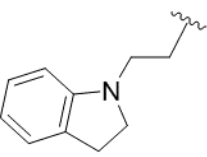
was held constant while surveying the amide moiety. Beginning from commercially available 4-substituted 3-hydroxy benzoic ester **1.27** and commercially available hydroxyl cycloalkyl amine **1.28**, Mitsunobu reaction conditions were employed to couple the two chemical building blocks together to provide compound **1.29**. Next, ester **1.29** was hydrolyzed to carboxylic acid **1.30** using mild basic conditions, followed by HATU mediated amide couplings with various primary and secondary amines to access analogs **1.33-1.64**. SAR data for the eastern amide portion of the molecule utilizing primary amines is highlighted in **Table 1.2** and SAR data utilizing secondary amines is highlighted in **Table 1.3**.

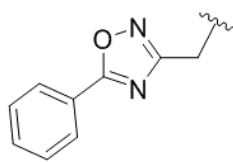


1.33 - 1.65

R	Compound Number	VOID	CHT % activity remaining	CHT IC ₅₀ (μM)
	1.33	VU6001044	Inactive	N/A
	1.34	VU6001045	Inactive	N/A

	1.35	VU6001046	Inactive	N/A
	1.36	VU6001047	Inactive	N/A
	1.37	VU6001048	Inactive	N/A
	1.38	VU6001049	Inactive	N/A
	1.39	VU6001050	Inactive	N/A
	1.40	VU6001051	Inactive	N/A
	1.41	VU6001052	Inactive	N/A
	1.42	VU6001053	Inactive	N/A
	1.43	VU6001054	Inactive	N/A

	1.44	VU6001055	Inactive	N/A
	1.45	VU6001056	Inactive	N/A
	1.46	VU6001057	Inactive	N/A
	1.47	VU6001058	Inactive	N/A
	1.48	VU6001059	Inactive	N/A
	1.49	VU6001060	Inactive	N/A
	1.50	VU6001061	Inactive	N/A
	1.51	VU6001062	Inactive	N/A

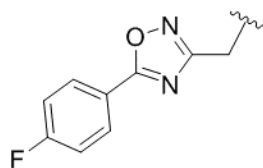


1.52

VU6001063

43.3

N/A

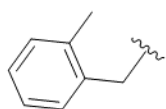


1.53

VU6001565

Inactive

N/A

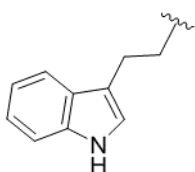


1.54

VU6001562

Inactive

N/A

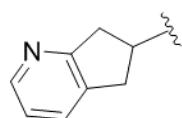


1.55

VU6001563

Inactive

N/A

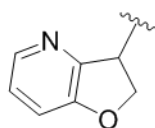


1.56

VU6001564

Inactive

N/A

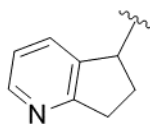


1.57

VU6001566

Inactive

N/A

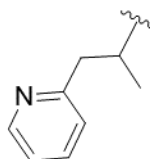


1.58

VU6001567

Inactive

N/A

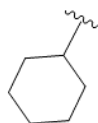


1.59

VU6001560

Inactive

N/A

**1.60**

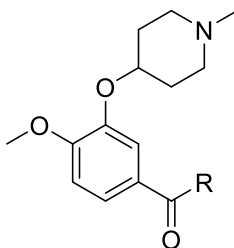
VU6001561

Inactive

N/A

Table 1.2 SAR around the amide moiety: 2° amides – analogs **1.33-1.60**.

The data in **Table 1.2** shows steep SAR, which is not entirely unanticipated due to the allosteric nature of the series. Only one compound within this group displayed CHT inhibition greater than 50%. Although **1.52** is considered to be active by the standards we laid out, it is only mildly so and therefore not pursued further. A few tertiary amides were also incorporated (**Table 1.3**). However, these amide analogs turned out to be unfruitful as well. Unable to find a compound of equal or greater potency as ML352, we moved away from modifying branches of the molecule to focusing on changing the electronics of the core.

**1.61 - 1.64**

R	Compound Number	VOID	CHT % activity remaining	CHT IC₅₀ (μM)
	1.61	VU6001267	Inactive	N/A

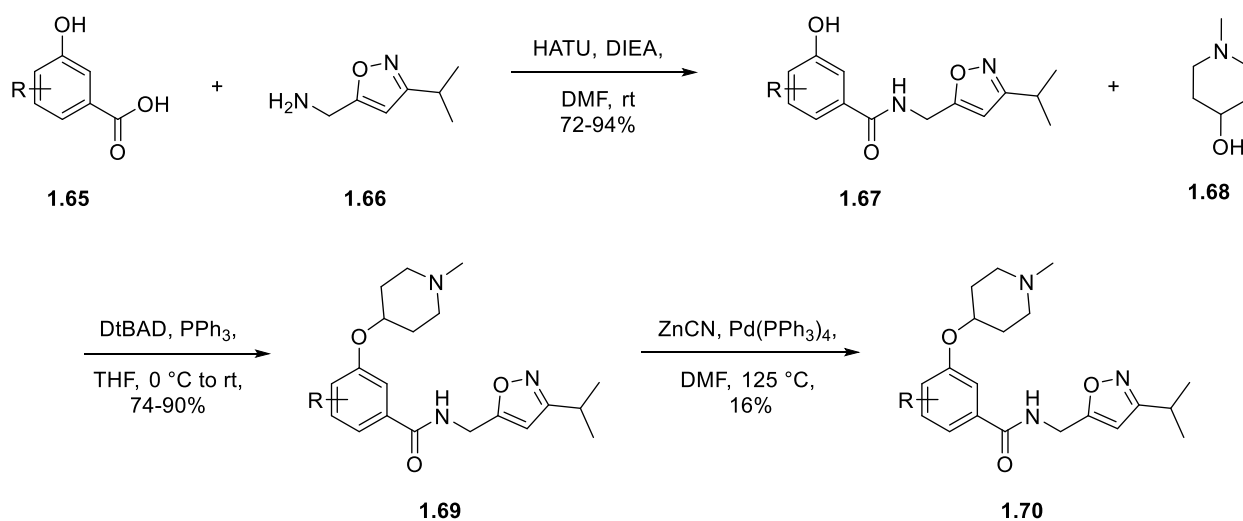
	1.62	VU6001266	Inactive	N/A
	1.63	VU6001265	Inactive	N/A
	1.64	VU6001264	Inactive	N/A

Table 1.3 SAR around the amide moiety: 3° amides – analogs **1.61-1.64**.

Tuning the Electronics of the Central Core: Analogs 1.71-1.74

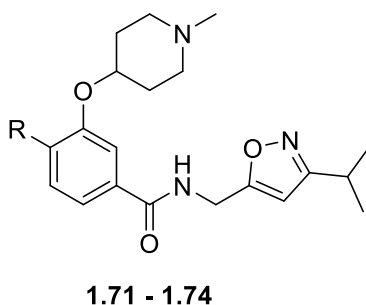
We hypothesized that the electron rich core induced by the electron donating methoxy substituent made this moiety especially susceptible to metabolism. Therefore, we decided to remove the methoxy group, as well as incorporate electron withdrawing groups in its place. Congeners such as these were synthesized via **Scheme 1.3**.

Commercially available primary amine **1.66** was coupled to the appropriate hydroxy



Scheme 1.3 Synthetic route to access core analogs **1.71-1.74**.

benzoic acid via a HATU mediated amide coupling to provide **1.67** analogs. Mitsunobu reaction conditions were then employed to couple **1.67** and **1.68** to provide congeners **1.71-1.73**. Analog **1.74** was accessed through palladium-catalyzed cyanation conditions to provide the final nitrile compound. Potency data for compounds **1.71-1.74** can be observed in **Table 1.4**. Excitingly, these efforts afforded active CHT inhibitors. The des-methoxy compound **1.71** showed moderate nanomolar activity. Electron-withdrawing groups were also tolerated with fluorine (**1.72**) and chlorine (**1.73**) congeners displaying nanomolar activity, while cyano analog **1.74** showed weak activity ($IC_{50} = 3.35 \mu M$).



R	Compound Number	VUID	CHT IC_{50} (μM)
H	1.71	VU6001550	0.64
F	1.72	VU6003896	0.47
Cl	1.73	VU6001221	0.27
CN	1.74	VU6003902	3.35

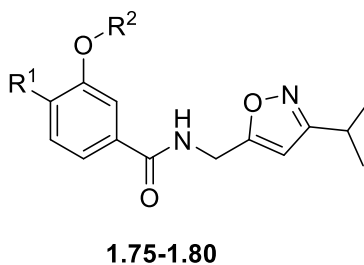
Table 1.4 SAR around the central core – analogs **1.71-1.74**.

While these analogs showed a loss in potency compared to ML352, it was a step in the right direction. Therefore, chloro analog **1.73** emerged as the most promising compound thus far in this optimization campaign and selected for further evaluation. In parallel, we

decided to further explore the SAR around analogs **1.71-1.73** in light of their activity as CHT inhibitors.

SAR around fluoro, chloro, and des-methoxy congeners of ML352: Analogs 1.75-1.94

With these new active cores in hand, we explored the replacements of the methyl piperidine and the amide moieties to further probe SAR in search of a more potent compound. These analogs were synthesized in the same manner depicted in **Scheme 1.1** using the appropriate commercially available hydroxy benzoic acid. Because the *N*-methyl piperidine appears to play a crucial role in compound activity, we did very little SAR around it. The very subtle alterations that were made to the northern cycloalkyl region can be viewed in **Table 1.5**.



R¹	R²	Compound Number	VOID	CHT IC₅₀ (μM)
H		1.75	VU6001554	1.8
F		1.76	VU6003527	>10

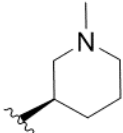
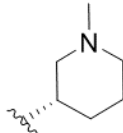
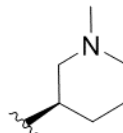
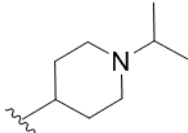
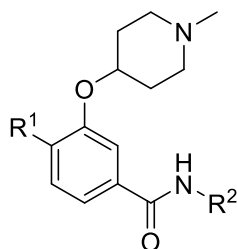
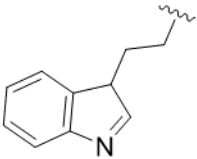
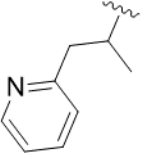
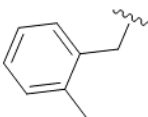
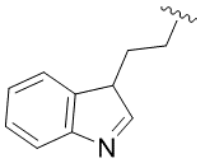
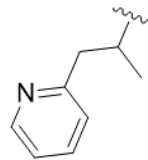
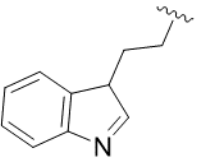
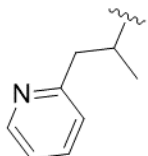
F		1.77	VU6003138	3.2
Cl		1.78	VU6003141	>10
Cl		1.79	VU6005261	6.5
Cl		1.80	VU6003899	0.31

Table 1.5 SAR around the northern cycloalkylamine with new central cores – analogs **1.75-1.80**.

Compounds of this nature displayed weak active, apart from analog **1.80**, which exhibited nanomolar potency. Despite compound **1.80** displaying nanomolar activity, it was not pursued further due to it being less potent than our current lead compound (**1.73**). Encountering steep SAR around the cycloalkylamine moiety, we diverted our attention to surveying different amides, which are highlighted in **Table 1.6**, utilizing the new core pieces described in previous sections.



1.81-1.94

R ¹	R ²	Compound Number	VOID	CHT IC ₅₀ (μM)
H		1.81	VU6001551	Inactive
H		1.82	VU6001552	Inactive
H		1.83	VU6001553	Inactive
F		1.84	VU6003898	2.5
F		1.85	VU6003897	4.3
Cl		1.86	VU6001262	Inactive
Cl		1.87	VU6003901	1.6

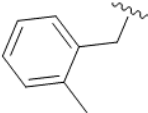
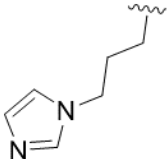
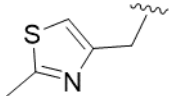
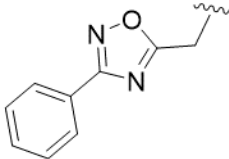
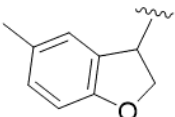
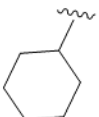
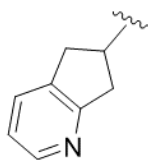
Cl		1.88	VU6001263	Inactive
Cl		1.89	VU6003244	Inactive
Cl		1.90	VU6001223	Inactive
Cl		1.91	VU6001220	Inactive
Cl		1.92	VU6001214	Inactive
Cl		1.93	VU6001222	Inactive
Cl		1.94	VU6001555	Inactive

Table 1.6 SAR around amide moiety with new central cores – analogs **1.81-1.94**.

Unfortunately, modifications to the amide region of 4-F, 4-Cl, and 4-des-methoxy compounds resulted in a considerable loss in potency. With SAR being incredibly steep within this series, our efforts shifted from making additional analogs to exploring the DMPK profile of lead compound **1.73** to evaluate its potential as an *in vivo* probe molecule.

Assessment of VU6001221(1.73) as a Viable Tool Compound

Like ML352, **1.73** has a low molecular weight (MW <400), attractive cLogP, and a low total polar surface area (TPSA; **Table 1.7**). The two CHT inhibitors also display clean CYP profiles, great free fraction in rat and human, and good brain homogenate binding data in rat. One large improvement **1.73** has over ML352 is its low *in vitro*

Property	ML352	1.73
MW	387.2	391.1
cLogP	2.49	2.71
TPSA	77.1	63.6
<i>In vitro pharmacokinetic parameters</i>		
CL _{INT} (mL/min/kg), rat	95.0	42.5
CL _{HEP} (mL/min/kg), rat	40.0	28.9
CL _{INT} (mL/min/kg), human	10.4	10.4
CL _{HEP} (mL/min/kg), human	6.90	6.90
PPB (f _u), rat	0.35	0.19
PPB (f _u), human	0.67	0.31
BHB (f _u), rat	0.36	0.65
Cytochrome P ₄₅₀ (IC ₅₀ μM)		
1A2	>30	>30
2C9	>30	>30
2D6	>30	>30
3A4	>30	>30
<i>In vivo PK (Sprague-Dawley rats, Intravenous 1 mg/kg)</i>		
CL _p (mL/min/kg)	107	1.54

$t_{1/2}$ (min)	33.0	117
V_{SS} (L/kg)	3.2	0.30
<i>Tissue distribution (1 mg/kg, Intraperitoneal, 0.25 h sample time)</i>		
C_n plasma (ng/mL)	129	47.2
C_n brain (ng/mL)	23.4	16.3
K_p , brain	0.18	0.34

Table 1.7 *In vitro* and *in vivo* DMPK profiles of ML352 and **1.73**.

predicted hepatic clearance (CL_{HEP}) from liver microsomes, as well as over a 70-fold reduction in rat *in vivo* plasma clearance ($CL_p = 1.54$ mL/min/kg versus 107 mL/min/kg for ML352). We believe that the tuning of electronics of the central phenyl core by changing the electron donating group to an electron withdrawing group is responsible for this improvement in clearance. As expected, the improvement in clearance resulted in an increased half-life from 33 minutes (ML352) to 117 minutes (**1.73**), which is sufficient enough to run behavioral experiments. In addition to the large improvement in clearance, CNS penetration is doubled for **1.73** ($K_p = 0.34$) over ML352 ($K_p = 0.18$). When considering fraction unbound data with the plasma/brain ratio (K_p), the unbound partition coefficient ($K_{p,uu}$) is approaching unity at a ratio of 0.71; meaning **1.73** freely diffuses across the blood-brain barrier (BBB). With a great clearance value, increased half-life, and improvement in brain penetration, we deduced that **1.73** had an acceptable DMPK profile for an *in vivo* tool molecule to probe the physiological roles of CHT. Lastly, **1.73** was tested against 68 CNS relevant GPCRs, ion channels, and transporters in the EuroFin Lead Profiling Screen, which showed a clean ancillary pharmacology profile (**Table 1.8**; no inhibition of >50% at 10 μ M **1.73** in a radioligand binding panel).

Target/Protein	Species	% Inhibition
Adenosine A ₁	Human	-5
Adenosine A _{2A}	Human	0
Adenosine A ₃	Human	4
Adrenergic α_{1A}	Rat	23
Adrenergic α_{1B}	Rat	3
Adrenergic α_{1D}	Human	24
Adrenergic α_{2A}	Human	43
Adrenergic β_1	Human	2
Adrenergic β_2	Human	43
Androgen (Testosterone)	Human	8
Bradykinin B ₁	Human	6
Bradykinin B ₂	Human	-3
Calcium Channel L-Type, Benzothiazepine	Rat	3
Calcium Channel L-Type, Dihydropyridine	Rat	13
Calcium Channel N-Type	Rat	-1
Cannabinoid CB ₁	Human	4
Dopamine D ₁	Human	9
Dopamine D _{2S}	Human	18
Dopamine D ₃	Human	15
Dopamine D _{4.2}	Human	-3
Endothelin ET _A	Human	-3
Endothelin ET _B	Human	-2
Epidermal Growth Factor (EGF)	Human	5
Estrogen Era	Human	4
GABA _A , Flunitrazepam, Central	Rat	6
GABA _A , Muscimol, Central	Rat	9
GABA _{B1A}	Human	-9
Glucocorticoid	Human	-1
Glutamate, Kainate	Rat	-2
Glutamate, NMDA, Agonism	Rat	1
Glutamate, NMDA, Glycine	Rat	4
Glutamate, NMDA, Phencyclidine	Rat	-5
Histamine H ₁	Human	37
Histamine H ₂	Human	20
Histamine H ₃	Human	7
Imidazoline I ₂ , Central	Rat	16
Interleukin IL-1	Mouse	-2
Leukotriene, Cysteinyl CysLT ₁	Human	-3
Melatonin MT ₁	Human	5
Muscarinic M ₁	Human	32

Muscarinic M ₂	Human	12
Muscarinic M ₃	Human	26
Neuropeptide Y Y ₁	Human	-2
Neuropeptide Y Y ₂	Human	7
Nicotinic Acetylcholine	Human	13
Nicotinic Acetylcholine α 1, Bungarotoxin	Human	7
Opiate δ ₁ (OP1, DOP)	Human	-2
Opiate κ (OP2, KOP)	Human	22
Opiate μ (OP3, MOP)	Human	8
Phorbol Ester	Mouse	5
Platelet Activating Factor (PAF)	Human	-4
Potassium Channel [K _{ATP}]	Hamster	4
Potassium Channel hERG	Human	16
Prostanoid EP ₄	Human	-7
Purinergic P2X	Rabbit	22
Purinergic P2Y	Rat	19
Rolipram	Rat	1
Serotonin (5-HT _{1A})	Human	40
Serotonin (5-HT _{2B})	Human	-7
Serotonin (5-HT ₃)	Human	2
Sigma σ ₁	Human	-1
Sodium Channel, Site 2	Rat	20
Tachykinin NK ₁	Human	22
Thyroid Hormone	Rat	6
Transporter, Dopamine (DAT)	Human	4
Transporter, GABA	Rat	11
Transporter, Norepinephrine (NET)	Human	12
Transporter, Serotonin (SERT)	Human	2

Table 1.8 Eurofins lead profile panel for VU6001221 (**1.73**). Significant activity is defined as >50% inhibition at a 10 μ M concentration of **1.73**. Data courtesy of Eurofins.

While **1.73** took a slight hit in potency compared to ML352, it had significantly improved *in vitro* and *in vivo* DMPK properties. Overall, **1.73** emerged as a best-in-class probe to study the modulation of CHT *in vivo*.³⁸

Behavioral Pharmacology of VU6001221 (1.73) in Models of Cognition

With a viable *in vivo* tool molecule in hand, we were able to evaluate the physiological role that selective CHT inhibition plays in rodent models of cognition. The behavioral model that was utilized in rodents for the assessment of **1.73** was the novel object recognition (NOR), a paradigm sensitive to cholinergic intervention. Muscarinic acetylcholine receptor (mAChR) agonists and positive allosteric modulators (PAMs), as well AChE inhibitors, are known to be efficacious in the NOR model of cognitive enhancement. Therefore, we can confirm **1.73**'s involvement in the cholinergic system through the utilization of this paradigm. The NOR paradigm evaluates the rodents' ability to recognize a novel object in their environment compared to a familiar object of which they have already been exposed to. All NOR studies were conducted by Jerri Rook's lab at Vanderbilt University.

Rats were dosed with **1.73** at 1, 3, and 10 mg/kg intraperitoneally (i.p.) 30 minutes prior to exposing them to two identical objects. The rats were allowed to explore the objects for 10 minutes before being removed from the arena. The animals were then returned to the arena 24 hours later where one of the previous objects was replaced with a novel object. The recognition index was calculated as [(time spent exploring the novel object) – (time spent exploring the familiar object)]/total time exploring objects. The results of the NOR task revealed a significant dose-dependent increase in the recognition index ($p = 0.0094$). This data showed for the first time that the inhibition of CHT results in the enhancement of cognition similar to AChE inhibitors, such as donepezil (**Figure 1.5**). The rats that received the 3 mg/kg dose displayed the largest enhancement in recognition index with an increase of 28% relative to vehicle

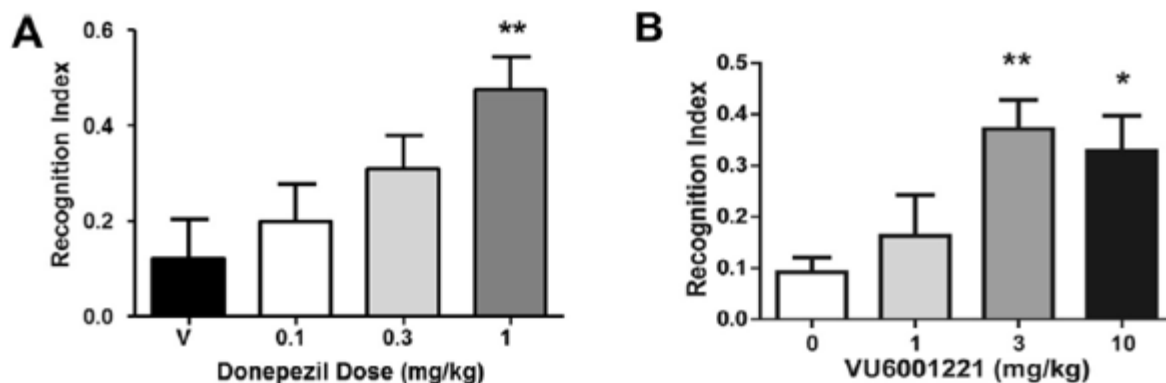


Figure 1.5 Cognitive behavioral assays of VU6001221 (**1.73**): A) NOR assay using Donepezil, B) NOR assay using **1.73**.

treated controls ($p < 0.01$). The rats dosed at 10 mg/kg displayed a slightly lower effect of 24% increase ($p < 0.05$) relative to controls, which could be due to dose-dependent cholinergic side effects such as fatigue or sedation. These data are expressed as a mean \pm SEM ($n = 5-8$) and statistical analysis was done using a Dunnett's post hoc test with significance determined as $p < 0.05$.

The mechanism by which NOR enhancement occurs is unclear, as we expected inhibition of CHT and the resulting decrease in synaptic ACh would diminish cognitive function. A possible explanation could be that **1.73** is having an agonistic effect on the $\alpha 7$ nicotinic acetylcholine receptors (nAChRs) via an elevation in synaptic or extrasynaptic choline levels due to lack of choline clearance. Although **1.73** had a clean pharmacological profile with no ancillary pharmacology observed in the panel of 68 GPCRs, ion channels, and other transporters, this does not preclude the possibility of it interacting with another target absent from the EuroFins panel.

Conclusions

To summarize, an SAR campaign was conducted around ML352 where steep, intractable SAR was encountered. Subtle electronic manipulation of the central phenyl core of ML352 provided **1.73**, a potent and selective CHT inhibitor with significantly improved pharmacokinetics and CNS penetration. The discovery of **1.73** afforded an *in vivo* tool molecule that produced, cognitive enhancing efficacy in the NOR rodent model for the first time. However, these findings of enhanced cognition were perplexing and thus require further investigations into the mechanism of action. In addition, it was also observed that non-competitive inhibition of CHT with **1.73** causes on-target distress and toxicity when dosed above 10 mg/kg i.p. Therefore, while CHT is a druggable and unexplored target to modulate cholinergic response in the context of cognition, the dose-limiting toxicity results in a narrow window of utility. It is unknown whether or not the non-competitive nature of CHT inhibitors is an essential component for behavioral efficacy. Therefore, further investigation of competitive CHT inhibitors must be explored to elucidate this phenomenon. Furthermore, the development of a competitive inhibitor would determine whether a competitive mode of inhibition would afford a broader window of utility.

Experimental Methods

General Synthetic Methods and Instrumentation

Unless otherwise stated, all reactions were conducted in flame-dried or oven-dried glassware under inert atmospheres of argon. All commercially available reagents and reaction solvents were used as received, unless otherwise noted. Reactions were

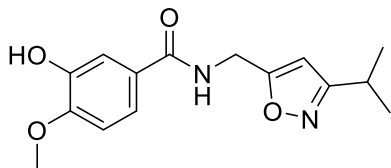
conducted at room temperature (rt, approximately 23 °C) unless otherwise noted. All NMR spectra were recorded on a 400 MHz AMX Bruker NMR spectrometer. ¹H and ¹³C chemical shifts are reported in δ values in ppm downfield with the deuterated solvent as the internal standard. Data are reported as follows: chemical shift, multiplicity (s = singlet, d = doublet, t = triplet, q = quartet, b = broad, m = multiplet), integration, coupling constant (Hz). Low resolution mass spectra were obtained on an Agilent 6120 or 6150 with ESI source. MS parameters were as follows: fragmentor: 70, capillary voltage: 3000 V, nebulizer pressure: 30 psig, drying gas flow: 13 L/min, drying gas temperature: 350 °C. Samples were introduced via an Agilent 1290 UHPLC comprised of a G4220A binary pump, G4226A ALS, G1316C TCC, and G4212A DAD with ULD flow cell. UV absorption was generally observed at 215 nm and 254 nm with a 4 nm bandwidth. Column: Waters Acquity BEH C18, 1.0 x 50 mm, 1.7 μm. Gradient conditions: 5% to 95% CH₃CN in H₂O (0.1% TFA) over 1.4 min, hold at 95% CH₃CN for 0.1 min, 0.5 mL/min, 55 °C. High resolution mass spectra were obtained on an Agilent 6540 UHD Q-TOF with ESI source. MS parameters were as follows: fragmentor: 150, capillary voltage: 3500 V, nebulizer pressure: 60 psig, drying gas flow: 13 L/min, drying gas temperature: 275 °C. Samples were introduced via an Agilent 1200 UHPLC comprised of a G4220A binary pump, G4226A ALS, G1316C TCC, and G4212A DAD with ULD flow cell. UV absorption was observed at 215 nm and 254 nm with a 4 nm bandwidth. Column: Agilent Zorbax Extend C18, 1.8 μm, 2.1 x 50 mm. Gradient conditions: 5% to 95% CH₃CN in H₂O (0.1% formic acid) over 1 min, hold at 95% CH₃CN for 0.1 min, 0.5 mL/min, 40 °C. For compounds that were purified on a Gilson preparative reversed-phase HPLC, the system comprised of a 333 aqueous pump with

solvent-selection valve, 334 organic pump, GX-271 or GX-281 liquid handler, two column switching valves, and a 155 UV detector. UV wavelength for fraction collection was user-defined, with absorbance at 254 nm always monitored. Method 1: Phenomenex Axiapacked Luna C18, 30 x 50 mm, 5 μ m column. Mobile phase: CH₃CN in H₂O (0.1% TFA). Gradient conditions: 0.75 min equilibration, followed by user defined gradient (starting organic percentage, ending S3 organic percentage, duration), hold at 95% CH₃CN in H₂O (0.1% TFA) for 1 min, 50 mL/min, 23 °C. Method 2: Phenomenex Axia-packed Gemini C18, 50 x 250 mm, 10 μ m column. Mobile phase: CH₃CN in H₂O (0.1% TFA). Gradient conditions: 7 min equilibration, followed by user defined gradient (starting organic percentage, ending organic percentage, duration), hold at 95% CH₃CN in H₂O (0.1% TFA) for 7 min, 120 mL/min, 23 °C. All reagents were purchased from Aldrich Chemical Co. and were used without purification. Sure-Seal solvents were purchased from Sigma Aldrich. Analytical thin layer chromatography was performed on 250 μ M silica gel 60 F₂₅₄ plates. Visualization was accomplished with UV light, and/or the use of potassium permanganate or Seebach stain followed by development with a heat gun.

General Procedure 1: Synthesis of Amides

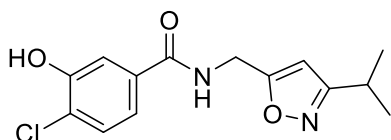
To a solution of 4-substituted 3-hydroxy benzoic acid (1.0 eq), HATU (1.1 eq), and the appropriate amine (1.1 eq) in DMF (0.25 M) was added *N,N*-diisopropylethylamine (3 eq). The reaction was stirred at rt for 1-2 h. The reaction was then diluted with H₂O and extracted with EtOAc (3x). The combined organic material was dried over MgSO₄, filtered, and concentrated. The crude material was purified using a Gilson HPLC system (30 x 50 mm column; H₂O with 0.1% TFA:acetonitrile). Fractions containing the desired

product were quenched with saturated NaHCO₃, extracted with DCM, passed through a phase separator, and concentrated to liberate the product as the free base.



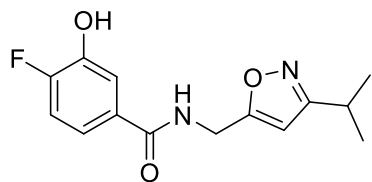
Synthesis of 3-hydroxy-*N*-((3-isopropylisoxazol-5-yl)methyl)-4-methoxybenzamide

This compound was synthesized according to general procedure 1. Clear oil (36% yield). ¹H NMR (400 MHz, CDCl₃) δ 7.40 – 7.33 (m, 2H), 6.90 – 6.84 (m, 1H), 6.62 (t, *J* = 5.9 Hz, 1H), 6.10 (s, 1H), 4.70 (d, *J* = 5.9 Hz, 2H), 3.93 (s, 3H), 3.02 (hept, *J* = 7.0 Hz, 1H), 1.26 (d, *J* = 7.0 Hz, 7H). ¹³C NMR (101 MHz, CDCl₃) δ = 169.6, 168.3, 166.8, 149.6, 145.5, 126.7, 119.8, 113.3, 110.1, 100.4, 77.3, 76.9, 76.6, 56.0, 35.6, 26.4, 21.6. LC-MS [*m/z*+H] = 291.0.



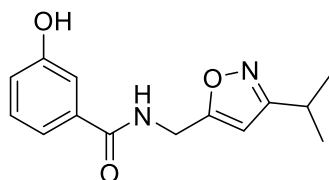
Synthesis of 4-chloro-3-hydroxy-*N*-[(3-isopropylisoxazol-5-yl)methyl]benzamide (1.73a)

This compound was synthesized according to general procedure 1. Clear oil (1.60 g, 93%). ¹H NMR (400 MHz, (CD₃)₂SO) δ 10.46 (s, 1H), 9.09 (t, *J* = 5.8 Hz, 1H), 7.49 – 7.37 (m, 2H), 7.31 (dd, *J* = 8.3, 2.0 Hz, 1H), 6.28 (s, 1H), 4.52 (d, *J* = 5.5 Hz, 2H), 2.95 (hept, *J* = 6.9 Hz, 1H), 1.18 (d, *J* = 6.9 Hz, 5H). ¹³C NMR (101 MHz, (CD₃)₂SO) δ 170.0, 169.2, 165.9, 153.4, 134.1, 130.1, 123.5, 119.0, 116.2, 100.5, 40.5, 40.3, 40.1, 39.9, 39.7, 39.5, 39.3, 35.6, 26.3, 21.8. LC-MS [*m/z*+H] = 295.0.



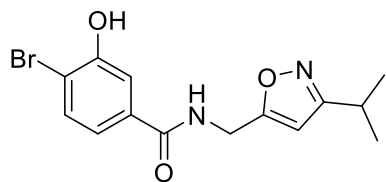
Synthesis of 4-fluoro-3-hydroxy-*N*-((3-isopropylisoxazol-5-yl)methyl)benzamide

This compound was synthesized according to general procedure 1. Clear oil (36% yield). ¹H NMR (400 MHz, (CD₃)₂SO) δ 10.16 (s, 1H), 9.04 (t, *J* = 5.8 Hz, 1H), 7.49 (dd, *J* = 8.7, 2.2 Hz, 1H), 7.34 (ddd, *J* = 8.5, 4.3, 2.2 Hz, 1H), 7.22 (dd, *J* = 11.0, 8.5 Hz, 1H), 6.28 (s, 1H), 4.52 (d, *J* = 5.8 Hz, 2H), 2.95 (hept, *J* = 6.9 Hz, 1H), 1.18 (d, *J* = 7.0 Hz, 6H). ¹³C NMR (100 MHz, (CD₃)₂SO) δ 170.13, 169.20, 165.86, 153.45 (d, ¹*J*_{CF} = 246.2 Hz), 145.3, 145.1, 130.9 (d, ⁴*J*_{CF} = 3.2 Hz), 119.0 (d, ³*J*_{CF} = 7.4 Hz), 117.8 (d, ³*J*_{CF} = 4.0 Hz), 116.3 (d, ²*J*_{CF} = 18.9 Hz), 100.4, 40.5, 40.3, 40.1, 39.9, 39.7, 39.5, 39.3, 35.6, 26.3, 21.8. LC-MS [*m/z*+H] = 279.0.



Synthesis of 3-hydroxy-*N*-((3-isopropylisoxazol-5-yl)methyl)benzamide

This compound was synthesized according to general procedure 1. Clear oil (37% yield). ¹H NMR (400 MHz, (CD₃)₂SO) δ 9.67 (s, 1H), 9.01 (t, *J* = 5.8 Hz, 1H), 7.35 – 7.22 (m, 3H), 6.93 (ddd, *J* = 7.8, 2.6, 1.3 Hz, 1H), 6.28 (s, 1H), 4.53 (d, *J* = 5.9 Hz, 2H), 2.95 (hept, *J* = 6.9 Hz, 1H), 1.19 (d, *J* = 6.9 Hz, 6H). ¹³C NMR (100 MHz, DMSO) δ 170.2, 169.2, 166.7, 157.8, 135.6, 129.8, 118.8, 118.2, 114.7, 100.4, 40.5, 40.3, 40.1, 39.9, 39.7, 39.5, 39.3, 35.6, 26.3, 21.8. LC-MS [*m/z*+H] = 261.0.

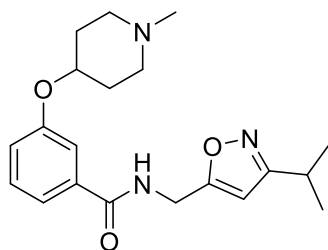


Synthesis of 4-bromo-3-hydroxy-N-((3-isopropylisoxazol-5-yl)methyl)benzamide

This compound was synthesized according to general procedure 1. Clear oil (77% yield). ¹H NMR (400 MHz, (CD₃)₂SO) δ 10.54 (s, 1H), 9.10 (t, *J* = 5.7 Hz, 1H), 7.59 (d, *J* = 8.3 Hz, 1H), 7.45 (d, *J* = 2.0 Hz, 1H), 7.25 (dd, *J* = 8.3, 2.0 Hz, 1H), 6.29 (s, 1H), 4.53 (d, *J* = 5.8 Hz, 2H), 2.95 (hept, *J* = 7.0 Hz, 1H), 1.19 (d, *J* = 6.9 Hz, 6H). ¹³C NMR (101 MHz, (CD₃)₂SO) δ 170.0, 169.2, 166.0, 154.5, 134.8, 133.2, 119.3, 115.9, 113.4, 100.5, 40.5, 40.3, 40.1, 39.9, 39.7, 39.5, 39.3, 35.6, 26.3, 21.8. LC-MS [*m/z*+H] = 338.9.

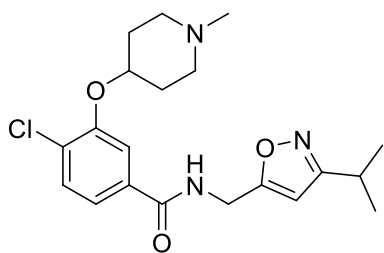
General Procedure 2: Synthesis of Ethers

A solution of the appropriate 4-substituted 3-hydroxy benzamide (1.0 eq), 4-hydroxy *N*-alkyl or 4-hydroxy *N*-boc (3.0 eq), and triphenylphosphine (1.2 eq) in THF (0.25M) was cooled to 0 °C. DtBad (1.5 eq) was then added and the reaction was warmed to rt and stirred for 14 h. Reaction was diluted in H₂O and extracted with EtOAc (3x). Combined organics were washed with brine, dried over MgSO₄, filtered, and concentrated. Crude material was purified using flash chromatography (Teledyne ISCO system, silica gel column, DCM/MeOH/NH₄OH (89:10:1) to afford the desired product.



Synthesis of *N*-((3-isopropylisoxazol-5-yl)methyl)-3-((1-methylpiperidin-4-yl)oxy)benzamide (1.71)

This compound was synthesized according to general procedure 2. Clear oil. ¹H NMR (400 MHz, (CD₃)₂SO) δ 9.09 (t, *J* = 5.8 Hz, 1H), 7.49 – 7.41 (m, 2H), 7.37 (t, *J* = 7.8 Hz, 1H), 7.13 (ddd, *J* = 8.2, 2.6, 1.1 Hz, 1H), 6.30 (s, 1H), 4.55 (d, *J* = 5.8 Hz, 2H), 4.43 (tt, *J* = 8.2, 3.9 Hz, 1H), 3.03 – 2.88 (m, 1H), 2.60 (dt, *J* = 10.8, 5.1 Hz, 2H), 2.23 – 2.20 (m, 1H), 2.18 (s, 5H), 1.98 – 1.87 (m, 2H), 1.64 (dtd, *J* = 12.5, 8.6, 3.6 Hz, 2H), 1.39 (s, 1H), 1.19 (d, *J* = 7.1 Hz, 6H). ¹³C NMR (100 MHz, DMSO) δ 171.4, 170.1, 169.2, 166.4, 157.5, 135.6, 130.0, 120.1, 119.4, 114.9, 100.4, 99.9, 72.5, 52.7, 46.2, 42.5, 40.8, 40.6, 40.3, 40.1, 39.9, 39.7, 39.5, 39.3, 36.0, 35.6, 30.9, 28.5, 26.3, 26.3, 21.9, 21.8. LC-MS [m/z+H] = 261.0

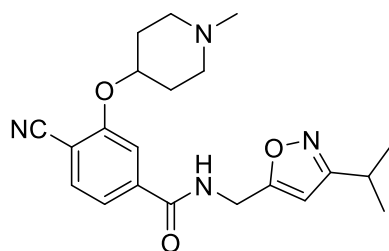


Synthesis of 4-chloro-*N*-[(3-isopropylisoxazol-5-yl)methyl]-3-[(1-methyl-4-piperidyl)oxy]benzamide (1.73)

This compound was synthesized according to general procedure 2. Clear oil (1.03 g, 77%). ¹H NMR (400.1 MHz, CDCl₃) δ 7.65 (1H, t, *J* = 5.6 Hz), 7.45 (1H, d, *J* = 1.4 Hz), 7.27 (2H, m), 6.04 (1H, s), 4.58 (d, *J* = 5.8 Hz, 2H), 4.42 (1H, s), 3.35 (1H, s), 2.91 (1H, m), 2.62 (2H, m), 2.32 (2H, m), 2.24 (3H, s), 1.92 (2H, m), 1.83 (2H, m), 1.16 (6H, d, *J* = 7.0 Hz). ¹³C NMR (100 MHz, CDCl₃) δ 169.6, 168.3, 166.5, 153.1, 133.1, 130.3, 128.2,

119.8, 114.8, 100.6, 77.3, 77.0, 76.7, 51.8, 50.2, 45.8, 35.6, 30.1, 26.4, 21.5. LC-MS

[m/z+H] = 392.1.



Synthesis of 4-cyano-N-[(3-isopropylisoxazol-5-yl)methyl]-3-[(1-methyl-4-piperidyl)oxy]benzamide (1.74)

To a MW vial equipped with a stir bar, 4-bromo-N-[(3-isopropylisoxazol-5-yl)methyl]-3-[(1-methyl-4-piperidyl)oxy]benzamide (1 eq) zinc cyanide (1.1 eq) and DMF (0.1M) were added and reaction was subjected to MW irradiation at 125 °C for 30 min.

Reaction diluted in H₂O, extracted with DCM (3x), passed through a phase separator, and concentrated. The crude material was purified using a Gilson HPLC system (30 x 50 mm column; H₂O with 0.5mL/L NH₄OH:acetonitrile; 25-85% acetonitrile gradient) to provide the titled compound as a brown oil (5.5 mg, 16% yield). ¹H NMR (400

MHz, (CD₃)₂SO) δ 9.34 (t, *J* = 5.8 Hz, 1H), 7.86 (d, *J* = 8.0 Hz, 1H), 7.66 (d, *J* = 1.4 Hz, 1H), 7.55 (dd, *J* = 8.0, 1.4 Hz, 1H), 6.35 (s, 1H), 4.72 (hept, *J* = 7.1 Hz, 1H), 4.59 (d, *J* = 5.7 Hz, 2H), 3.04 – 2.89 (m, 2H), 2.29 (m, 2H), 2.19 (s, 3H), 2.00 – 1.91 (m, 1H), 1.74 (m, 2H), 1.20 (d, *J* = 6.9 Hz, 6H). ¹³C NMR (101 MHz, (CD₃)₂SO) δ 169.6, 169.3, 165.2, 159.3, 139.8, 134.4, 120.4, 116.3, 113.3, 104.7, 100.7, 73.8, 52.1, 46.3, 42.5, 40.8, 40.6, 40.3, 40.1, 39.9, 39.7, 39.5, 39.3, 35.7, 30.5, 26.3, 21.8. LC-MS [m/z+H] = 383.4.

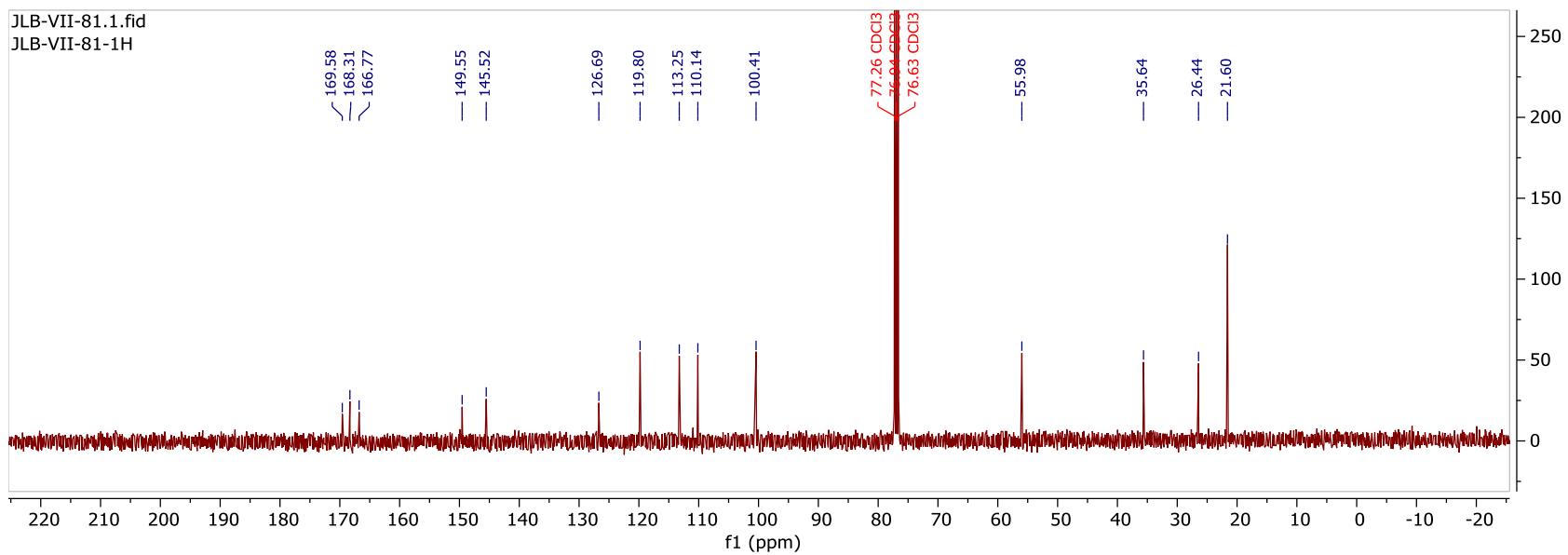
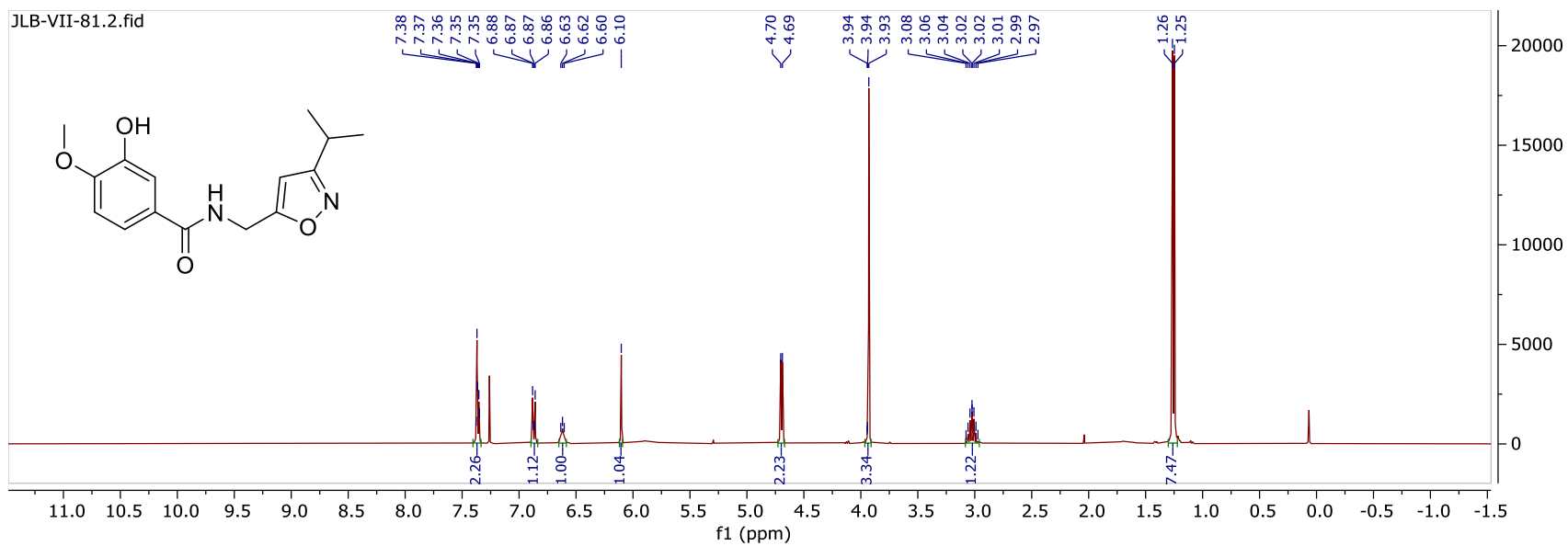
References for Chapter I

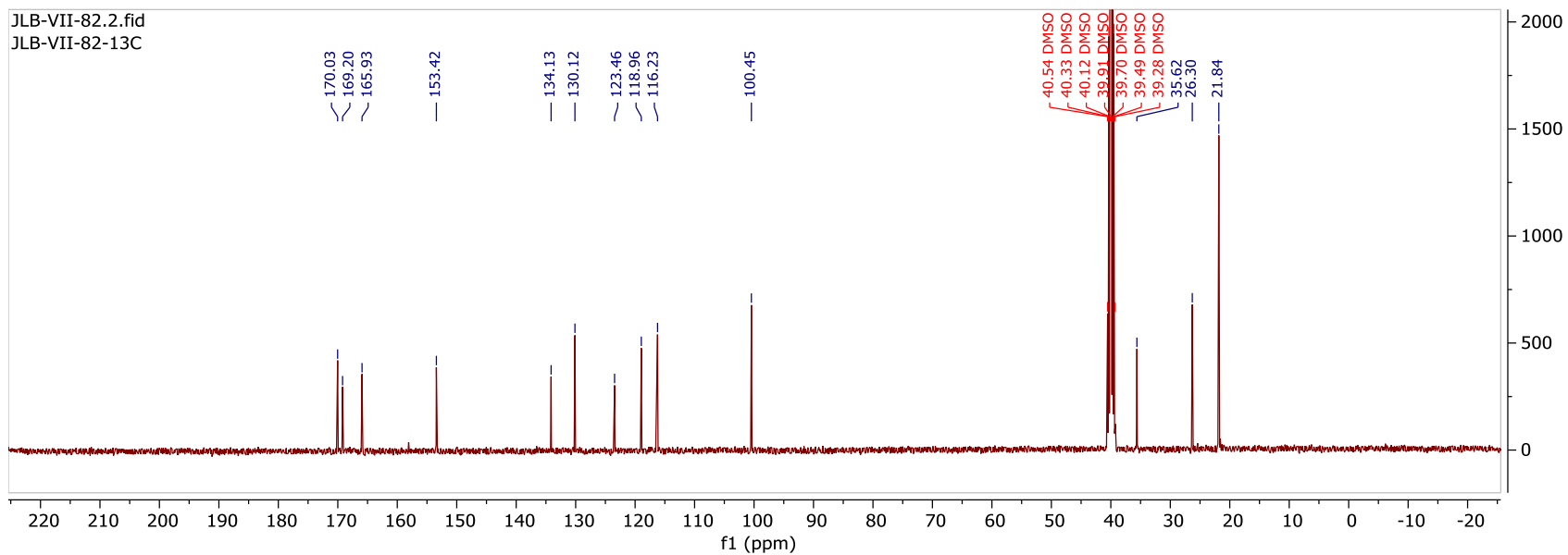
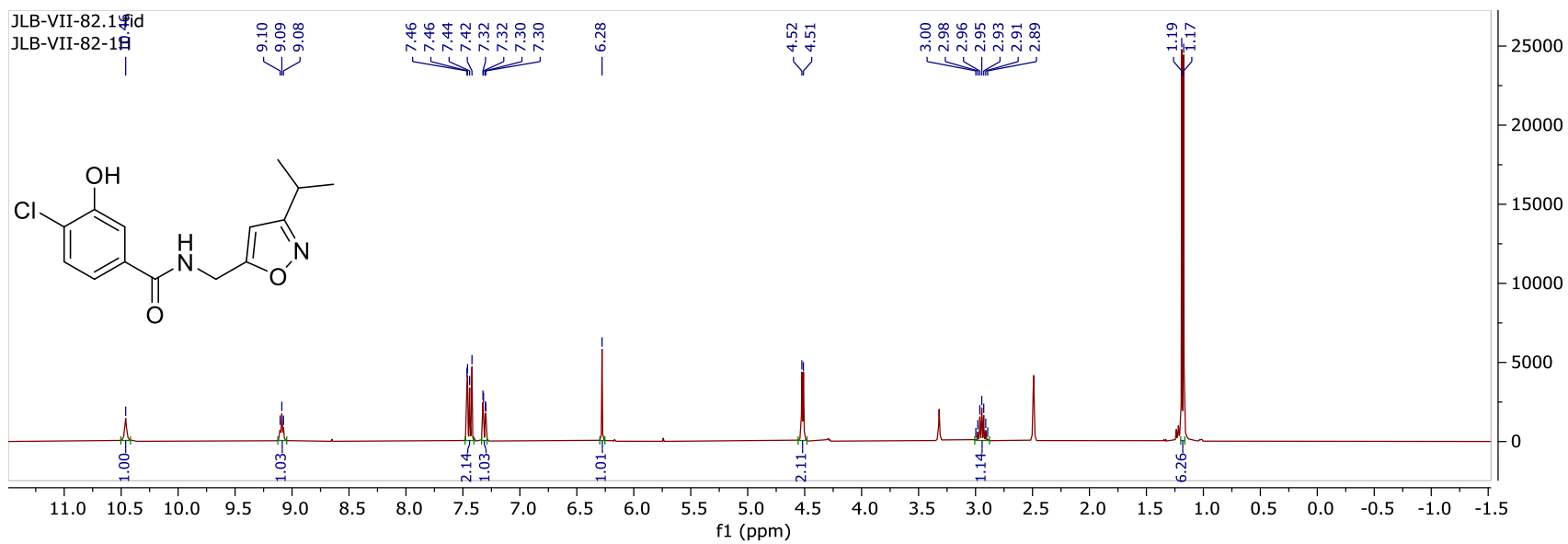
- 1) Okuda, T.; Haga, T. *Neurochemical research* **2003**, *28*, 483.
- 2) Wright, E. M.; Turk, E. *Pflugers Archiv : European journal of physiology* **2004**, *447*, 510.
- 3) Okuda, T.; Haga, T.; Kanai, Y.; Endou, H.; Ishihara, T.; Katsura, I. *Nature neuroscience* **2000**, *3*, 120.
- 4) Kwon, E.; Kim, D. Y.; Ngo, T. D.; Gross, C. A.; Gross, J. D.; Kim, K. K. *Protein science : a publication of the Protein Society* **2012**, *21*, 1334.
- 5) Okuda, T.; Osawa, C.; Yamada, H.; Hayashi, K.; Nishikawa, S.; Ushio, T.; Kubo, Y.; Satou, M.; Ogawa, H.; Haga, T. *The Journal of biological chemistry* **2012**, *287*, 42826.
- 6) Barwick, K. E.; Wright, J.; Al-Turki, S.; McEntagart, M. M.; Nair, A.; Chioza, B.; Al-Memar, A.; Modarres, H.; Reilly, M. M.; Dick, K. J.; Ruggiero, A. M.; Blakely, R. D.; Hurles, M. E.; Crosby, A. H. *American journal of human genetics* **2012**, *91*, 1103.
- 7) Ennis, E. A.; Blakely, R. D. *Advances in pharmacology (San Diego, Calif.)* **2016**, *76*, 175.
- 8) Neumann, S. A.; Linder, K. J.; Muldoon, M. F.; Sutton-Tyrrell, K.; Kline, C.; Shrader, C. J.; Lawrence, E. C.; Ferrell, R. E.; Manuck, S. B. *The international journal of cardiovascular imaging* **2012**, *28*, 243.
- 9) English, B. A.; Hahn, M. K.; Gizer, I. R.; Mazei-Robison, M.; Steele, A.; Kurnik, D. M.; Stein, M. A.; Waldman, I. D.; Blakely, R. D. *Journal of neurodevelopmental disorders* **2009**, *1*, 252.
- 10) Hahn, M. K.; Blackford, J. U.; Haman, K.; Mazei-Robison, M.; English, B. A.; Prasad, H. C.; Steele, A.; Hazelwood, L.; Fentress, H. M.; Myers, R.; Blakely, R. D.; Sanders-Bush, E.; Shelton, R. *Genes, brain, and behavior* **2008**, *7*, 487.
- 11) Ribeiro, F. M.; Black, S. A.; Prado, V. F.; Rylett, R. J.; Ferguson, S. S.; Prado, M. A. *Journal of neurochemistry* **2006**, *97*, 1.
- 12) Holmstrand, E. C.; Lund, D.; Cherian, A. K.; Wright, J.; Martin, R. F.; Ennis, E. A.; Stanwood, G. D.; Sarter, M.; Blakely, R. D. *Neurochemistry international* **2014**, *73*, 217.
- 13) Bollinger, S. R.; Engers, D. W.; Ennis, E. A.; Wright, J.; Locuson, C. W.; Lindsley, C. W.; Blakely, R. D.; Hopkins, C. R. *Bioorg Med Chem Lett* **2015**, *25*, 1757.
- 14) Yamamura, H. I.; Snyder, S. H. *Proceedings of the National Academy of Sciences of the United States of America* **1974**, *71*, 1725.
- 15) Guyenet, P.; Lefresne, P.; Rossier, J.; Beaujouan, J. C.; Glowinski, J. *Molecular pharmacology* **1973**, *9*, 630.
- 16) Amenta, F.; Tayebati, S. K. *Current medicinal chemistry* **2008**, *15*, 488.
- 17) Jope, R. S. *Brain research* **1979**, *180*, 313.
- 18) Tansey, E. M. *Comptes rendus biologies* **2006**, *329*, 419.
- 19) Picciotto, M. R.; Higley, M. J.; Mineur, Y. S. *Neuron* **2012**, *76*, 116.
- 20) Eckhardt, E. T.; Schueler, F. W. *The Journal of pharmacology and experimental therapeutics* **1963**, *141*, 343.
- 21) Higley, M. J.; Picciotto, M. R. *Current opinion in neurobiology* **2014**, *29*, 88.
- 22) Sarter, M.; Parikh, V. *Nature reviews. Neuroscience* **2005**, *6*, 48.
- 23) Casey, D. E.; Gerlach, J.; Christensson, E. *Psychopharmacology* **1980**, *70*, 83.

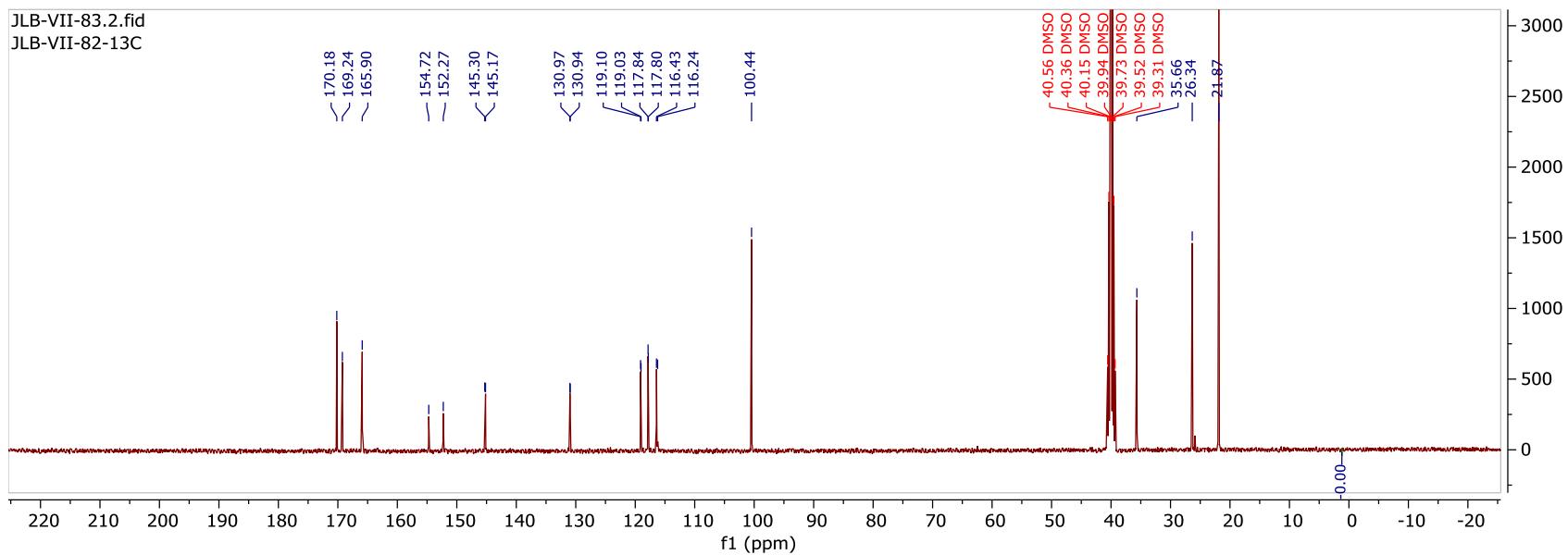
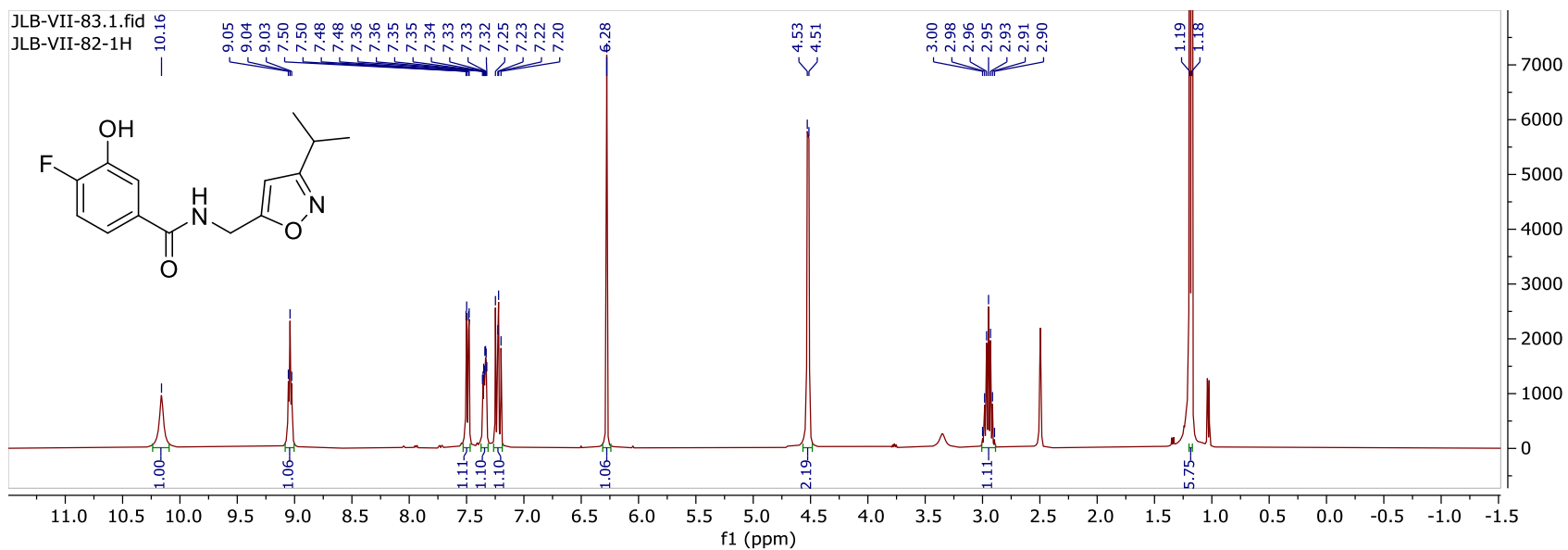
- 24) Salter, C. G.; Beijer, D.; Hardy, H.; Barwick, K. E. S.; Bower, M.; Mademan, I.; De Jonghe, P.; Deconinck, T.; Russell, M. A.; McEntagart, M. M.; Chioza, B. A.; Blakely, R. D.; Chilton, J. K.; De Bleecker, J.; Baets, J.; Baple, E. L.; Walk, D.; Crosby, A. H. *Neurology. Genetics* **2018**, *4*, e222.
- 25) Surgeons, A. A. o. N.
- 26) Foundation, D. M. R.
- 27) Dressler, D.; Altenmueller, E.; Bhidayasiri, R.; Bohlega, S.; Chana, P.; Chung, T. M.; Frucht, S.; Garcia-Ruiz, P. J.; Kaelin, A.; Kaji, R.; Kanovsky, P.; Laskawi, R.; Micheli, F.; Orlova, O.; Relja, M.; Rosales, R.; Slawek, J.; Timerbaeva, S.; Warner, T. T.; Saberi, F. A. *Journal of neural transmission (Vienna, Austria : 1996)* **2016**, *123*, 251.
- 28) Foundation, D. M. R.
- 29) Chang, E.; Ghosh, N.; Yanni, D.; Lee, S.; Alexandru, D.; Mozaffar, T. *Crit Rev Phys Rehabil Med* **2013**, *25*, 11.
- 30) Furr-Stimming, E.; Boyle, A. M.; Schiess, M. C. *Seminars in neurology* **2014**, *34*, 591.
- 31) Awaad, Y.; Rizk, T.; Siddiqui, I.; Roosen, N.; McIntosh, K.; Waines, G. M. *ISRN neurology* **2012**, *2012*, 575168.
- 32) Woolf, S. M.; Baum, C. R. *Pediatric emergency care* **2017**, *33*, 271.
- 33) Termsarasab, P. T., T; Furcht, S.J. *Journal of Clinical Movement Disorders* **2016**, *3*.
- 34) Petursson, H. *Addiction (Abingdon, England)* **1994**, *89*, 1455.
- 35) Randby, H.; Salvador, C. L.; Oppeboen, M.; Skogseid, I. M.; Koht, J. *Tidsskrift for den Norske laegeforening : tidsskrift for praktisk medicin, ny raekke* **2018**, *138*.
- 36) Ramirez-Castaneda, J.; Jankovic, J. *Toxins (Basel)* **2013**, *5*, 249.
- 37) Ennis, E. A.; Wright, J.; Retzlaff, C. L.; McManus, O. B.; Lin, Z.; Huang, X.; Wu, M.; Li, M.; Daniels, J. S.; Lindsley, C. W.; Hopkins, C. R.; Blakely, R. D. *ACS chemical neuroscience* **2015**, *6*, 417.
- 38) Bertron, J. L.; Ennis, E. A.; Tarr, C. J.; Wright, J.; Dickerson, J. W.; Locuson, C. W.; Blobaum, A. L.; Rook, J. M.; Blakely, R. D.; Lindsley, C. W. *Bioorg Med Chem Lett* **2016**, *26*, 4637.

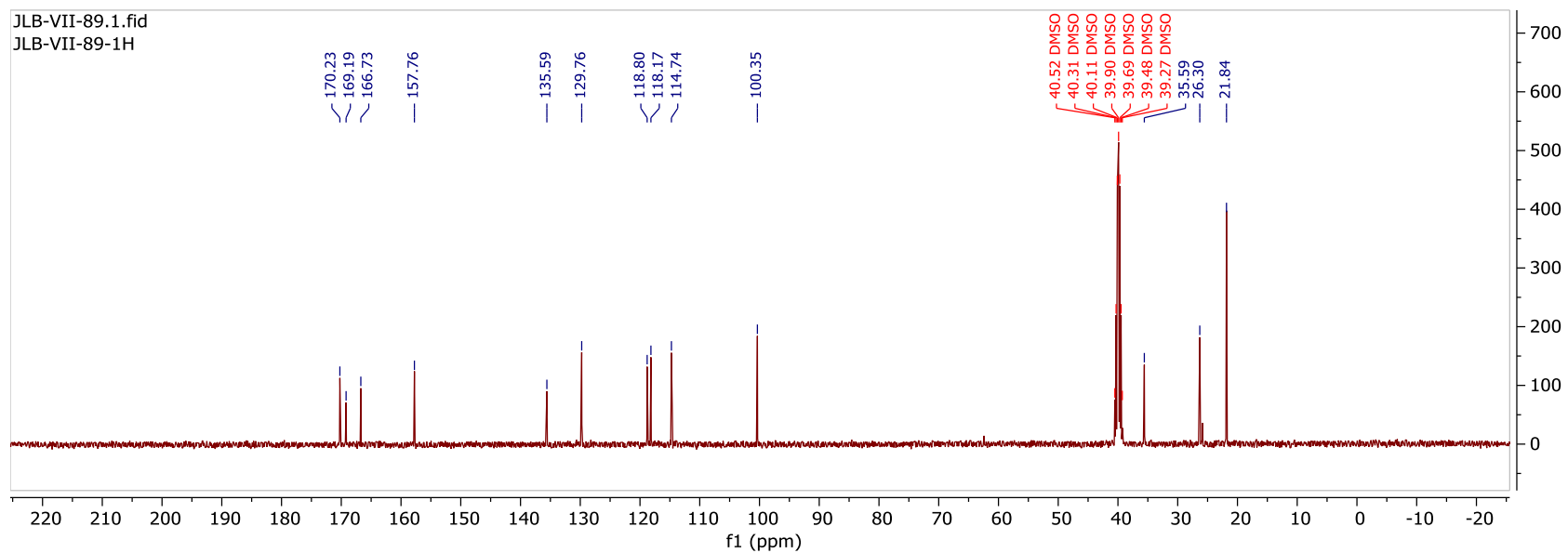
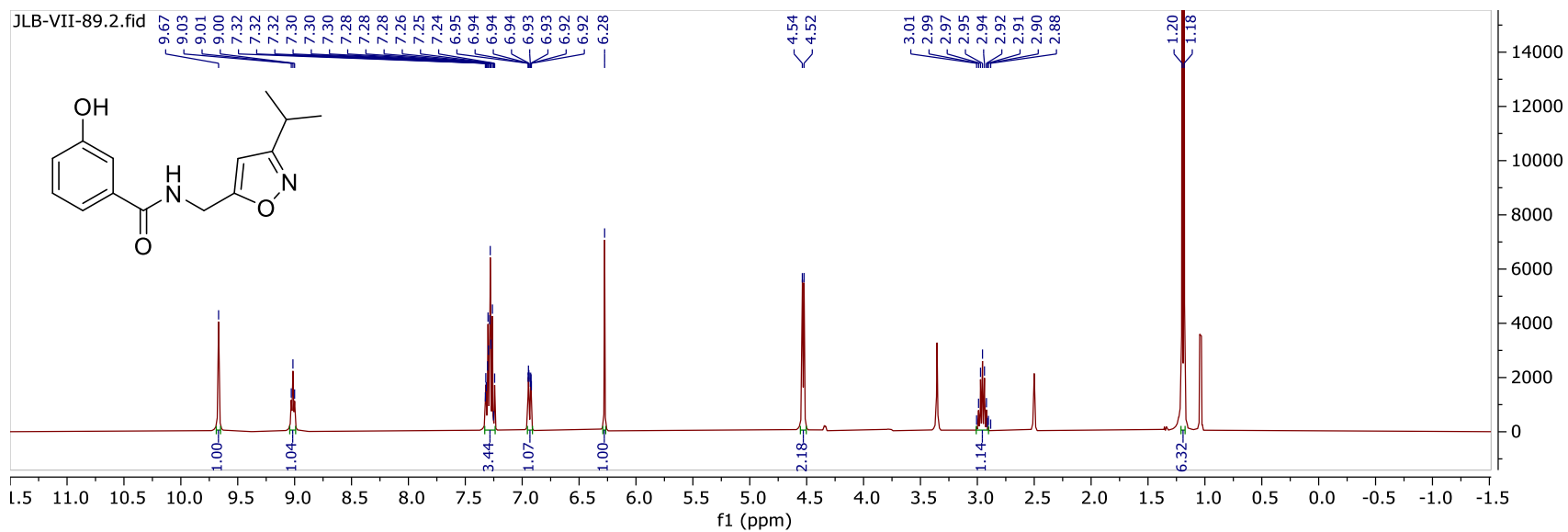
Appendix A

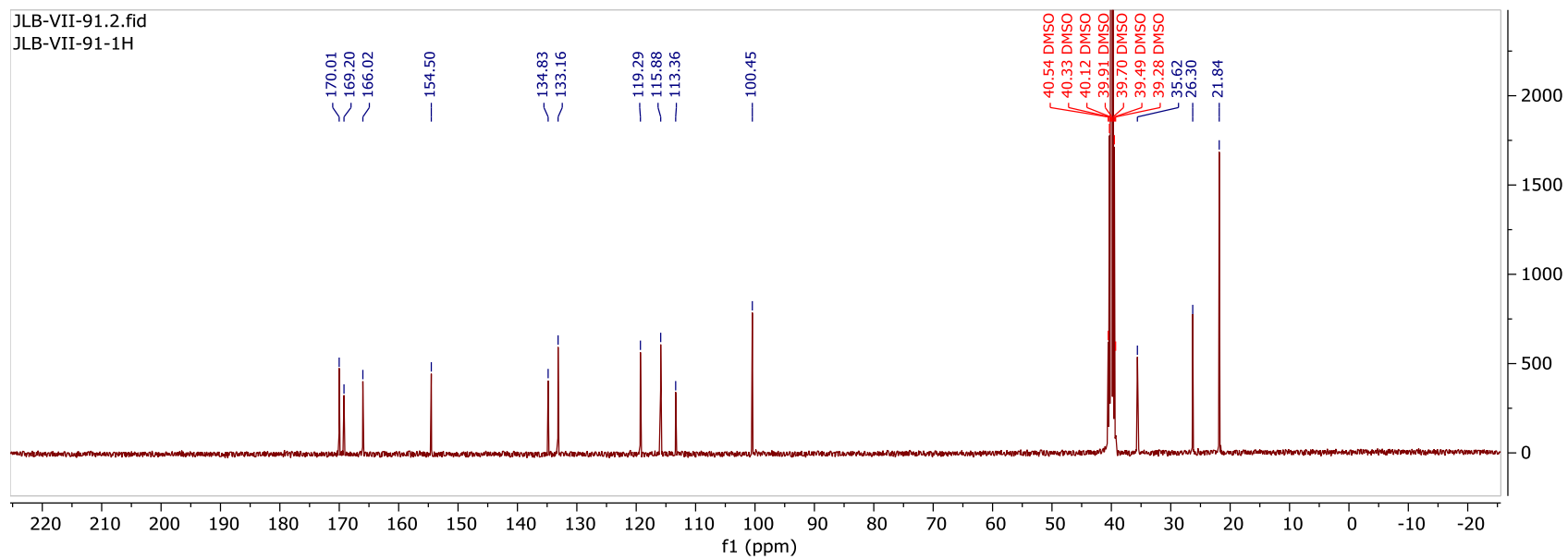
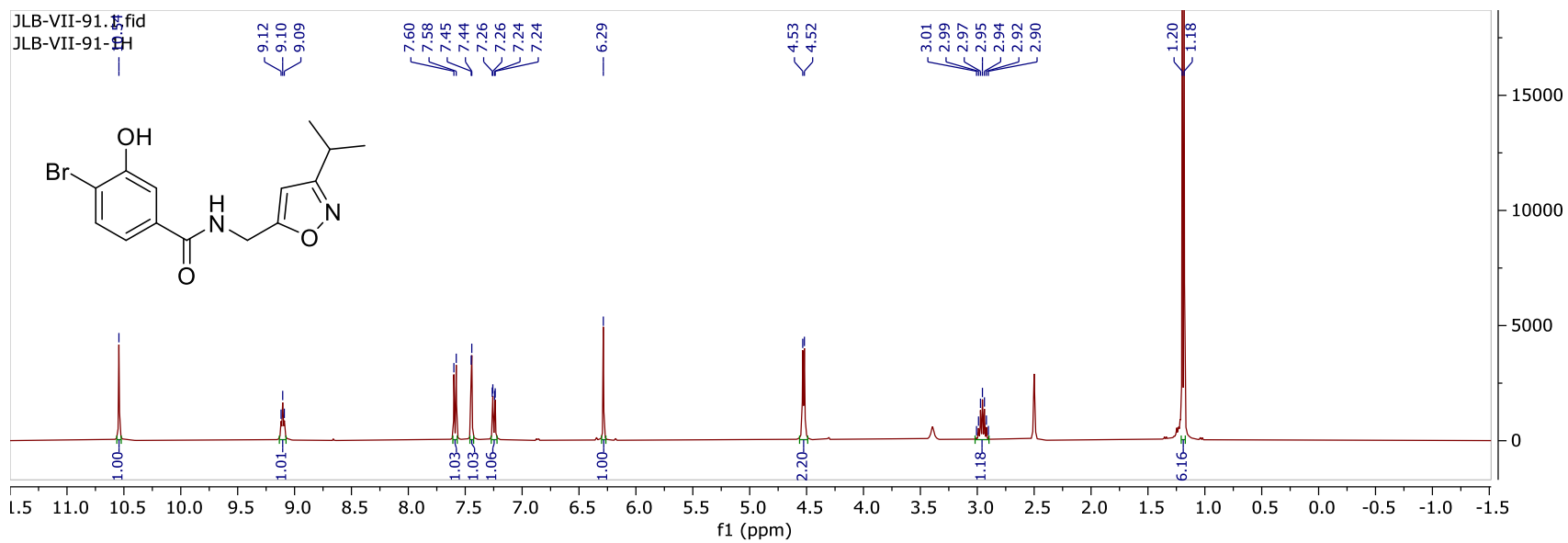
Relevant Spectra for Chapter I

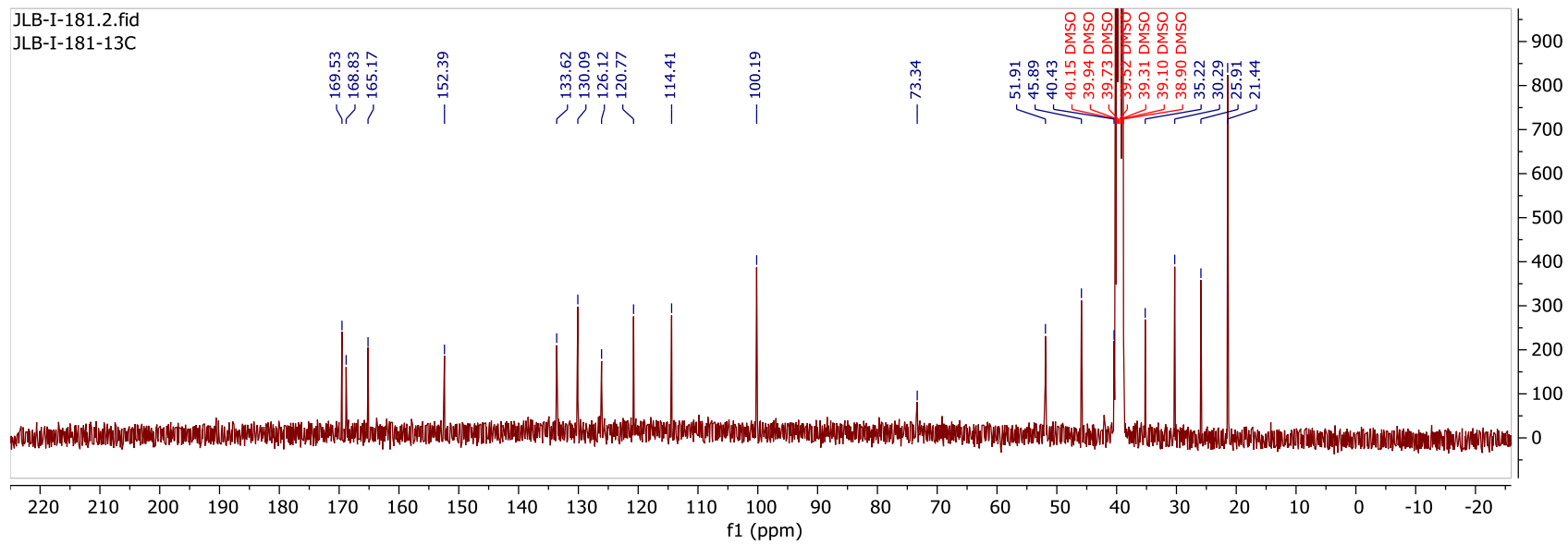
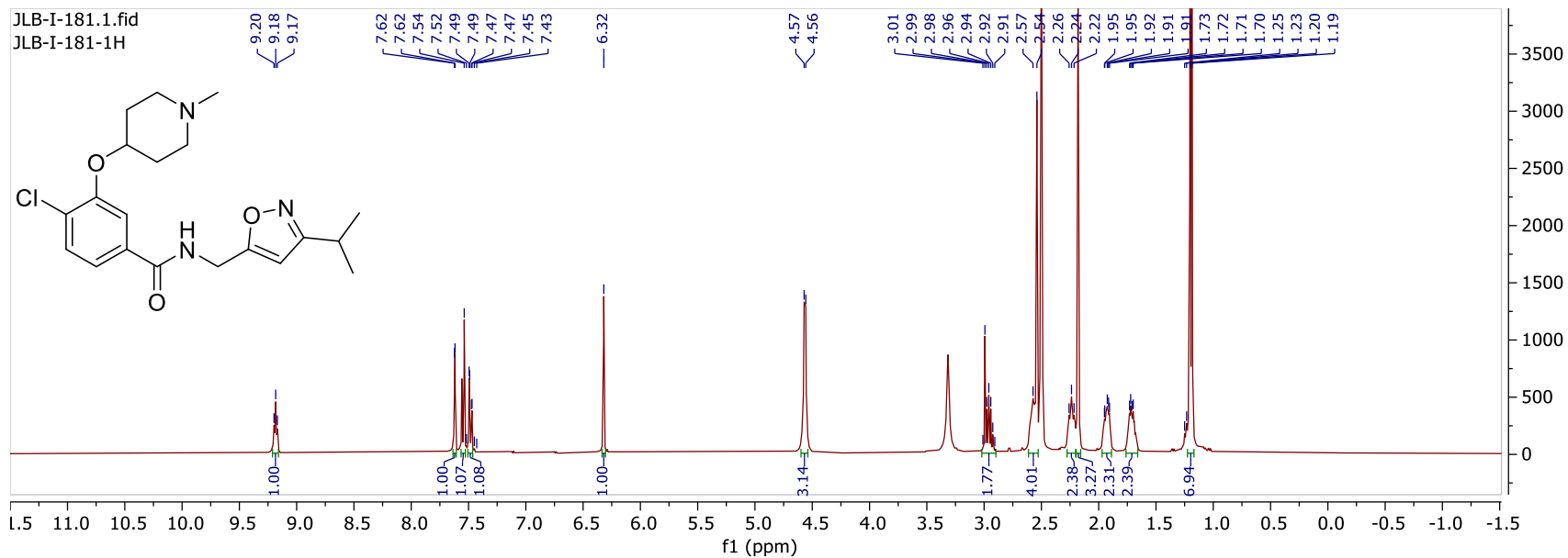


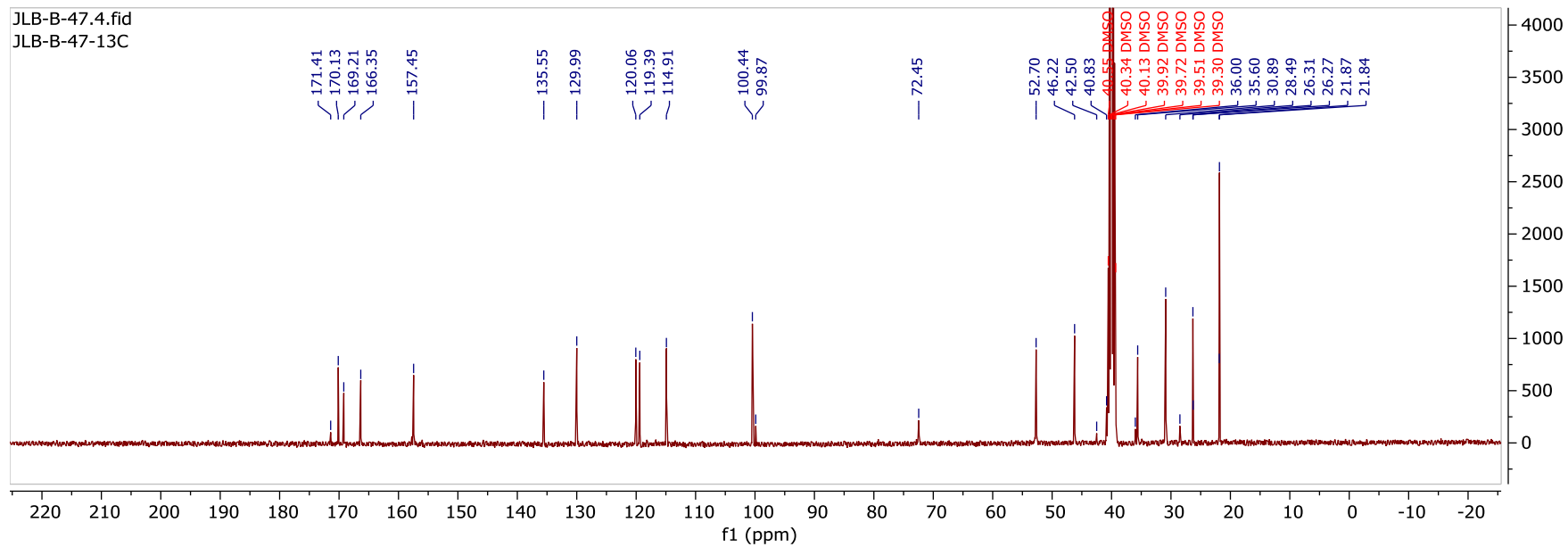
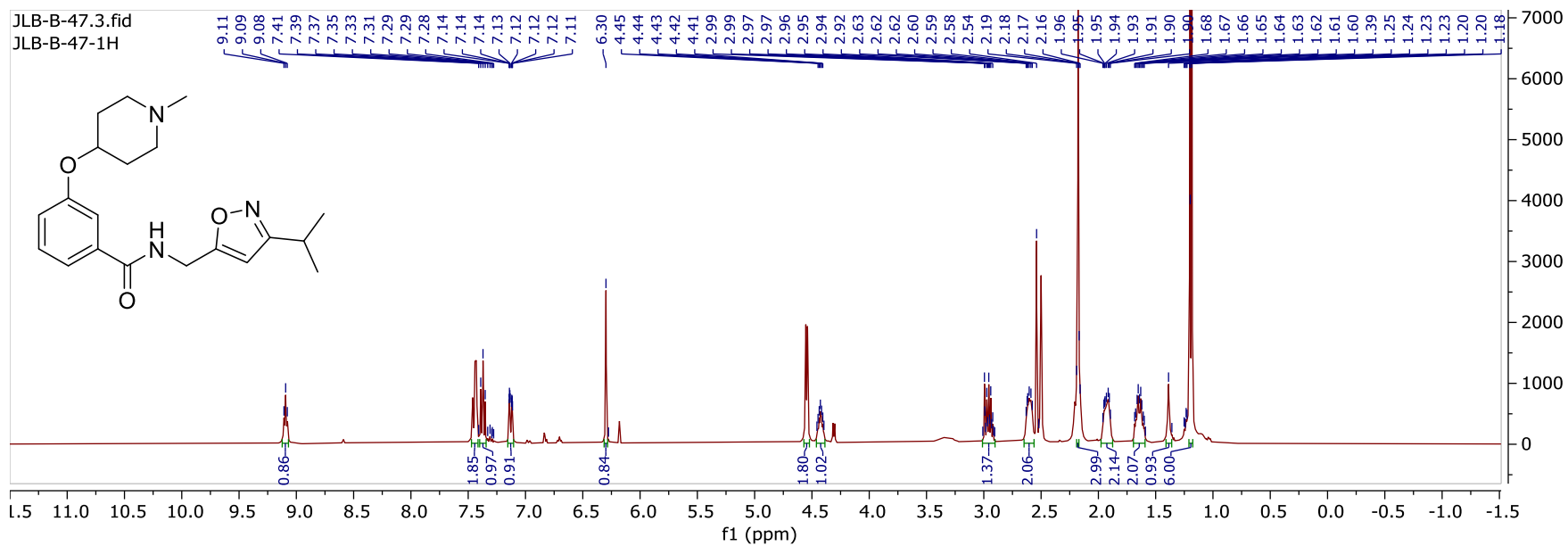




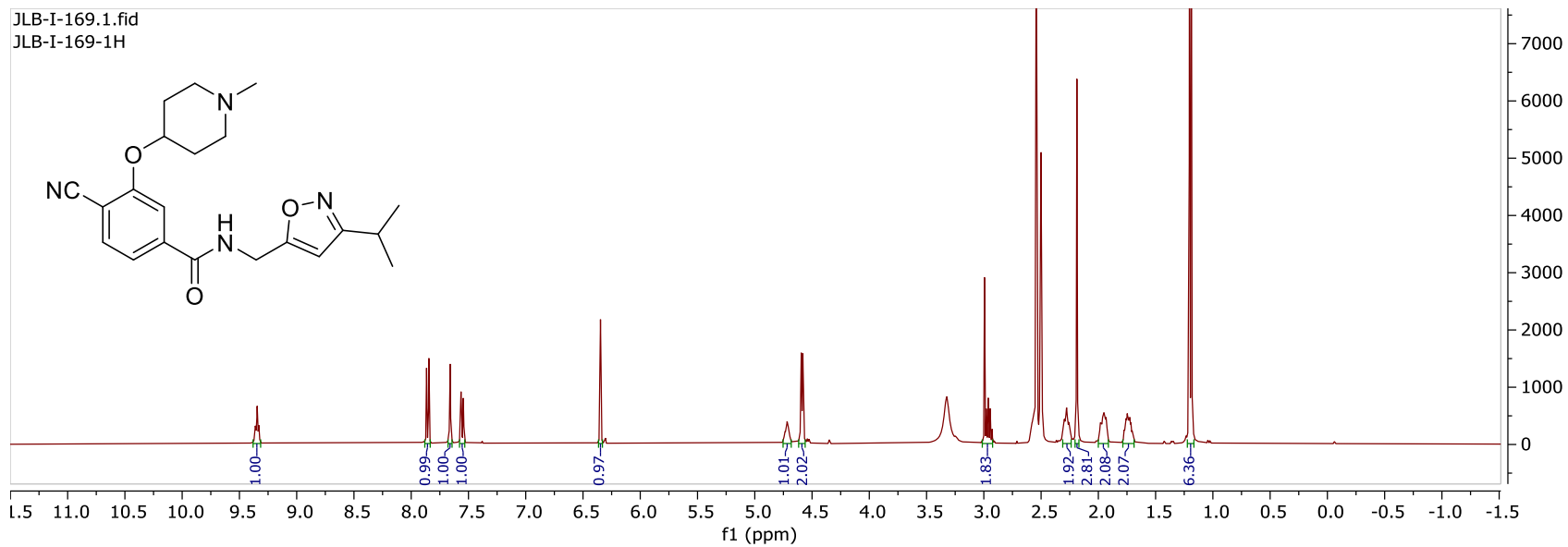




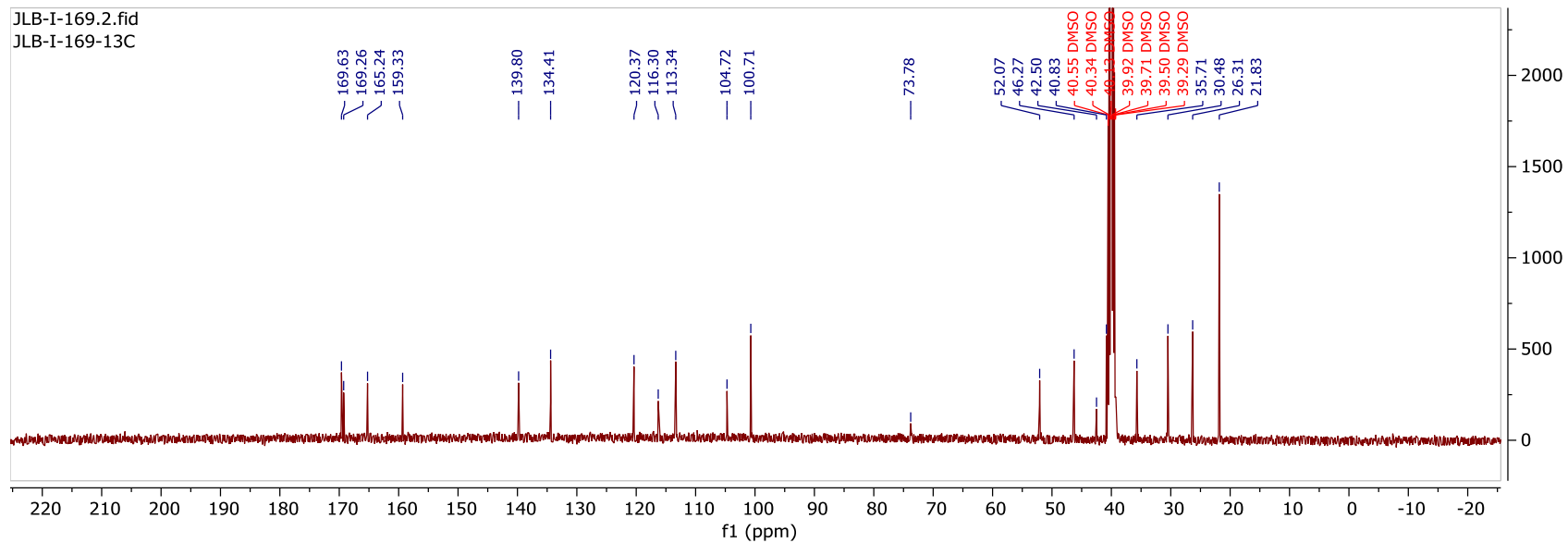




JLB-I-169.1.fid
JLB-I-169-1H



JLB-I-169.2.fid
JLB-I-169-13C



CHAPTER II

DISCOVERY AND DEVELOPMENT OF M₁ PAMS: BENZOMORPHOLINE AND TETRAHYDROQUINOLINE SERIES

Background and Introduction

G-Protein Coupled Receptors: Muscarinic Acetylcholine Receptors

G-protein coupled receptors (GPCRs) are the most prevalent membrane proteins in eukaryotes and play a crucial role in regulating cellular responses to neurotransmitters and hormones.^{1,2} Because of this, GPCRs are commonly targeted in drug development research. To date, roughly 826 GPCRs have been identified in the human genome.³ Approximately 34% of food and drug administration (FDA)-approved drugs target one of these GPCRs and gross about 180 billion US dollars annually, thus further supporting their importance and attractiveness as therapeutic targets.⁴

GPCRs are characterized by their seven-transmembrane (7-TM) domain, with loops alternating between extracellular space and intracellular space. They are activated extracellularly by a host of different ligands such as hormones, neurotransmitters, odorants, and photons.⁵ Ligand binding results in the induction of intracellular signal transduction pathways to elicit a biological response. Perturbations in these systems such as mutations and polymorphisms have been detected and associated with a multitude of biological disorders and disease states.⁶ In particular,

GPCRs are abundantly expressed in the central nervous system (CNS), and thus have been the focus of many drug discovery efforts.^{7,8}

The cholinergic system is known to modulate a variety of different neurological processes that when altered can result in a variety of disorders including attention-deficit/hyperactivity disorder (ADHD), schizophrenia, depression, dementias such as Alzheimer's disease, and dystonia.⁹⁻¹⁴ Cholinergic receptors are broadly categorized as either muscarinic acetylcholine receptors (mAChRs) or nicotinic acetylcholine receptors (nAChRs). It has been well established that cholinergic transmission at the mAChRs is associated with higher brain function, learning, and memory.^{12,15-17} Therefore, substantial research efforts have focused towards altering cholinergic signaling through the agonism or antagonism of the mAChR system. mAChRs belong to the Family A, rhodopsin-like, 7-TM GPCRs, of which there are five subtypes (M₁₋₅).^{18,19} When activated, the mAChRs signal through heterotrimeric G-proteins consisting of α , β , and γ subunits (**Figure 2.1**). The mAChR subtypes 1-5 are further categorized by their α -subunit coupling partners and downstream effects. M₁, M₃, and M₅ have been known to couple to G $\alpha_{q/11}$ subunits while M₂ and M₄ couple with G $\alpha_{i/o}$ subunits. Activation of the

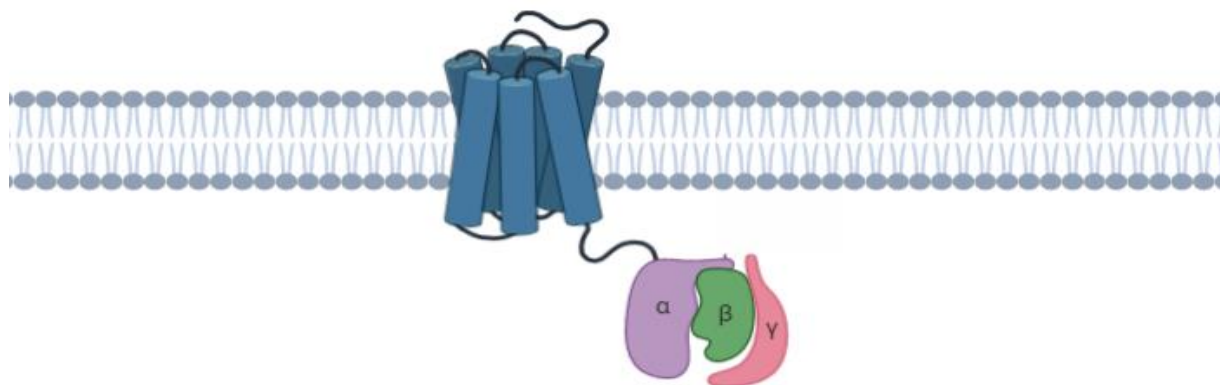


Figure 2.1 Generic representation of M₁ receptor and heterotrimeric protein.

$G_{i/o}$ signaling cascade results in a reduction of intracellular cyclic adenosine monophosphate (cAMP) through the inhibition of adenylyl cyclase. Concurrently, a reduction in $[Ca^{2+}]$ occurs via modulation of the $G_{\beta\gamma}$ dimer, which can result in the inhibition of neurotransmitter release. Contrarily, initiation of the $G_{\alpha q/11}$ pathway activates phospholipase-c (PLC), which results in the hydrolysis of plasma membrane phosphoinositides into inositol 1,4,5-triphosphate (IP_3) and diacyl glycerol. Release of IP_3 results in an increase of intracellular $[Ca^{2+}]$ which can promote neuronal excitability.^{17,20}

Muscarinic Acetylcholine Receptor 1 (M_1) and its Therapeutic Relevance

The Alzheimer's Association estimates around 5.8 million people currently living with Alzheimer's disease (AD) in the United States.²¹ AD is a form of dementia characterized by memory loss and other cognitive deficits that gradually worsen and interfere with daily functions.²² AD is the sixth leading cause of death in the United States and currently there is no cure for it.²³ AD has been associated with perturbations in the cholinergic signaling pathway. More specifically, it has been hypothesized that the loss of cholinergic neurons, and thus a decreased level of ACh, contributes to the development of AD.^{15,24,25} While there is no cure, there are therapies available to treat symptoms of AD. The classical form of treatment for AD is the administration of AChE inhibitors, which prevent or slow hydrolysis of ACh to choline and acetate upon presynaptic release.²⁶ The prevention of hydrolysis results in an increase in synaptic ACh concentration, which has been shown to enhance memory and learning. Unfortunately, AChE inhibitors have been known to induce cholinergic toxicity and undesirable side effects.^{27,28} Therefore, a safer therapeutic target within the cholinergic system should be explored.

As previously mentioned, the mAChR system is involved in mediating cognitive functions such as learning and memory processing. Extensive biochemical, genetic, and clinical data have implicated selective activation of M₁ could be a viable treatment for the cognitive deficits associated with neurodegenerative disorders like schizophrenia and Alzheimer's disease (AD).^{9,15,24,25} M₁ receptors are heavily localized to the cerebral cortex and hippocampus, which are known for regulating cognition, learning, and memory.^{16,25} Furthermore, studies have indicated that the reduction of M₁ receptors in transgenic mice significantly decreases cognitive behavior and working memory, further suggesting that M₁ could be an attractive target for diseases displaying cognitive and memory impairment.²⁴ Of note, M₁ knock-out (KO) mice demonstrated that the lack of M₁ receptors exacerbated the decline in cognitive abilities associated with AD, compared to control mice.²⁹

The evaluation of biopsied brain tissue from AD patients roughly three and a half years after onset, indicated pathogenesis within in the cholinergic system. Specifically, it has been noted that presynaptic ACh release is markedly reduced in patients presenting with AD. The disclosure of M₁/M₄ preferring agonist xanomeline (**2.1**) displaying clinical efficacy in human AD and schizophrenia trials provided confirmation that activation of the mAChRs, especially M₁ and M₄, play an important role in cognitive function.³⁰

Xanomeline as an M₁ tool compound

Xanomeline is a pan-mAChR orthosteric agonist. However, it displays a preference for activating receptors M₁ and M₄.³¹ In addition to activating the mAChRs, xanomeline also binds and activates 5-HT₁ and 5-HT₂ serotonin receptors, albeit with

markedly less affinity.³² Xanomeline advanced into clinical trials, where it displayed significant efficacy in improving the behavioral disturbances associated with AD and schizophrenia patients. Post-administration observations include a robust reduction in outbursts, suspiciousness, delusions, agitation, and hallucinations in AD patients as well as improvements in cognitive function. Unfortunately, xanomeline also causes several gastrointestinal (GI) related adverse effects (AEs) such as nausea, vomiting, dyspepsia, increased salivation, and increased diaphoresis and therefore, has yet to be approved by the FDA.³³ Although this compound did not display therapeutic selectivity, it served as a great tool molecule to probe the biological function of M₁ and M₄ signaling pathways.

As there are no selective tool compounds, M₁ and M₄ KO mice were used in conjunction with xanomeline to examine the individual physiological roles of M₁ and M₄ in rodent models of schizophrenia and AD. An amphetamine induced hyperlocomotion (AHL) paradigm, which is predictive of antipsychotic-like activity, was used to further investigate receptor-specific effects. In wild type animals, xanomeline was able to reverse the amphetamine-induced hyperactivity, whereas xanomeline showed no effect in M₄ KO mice, and only partial reversal in M₁ KO mice.^{30,34} These data suggest that the antipsychotic-like effects of xanomeline are primarily mediated through the activation of M₄. It was inferred from this data that the enhancement of cognitive or negative symptoms (reduced motivation, anhedonia, and deficits in attention and memory) in schizophrenia and AD patients were associated with the activation of the M₁ signaling pathway.³⁵ Additional M₁ KO studies deduced that deficits in M₁ signaling results in the disruption of mitogen-activated protein kinase (MAPK) activation leading to observations of working memory and consolidation impairment and overall deficits in long-term

plasticity.³⁶ These monumental studies demonstrated the biological rationalization for the development of selective M₁ tool compounds by employing an allosteric approach, which will be discussed in the following section.

Considering an Orthosteric Versus Allosteric Approach

In order to investigate the physiological function of the M₁ signaling pathway, a selective tool compound must be developed. A classical approach to tool molecule development and drug discovery is through activation of the orthosteric site where the endogenous ligand binds.^{37,38} The binding and activation of the orthosteric site with a small molecule instead of the native ligand is known as an agonist. Conversely, a small molecule that binds and diminishes the activation of the receptor is referred to as an antagonist. Orthosteric binding with an endogenous ligand, agonist, or antagonist can lock the receptor in an “on” or “off” state. In many cases this approach can be highly successful in selective activation or deactivation of a receptor.^{39,40} However, an agonist approach can be problematic in a situation where the therapeutic window is extremely narrow, as observed with M₁ agonist, xanomeline.³²

The undesired side-effects characteristic with cholinergic activation, often referred to as “SLUD” (salivation, lacrimation, urination, defecation), associated with taking pan-agonist xanomeline are due in part to off-target activation of peripheral M₂ and M₃ receptors.³¹ While xanomeline displays a preference for M₁ and M₄ receptors, it still activates all five muscarinic subtypes due to the high conservation of their active sites. The amino-acid sequences across all five muscarinic subtypes are highly conserved, with an average of 56.6% sequence similarity.⁴¹ The 7-TM domains are structured in a cylindrical manner, forming a central pore where the native ligand ACh

binds. This site is known as the orthosteric site. Because the orthosteric site is highly conserved, classic orthosteric approaches to therapeutic intervention unfortunately cannot be utilized in the development of effective *in vivo* tool molecules in the case of M_1 . Therefore, different strategies such as allosteric modulation must be considered.

An allosteric approach utilizes a binding site on the receptor that is distinct from the orthosteric site where the endogenous ligand binds (**Figure 2.2**). It is well known that GPCR's operate as dynamic systems where the protein is constantly undergoing

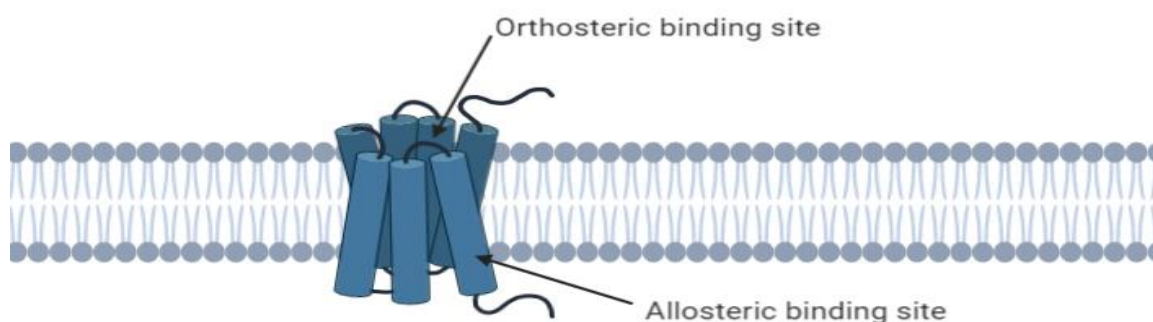


Figure 2.2 Orthosteric and putative allosteric binding sites for M_1 receptors.

micromovements. When the endogenous ligand ACh binds to M_1 , it stabilizes the receptor in an active or “on” state where full activation is achieved. M_1 , like all GPCRs, can adopt multiple different conformations stabilized by a myriad of ligands to “dial in” levels of activity ranging from fully active to fully inactive. Upon binding, allosteric modulators can stabilize active forms of the receptor that encourage endogenous orthosteric ligand binding (positive allosteric modulators; PAMs) or they can stabilize inactive conformations of the receptor hindering ACh orthosteric binding (negative allosteric modulators; NAMs).^{42,43} Employing an allosteric strategy allows for the

modulation of the receptor at varying degrees of activity between “on” and “off” states, therefore making allosteric modulation an attractive approach for targeting M₁.⁴⁴

M₁ Tool Compounds: Positive Allosteric Modulators (PAMs)

Merck and Co. developed the first M₁ PAM tool molecule, BQCA (**2.2**), which was further developed into clinical candidate, MK-7622 (**2.3**)(**Figure 2.3**).^{45,46} Unfortunately,

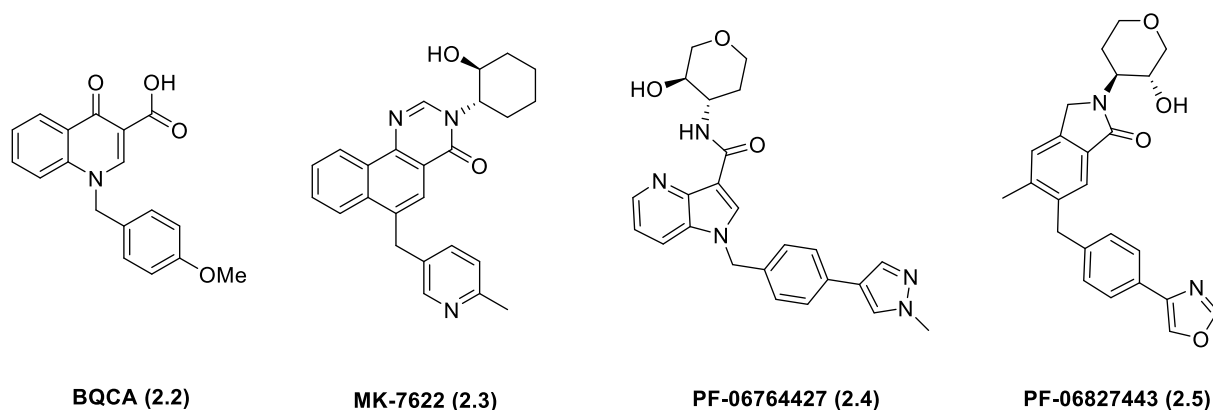


Figure 2.3 Known M₁ ago-PAMs disclosed in the literature.

these compounds and closely related analogs displayed robust ago-PAM activity, meaning they elicit direct agonist activity as well as PAM activity in both *in vitro* cellular assays as well as in native tissues. Both BQCA and MK-7622 display seizure activity and other side effects commonly observed with cholinergic toxicity. It has been posited that the agonist activity could be responsible for the seizure liability and other AEs commonly observed with cholinergic toxicity. Pfizer disclosed PF-06764427 (**2.4**) and PF-06827443 (**2.5**), an M₁ ago-PAM and a reported M₁ PAM, respectively. Due to its agonistic nature, PF-06764427 expectedly displayed AEs and seizure activity when administered to mice.⁴⁷ Interestingly, PF-06827443 showed very minimal agonist activity in a recombinant *in vitro* cell line and still displayed robust AEs across multiple

different species, in addition to inducing seizure activity in mice.⁴⁸ Recently, Moran et. al. demonstrated that while PF-06827443 showed very low agonist activity in *in vitro* cell lines, potent agonist activity was observed in native tissues when subjected to electrophysiology experiments. Agonist activity is dependent on the level of cellular receptor expression.⁴⁹ Therefore, compounds may exhibit a wide range of activity, depending on receptor expression within a given tissue or cell culture. Thus, agonist activity in native tissues more accurately predicts the level of *in vivo* toxicity over *in vitro*, cell-based assays.

Our lab also reported on the development of M₁ PAM tool molecules that, unlike the Merck and Pfizer compounds, do not elicit seizure activity or other cholinergic AEs. VU0453595 (**2.6**) and VU6004256 (**2.7**) were both derived from individual hit molecules identified from our internal high-throughput screening (HTS) campaign (**Figure 2.4**).⁵⁰⁻⁵² Compound **2.6** was determined to be a pure PAM without displaying any agonist activity in recombinant or native systems. When tested *in vivo*, **2.6** was indeed devoid of AEs and elicited procognitive activity, albeit to a minor extent due to its weak potency in the low micromolar range. Due to the weak activity of **2.6**, an alternative scaffold from the

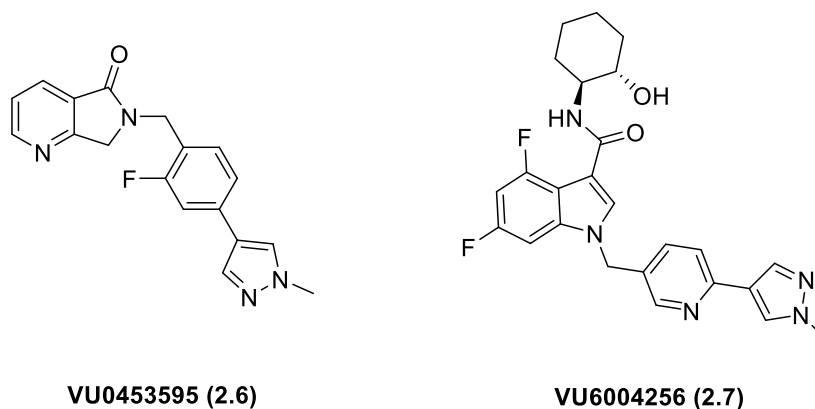


Figure 2.4 Previous M₁ PAMs developed in the Lindsley Lab.

HTS campaign was pursued, which gave rise to compound **2.7**, a more potent M₁ PAM. Interestingly, **2.7** displayed agonist activity in our high receptor reserve recombinant *in vitro* cell assay, yet showed no seizure activity or AEs in rodents, which contradicts the theory that agonistic activity is responsible for causing severe convulsions and other AEs. In addition, dissimilar to previous ago-PAMs, compound **2.7** exhibits procognitive effects in rodents, thus validating M₁ as a viable target for improving the cognitive deficits in Alzheimer's Disorder (AD) and schizophrenia patients. While **2.7** displays procognitive efficacy in rodents, the data is only trending towards significance and therefore a more robust *in vivo* M₁ PAM with desirable drug metabolism and pharmacokinetic (DMPK) properties is necessary to critically evaluate the physiological role of M₁.⁵³ Furthermore, additional studies must be conducted to elucidate the mechanism by which M₁ ago-PAMs induce cholinergic AEs in animal models to aid the field in the development of an effective therapeutic agent.

Conclusions

Having exhausted the SAR surrounding our indole-based series of M₁ PAMs, we began thinking of alternative approaches. Instead of beginning from another unoptimized HTS hit, we decided to revisit the first disclosed M₁ PAM, BQCA. Beginning from BQCA, we will modify the core of the scaffold using traditional medicinal chemistry approaches to develop a tool compound which can be utilized in probing the induction of M₁ cholinergic AEs as well as its physiological role in diseased brain states. Our optimization efforts will be driven by SAR and DMPK data, as there is no known crystal structure for the M₁ allosteric binding site of this series of compounds. By targeting the allosteric site, we hope to develop a pure PAM devoid of agonist activity or AEs and

achieve subtype selectivity. The following chapter reports on the efforts towards the development of a potent and selective M₁ PAM *in vivo* tool molecule devoid of AEs.

Materials and Methods

General Synthetic Methods and Instrumentation

All NMR spectra were recorded on a 400 MHz AMX Bruker NMR spectrometer. ¹H and ¹³C chemical shifts are reported in δ values in ppm downfield with the deuterated solvent as the internal standard. Data are reported as follows: chemical shift, multiplicity (s = singlet, d = doublet, t = triplet, q = quartet, b = broad, m = multiplet), integration, coupling constant (Hz). Low resolution mass spectra were obtained on an Agilent 6120 or 6150 with ESI source. MS parameters were as follows: fragmentor: 70, capillary voltage: 3000 V, nebulizer pressure: 30 psig, drying gas flow: 13 L/min, drying gas temperature: 350 °C. Samples were introduced via an Agilent 1290 UHPLC comprised of a G4220A binary pump, G4226A ALS, G1316C TCC, and G4212A DAD with ULD flow cell. UV absorption was generally observed at 215 nm and 254 nm with a 4 nm bandwidth. Column: Waters Acquity BEH C18, 1.0 x 50 mm, 1.7 μm. Gradient conditions: 5% to 95% CH₃CN in H₂O (0.1% TFA) over 1.4 min, hold at 95% CH₃CN for 0.1 min, 0.5 mL/min, 55 °C. High resolution mass spectra were obtained on an Agilent 6540 UHD Q-TOF with ESI source. MS parameters were as follows: fragmentor: 150, capillary voltage: 3500 V, nebulizer pressure: 60 psig, drying gas flow: 13 L/min, drying gas temperature: 275 °C. Samples were introduced via an Agilent 1200 UHPLC comprised of a G4220A binary pump, G4226A ALS, G1316C TCC, and G4212A DAD

with ULD flow cell. UV absorption was observed at 215 nm and 254 nm with a 4 nm bandwidth. Column: Agilent Zorbax Extend C18, 1.8 μm , 2.1 x 50 mm. Gradient conditions: 5% to 95% CH_3CN in H_2O (0.1% formic acid) over 1 min, hold at 95% CH_3CN for 0.1 min, 0.5 mL/min, 40 $^\circ\text{C}$. For compounds that were purified on a Gilson preparative reversed-phase HPLC, the system comprised of a 333 aqueous pump with solvent-selection valve, 334 organic pump, GX-271 or GX-281 liquid handler, two column switching valves, and a 155 UV detector. UV wavelength for fraction collection was user-defined, with absorbance at 254 nm always monitored. Method 1: Phenomenex Axia-packed Luna C18, 30 x 50 mm, 5 μm column. Mobile phase: CH_3CN in H_2O (0.1% TFA). Gradient conditions: 0.75 min equilibration, followed by user defined gradient (starting organic percentage, ending organic percentage, duration), hold at 95% CH_3CN in H_2O (0.1% TFA) for 1 min, 50 mL/min, 23 $^\circ\text{C}$. Method 2: Phenomenex Axia-packed Gemini C18, 50 x 250 mm, 10 μm column. Mobile phase: CH_3CN in H_2O (0.1% TFA). Gradient conditions: 7 min equilibration, followed by user defined gradient (starting organic percentage, ending organic percentage, duration), hold at 95% CH_3CN in H_2O (0.1% TFA) for 7 min, 120 mL/min, 23 $^\circ\text{C}$. All reagents were purchased from Aldrich Chemical Co. and were used without purification. All final compounds were >98% pure by LCMS (254 nm, 214 nM and ELSD). Following these purification protocols, final compounds were transferred to a barcode vial and diluted to a concentration of 10 μM using molecular biology grade dimethylsulfoxide (DMSO). These compounds were registered into Dotmatics and assigned a VU identification number before being tested in the primary screening assay.

Cell Lines

Chinese hamster ovary (CHO) cells stably expressing muscarinic receptor isoforms were maintained in Ham's F-12 growth medium containing 10% FBS, 20 mM HEPES, antibiotic/antimycotic, 500 µg/mL G418 in the presence of 5% CO₂ at 37 °C. For Gi-coupled M2 and M4 receptors, chimeric Gqi5 was stably coexpressed to elicit Ca response. To determine the functional activity at dog M1, the dog M1 full-length open reading frame (ORF) was amplified from the dog hippocampus cDNAs (Zyagen, San Diego, CA). The ORF was then subcloned into the EcoR I and Xho I sites of pcDNA3.1 (+) vector (Life Technologies, Carlsbad, CA). Sequencing of the plasmid confirmed the presence of dog M1 ORF (XM_540897). CHO cells were transfected with dog M1 expression plasmid using Fugene 6 (Promega, Madison, WI), the transfected cells were incubated with the selection medium containing 1 mg/mL G418 for 2 weeks, and the resulting polyclones were used for the calcium mobilization assay described below.

Calcium Mobilization Assay

To determine the potency and efficacy of M1 ago-PAMs, calcium flux was measured using the Functional Drug Screening System (FDSS7000, Hamamatsu, Japan) as previously described (Rook et al. 2016). Briefly, All muscarinic receptor-CHO cells including multi species M1 and M2–M5 cells were plated in black-walled, clear-bottomed 384 well plates (Greiner BioOne, Monroe, NC) at 20,000 cells/well in 20 µL of growth medium without G418 the day before assay. The following day, cells were washed with assay buffer (Hank's balanced salt solution, 20 mM HEPES, and 2.5 mM probenecid) and immediately incubated with 20 µL of 1.15 µM fluo-4-acetomethoxyester (Fluo-4 AM) dye solution prepared in assay buffer for 45 min at 37 °C. During the

incubation time, all compounds were serially diluted (1:3) in DMSO for 10-point concentration–response curves (CRC), and further diluted in assay buffer at starting final concentration 30 μ M using Echo liquid handler (Labcyte, Sunnyvale CA). Dye was removed and replaced with assay buffer. Immediately, calcium flux was measured using the FDSS7000. The CRC of compounds or vehicle was added to cells for 2.5 min and then an EC₂₀ concentration of acetylcholine (ACh) was added and incubated for 1 min. EC_{max} concentration was also added to cells that were incubated with DMSO vehicle to calculate the EC₂₀ calcium response. Using a four-point logistical equation in GraphPad Prism 5.0 (GraphPad Software, Inc., La Jolla, CA), the concentration response curves were generated for determination of the potency and efficacy of the agonist and PAM.

Radioligand Binding Assay

Competition binding assays were performed using [³H]-N-methylscopolamine ([³H]-NMS, PerkinElmer, Boston, MA) as previously described. Briefly, compounds were serially diluted 1:3 in DMSO for an 11-point CRC, then further diluted for a final top concentration of 30 μ M in binding buffer (20 mM HEPES, 10 mM MgCl₂, and 100 mM NaCl, pH 7.4). Membranes from rat M1-CHO cells (10 μ g) were incubated with the serially diluted compounds in the presence of a K_d concentration of [³H]-NMS, 0.088 nM, at room temperature for 1 h with constant shaking. Nonspecific binding was determined in the presence of 10 μ M atropine. Binding was terminated by rapid filtration through GF/B Unifilter plates (PerkinElmer) using a Brandel 96-well plate Harvester (Brandel Inc., Gaithersburg, MD), followed by three washes with ice-cold harvesting buffer (25 mM Tris-HCl, pH 7.4, 150 mM NaCl). Plates were airdried overnight, 50 μ L of

Microscint20 added to the plate, and radioactivity was counted using a TopCount Scintillation Counter (PerkinElmer Life and Analytical Sciences).

Drug Metabolism Methods: In Vitro

Protein binding of M1 PAMs was determined in plasma via equilibrium dialysis employing Single-Use RED Plates with inserts (ThermoFisher Scientific, Rochester, NY). Briefly plasma (220 μ L) was added to the 96-well plate containing test article (5 μ L) and mixed thoroughly. Subsequently, 200 μ L of the plasma–test article mixture was transferred to the cis chamber (red) of the RED plate, with an accompanying 350 μ L of phosphate buffer (25 mM, pH 7.4) in the trans chamber. The RED plate was sealed and incubated 4 h at 37 °C with shaking. At completion, 50 μ L aliquots from each chamber were diluted 1:1 (50 μ L) with either plasma (cis) or buffer (trans) and transferred to a new 96-well plate, at which time ice-cold acetonitrile (2 volumes) was added to extract the matrices. The plate was centrifuged (3000 rpm, 10 min), and supernatants were transferred to a new 96-well plate. The sealed plate was stored at –20 °C until LC/MS/MS analysis. A cocktail of substrates for cytochrome P450 enzymes (1A2: phenacetin, 10 μ M; 2C9: diclofenac, 5 μ M; 2D6: dextromethorphan, 5 μ M; 3A4: midazolam, 2 μ M) were mixed to assess the ability of compounds to inhibit the major cytochrome P450 enzymes. A reaction mixture of 100 mM Kpi, pH 7.4, 0.1 mg/mL human liver microsomes (HLM) and Substrate Mix was prepared and aliquoted into a 96-deepwell block. Test compound and positive control (in duplicate) were then added such that the final concentration of test compound ranged from 0.1–30 μ M. The plate was vortexed briefly and then preincubated at 37 °C while shaking for 15 min. The reaction was initiated with the addition of NADPH (1 mM final concentration). The

incubation continued for 8 min and the reaction quenched by 2x volume of cold acetonitrile containing internal standard (50 nM carbamazepine). The plate was centrifuged for 10 min (4000 rcf, 4 °C) and the resulting supernatant diluted 1:1 with water for LC/MS/MS analysis. A 12 point standard curve of substrate metabolites over the range of 0.98 nM to 2000 nM. The IC₅₀ values for each compound were obtained for the individual CYP enzymes by quantitating the inhibition of metabolite formation for each probe substrate. A 0 μM compound condition (or control) was set to 100% enzymatic activity and the effect of increasing test compound concentrations on enzymatic activity could then be calculated from the % of control activity. Curves were fitted using XLfit 5.2.2 (four-parameter logistic model, eq 201) to determine the concentration that produces halfmaximal inhibition (IC₅₀). The *in vitro* biotransformation of compounds was investigated using hepatic microsomes incubated with or without NADPH (1 mM). Reactions were terminated by adding 1 volume of acetonitrile, and proteins were removed by centrifugation. The supernatants were saved for HPLC/UV/MS analysis. Samples were analyzed on a Waters Acquity UPLC system with PDA detector with a flow rate of 0.5 mL/ min (A: Water/Acetonitrile 95/5 with 0.1% formic acid; B: Acetonitrile) and a Waters Xevo QTOF mass spectrometer with positive ESI source. The metabolic stability of M1 PAMs was investigated in multispecies hepatic microsomes (BD Biosciences, Billerica, MA) using substrate depletion methodology (% test article remaining). A potassium phosphate-buffered reaction mixture (0.1 M, pH 7.4) of test article (1 μM) and microsomes (0.5 mg/mL) was preincubated (5 min) at 37 °C prior to the addition of NADPH (1 mM). The incubations, performed in 96-well plates, were continued at 37 °C under ambient oxygenation and

aliquots (80 μL) were removed at selected time intervals (0, 3, 7, 15, 25, and 45 min). Protein was precipitated by the addition of chilled acetonitrile (160 μL), containing glyburide as an internal standard (50 ng/mL), and centrifuged at 3000 rpm (4 $^{\circ}\text{C}$) for 10 min. Resulting supernatants were transferred to new 96-well plates in preparation for LC/MS/MS analysis. The *in vitro* half-life ($t_{1/2}$, min, eq 1), intrinsic clearance (CL_{int} , mL/min/kg, eq 2) and subsequent predicted hepatic clearance (CL_{hep} , mL/min/kg, eq 3) was determined employing the following equations:

$$(1) \quad T_{1/2} = \frac{\text{Ln}(2)}{k}$$

where k represents the slope from linear regression analysis of the natural log percent remaining of test compound as a function of incubation time

$$(2) \quad CL_{\text{int}} = \frac{0.693}{\text{in vitro } T_{1/2}} \times \frac{\text{mL incubation}}{\text{mg microsomes}} \times \frac{45 \text{ mg microsomes}}{\text{gram liver}} \times \frac{45^a \text{ gram liver}}{\text{kg body wt}}$$

^a scale-up factor that is species specific

$$(3) \quad CL_{\text{hep}} = \frac{Q_h \cdot CL_{\text{int}}}{Q_h + CL_{\text{int}}}$$

where Q_h (hepatic blood flow) is species specific.

Drug Metabolism Methods: In Vivo

All animal studies were approved by the Vanderbilt University Medical Center Institutional Animal Care and Use Committee. The animal care and use program is fully accredited by the Association for Assessment and Accreditation of Laboratory Animal Care, International. Male Sprague–Dawley rats ($n = 2$) weighing around 300 g were

purchased from Harlan laboratories (Indianapolis, IN) and implanted with catheters in the carotid artery and jugular vein. The cannulated animals were acclimated to their surroundings for approximately 1 week before dosing and provided food and water ad libitum. IV cassette PK experiments in rats were carried out according to methods described previously (Bridges et al. Pharmacol. Res. Perspect. 2014; reference 49). Briefly, A cassette of compounds (n =4 –5/cassette) were formulated from 10 mM solutions of compounds in DMSO. In order to reduce the absolute volume of DMSO that was administered, the compounds were combined and diluted with ethanol and PEG400 to achieve a final concentration of 0.4–0.5 mg/mL for each compound (2 mg/mL total) administered in each cassette. The final dosing solutions consisted of approximately 10% ethanol, 40% PEG400, and 50% DMSO (v/v). Each cassette dose was administered IV via the jugular vein to two dual-cannulated (carotid artery and jugular vein) adult male Sprague–Dawley rats, each weighing between 250 and 350 g (Harlan, Indianapolis, IN) for a final dose of 0.2–0.25 mg/kg per compound. Whole blood collections via the carotid artery were performed at 0.033, 0.117, 0.25, 0.5, 1, 2, 4, 7, and 24 h post dose and plasma samples prepared for bioanalysis. For tissue distribution studies in cassette format, brain dissection and blood collections via the carotid artery were performed at 0.25 h post dose. Blood samples were collected into chilled, EDTA-fortified tubes, centrifuged for 10 min at 3000 rpm (4 °C), and resulting plasma aliquoted into 96-well plates for LC/MS/MS analysis. The brain samples were rinsed in PBS, snap frozen and stored at –80 °C. Prior to LC/MS/MS analysis, brain samples were thawed to room temperature and subjected to mechanical homogenation employing a Mini-Beadbeater and 1.0 mm Zirconia/Silica Beads (BioSpec Products). Discrete IV PK

experiments in rats (n = 2) were carried out analogously at a dose of 1.0 mg/kg in 10% EtOH, 50% PEG 400, 40% saline, while discrete PO PK experiments in rats (n = 2) were carried out using a 3 mg/kg dose of compounds in a fine microsuspension in 30% Captisol in H₂O via oral gavage to fasted animals. Whole blood collections via the carotid artery were performed at 0.117, 0.25, 0.5, 1, 2, 4, 7, and 24 h post dose. Plasma samples were prepared for bioanalysis as described above. Determination of the pharmacokinetic profile of VU0486846 following a single IV bolus dose of 1 mg/kg (Ethanol: Peg400: Saline, 10:60:30, v/v/v) and a single PO dose of 3 mg/kg (30% aqueous Captisol) to male Cynomolgus monkeys (n = 3) was carried out at Frontage Laboratories (Exton, Pennsylvania). Blood was collected at standard PK time points and plasma prepared for bioanalysis as per internal protocols at Frontage. All bioanalysis and calculation of PK parameters was carried out by Frontage and a final report issued upon study completion.

Liquid Chromatography/Mass Spectrometry Analysis. M1 PAMs were analyzed via electrospray ionization (ESI) on an AB Sciex API4000 (Foster City, CA) triple-quadrupole instrument that was coupled with Shimadzu LC-10AD pumps (Columbia, MD) and a Leap Technologies CTC PAL autosampler (Carrboro, NC). Analytes were separated by gradient elution using a Fortis C18 2.1 × 50 mm, 3.5 μm column (Fortis Technologies Ltd., Cheshire, UK) thermostated at 40 °C. HPLC mobile phase A was 0.1% formic acid in water (pH unadjusted), mobile phase B was 0.1% formic acid in acetonitrile (pH unadjusted). The gradient started at 30% B after a 0.2 min hold and was linearly increased to 90% B over 0.8 min; held at 90% B for 0.5 min and returned to 30% B in 0.1 min followed by a re-equilibration (0.9 min). The total run time was 2.5 min

and the HPLC flow rate was 0.5 mL/min. The source temperature was set at 500 °C and mass spectral analyses were performed using multiple reaction monitoring (MRM) utilizing a Turbo-Ionspray source in positive ionization mode (5.0 kV spray voltage). All data were analyzed using AB Sciex Analyst 1.4.2 software. For *in vivo* studies, the final PK parameters were calculated by noncompartmental analysis using Phoenix (version 6.2) (Pharsight Inc., Mountain View, CA).

Mouse Plasma-Brain Exposure

M1 PAMs were dissolved in 10% Tween 80 at the concentration of 1–10 mg/mL (base form) and administered intraperitoneally to male C57BL/6J (Jackson Laboratory, Sacramento, CA) mice aged 7–9 weeks at a volume of 10 mL/kg. The blood and brain were collected at 0.25 h. Animals were euthanized and decapitated, and the brains were removed, thoroughly washed with cold saline and immediately frozen on dry ice. Trunk blood was collected in EDTA coated Eppendorf tubes, and plasma was separated by centrifugation and stored at –80 °C until processed for LC/MS/MS analysis as previously described. Three animals were used for each time point.

Electrophysiology

Animals. All animal studies were approved by the Vanderbilt University Medical Center Institutional Animal Care and Use Committee and were conducted in accordance with the National Institutes of Health Guide for the Care and Use of Laboratory Animals. Male C57BL6/J mice (Jackson laboratories) were used in electrophysiology and behavioral studies (6–10 weeks old). Animals were group housed 4–5 per cage, maintained on a 12 h light/ dark cycle, and provided food and water *ad libitum*.

Extracellular Field Electrophysiology. Briefly, 6–10 week old male C57BL6/J mice were anesthetized using a mixture of ketamine and xylazine (100 mg/kg and 10 mg/kg, respectively, intraperitoneal injection) then transcardially perfused with ice-cold cutting solution (in mM: 230 sucrose, 2.5 KCl, 8 MgSO₄, 0.5 CaCl₂, 1.25 NaH₂PO₄, 10 D-glucose, 26 NaHCO₃), and then the brains were removed and submerged in ice-cold cutting solution. Coronal slices containing the prelimbic prefrontal cortex were cut at 400 μ m using Leica VT1200 vibratome and were transferred to a holding chamber containing NMDG-HEPES recovery solution (in mM: 93 NMDG, 2.5 KCl, 1.2 NaH₂PO₄, 30 NaHCO₃, 20 HEPES, 25 D-glucose, 5 sodium ascorbate, 2 thiourea, 3 sodium pyruvate, 10 MgSO₄, 0.5 CaCl₂, 12N-acetyl-L-cysteine, pH 7.3, <310 mOsm) for 8–10 min at 32 °C. Slices were then transferred to a room temperature holding chamber for at least 1.5 h containing ACSF (in mM: 126 NaCl, 1.25 NaH₂PO₄, 2.5 KCl, 10 D-glucose, 26 NaHCO₃, 2 CaCl₂, 1 MgSO₄) supplemented with 600 μ M sodium ascorbate for slice viability. All buffers were continuously bubbled with 95% O₂/5% CO₂. Subsequently, slices were transferred to a 30–32 °C submersion recording chamber (Warner Instruments) where they were perfused with ACSF at a rate of 2 mL/min. Field excitatory postsynaptic potentials (fEPSPs) were recorded from layer V of the prelimbic cortex and evoked electrically by a concentric bipolar stimulating electrode (200 μ s duration, 0.05 Hz; interpulse interval of 50 ms) in the superficial layers II–III as described previously (Ghoshal et al., 2017). VU0486846 was diluted to the appropriate concentrations in DMSO (<0.1% final) in ACSF and applied to the bath for 20 min using a peristaltic pump perfusion system. Carbachol and OxoM (Tocris Bioscience, Bristol, UK) were diluted in H₂O. See the Supporting Information for additional information.

Stereotaxic Viral Injections. Mice underwent stereotaxic injections for viral-mediated gene transfer of channelrhodopsin-2 (ChR2) at 4–5 weeks of age. Mice were anaesthetized with 1–2% isoflurane for the duration of the surgery and were administered carprofen (10 mg/kg, s.c.) before the surgery commenced. Following a craniotomy, one injection per hemisphere (800 nL at a rate of 100 nL/min) of AAV5CaMKII-ChR2- EYFP (UNC Viral Vector Core) was delivered into the target regions through a 28G needle attached to a 10 μ L Hamilton syringe. Injection site coordinates were as follows (relative to bregma): vHipp [ML: \pm 3.4, AP: -3.4, DV: -4.0]. Carprofen (10 mg/kg, s.c.) was administered for at least 72 h post procedure. Recordings were made 4–5 weeks following surgery to allow sufficient expression of ChR2 in axon terminals within the PFC.

Optical Extracellular Field Electrophysiology. Brain slices from viral injected mice were prepared in a similar manner described above. For studies involving optical stimulation, blue light (470 nm) was delivered using a High-Power LED (Thorlabs Inc. Newton, NJ), which was mounted to the epi-illumination port of an Olympus BX50WI upright microscope (Olympus). Blue light was shined onto slices through the 40 \times objective lens at 0.05 Hz (Maximum light intensity at the site of illumination is 2.6 mW).

Eurofins Lead Profiling Data

A radioligand binding panel of 68 targets (GPCRs, ion channels, transporters, and nuclear hormones) with data reported as % inhibition of radioligand binding at a 10 μ M concentration of VU6010608 and VU6012962 from two independent determinations.

Behavioral Pharmacology Studies

Animals. *In vivo* studies utilized either 7–8 week old male C57Bl/6 mice (Jackson Laboratory, Sacramento, CA) or male Sprague–Dawley rats weighing 275–300 g (Envigo, Indianapolis, IN). The animals were cared for in accordance with the National Institutes of Health Guide for the Care and Use of Laboratory Animals. All experimental procedures were approved by the Vanderbilt University Animal Care and Use Committee.

Novel Object Recognition Task. Novel object recognition memory was assessed as previously described.²⁶ Briefly, rats were habituated to an empty novel object recognition (NOR) arena. On test day, rats were administered vehicle (10% tween 80) or VU0486846 (1–10 mg/ kg, intraperitoneally (i.p.), 1 mL/kg, n = 12) and returned to their home cage for 30 min. Rats were then placed in the NOR arena containing 2 identical objects for 10 min. Following the exposure period, rats were placed back into their home cages for 24 h. The rats were then returned to the arena in which one of the previously exposed (familiar) objects was replaced by a novel object and exploration behavior was assessed for 3 min. Time spent exploring each object was scored by an observer blinded to the experimental conditions and the recognition index was calculated as [(time spent exploring novel object) – (time spent exploring familiar object)]/total time exploring objects.

Contextual Fear Conditioning. The effects of VU0486846 on acquisition of contextual fear conditioning were evaluated in rats as previously described.⁴² Rats were given a 30 min pretreatment of vehicle (10% Tween 80), risperidone alone (3 mg/kg, i.p., 1 mL/kg), or risperidone coadministered with VU0486846 (1–10 mg/kg) and

placed in a sound-attenuating conditioning chamber (Med Associates). Following a 2 min habituation period, rats received three shock-tone pairing trials (30 s 3000 Hz 80 dB tone coterminated with a 1 s, 0.5 mA shock) in the presence of a 10% vanilla solution scent and then returned to their home cages. Twenty four hours later, acquisition of fear conditioning was assessed in the same conditioning environment for 4 min by measuring freezing behavior in the absence of any shock stimuli or drug. Testing sessions were recorded and time spent freezing was automatically scored using video freeze software (MEDVFC-RS, MedAssociates).

Modified Irwin Toxicology Battery

The potential CNS adverse effects of VU0486846 were evaluated using the Modified Irwin Toxicology Battery. Baseline assessments were conducted prior to administration of compounds. Mice were administered vehicle or VU0486846 (100 mg/kg, 10% Tween 80, 10 mL/kg, i.p., n = 3) while rats were administered vehicle or VU0486846 (56.6 mg/kg, 10% Tween 80, 2 mL/kg, i.p., n = 3). Animals were then placed back into their home cages and evaluated by an observer blinded to dosing conditions at 15, 30, 60, 180, and 360 min for autonomic nervous and somatomotor system parameters. Animals were assigned a score for each parameter of 0 (normal), 1 (slight/light), 2 (moderate), or 3 (marked) relative to vehicle-treated controls. The mean Modified Irwin Toxicology Battery test scores are classified as follows: - no effect, (+) 0.01 to 0.25, + 0.251 to 0.50, ++ 0.51 to 1.0. Pretreatment of VU0486846 (100 mg/kg, i.p.) did not cause significant observable adverse effects in normal, healthy mice.

The Discovery and Development of M₁ Positive Allosteric Modulators: Benzomorpholine and Tetrahydroquinoline Series

Scaffold hopping: Quinolone to Benzomorpholine core

The quinolone series that produced BQCA was further explored by Merck and Co., which led to the seminal discovery of (1*S*,2*S*)-2-aminocyclohexan-1-ol amide moiety as a replacement for the carboxylic acid functional group. The incorporation of (1*S*,2*S*)-2-aminocyclohexan-1-ol amide prompted the realization and recognition that the secondary N-H amide formed an intramolecular hydrogen bond (IMHB) with the carbonyl oxygen of the quinolone moiety. The IMHB discovery influenced the development of the tricyclic core of MK-7622, disclosed by Merck and Co., and azaindole core of PF-06764427, disclosed by Pfizer.^{48,54,55}

When designing our central core, we opted to utilize the BQCA 6,6-fused ring system with the (1*S*,2*S*)-2-aminocyclohexan-1-ol amide moiety (**2.8**) to simultaneously increase sp³ character and internalize the Lewis basic oxygen of the quinolone into the ring by scaffold hopping to a benzomorpholine core (**2.9**) as depicted in **Figure 2.5**.⁵³ In addition to increasing sp³ character, scaffold hopping to the benzomorpholine core also introduced an additional chiral center, which presents the opportunity to improve

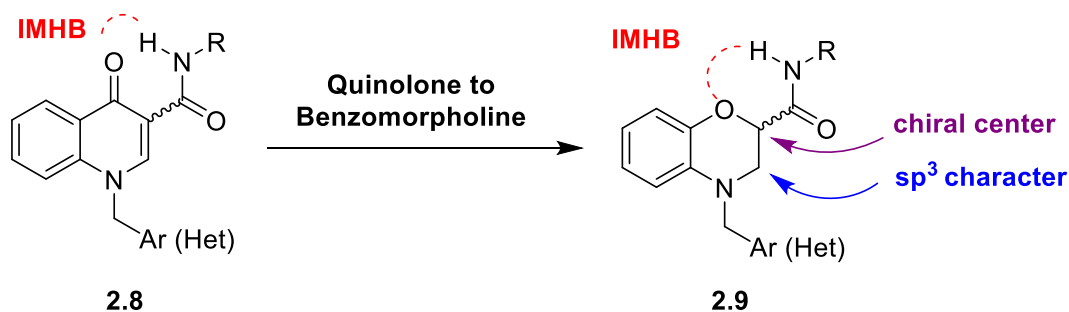


Figure 2.5 Scaffold hopping from a BQCA derived, Merck compound to a novel benzomorpholine core.

potency and efficacy by resolving the diastereomers. With a new core in hand, we were able to move forward with optimization efforts.

SAR and Synthesis of Benzomorpholine Series

While holding the morpholine and secondary amide in place to maintain the IMHB, we plan to make minor perturbations to the remaining portions of the scaffold, highlighted in **Figure 2.6**. Early SAR around the eastern amide were brief, as it rapidly

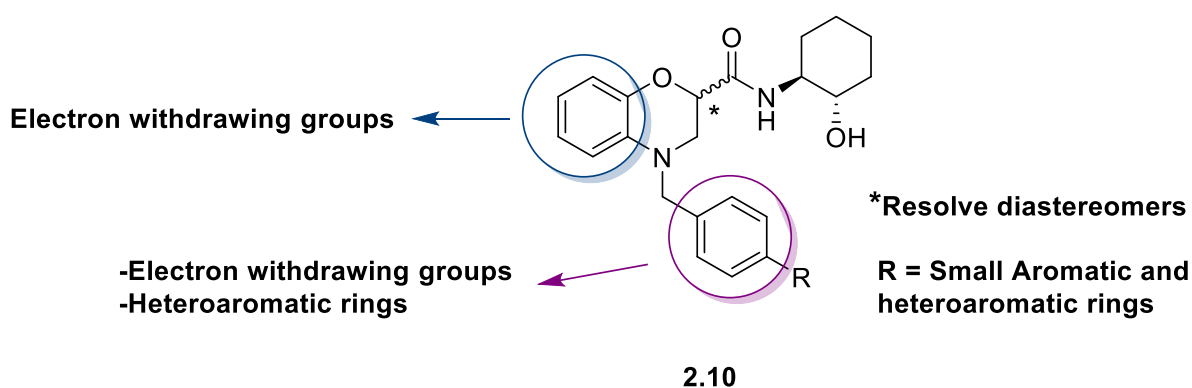
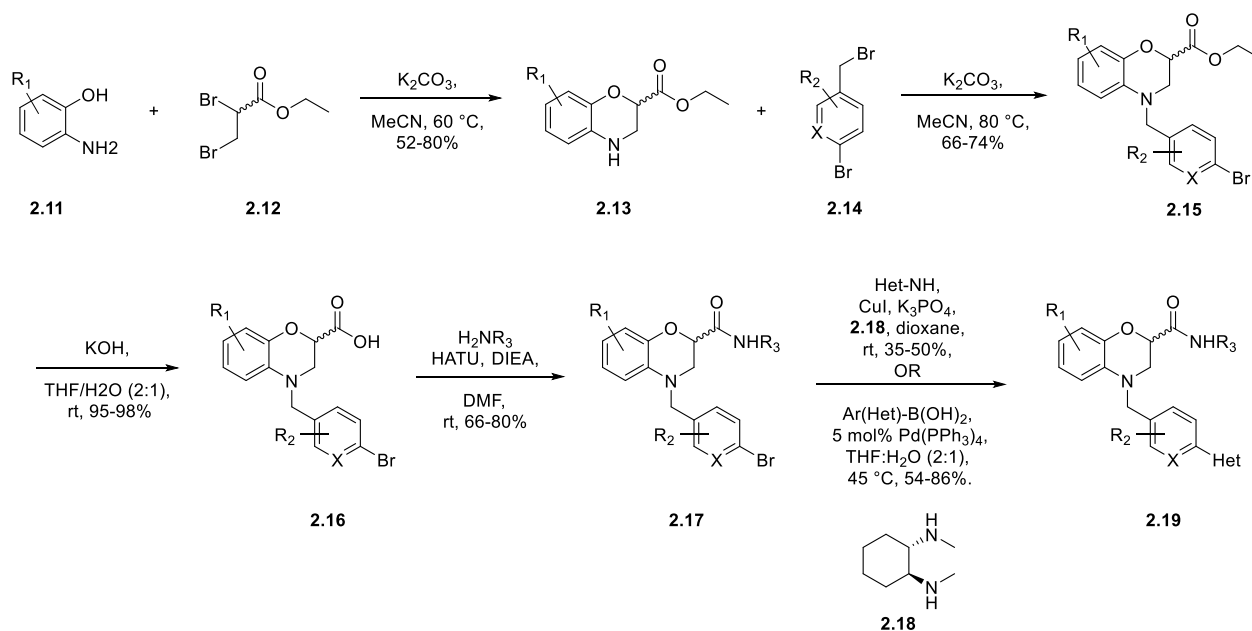


Figure 2.6 Our SAR strategy around new benzomorpholine core.

became apparent that the (1*S*,2*S*)-2-aminocyclohexan-1-ol moiety was crucial for activity and therefore the cyclic amide moiety will be held constant. We plan to explore the addition of small functional groups at R and incorporate electron withdrawing groups and heterocycles into the western phenyl group as well as the southern benzyl group to improve DMPK properties. We plan to screen all analogs in our cell-based *in vitro* assay as the mixture of diastereomers to facilitate a more rapid SAR. The mixture of diastereomers that engender sub-micromolar activity will be resolved and screened as a single diastereomer to evaluate potency and efficacy. The optimization efforts of the

benzomorpholine series described in the following sections was a collaborative effort between Dr. Pedro Garcia-Barrantes and myself.

Analogs of this nature were readily synthesized and diversified via **Scheme 2.1** from commercially available starting materials. Ethyl 2,3-dibromopropanoate (**2.12**) was



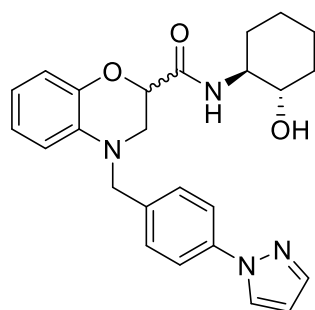
Scheme 2.1 Synthetic route to access benzomorpholine analogs **2.20-2.42**.

condensed with 2-aminophenol's to provide racemic substituted and unsubstituted benzomorpholine cores (**2.13**). The benzomorpholine cores can then be reacted with various benzyl bromides using standard alkylating conditions to provide analogs of **2.15**. Ester congeners of **2.15** are then hydrolyzed to generate carboxylic acids **2.16** at a near quantitative yield. HATU mediated amide couplings were then performed, reacting **2.16** with several primary cyclic and non-cyclic amines to provide derivatives of **2.17** as mixtures of diastereomers. Finally, **2.17** congeners were subjected to either copper-mediated or Suzuki cross-coupling reaction conditions to install the southern heteroaromatic ring, giving rise to our putative M₁ PAMs. The mixture of diastereomers

are separated by either flash column chromatography or by supercritical fluid chromatography (SFC) if the diastereomers are unable to be resolved by flash chromatography.

Benzomorpholine Core Modifications: *Analogs 2.20-2.29*

Significant work had been previously done around this scaffold, with the racemic compound VU0484043 (**2.20**) emerging as the lead contender and reference compound for future analogs (**Figure 2.7**). Electron withdrawing groups, specifically fluorine, have



VU0484043 (**2.20**)
 M_1 EC₅₀ = 0.92 μ M
ACh Max = 83%
 f_u plasma > 0.11
CL_{HEP} human = 11.1 mL/min/kg
CL_{HEP} rat = 43.2 mL/min/kg
 K_p = 0.17

Figure 2.7 Structure and *in vitro* DMPK profile of VU0484043 (**2.20**).

been known to attenuate lipophilicity and amine basicity of compounds to increase brain penetration and improve DMPK properties. Therefore, fluorine substituents and nitrogen heteroatoms were strategically incorporated into the scaffold at different locations to attenuate the electronics of the molecule. We began by initiating a ‘fluorine walk’ around the aromatic ring of the central benzomorpholine core (**Figure 2.8**). The ‘fluorine walk’ has been a highly successful technique in the optimization of allosteric modulators, especially for previous M_1 PAM scaffolds. Compounds **2.21** and **2.23** with the fluorine substituents in the 5 and 7 position, respectively, displayed a diminution in activity with

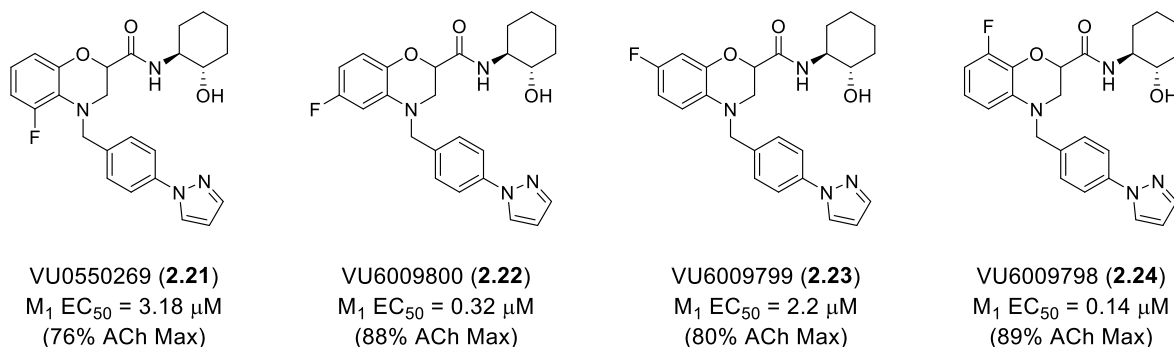


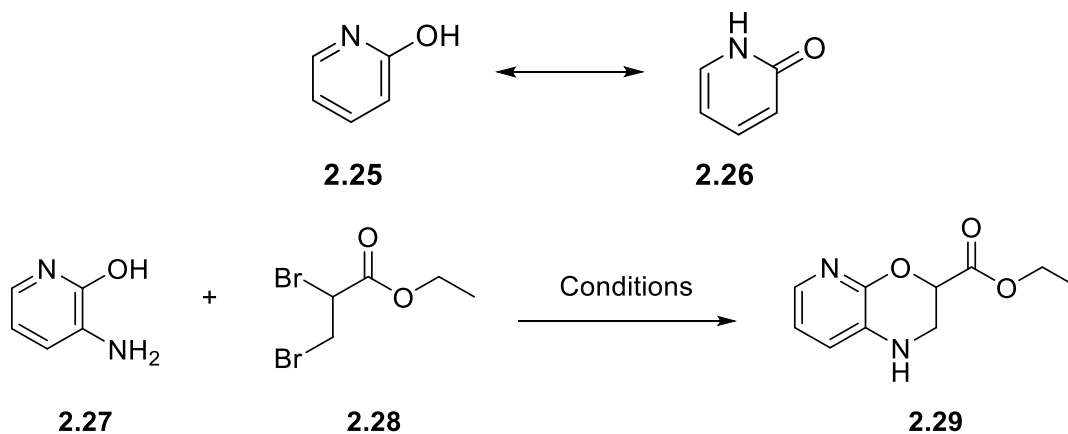
Figure 2.8 Fluorine ‘walk’ around benzomorpholine core.

respect to VU0484043. On the other hand, compounds **2.22** and **2.24** showed an improvement in potency, with an approximate 7-fold increase observed with **2.24**. In addition, rat CNS penetration was improved relative to VU0484043 as expected. Unfortunately, the incorporation of the fluorine substituents negatively impacted the DMPK profiles of **2.21-2.24**. Unlike VU0484043 with good fraction unbound in plasma and moderate predicted hepatic clearance, the fluorinated analogs all displayed unacceptable fraction unbound ($f_u < 0.02$) and high predicted hepatic clearance in both human ($CL_{HEP} \sim 20$ mL/min/kg) and rat ($CL_{HEP} > 65$ mL/min/kg) liver microsomes. Thus, while the ‘fluorine walk’ improved potency and CNS penetration, the predicted clearance suffered greatly. To improve the predicted clearance while maintaining potency and CNS penetration, we envisioned replacing the fluorine substituent in the 8 position of **2.24** with an alternative hydrogen bonding accepting group containing different electronic properties.

We began from commercially available 3-aminopyridin-2-ol (**2.27**) and the dibromopropionate (**2.28**) utilizing the conditions outlined in **Scheme 2.1** in the attempt to form aza benzomorpholine **2.29**. However only trace amount of desired product was observed by LC-MS. We believe the reaction only proceeded in trace amounts due to

the nature of the polar solvent shifting equilibrium primarily to the pyridone tautomer

2.26.⁵⁶ Therefore, a solvent screen with varying polarities was enough to promote



Solvent	Base	Temp (°C)	Yield
Acetonitrile	K ₂ CO ₃	50	Trace
DMF	K ₂ CO ₃	50	n.p.
1,4-Dioxane	K ₂ CO ₃	50	n.p.
THF	K ₂ CO ₃	50	n.p.
CHCl ₃	K ₂ CO ₃	50	n.p.
CCl ₄	K ₂ CO ₃	50	n.p.
Acetone	K ₂ CO ₃	50	n.p.
EtOH	K ₂ CO ₃	50	n.p.
tBuOH	K ₂ CO ₃	50	n.p.
Pyridine	K ₂ CO ₃	50	n.p.
Acetonitrile	TEA	80	Trace
Acetonitrile	Cs ₂ CO ₃	80	Not isolable
Acetonitrile	tBuOH	80	n.p.
Acetonitrile	NaH	80	Not isolable

Table 2.1 Solvent and base screen to influence the conformation of **2.27**, where it exists primarily as exemplary 2-hydroxypyridine **2.25** rather than the undesired tautomer **2.26**. **2.27** reacts with **2.28** to generate the desired azabenzomorpholine core **2.29**.

conducted to identify a solvent non-polar enough to access tautomer **2.25** but polar substrate solubility. As can be observed in **Table 2.1**, the only solvent to produce the desired product in any capacity was our original solvent, acetonitrile. Thus, moving

forward, acetonitrile was maintained while screening stronger, alternative bases at a higher temperature to see if we could force deprotonation and nucleophilic addition of the 2-hydroxypyridine. Triethylamine (TEA) afforded a trace amount of desired product by LC-MS, which is unsurprising as TEA is only slightly more basic than K_2CO_3 . While a much stronger base than K_2CO_3 , *tert*-butyl hydroxide (tBuOH) generated no desired product, likely due to the steric bulk of the base. The use of Cs_2CO_3 and NaH on the other hand, both forced the reaction to completion, where the desired mass was appreciably observed by LC-MS. However, we were never able to isolate the product for further characterization and *in vitro* studies. This is likely due to decomposition of the molecule upon work up or purification. Therefore, the poor clearance of analogs **2.21-2.24** and the inability to isolate core **2.29** led us to move away from the fluoro-substituted and aza-benzomorpholine cores and evaluate alternative regions of the molecule.

SAR Around the Southern Biaryl Rings: Analogs 2.30-2.36

Metabolite identification studies revealed that the primary mode of metabolism is driven by P_{450} -mediated debenzoylation of **2.20** liberating **2.30** (Figure 2.9). Therefore, returning to the unsubstituted benzomorpholine core, we shifted focus to the southern

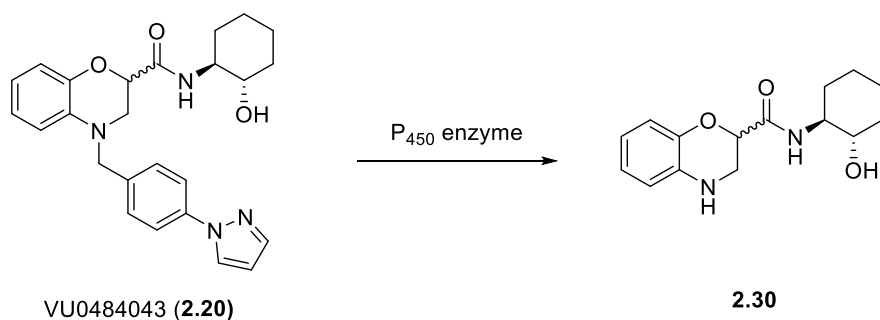
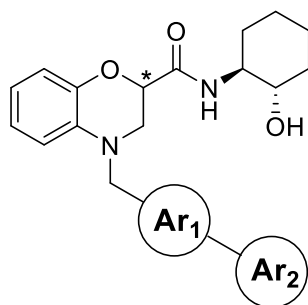


Figure 2.9 Predominant mechanism by which VU0484043 (**2.20**) is metabolized.

region of the molecule, where we surveyed alternative substituted biaryl and heterobiaryl rings to manipulate the electronics in the hopes of inhibiting the debenzoylation.

Previous work around this area revealed that replacement of the benzyl group with a 3-pyridine produced the most active compounds in the series. However, none of these analogs possessed a balanced pharmacological profile suitable for *in vivo* testing. Re-evaluating these historic analogs, we attempted again to perturb the electronics in the system to improve DMPK properties. We investigated the addition of 2-fluorobenzene substituents as well as 2-pyridines with a few of the more active heteroaryl groups at Ar₂ (**Table 2.2**). As shown in **Table 2.2**, moving the pyridine nitrogen over one position resulted in a drastic loss in potency from (M₁ EC₅₀ < 0.60 μM) to mid to high micromolar activity. Changing the electronics by swapping the pyridine with a 2-fluorobenzene was able to rescue activity to the high nanomolar range. Unfortunately, these modifications did not produce a molecule with a balanced DMPK



Topicity ^a	Ar ₁	Ar ₂	Compound Number	VOID	M ₁ EC ₅₀ (μM)	% ACh Max
racemic			2.31	VU6011231	6.0	77

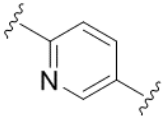
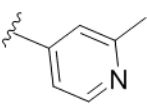
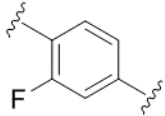
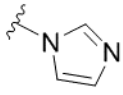
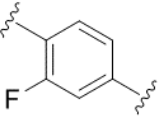
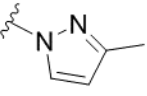
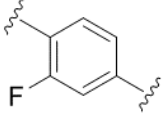
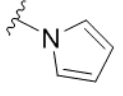
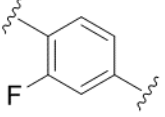
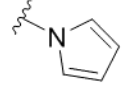
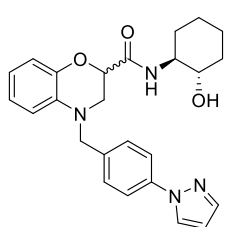
racemic			2.32	VU6011273	8.5	87
racemic			2.33	VU6011288	0.87	84
racemic			2.34	VU6011286	0.79	81
Diastereomer 1			2.35	VU6009718	2.4	69
Diastereomer 2			2.36	VU6009717	0.67	76

Table 2.2 SAR around the southern biaryl system – analogs **2.31-2.36**.

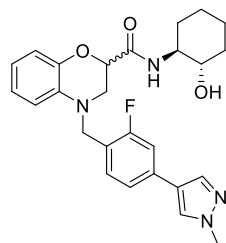
profile. Thus, VU0484043 remained the most attractive and balanced compound to date. Encountering steep SAR, we decided to revisit a few historic compounds ≥ 500 nM and resolve the enantiomers for *in vitro* potency and DMPK testing. Efforts surrounding these analogs will be discussed in the following section.

Resolving and Evaluating Single Diastereomers: Analogs 2.37-2.46

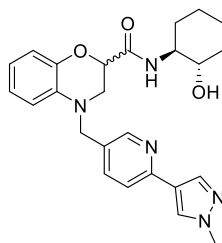
While we were resolving and assessing the potency, efficacy, and DMPK properties of the single diastereomers of compounds **2.37-2.39**, we simultaneously probed the 3-dimensional space of the pocket by introducing a quaternary carbon at the chiral center with a methyl group (**Figure 2.10**). Unfortunately, the addition of the methyl group at the chiral center resulted in a large loss of activity and was therefore, not



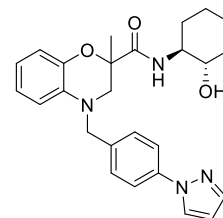
VU0484043 (**2.37**)
 M_1 EC₅₀ = 0.54 μ M
 (83% ACh Max)



VU0650437 (**2.38**)
 M_1 EC₅₀ = 0.29 μ M
 (81% ACh Max)



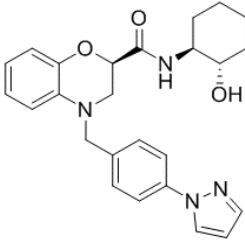
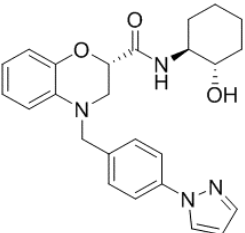
VU0604445 (**2.39**)
 M_1 EC₅₀ = 0.19 μ M
 (88% ACh Max)



VU6010006 (**2.40**)
 M_1 EC₅₀ = 7.3 μ M
 (61% ACh Max)

Figure 2.10 Analogs **2.37-2.39** to be separated and assayed as single diastereomers. The addition of a methyl group at the chiral center results in a loss of activity (**2.40**).

pursued further (**2.40**). The mixture of diastereomers of **2.37** were readily separated via flash column chromatography whereas the diastereomers of **2.38** and **2.39** were resolved by SFC. Activities of the single diastereomers of unknown absolute stereochemistry are highlighted in **Table 2.3**. Here we see that both diastereomers **2.43** and **2.44** are far less potent than the racemate and we therefore elected to move forward without further pursuit of these compounds. Contrarily, compounds **2.45** and

Compound*	Compound Number	VOID	M_1 EC ₅₀ (μ M)	% ACh Max
	2.41	VU0486846	0.31	85
	2.42	VU0486834	0.96	76

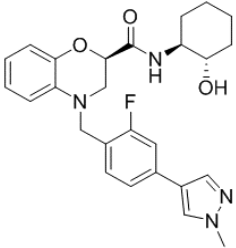
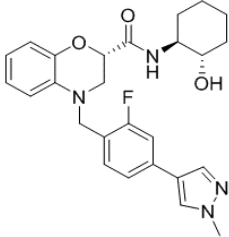
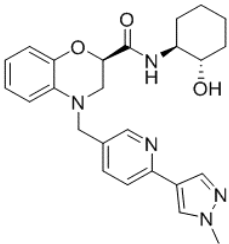
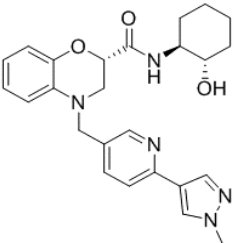
	2.43	VU6009807	8	77
	2.44	VU6009806	2.3	87
	2.45	VU6009801	0.23	86
	2.46	VU6009802	0.40	82

Table 2.3 Structures and activities of single diastereomers of the most attractive compounds in this series – analogs **2.41-2.46**.

2.46 displayed acceptable potency and efficacy. However, they suffered from poor predicted clearance in human and liver microsomes and were also not pursued further. As a result, the more active diastereomer of the two, VU0486846 (**2.41**), emerged as the most attractive and balanced compound from the overall series and was carried forward for further evaluation.

Assessment of VU0486846 (2.41) as a Viable *In Vivo* Tool Compound

A battery of tests were performed on VU0486846 to evaluate selectivity, adverse effects, and DMPK properties to ensure the compound is suitable for *in vivo* pharmacological assays. In order to accomplish this, VU0486846 was prepared on a 25-gram scale to generate sufficient material for numerous *in vivo* behavioral studies. Gratifyingly, our synthetic route toward VU0486846 is highly scalable between 100 mg and 25 grams. Following synthesis, a crystal was grown and a structure obtained of VU0486846 to determine the absolute stereochemistry of the newly formed stereocenter generated by scaffold hopping from the quinolone to the benzomorpholine

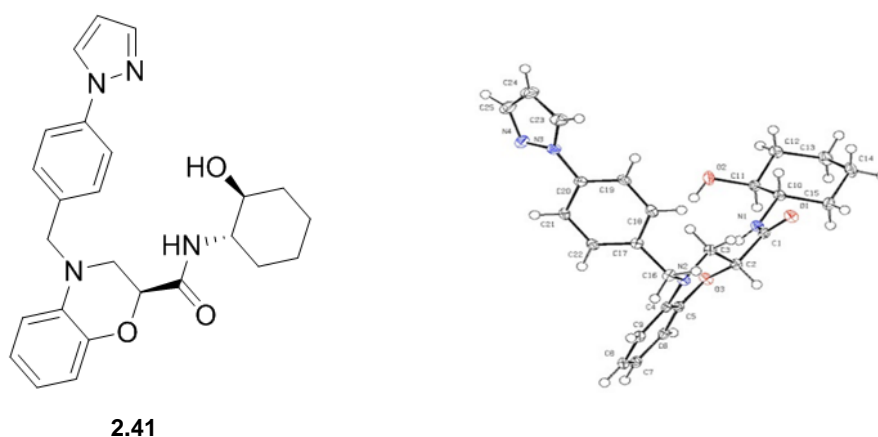


Figure 2.11 Structure and x-ray crystal structure of VU0486846 (**2.41**). X-Ray crystal structure courtesy of Joel Harp.

core. The crystal structure depicted in **Figure 2.11** confirmed the stereochemistry of our more active diastereomer, VU0486846 (**2.41**), as the *R*-enantiomer and its counterpart, VU0486834 (**2.42**) presumed to be the *S*-enantiomer.

Following confirmation of the absolute stereochemistry of VU0486846, we tested subtype selectivity against M₂-M₅ in our high expression human and rat cell lines. As can be seen in **Figures 2.12A** and **2.12B**, VU0486846 is selective for M₁ in both human

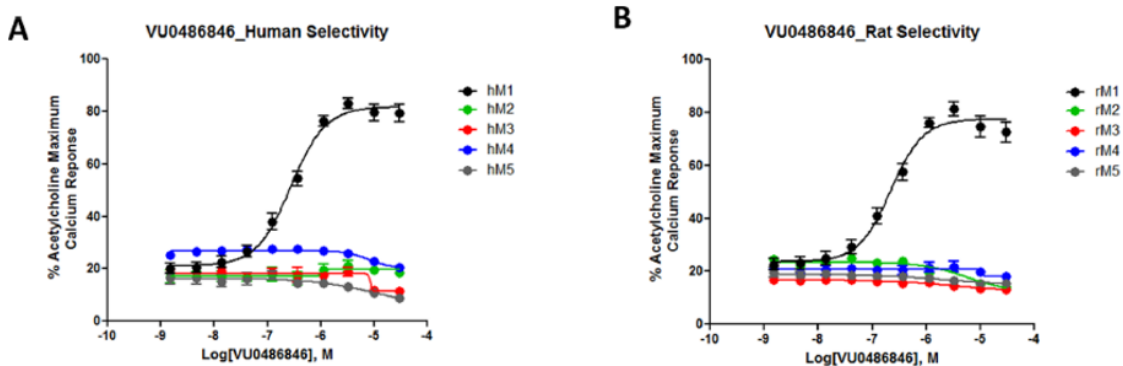


Figure 2.12 A) VU0486846 does not elicit a calcium mobilization response in human cells expressing M₂-M₅, B) VU0486846 also does not engender a calcium mobilization response in rat cells expressing M₂-M₅.

and rat cell lines with no activity observed at M₂-M₅. To get a broader assessment of ancillary pharmacology, VU0486846 was outsourced to Eurofins to perform a radioligand binding panel of 68 targets to investigate potential off-target activity at alternative GPCRs, ion channels, transporters, and nuclear hormones. At a 10 μ M concentration of VU0486846, no significant off-target activity was observed at the 68 CNS targets highlighted in **Table 2.4** (no inhibition >50% at 10 μ M).

Target/Protein	Species	% Inhibition
Adenosine A ₁	Human	3
Adenosine A _{2A}	Human	-2
Adenosine A ₃	Human	7
Adrenergic α_{1A}	Rat	12
Adrenergic α_{1B}	Rat	5
Adrenergic α_{1D}	Human	2
Adrenergic α_{2A}	Human	21
Adrenergic β_1	Human	-1
Adrenergic β_2	Human	-1
Androgen (Testosterone)	Human	1
Bradykinin B ₁	Human	-9
Bradykinin B ₂	Human	16
Calcium Channel L-Type, Benzothiazepine	Rat	7
Calcium Channel L-Type, Dihydropyridine	Rat	5
Calcium Channel N-Type	Rat	-1

Cannabinoid CB ₁	Human	-1
Dopamine D ₁	Human	-2
Dopamine D _{2S}	Human	-9
Dopamine D ₃	Human	2
Dopamine D _{4.2}	Human	-2
Endothelin ET _A	Human	0
Endothelin ET _B	Human	2
Epidermal Growth Factor (EGF)	Human	-5
Estrogen E _α	Human	2
GABA _A , Flunitrazepam, Central	Rat	4
GABA _A , Muscimol, Central	Rat	-4
GABA _{B1A}	Human	2
Glucocorticoid	Human	0
Glutamate, Kainate	Rat	2
Glutamate, NMDA, Agonism	Rat	-2
Glutamate, NMDA, Glycine	Rat	-5
Glutamate, NMDA, Phencyclidine	Rat	-3
Histamine H ₁	Human	2
Histamine H ₂	Human	-8
Histamine H ₃	Human	4
Imidazoline I ₂ , Central	Rat	22
Interleukin IL-1	Mouse	16
Leukotriene, Cysteinyl CysLT ₁	Human	-2
Melatonin MT ₁	Human	2
Muscarinic M ₁	Human	12
Muscarinic M ₂	Human	-2
Muscarinic M ₃	Human	-14
Neuropeptide Y Y ₁	Human	-1
Neuropeptide Y Y ₂	Human	2
Nicotinic Acetylcholine	Human	-2
Nicotinic Acetylcholine α ₁ , Bungarotoxin	Human	-2
Opiate δ ₁ (OP1, DOP)	Human	-3
Opiate κ (OP2, KOP)	Human	5
Opiate μ (OP3, MOP)	Human	-9
Phorbol Ester	Mouse	5
Platelet Activating Factor (PAF)	Human	-4
Potassium Channel [K _{ATP}]	Hamster	3
Potassium Channel hERG	Human	10
Prostanoid EP ₄	Human	2
Purinergic P2X	Rabbit	19
Purinergic P2Y	Rat	-9

Rolipram	Rat	2
Serotonin (5-HT _{1A})	Human	-10
Serotonin (5-HT _{2B})	Human	-3
Serotonin (5-HT ₃)	Human	-11
Sigma σ_1	Human	2
Sodium Channel, Site 2	Rat	19
Tachykinin NK ₁	Human	-1
Thyroid Hormone	Rat	-3
Transporter, Dopamine (DAT)	Human	4
Transporter, GABA	Rat	4
Transporter, Norepinephrine (NET)	Human	0
Transporter, Serotonin (SERT)	Human	0

Table 2.4 Eurofins lead profile panel for VU0486846 (**2.42**). Significant activity is defined as >50% inhibition at a 10 μ M concentration of VU0486846 (**2.42**). Data courtesy of Eurofins.

After VU0486846 was determined to be a selective M₁ PAM, DMPK studies were employed to assess its pharmacology profile in rodents and nonhuman primates. *In vitro* studies predicted VU0486846 to be low to moderately cleared compound in human and rat liver microsomes with attractive fraction unbound in plasma and rat brain homogenate (**Table 2.5A**). On the other hand, predicted clearance in cynomolgus (cyno) monkeys was high with a low fraction unbound in plasma. Cytochrome P450 (CYP₄₅₀) enzyme inhibition was also assessed against CYP 3A4, 1A2, 2C9, and 2D6, as these four enzymes are involved in approximately 90% of phase one metabolism of marketed drugs (**Table 2.5B**). The overall CYP₄₅₀ profile was acceptable for a tool compound. Unfortunately, inhibition of 3A4 precluded VU0486846 from advancing as a putative clinical candidate. With a suitable *in vitro* profile, the DMPK properties of VU0486846 were further evaluated in *in vivo* systems (**Table 2.5C**). A lack of *in vitro:in vivo* correlation (IVIVC) was observed in a standard PK IV/PO cross over study in rats,

reporting a high clearance value of 89 mL/min/kg *in vivo*. VU0486846 also displayed a 1.2 hour half-life ($t_{1/2}$), an acceptable volume of distribution (V_{ss}), and exceptional

A.					B.			
Species	CL _{INT} (mL/min/kg)	CL _{HEP} (mL/min/kg)	PPB (f _u)	BHB (f _u)	CYP ₄₅₀ IC ₅₀ (μM)			
					3A4	1A2	2C9	2D6
Human	23	11	0.12	-	5	>30	18.8	29.8
Rat	36	24	0.11	0.03				
Cyno	1389	43	0.02	-				

C.						
Species	CL _p (mL/min/kg)	t _{1/2} (hrs)	V _{ss} (L/kg)	%F	K _p	K _{p,uu}
Rat	89	1.2	1.8	96	0.18	0.05
Mouse	-	-	-	-	0.67	0.17
Cyno	18	4.2	1.0	37	-	-

Table 2.5 A) *in vitro* DMPK profile for human, rat and, cynomolgus (cyno) monkey, B) Inhibition of common CYP₄₅₀ enzymes involved in drug metabolism, C) *in vivo* DMPK profile in rat, mouse, and cyno monkey.

bioavailability (%F) in rat. The cyno monkey PK profile was more balanced and favorable, with a longer half-life of 4.2 hours, a moderate clearance, good volume of distribution, and decent bioavailability. Finally, the CNS penetration of VU0486846 was evaluated prior to adverse effects and seizure liability testing.

As seen with previous (1*S*,2*S*)-2-aminocyclohexan-1-ol amide containing M₁ PAMs, CNS exposure varied across rodent species (K_p and K_{p,uu}). Despite the variance in CNS penetration among species, VU0486846 possesses a favorable central nervous system multiparameter optimization (CNS MPO) score (>5). The CNS MPO is a desirability tool utilizing six important physiochemical parameters when evaluating small molecules for therapeutic applications: calculated partition coefficient (ClogP), calculated distribution coefficient at pH 7.4 (ClogD), molecular weight (MW), topological

polar surface area (TPSA), number of hydrogen-bond donors (HBDs), and most basic center (pKa). A good CNS MPO value is defined as >4 on a 0-6 scale. Therefore, based on its CNS MPO score, VU0486846 has a higher probability of crossing the blood-brain-barrier (BBB). In addition, VU0486846 is not a substrate recognized by human P-glycoprotein 1 (MDCK Efflux Ratio = 0.9, $P_{app} = 30 \times 10^{-6}$ cm/s), an ATP-dependent efflux pump designed to expel foreign substances from cells located in the BBB. Therefore, these data predict brain penetration of VU0486846 in animal behavior models.

Next, VU0486846 was heavily tested for agonists activity and adverse effects before being subjected to behavioral assays. Unlike Pfizer and Merck M₁ PAMs, VU0486846 show no interaction with the orthosteric site (**Figure 2.13A**). Pfizer and Merck compounds with reported adverse effect liability show weak to significant displacement of [³H]-NMS binding and in some cases are shown to possess negative cooperativity. We believe that this overlap, and therefore dual mode of activation, causes overstimulation of the M₁ receptor, which results in cholinergic toxicity and adverse events limiting its procognitive effects and therapeutic utility.

While VU0486846 displays weak, micromolar agonist activity in our high expression cell lines (M₁ = 4.5 μM), electrophysiological data in prefrontal cortex (PFC) brain tissue exhibits no long-term depression (LTD), indicating that VU0486846 does not elicit agonist activity when administered on its own (**Figure 2.13B**). As a control, a separate experiment was run in PFC brain tissue using 3μM of OxoM, a selective muscarinic agonist. **Figure 2.13C** illustrates the significant change in field excitatory

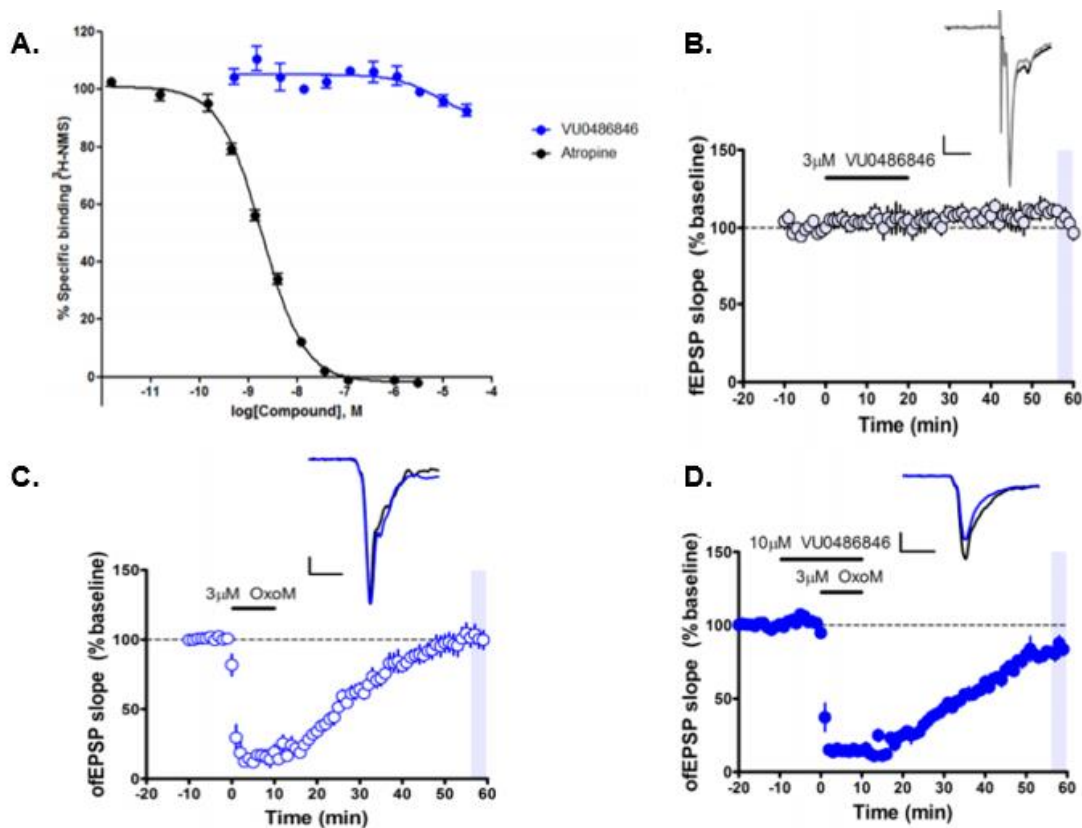


Figure 2.13 A) Competition binding assay displaying no interactions of VU0486846 with the orthosteric site, B) VU0486846 does not induce LTD in PFC brain tissue, C) Muscarinic agonist, OxoM, induces LTD in PFC brain tissue, D) Co-application of VU0486846 significantly enhances LTD observed in native brain tissue.

post synaptic potentials (fEPSPs), demonstrating agonist activity. In addition, as can be seen in **Figure 2.13D**, co-application of 10 μM VU0486846 + 3 μM OxoM significantly enhanced the magnitude of LTD compared to 3 μM OxoM on its own. Therefore, VU0486846 displays no agonist activity alone. However, it can potentiate the effects of muscarinic agonists. The ability for VU0486846 to potentiate the effects of a muscarinic agonist, acts as a proof of concept for the utility as an *in vivo* PAM to assess its procognitive effects in rodent models.

In addition to *in vitro* studies, VU0486846 was tested in a high dose (100 mg/kg intraperitoneal (i.p.)) phenotypic mouse screen to assess seizure liability. The scale by

which the seizure activity will be measured is known as the Racine scale, where a score of zero represents no change in behavior and a score of five represents generalized clonic activity that can often be severe enough to be fatal. At a 100mg/kg dose,

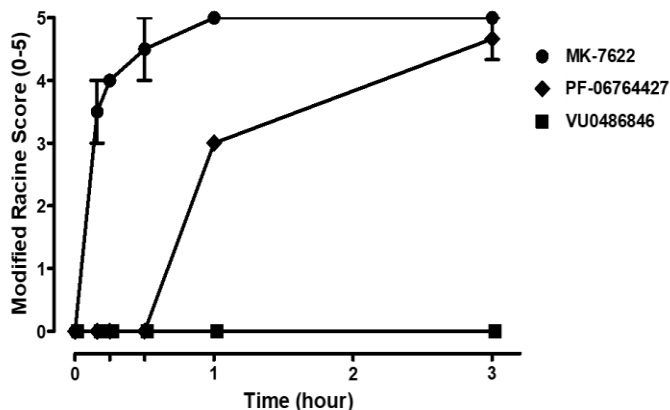


Figure 2.14 The Racine Scale is a phenotypic measurement of seizure activity. At a 100mg/kg dose, VU846 displayed no seizure activity, while MK-7622 and PF-06764427 both displayed a 4/5 on the Racine Scale. Seizure activity with MK-7622 began immediately after administration and PF-06765527 began 60-minutes post administration with both lasting the duration of the 3 hour experiment.

VU0486846 displayed no seizure activity in mice up to 3 hours, while Merck (MK-7622) and Pfizer (PF-06764427) compounds both exhibited a 4/5 on the Racine scale (**Figure 2.14**). Seizure activity with MK-7622 began immediately after administration and PF-06765527 began 60-minutes post administration, with both lasting the duration of the 3-hour experiment. In addition to seizure liability, VU0486846 was also monitored for any other somatomotor or autonomic nervous system adverse effects (**Table 2.6**). A modified Irwin Toxicology Battery test in mice revealed that pre-treatment of VU0486846, reaching plasma levels of 18.2 μ M, did not cause any other significantly observable adverse effects.

	VU0486846 (100 mg/kg)				
Time (min):	15	30	60	120	180
Autonomic Nervous System					
Ptosis	-	-	-	-	-
Exophthalmos	-	-	-	-	-
Miosis	-	-	-	-	-
Mydriasis	-	-	-	-	-
Corneal reflex loss	-	-	-	-	-
Pinna reflex loss	-	-	+	+	-
Piloerection	-	++	++	++	++
Respiratory rate	-	-	-	-	-
Writhing	-	-	-	-	-
Tail erection	-	-	-	-	-
Lacrimation	-	-	-	-	-
Defecation	-	-	-	-	-
Salivation	-	-	-	-	-
Vasodilation	-	-	-	-	-
Skin color	-	-	-	-	-
Irritability	-	-	-	-	-
Somatomotor Systems					
Motor Activity	-	-	-	-	-
Convulsions	-	-	-	-	-
Arch/roll	-	-	-	-	-
Tremors	-	-	-	-	-
Leg weakness	-	-	-	-	-
Rigid stance	-	-	-	-	-
Spraddle	-	-	-	-	-
Placing loss	-	-	-	-	-
Grasping loss	-	-	-	-	-
Righting loss	-	-	-	-	-
Catalepsy	-	-	-	-	-
Tail pinch	-	-	-	-	-
Escape loss	-	-	-	-	-

Table 2.6 Modified Irwin Toxicology Battery test in mice was used to assess any potential adverse effects of VU0486846 on the CNS.

An *in vivo* non-human primate study was also attempted to assess adverse effect liabilities. However, physiochemical properties of VU0486846 did not allow for higher dose formulations and precluded definitive data. Nevertheless, we were able to achieve roughly 2 μ M total plasma levels in non-human primates without observing any adverse effects. Thus, VU0486846 was confirmed as a pure PAM, devoid of agonist activity and adverse effects, with good CNS penetration and an attractive DMPK profile. With VU0486846 deemed an acceptable *in vivo* tool compound by our standards, it was advanced into behavioral pharmacology assays for further evaluation.

Behavioral Pharmacology of VU0486846

After being fully vetted, VU0486846 was subjected to behavioral testing in rodent models of cognition. A novel object recognition (NOR) paradigm was utilized to evaluate recognition memory in rats. The NOR task assesses the rat's ability to recognize a novel object with respect to a familiar object within its environment. Rats were pretreated with vehicle or 1, 3, and 10 mg/kg of VU0486846 (i.p., 10% Tween 80 in water) 30 minutes prior to exposure to two identical objects. The rats were then allowed to explore the objects for 10 minutes before being removed from the arena. Twenty-four hours later, the rats were reintroduced to the arena where one of the identical objects was replaced by a novel one. The time spent exploring each object was calculated as [(time spent exploring novel object) – (time spent exploring familiar object)]/total time exploring objects to provide a recognition index value. Excitingly, VU0486846 was observed to dose-dependently enhance recognition index in rats, with a minimum efficacious dose of 3 mg/kg i.p. ($n = 12$; $p = 0.0133$)(**Figure 2.15A**).⁵³ VU0486846

displaying robust procognitive activity in the NOR paradigm suggests it could prove efficacious in other models of cognition.

Briefly mentioned earlier, the cognitive symptoms of schizophrenia are another large unmet need in the neuroscience community. Furthermore, primary treatment of

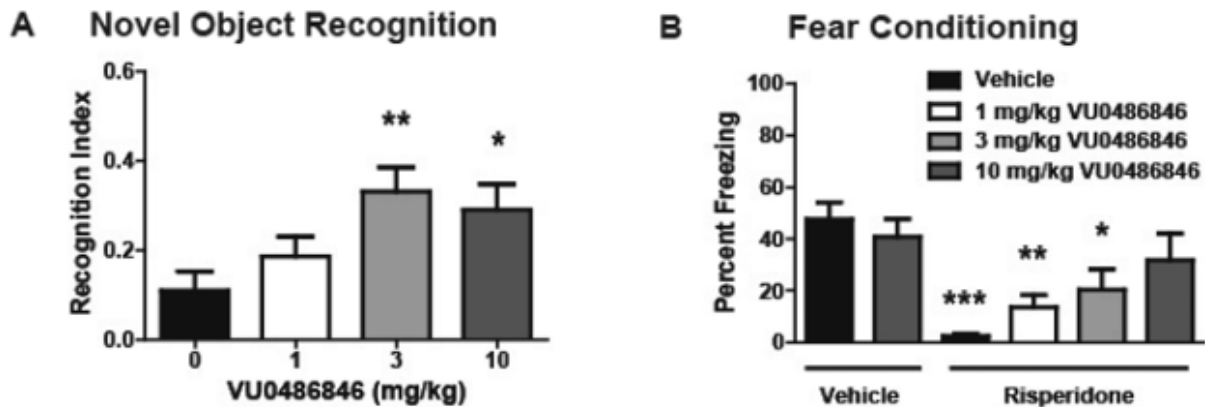


Figure 2.15 A) VU0486846 displays robust procognitive activity in rodent novel object recognition paradigm, B) VU0486846 also reverses risperidone induced cognitive deficits in a rodent fear conditioning paradigm.

the positive symptoms (hallucinations, delusions, agitated body movements, and dysfunctional ways of thinking) of schizophrenia, such as risperidone, are known to elicit added cognitive dysfunction. To measure the effects of VU0486846 in the context of a drug induced cognitive deficit, a contextual fear conditioning paradigm was employed in rats. The rats were pretreated with vehicle, risperidone by itself, or risperidone co-administered with 1, 3, and 10 mg/kg of VU0486846 thirty minutes prior to placing them in a sound-attenuating conditioning chamber. The rats were given three shock-tone pairing trials and then returned to their home cages. Twenty-four hours later, acquisition of fear conditioning was assessed in the same environment by measuring freezing behavior sans shock stimuli. **Figure 2.15B** displays, for the first time, the ability for an M₁ PAM to reverse the cognitive deficits induced by the antipsychotic risperidone ($n =$

11-13; $p < 0.0001$) with a 1 mg/kg minimum effective dose. When 3 mg/kg of risperidone is co-administered with 10 mg/kg VU0486846, conditioned freezing was restored to vehicle-treated control levels. This data suggests that a pure M_1 PAM could be co-administered with atypical antipsychotics in schizophrenic patients to ameliorate their existing cognitive impairments in addition to the drug induced cognitive deficits.

In summary, we provided the scientific community with a novel M_1 PAM with enhanced potency, physiochemical properties, and DMPK profile. VU0486846 is a highly selective, pure M_1 PAM, devoid of agonist activity in native tissues and adverse effects across species. VU0486846 also displays robust procognitive activity in rodent models of cognition, thus affording the best-in-class M_1 PAM tool compound for investigating neurological processes.

Challenging the Intramolecular Hydrogen Bond Theory: Analogs 2.47-2.82

Perhaps the most interesting finding in the benzomorpholine series from an SAR standpoint was the discovery that the des-oxy tetrahydroquinoline analog (**2.47**; M_1 $EC_{50} = 1.4 \mu M$, 75 ACh Max) was virtually equipotent to VU0484043, indicating that the putative IMHB of previous M_1 PAMs may not be a key pharmacophore in this series

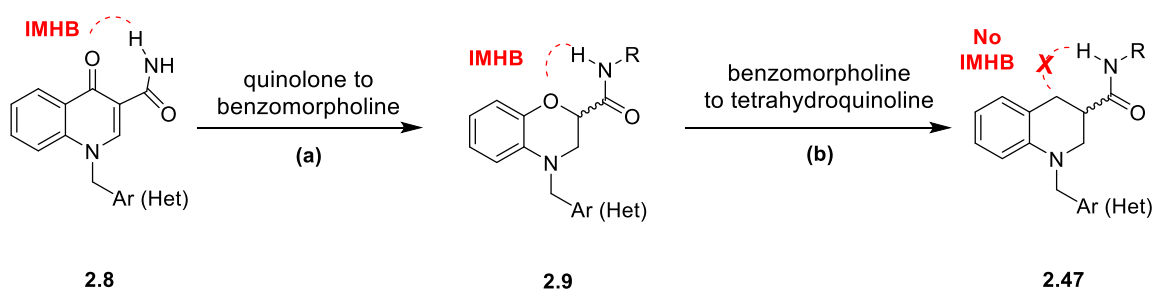
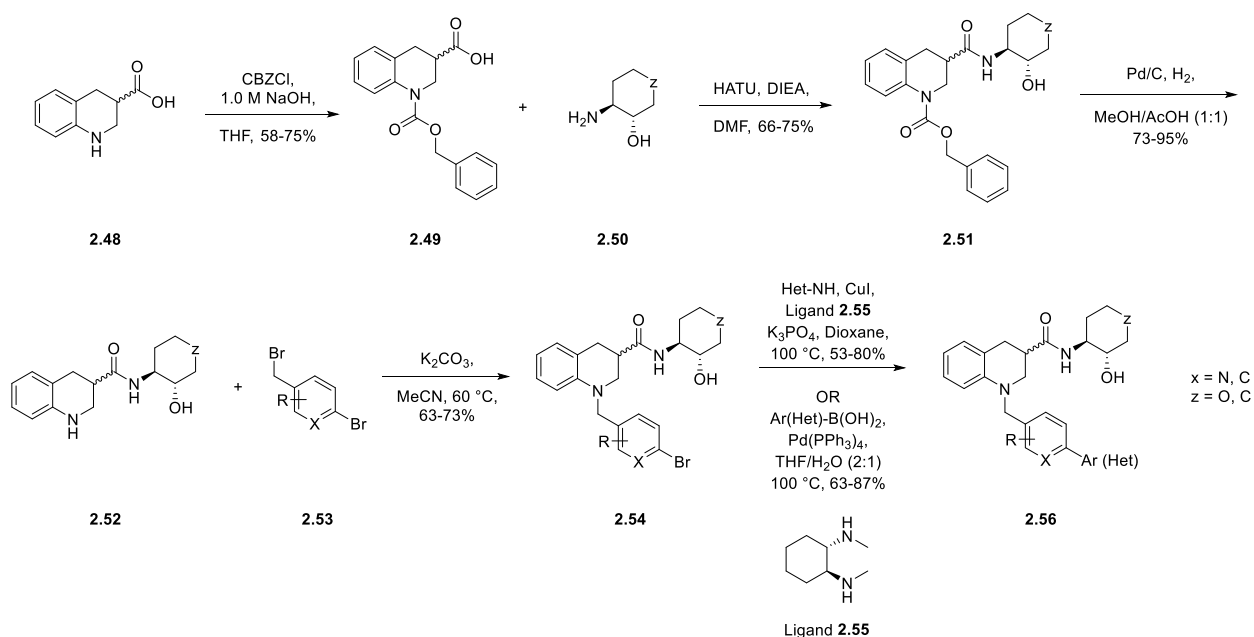


Figure 2.16 Scaffold hopping from quinolone core to a benzomorpholine cored and finally to a tetrahydroquinoline core.

(Figure 2.16). To investigate this further, we elected to do a small, targeted SAR campaign around the new tetrahydroquinoline core. To access these tetrahydroquinoline congeners, the synthetic route highlighted in **Scheme 2.2** was developed. First, commercially available 1,2,3,4-tetrahydroquinoline-3-carboxylic acid (**2.48**) was Cbz protected under mildly basic conditions. Next, carboxylic acid **2.49** and cyclohexylamine derivatives of **2.50** were connected via a HATU mediated amide

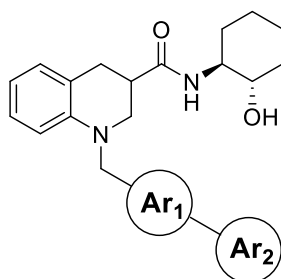


Scheme 2.2 Synthetic route to access tetrahydroquinoline analogs **2.57-2.92**.

coupling, followed by a subsequent palladium catalyzed Cbz deprotection to afford compound **2.52** as the free amine. **2.52** was then reacted with various benzyl bromides using standard S_N2 conditions to provide analogs of **2.54** in decent yields. Finally, **2.54** congeners were subjected to either a copper-mediated, Ullmann-like cross-coupling utilizing ligand **2.55** or a Suzuki cross-coupling using standard conditions to afford M₁ PAMs as the racemate for activity screening. The racemates were unable to be separated by flash column chromatography therefore, the racemic M₁ PAMs displaying

potency below 1.0 μM were resolved via SFC for further evaluation as a single diastereomer. With an optimized synthetic route in hand, we could begin making tetrahydroquinoline analogs.

In the attempt to drive down potency into the nanomolar range, we incorporated some of the most active southern aryl groups from our benzomorpholine series into our tetrahydroquinoline series. Analogs of this nature can be observed in **Table 2.7**. Several of these congeners were in the low micromolar range, however we were unable to drop



Ar ₁	Ar ₂	Compound Number	VOID	M ₁ EC ₅₀ (μM)	% ACh Max
		2.57	VU0516639	1.4	75
		2.58	VU6019905	2.0	77
		2.59	VU6021486	8.6	86
		2.60	VU6021490	8.2	56

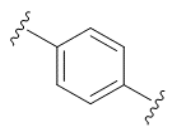
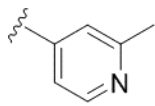
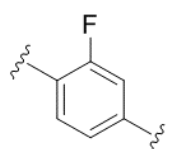
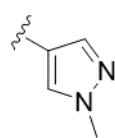
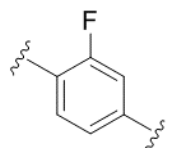
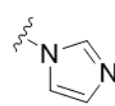
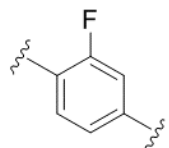
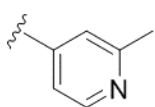
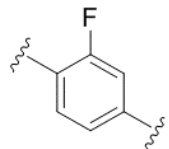
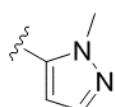
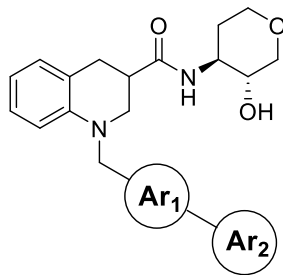
		2.61	VU6021494	3.0	82
		2.62	VU6019903	3.5	81
		2.63	VU6021478	5.2	83
		2.64	VU6021480	3.2	83
		2.65	VU6021482	8.5	86

Table 2.7 SAR around southern biaryl system with cyclohexanol amide – analogs **2.57-2.65**.

below 1.0 μM . Therefore, VU0516639 (**2.57**) remained the most active compound in this series. We knew from the benzomorpholine series that by replacing the aminocyclohexanol with an aminotetrahydropyranol we could improve potency thus, we employed the same strategy with the tetrahydroquinoline series (**Table 2.8**). Indeed, the tetrahydropyranol amide moiety displayed a great improvement in activity over the cyclohexanol amide. Congeners with potency less than 1.0 μM in addition to the parent molecules (**2.57** and **2.66**), were resolved via SFC and screened in our M_1 PAM assay as single diastereomers (**Table 2.9**). Congeners possessing the pyrazole connected



Ar ₁	Ar ₂	Compound Number	VOID	M ₁ EC ₅₀ (μM)	% ACh Max
		2.66	VU6018311	1.6	87
		2.67	VU6019904	0.89	75
		2.68	VU6021483	4.2	75
		2.69	VU6021484	1.3	80
		2.70	VU6021485	2.6	82
		2.71	VU6021489	1.1	80
		2.72	VU6018312	2.1	82

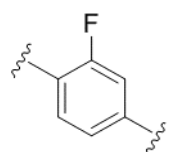
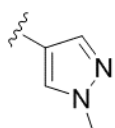
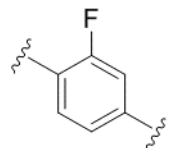
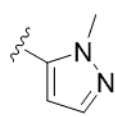
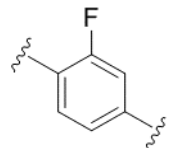
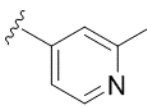
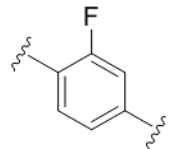
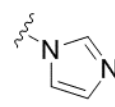
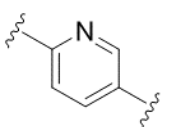
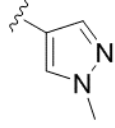
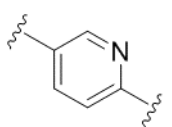
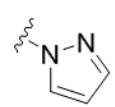
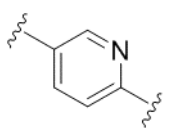
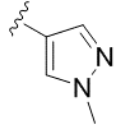
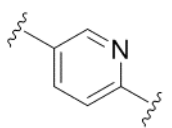
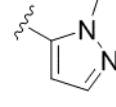
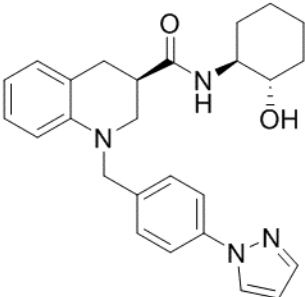
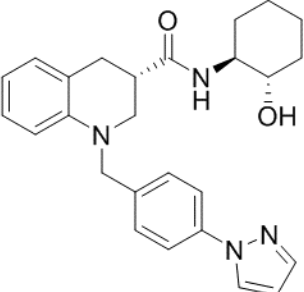
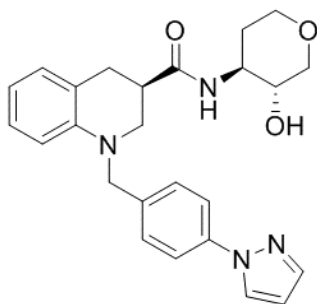
		2.73	VU6019900	0.89	75
		2.74	VU6019901	>10	77
		2.75	VU6021466	1.6	76
		2.76	VU6021467	2.7	80
		2.77	VU6019902	>10	76
		2.78	VU6021498	7.0	79
		2.79	VU6021510	0.71	68
		2.80	VU6021511	>10	67

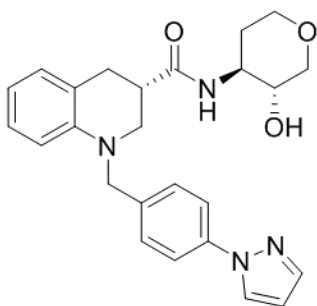
Table 2.8 SAR around southern biaryl system with tetrahydropyranol amide – analogs **2.66-2.80**.

through the nitrogen (**2.81-2.84**, **2.91** and **2.92**) exhibited decent potency hovering around a micromolar with **2.83** as an outlier showcasing an M₁ PAM EC₅₀ equaling roughly 330 nM. These analogs also showed an enantiomeric preference whereas interestingly, analogs containing the *N*-methyl pyrazole moiety (**2.85-2.90**) did not display an enantiomeric preference when tested as single diastereomers. However, they excitingly exhibited low hundred nanomolar potency and were therefore advanced further into DMPK studies.

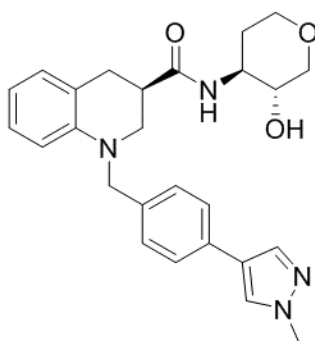
Compound ^a	Compound Number	VOID	M ₁ EC ₅₀ (μM)	% ACh Max	Agonist EC ₅₀ (μM)
	2.81	VU6029430	0.95	84	>10
	2.82	VU6029431	3.0	84	>10



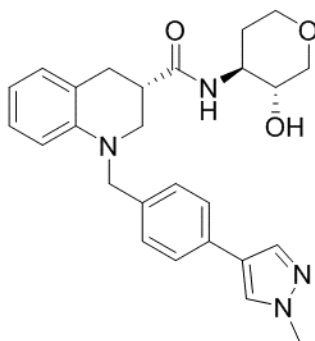
2.83 VU6024711 0.33 82 >10



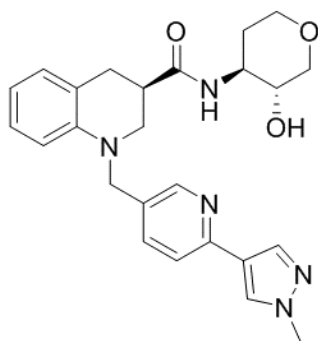
2.84 VU6024712 1.0 67 >10



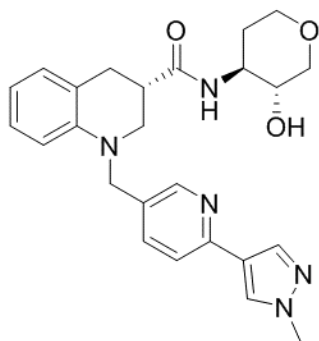
2.85 VU6024715 0.38 72 3.1



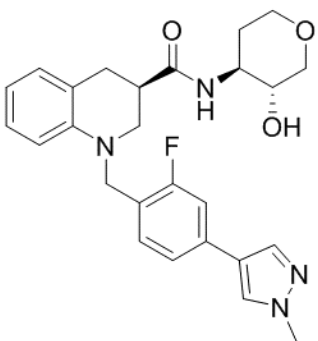
2.86 VU6024716 0.24 67 8.2



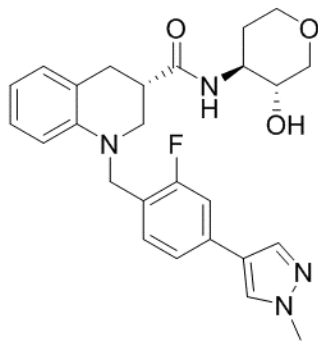
2.87 VU6024719 0.44 72 9.4



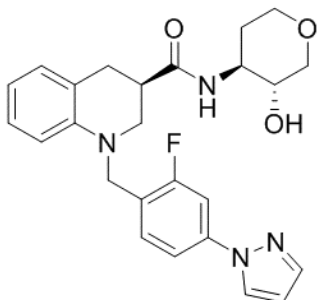
2.88 VU6024720 0.48 75 9.8



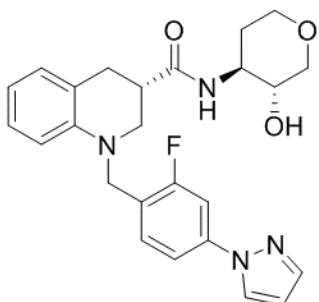
2.89 VU6024717 0.35 57 >10



2.90 VU6024718 0.39 67 7.8



2.91 VU6024713 1.2 77 >10



2.92 VU6024714 1.8 77 >10

Table 2.9 Structures and activity of single diastereomers – analogs **2.81-2.92**.

Compounds **2.85-2.90** were subjected to *in vitro* clearance (CL), plasma protein binding (PPB), and brain homogenate binding (BHB) assays in rat to determine whether they would be suitable for *in vivo* behavioral testing (**Table 2.10**). Compounds **2.86**, **2.89**, and **2.90** all suffer from high-hepatic clearance whereas **2.85**, **2.87**, and **2.88** exhibit a moderate clearance in both human and rat liver microsomes. Congeners **2.87** and **2.88** displayed the best overall PK profiles, yet were slightly less potent than we would like and therefore fell out of contention. Compound **2.85** was also not pursued, due to its significant agonist activity in our high expression cell lines. **2.89** has decent M₁ PAM activity and shows the least amount of agonist activity in our cell lines.

Compound Number	CL _{INT} Human	CL _{INT} Rat	CL _{HEP} Human	CL _{HEP} Rat	PPB (f _u) Human	PPB (f _u) Rat	BHB (f _u)
2.85	82	228	16.7	53.5	0.17	0.06	0.02
2.86	607	789	20.3	64.3	0.13	0.07	0.03
2.87	34	91	12.9	39.7	0.28	0.27	0.12
2.88	72	64	16.3	33.4	0.33	0.36	0.17
2.89	146	516	18.4	61.6	0.09	0.04	0.02
2.90	389	1423	19.9	66.7	0.09	0.04	0.02

Table 2.10 DMPK data for single diastereomers – analogs **2.85-2.2.90**.

Recognizing that the plasma protein binding of **2.89** was less than ideal in rat for *in vivo* behavioral studies, we decided to explore other options.

We decided to investigate the DMPK of **2.89** in mice to determine whether a mouse model would be a more appropriate choice for behavioral pharmacology assays. Plasma and brain exposure level studies of **2.89** in mouse after i.p. administration unfortunately revealed very low brain penetration and levels of drug unbound (**Table 2.11**). The low brain penetration observed is likely due to the tetrahydropyranol amide moiety, as diminution of brain penetration was also observed in the benzomorpholine

Compound Number	Dose (mg/kg)	Plasma (ng/mL)	Plasma Total (μM)	Plasma Free (nM)	Brain (ng/g)	Brain Total (μM)	Brain Free (nM)
2.89	3	569	1.22	42.9	21.3	0.05	0.73
	10	934	2.01	70.4	45.4	0.10	1.56

Table 2.11 CNS exposure of analog **2.89** in mice at 3 and 10 mg/kg doses.

series when the cyclohexanol amide was replaced with the tetrahydropyranol amide. *In vivo* studies were not pursued further, as our true purpose in this pursuit was to develop

a new hypothesis as to what is driving activity within this series if it isn't due to intramolecular hydrogen bonding.

The parent diastereomers VU6029430 (**2.81**) and VU6029431 (**2.82**) were revisited as they were the closest analogs to IMHB-containing compounds VU0486846 (**2.41**) and VU0486834 (**2.42**). Crystals were grown of both **2.81** and **2.82**. An X-Ray crystallography structure was only able to be obtained with compound **2.82**. **2.81** while crystalline, sadly did not produce crystals large and reflective enough to obtain a crystal structure. As can be seen in **Figure 2.17**, the crystal structure of **2.82** is completely

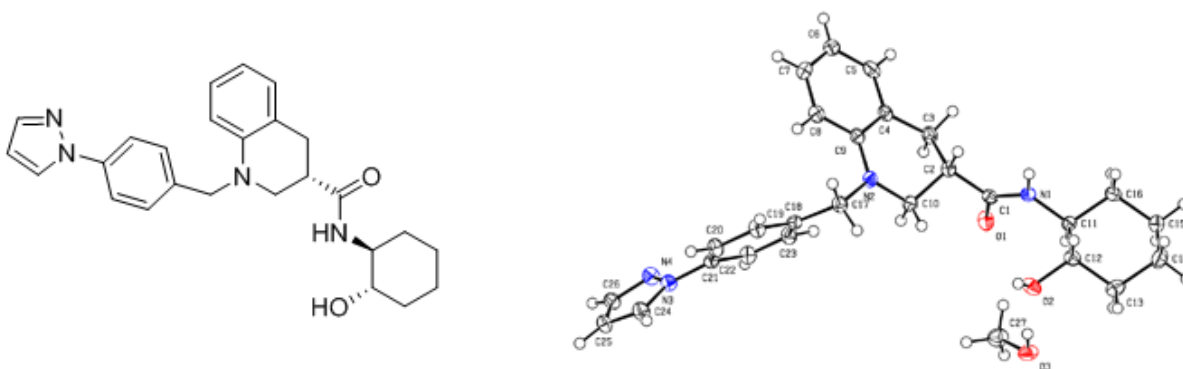


Figure 2.17 Structure and x-ray crystallography structure of VU6029431 (**2.82**). Structure courtesy of Nathan Schley.

extended. This could be due to the lack of an IMHB interaction or this could just be how the molecule is oriented in three-dimensional space. We hypothesize that the *S*-enantiomer is oriented in an extended, linear manner while the *R*-enantiomer has the cyclohexanol amide moiety folding back onto the molecule. To further support this hypothesis, we elected to do some computational modeling using the modeling software MOE (Molecular Operating Environment). Once the two diastereomers were built in MOE, their energies were minimized using default settings. **Figure 2.18A** depicts the

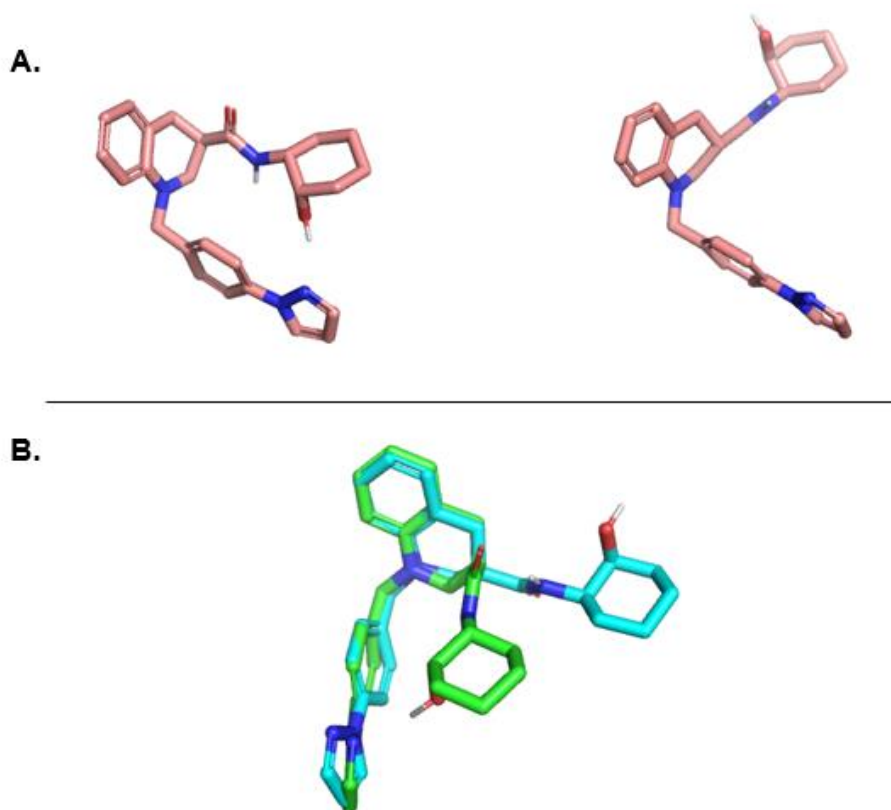


Figure 2.18 A) Computational modeling of single diastereomers VU6029430 and VU6029431, B) Computational modeling of overlaid single diastereomers VU6029430 and VU6029431.

computational prediction of how the two diastereomers exist in their lowest energetic state, with the *S*-enantiomer (**2.82**) predicted to display full extension of the cyclohexanol amide moiety, just as we confirmed with our X-Ray crystal structure. Therefore, we believe the conformational modeling is within reason and accurately depicts the lowest conformational state of both diastereomers. The *R*-configuration where the cyclohexanol amide folds back onto the molecule is the more active enantiomer in both the tetrahydroquinoline and benzomorpholine series. This leads us to believe that the IMHB is not what is driving activity in either of these series. Rather, we now believe it is a matter of how the M₁ PAMs are situated inside the allosteric

pocket. As depicted in **Figure 2.18B**, the two diastereomers are overlaid at its core, revealing a large difference in how the cyclohexanol amide sits in three-dimensional space. Therefore, it is possible that the fully extended diastereomer could potentially be clashing with certain residues within the pocket, whereas the compact, folded diastereomer fits in a manner that is conducive for potency. Efforts are currently underway in the laboratory of professor Arthur Christopoulos at Monash University to co-crystalize our M₁ PAM, VU0486846 in its M₁ allosteric site. This should give us a more complete picture as to what is driving activity within the series.

Conclusions

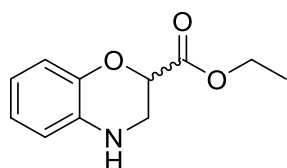
In summary, we scaffold hopped from Merck compound BQCA with the quinolone core to a benzomorpholine core, simultaneously adding a new chiral center and increasing sp³ character. Despite encountering steep SAR within this series, we managed to develop a potent and selective M₁ PAM, devoid of adverse effects that displays robust efficacy in rodent models of cognition.^{53,57} During our SAR campaign, we serendipitously discovered that in the absence of the IMHB, which we believed drove activity, was equally as active as VU0486846. Because of this, we chose to challenge the notion that an IMHB interaction is important for activity. A brief SAR campaign around the new tetrahydroquinoline core revealed that the IMHB is not crucial for activity, as we once believed. Instead, we now hypothesize that the more active diastereomer is resultant upon its compact conformation and the more elongated diastereomer is less active due to its possible clashing with amino acid residues within the active site.

Experimental Methods

General Synthetic Methods and Instrumentation

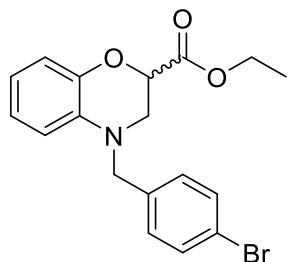
Unless otherwise stated, all reactions were conducted in flame-dried or oven-dried glassware under inert atmospheres of argon. All commercially available reagents and reaction solvents were used as received, unless otherwise noted. Reactions were conducted at room temperature (rt, approximately 23 °C) unless otherwise noted. All ¹H NMR and ¹³C NMR spectra were recorded on a Bruker AV-400 (400 MHz) or Bruker AV-NMR (600 MHz) instrument. Chemical shifts are reported in ppm relative to residual solvent peaks as an internal standard set to δ H 7.26 or δ C 77.0 (CDCl₃) and δ H 3.31 or δ C 49.0 (CD₃OD). Data are reported as follows: chemical shift, multiplicity (s = singlet, d = doublet, t = triplet, q = quartet, br = broad, m = multiplet), integration, and coupling constant (Hz). IR spectra were recorded as thin films and are reported in wavenumbers (cm⁻¹). Low resolution mass spectra were obtained on an Agilent 1200 LCMS with electrospray ionization. High resolution mass spectra were recorded on a Waters Qtof-API-US plus Acquity system. The value Δ is the error in the measurement (in ppm) given by the equation $\Delta = [(ME - MT)/MT] \times 106$, where ME is the experimental mass and MT is the theoretical mass. The HRMS results were obtained with ES as the ion source and leucine enkephalin as the reference. Optical rotations were measured on a PerkinElmer-341 polarimeter. Analytical thin layer chromatography was performed on 250 μ M silica gel 60 F254 plates. Visualization was accomplished with UV light, and/or the use of ninhydrin, anisaldehyde and ceric ammonium molybdate solutions followed by charring on a hot-plate. Chromatography on silica gel was performed using Silica Gel 60 (230–400 mesh) from Sorbent Technologies. Analytical

HPLC was performed on an Agilent 1200 analytical LCMS with UV detection at 214 and 254 nm along with ELSD detection. Solvents for extraction, washing, and chromatography were HPLC grade. All reagents were purchased from Aldrich Chemical Co. and were used without purification. All polymer-supported reagents were purchased from Biotage, Inc. Flame-dried (under vacuum) glassware was used for all reactions. All reagents and solvents were commercial grade and purified prior to use when necessary. High-resolution mass spectrometry (HRMS) data were obtained using a Micromass Q-ToF API-US mass spectrometer.



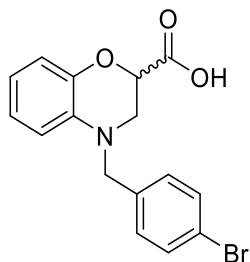
Synthesis of Ethyl 3,4-Dihydro-2H-1,4-benzoxazine-2-carboxylate

A solution of 2-aminophenol (1.0 eq), potassium carbonate (2.5 eq), ethyl 2,3-dibromopropionate (1.05 eq), and acetonitrile (0.2M) was heated to 80 °C and was allowed to stir for 16 hrs. The reaction was diluted with H₂O and extracted with EtOAc (3x). The layers were separated, and the organic phases were combined, washed with brine (1x), dried with MgSO₄, filtered, and concentrated in vacuo. Crude product was purified by flash chromatography (Teledyne ISCO Combi-Flash system, 0–30% EtOAc in hexanes) to provide a brown oil (73% yield). ¹H NMR (400 MHz, CDCl₃) δ 6.93 (dd, J = 7.92 Hz, 1.4 Hz, 1H), 6.79 (td, J = 7.5 Hz, 1.4 Hz, 1H), 6.72 (td, J = 7.6 Hz, 1.6 Hz, 1H), 6.61 (dd, J = 7.7 Hz, 1.6 Hz, 1H), 4.81–4.79 (m, 1H), 4.26 (m, 2H), 3.63–3.55 (m, 2H), 1.28 (t, J = 7.2, 3H). ¹³C NMR (100 MHz, CDCl₃) δ 169.4, 142.9, 132.6, 121.6, 119.5, 116.9, 115.7, 72.7, 61.5, 42.6, 14.1 ppm. HRMS (TOF, ES⁺) calculated for C₁₁H₁₃NO₃ m/z: 207.0895; found, 207.0892.



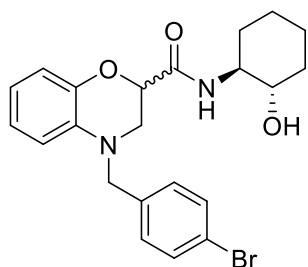
Synthesis of Ethyl 4-[(4-Bromophenyl)methyl]-2,3-dihydro-1,4-benzoxazine-2-carboxylate

A solution of ethyl 3,4-dihydro-2H-benzo[b]-[1,4]oxazine-2-carboxylate (1.0 eq), potassium carbonate (1.1 eq), 4-bromobenzyl bromide (1.1 eq), and acetonitrile (0.55M) was heated to 80 °C and allowed to stir for 16 h. The reaction was diluted with H₂O and extracted with EtOAc (3x). The layers were separated, and the organic phases were combined, washed with brine, dried over MgSO₄, filtered, and concentrated *in vacuo*. Crude product was purified using flash chromatography (Teledyne ISCO Combi-Flash system 0–40% EtOAc in hexanes) to provide an off-white solid (2935 mg, 7.80 mmol, 74% yield). ¹H NMR (400 MHz, CDCl₃) δ 7.45 (d, J = 8.4 Hz, 2H), 7.14 (d, J = 8.3 Hz, 2H), 6.97 (dd, J = 7.9 Hz, 1.5 Hz, 1H), 6.80 (td, J = 7.7 Hz, 1.5 Hz, 1H), 6.72 (td, J = 7.6 Hz, 1.4 Hz, 1H), 6.61 (dd, J = 8.0 Hz, 1.3 Hz, 1H), 4.83 (t, J = 4.0 Hz, 1H), 4.45–4.17 (m, 4H), 3.51 (d, J = 4.1 Hz, 2H), 1.25 (t, J = 7.1 Hz, 3H). ¹³C NMR (100 MHz, CDCl₃) δ 169.2, 142.9, 136.7, 134.4, 131.7, 128.7, 121.8, 121.0, 119.0, 116.6, 112.8, 72.5, 61.6, 54.4, 48.6, 14.1 ppm. HRMS (TOF, ES⁺) calculated for C₁₈H₁₈BrNO₃ m/z: 375.0470; found, 375.0467.



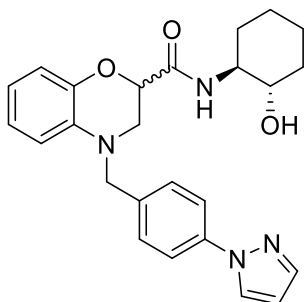
Synthesis of 4-[(4-Bromophenyl)methyl]-2,3-dihydro-1,4-benzoxazine-2-carboxylic acid

A solution of ethyl 4-[(4-bromophenyl)methyl]-2,3-dihydro-1,4-benzoxazine-2-carboxylate (1.0 eq), potassium hydroxide (3.0 eq), THF/H₂O (2:1) was heated to 60 °C and allowed to stir for 3 h. The reaction was diluted in H₂O, acidified to pH = 3, extracted with EtOAc (3x), and concentrated *in vacuo* to afford the desired material, which was carried forward to the next step without any further purification (2715 mg, quantitative yield). ¹H NMR (400 MHz, CDCl₃) δ 7.40 (d, J = 8.3 Hz, 2H), 7.13 (d, J = 8.2 Hz, 2H), 6.96 (dd, J = 7.8 Hz, 1.4 Hz, 1H), 6.82 (td, J = 8.0 Hz, 1.4 Hz, 1H), 6.73 (td, J = 7.4 Hz, 1.4 Hz, 1H), 6.63 (dd, J = 8.0 Hz, 1.1 Hz, 1H), 4.90 (t, J = 3.8, 1H), 4.44–4.28 (m, 2H), 3.52 (d, J = 3.80 Hz, 2H). ¹³C NMR (100 MHz, CDCl₃) δ 174.4, 142.7, 136.5, 134.5, 131.9, 129.0, 122.3, 121.3, 119.4, 116.8, 113.2, 72.4, 54.6, 48.4 ppm. HRMS (TOF, ES⁺) calculated for C₁₆H₁₄BrNO₃ m/z: 347.0157; found, 347.0150.



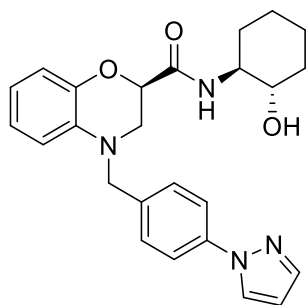
Synthesis of 4-[(4-Bromophenyl)methyl]-N-[(1S,2S)-2-hydroxycyclohexyl]-2,3-dihydro-1,4-benzoxazine-2 carboxamide

A solution of 4-[(4-bromophenyl)methyl]-2,3-dihydro-1,4-benzoxazine-2-carboxylic acid (1.0 eq), *N,N*-diisopropylethylamine (4.0 eq), HATU (1.1 eq), and DMF (0.2M) was pre-stirred for 10 min, to which was then added (1*S*,2*S*)-2-aminocyclohexanol (1.1 eq) and the reaction was allowed to stir for 12 h. The reaction was diluted with H₂O and extracted with EtOAc (3x). The layers were separated and the combined organics were washed with brine, dried over MgSO₄, filtered, and concentrated *in vacuo*. Crude product was purified using flash chromatography (Teledyne ISCO Combi-Flashsystem, 0–5% MeOH in DCM) to provide an off- white solid (2785 mg, 6.2535 mmol, 80% yield, 8:1 dr). ¹H NMR (400 MHz, CDCl₃) δ 7.44 (d, *J* = 8.3 Hz, 2H), 7.16 (d, *J* = 8.3 Hz, 2H), 6.92 (dd, *J* = 7.9 Hz, 1.3 Hz, 1H), 6.83 (td, *J* = 7.7 Hz, 1.3 Hz, 1H), 6.70 (td, *J* = 7.7 Hz, 1.2 Hz, 1H), 6.63 (dd, *J* = 8.1 Hz, 1.1 Hz, 1H), 6.50 (d, *J* = 7.4 Hz, 1H), 4.72 (dd, *J* = 6.7 Hz, 2.9 Hz, 1H), 4.43–4.42 (m, 2H), 3.72–3.63 (m, 1H), 3.59 (dd, *J* = 11.9 Hz, 3.0 Hz, 1H), 3.51–3.46 (m, 1H), 3.28–3.23 (m, 1H), 2.06–1.97 (m, 2H), 1.77–1.69 (m, 2H), 1.38–1.17 (m, 5H). ¹³C NMR (100 MHz, CDCl₃) δ 170.2, 141.9, 136.5, 134.8, 131.8, 128.8, 122.6, 121.0, 118.6, 116.3, 113.2, 74.9, 73.8, 55.5, 54.7, 49.0, 34.1, 31.2, 24.4, 23.8 ppm. HRMS (TOF, ES⁺) calculated for C₂₂H₂₅BrN₂O₃ *m/z*: 444.1049; found, 444.1048.



Synthesis of *N*-[(1*S*,2*S*)-2-Hydroxycyclohexyl]-4-[(4-pyrazol-1-ylphenyl)-methyl]-2,3-dihydro-1,4-benzoxazine-2-carboxamide

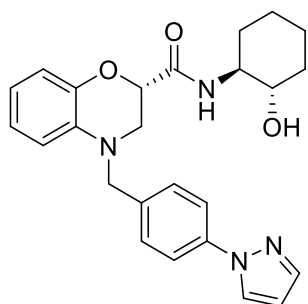
A degassed solution of 4-[(4-bromophenyl)methyl]-*N*-[(1*S*,2*S*)-2-hydroxycyclohexyl]-2,3-dihydro-1,4-benzoxazine-2-carboxamide (1.0 eq), pyrazole (1.1 eq), potassium phosphate (2.0 eq), copper(I) iodide (1.0 eq), *trans*-*N,N*-dimethylcyclohexane-2-diamine (1 eq), and 1,4-dioxane (0.2 M) was heated to 100 °C and was allowed to stir for 24 h. The reaction was diluted in H₂O and extracted with EtOAc (3x). The layers were separated, and the organic phases were combined, washed with saturated NH₄Cl (3x) and saturated brine, dried over MgSO₄, filtered, and concentrated *in vacuo*. Crude product was purified using flash chromatography (Teledyne ISCO Combi-Flash system, 0–60% EtOAc in hexanes) to afford two diastereomers, peak 1 and peak 2.



Synthesis of (2*R*)-*N*-[(1*S*,2*S*)-2-Hydroxycyclohexyl]-4-[(4-pyrazol-1-ylphenyl)-methyl]-2,3-dihydro-1,4-benzoxazine-2-carboxamide

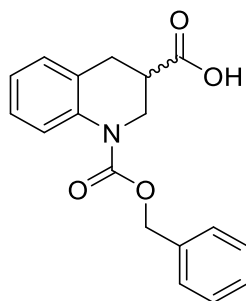
Peak 1. White solid (219 mg, 0.506 mmol, 25% yield). $[\alpha]_D^{21} +58.571$ ($c = 0.91$, MeOH). ¹H NMR (400 MHz, CDCl₃) δ 7.89 (d, $J = 2.3$ Hz, 1H), 7.70 (d, $J = 1.2$ Hz, 1H), 7.64 (d, $J = 8.5$ Hz, 2H), 7.36 (d, $J = 8.4$ Hz, 2H), 6.91 (dd, $J = 8.2$ Hz, 1.0 Hz, 1H), 6.84 (td, $J = 8.2$ Hz, 1.2 Hz, 1H), 6.73–6.68 (m, 2H), 6.52 (d, $J = 7.5$ Hz, 1H), 6.44 (t, $J = 2.0$ Hz, 1H), 4.73 (dd, $J = 6.7$ Hz, 2.9 Hz, 1H), 4.51–4.40 (m, 2H), 3.73–3.61 (m, 2H), 3.53–3.39 (m, 1H), 3.30–3.24 (m, 1H), 2.01 (d, $J = 10.9$ Hz, 2H), 1.76–1.68 (m, 2H), 1.38–1.20 (m, 5H). ¹³C NMR (100 MHz, CDCl₃) δ 170.3, 142.0, 140.9, 139.4, 135.7, 134.9, 128.1, 126.7, 122.6, 119.5, 118.5, 116.2, 113.3, 107.5, 74.8, 73.8, 55.5, 54.8, 49.0, 34.1, 31.2,

24.4, 23.8 ppm. HRMS (TOF, ES+) calculated for C₂₅H₂₈N₄O₃, 432.2161; found, 432.2161.



Synthesis of (2S)-N-[(1S,2S)-2-Hydroxycyclohexyl]-4-[(4-pyrazol-1-ylphenyl)-methyl]-2,3-dihydro-1,4-benzoxazine-2-carboxamide

Peak 1. Off-white solid. (19% yield). $[\alpha]_D^{22}$ -1.92 (c = 1.26, MeOH). ¹H NMR (400 MHz, CDCl₃) δ 7.90 (d, J = 2.5 Hz, 1H), 7.71 (d, J = 1.7 Hz, 1H), 7.64 (d, J = 8.5 Hz, 2H), 7.36 (d, J = 8.3 Hz, 2H), 6.93 (dd, J = 7.9, 1.5 Hz, 1H), 6.84 (td, J = 7.7, 1.5 Hz, 1H), 6.70 (t, J = 7.7 Hz, 2H), 6.58 (d, J = 7.6 Hz, 1H), 6.46 (t, J = 2.1 Hz, 1H), 4.76 (dd, J = 7.2, 2.9 Hz, 1H), 4.54 – 4.40 (m, 2H), 3.73 – 3.60 (m, 2H), 3.51 – 3.35 (m, 2H), 2.13 – 2.04 (m, 1H), 1.92 – 1.82 (m, 1H), 1.79 – 1.65 (m, 2H), 1.43 – 1.14 (m, 5H). ¹³C NMR (100 MHz, CDCl₃) δ 170.5, 142.2, 141.2, 139.6, 136.1, 135.0, 128.3, 126.9, 122.8, 119.7, 118.7, 116.6, 113.4, 107.7, 75.2, 73.8, 55.8, 55.0, 49.2, 34.6, 31.5, 24.6, 24.1. LC-MS (m/z + H) = 433.0.

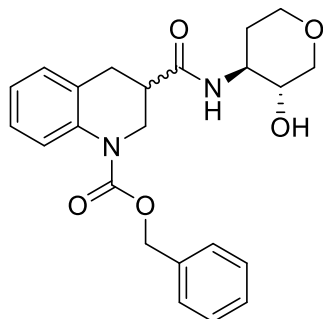


Synthesis of 1-benzoyloxycarbonyl-3,4-dihydro-2H-quinoline-3-carboxylic acid

A solution of 1-azatetralin-3-carboxylic acid (1.0 eq), 1.0 M sodium hydroxide (3.0 eq), and benzyl chloroformate (1.2 eq) in THF (0.25M) was stirred for 5 h. Upon completion the reaction mixture was acidified to pH = 3 and extracted with EtOAc (3x). Combined organics were dried over MgSO₄, filtered, and concentrated *in vacuo*. The crude material was purified via flash chromatography (Teledyne ISCO system, silica gel column, Hexanes:EtOAc) to provide the desired product as white solid (75% yield). ¹H NMR (400 MHz, (CD₃)₂SO) δ 7.63 (d, *J* = 8.1 Hz, 1H), 7.45-7.30 (m, 5H), 7.19-7.10 (m, 2H), 7.01 (t, *J* = 7.3 Hz, 1H), 5.18 (dd, *J* = 14.2, 12.8 Hz, 2H), 4.04 (dd, *J* = 12.6, 3.9 Hz, 1H), 3.77 (dd, *J* = 13.0, 6.8 Hz, 1H), 3.05-2.89 (m, 3H). ¹³C NMR (100 MHz, (CD₃)₂SO) δ = 173.9, 153.9, 137.5, 136.4, 128.9, 128.5, 128.1, 128.0, 127.8, 125.9, 123.7, 123.3, 67.0, 45.5, 38.7, 29.1. HRMS (TOF, ES+) calculated for C₁₈H₁₇NO₄ *m/z*: 311.1156; found, 311.1156.

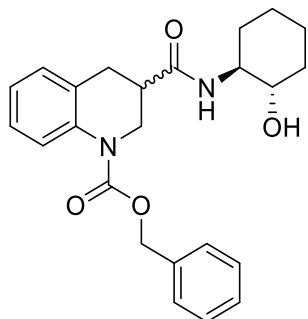
General Procedure 1: Synthesis of Amides

A solution of *N,N*-Diisopropylethylamine (4.0 eq), 1-benzyloxycarbonyl-3,4-dihydro-2H-quinoline-3-carboxylic acid (1.0 eq), HATU (1.1 eq) in DMF (0.2M) was pre-stirred for 30 min. The appropriate amine (1.1 eq) was then added and allowed to stir for an additional 3 h. Upon completion the reaction mixture was diluted with H₂O, and extracted with EtOAc (3x). The combined organics were dried over MgSO₄, filtered, concentrated *in vacuo*.



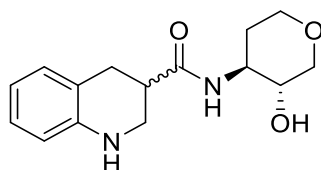
benzyl 3-[[[(3R,4S)-3-hydroxytetrahydropyran-4-yl]carbamoyl]-3,4-dihydro-2H-quinoline-1-carboxylate

This compound was synthesized according to general procedure 1. Crude product was purified via reverse phase chromatography (Gilson system, 50 x 30 mm, acetonitrile/0.1% TFA in H₂O). The desired fractions were dissolved in DCM and washed with saturated NaHCO₃ to liberate the desired product as the free base. White solid (75% yield). ¹H NMR (600 MHz, (CD₃)₂SO) δ 8.03 (t, *J* = 5.0 Hz, 1H), 7.62 (d, *J* = 4.2 Hz, 1H), 7.42-7.37 (m, 4H), 7.33 (tt, *J* = 4.6, 1.1 Hz, 1H), 7.12 (d, *J* = 5.0 Hz, 1H), 7.14 (tt, *J* = 5.1, 1.3 Hz, 1H), 7.02 (tt, *J* = 5.0, 0.9 Hz, 1H), 5.21-5.16 (m, 2H), 4.13-4.3.96 (m, 1H), 3.80-3.70 (m, 2H), 3.64-3.56 (m, 1H), 3.34-3.23 (m, 3H), 3.02-2.98 (m, 1H), 2.95-2.81 (m, 2H), 2.76-2.70 (m, 1H), 1.80-1.73 (m, 1H), 1.40-1.30 (m, 1H). ¹³C NMR (150 MHz, (CD₃)₂SO) δ = 171.8, 153.8, 153.8, 137.4, 137.3, 136.4, 128.8, 128.7, 128.7, 128.6, 128.5, 128.4, 128.0, 127.7, 127.7, 125.8, 125.7, 123.7, 123.3, 71.0, 68.2, 67.0, 66.9, 65.7, 52.0, 46.4, 46.3, 40.2, 40.1, 40.1, 31.3, 30.4, 30.0. HRMS (TOF, ES+) calculated for C₂₃H₂₆N₂O₅ m/z: 410.1842; found, 410.1849.



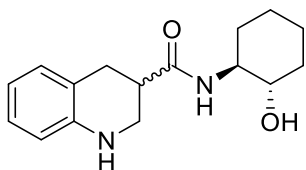
Benzyl 3-(((1S,2S)-2-hydroxycyclohexyl)carbamoyl)-3,4-dihydroquinoline-1(2H)-carboxylate

This compound was synthesized according to general procedure 1. Crude product was purified via flash chromatography (Teledyne ISCO system, silica gel column, hexanes:EtOAc) to provide the desired product as an off white solid (66% yield). ^1H NMR (400 MHz, CDCl_3) δ 7.63 (d, $J = 5.6$ Hz, 1H), 7.38-7.29 (m, 5H), 7.18-7.00 (m, 3H), 5.98 (d, $J = 5.4$, 1H), 5.30-5.17 (m, 2H), 4.17 (td, $J = 12.7, 4.0$ Hz, 1H), 3.76-3.54 (m, 2H), 3.29 (td, $J = 10.0, 4.2$ Hz, 1H), 3.17-3.08 (m, 1H), 2.91 (td, $J = 15.9, 6.2$ Hz, 1H), 2.74-2.65 (m, 1H), 2.07-2.00 (m, 1H), 1.96-1.88 (m, 1H), 1.75-1.64 (m, 2H), 1.37-1.08 (m, 5H). ^{13}C NMR (100 MHz, CDCl_3) $\delta = 174.0, 173.8, 154.9, 154.8, 137.6, 137.6, 136.2, 136.2, 129.1, 129.2, 128.7, 128.7, 128.3, 128.1, 128.1, 127.9, 127.9, 126.3, 124.5, 124.1, 75.1, 75.0, 68.0, 68.0, 56.1, 56.0, 46.7, 41.6, 41.4, 34.6, 34.5, 31.6, 31.5, 30.3, 30.2, 24.7, 24.2$. HRMS (TOF, ES+) calculated for $\text{C}_{24}\text{H}_{28}\text{N}_2\text{O}_4$ m/z : 408.2049; found, 408.2055.



N-[(3R,4S)-3-hydroxytetrahydropyran-4-yl]-1,2,3,4-tetrahydroquinoline-3-carboxamide

Benzyl 3-[[[(3R,4S)-3-hydroxytetrahydropyran-4-yl]carbamoyl]-3,4-dihydro-2H-quinoline-1-carboxylate (1.0 eq) was suspended in MeOH/AcOH (1:1, 0.2M) to which was added Pd/C (10 mol%). The reaction mixture was purged of air and under 1 atm of H₂ gas for 16 h. Upon completion, the solution was filtered through a syringe filter and concentrated *in vacuo*. The crude material was re-dissolved in MeOH, loaded onto a pre-wetted SCX cartridge, washed with MeOH, eluted with 7N NH₃/MeOH, and concentrated to provide the desired product as a white solid (95% yield). ¹H NMR (600 MHz, (CD₃)₂SO) δ 7.94-7.92 (m, 1H), 6.88-6.84 (m, 2H), 6.45 (d, *J* = 5.3 Hz, 1H), 6.42 (t, *J* = 4.8 Hz, 1H), 5.75 (s, 1H), 4.90 (d, *J* = 3.6 Hz, 1H), 3.80-3.72 (m, 2H), 3.65-3.58 (m, 1H), 3.32-3.25 (m, 3H), 3.06-2.98 (m, 2H), 2.84-2.76 (m, 1H), 2.73-2.65 (m, 1H), 2.55-2.51 (m, 1H), 1.82-1.76 (m, 1H), 1.41-1.33 (m, 1H). ¹³C NMR (150 MHz, (CD₃)₂SO) δ = 173.3, 173.2, 144.5, 144.4, 129.0, 129.0, 126.5, 119.2, 119.2, 115.3, 115.3, 113.3, 71.1, 68.3, 68.3, 65.7, 51.9, 43.6, 43.6, 40.1, 38.3, 31.4, 30.3, 30.2. HRMS (TOF, ES+) calculated for C₁₅H₂₀N₂O₃ m/z: 276.1474; found, 276.1476.



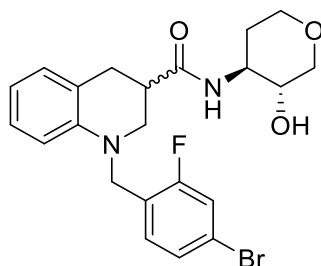
N-((1S,2S)-2-hydroxycyclohexyl)-1,2,3,4-tetrahydroquinoline-3-carboxamide

benzyl 3-[[[(1S,2S)-2-hydroxycyclohexyl]carbamoyl]-3,4-dihydro-2H-quinoline-1-carboxylate (1.0 eq) was suspended in MeOH (0.2M) to which was added Pd/C (10 mol%). The reaction mixture was purged of air and under 1 atm of H₂ gas for 2 h. Upon

completion, the solution was filtered through a syringe filter and concentrated. The crude material was re-dissolved in MeOH, loaded onto a pre-wetted SCX cartridge, washed with MeOH, eluted with 7N NH₃/MeOH, and concentrated to provide the desired product as a white solid (73% yield). ¹H NMR (600 MHz, (CD₃)₂SO) δ 7.75 (t, *J* = 6.8, 7.3 Hz, 1H), 6.88-6.82 (m, 2H), 6.45 (d, *J* = 7.9 Hz, 1H), 6.42 (tt, *J* = 7.3, 1.4 Hz, 1H), 5.73 (bs, 1H), 4.53 (d, *J* = 4.2 Hz, 1H), 3.46-3.39 (m, 1H), 3.32-3.21 (m, 3H), 3.02 (t, *J* = 11.1 Hz, 1H), 2.82-2.75 (m, 1H), 2.72-2.63 (m, 1H), 2.55-2.51 (m, 1H), 1.87-1.82 (m, 1H), 1.81-1.75 (m, 1H), 1.63-1.54 (m, 2H), 1.13-1.07 (m, 1H). ¹³C NMR (150 MHz, (CD₃)₂SO) δ = 173.1, 173.0, 144.5, 144.4, 129.0, 129.0, 126.4, 119.3, 119.2, 115.2, 115.2, 113.2, 71.2, 71.2, 54.1, 43.7, 43.6, 38.3, 38.3, 34.0, 31.0, 30.4, 30.2, 24.1, 24.1, 23.8. HRMS (TOF, ES⁺) calculated for C₁₆H₂₂N₂O₂ m/z: 274.1681; found, 274.1682.

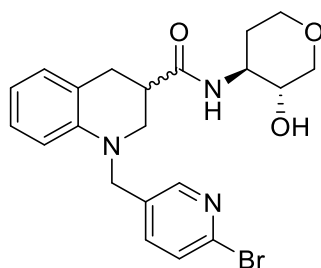
General Procedure 2: Alkylation synthesis

A solution of K₂CO₃ (2.5 eq), the appropriate benzyl bromide (1.1 eq), and the appropriate tetrahydroquinoline carboxamide (1.0 eq), in acetonitrile (0.4M) was heated to 60 °C and stirred for 16 h. Upon completion, the reaction mixture was diluted with H₂O, extracted with EtOAc (3x). The combined organics were dried over MgSO₄, filtered, concentrated, and purified via flash chromatography (Teledyne ISCO system, silica gel column, hexanes:EtOAc) to provide the desired product.



1-[(4-bromo-2-fluoro-phenyl)methyl]-N-[(3*R*,4*S*)-3-hydroxytetrahydropyran-4-yl]-3,4-dihydro-2*H*-quinoline-3-carboxamide

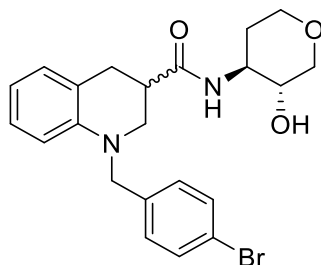
This compound was synthesized according to general procedure 2. Off-white solid (63% yield). ¹H NMR (600 MHz, (CD₃)₂SO) δ 7.98 (d, *J* = 5.2 Hz, 1H), 7.55 (d, *J* = 6.5 Hz, 1H), 7.35 (dt, *J* = 5.4, 1.5 Hz, 1H), 7.14 (td, *J* = 5.5, 2.7 Hz, 1H), 6.97 (d, *J* = 4.8 Hz, 1H), 6.92 (t, *J* = 5.2 Hz, 1H), 6.52 (t, *J* = 4.8 Hz, 1H), 6.45 (dd, *J* = 5.5, 1.4 Hz, 1H), 4.89 (dd, *J* = 10.7, 3.7 Hz, 1H), 4.57 (d, *J* = 11.6 Hz, 1H), 4.46 (dd, *J* = 11.6, 3.4 Hz, 1H), 3.80-3.71 (m, 2H), 3.65-3.58 (m, 1H), 3.41-3.25 (m, 4H), 3.02-2.97 (m, 1H), 2.91-2.71 (m, 3H), 1.81-1.75 (m, 1H), 1.42-1.31 (m, 1H). ¹³C NMR (150 MHz, (CD₃)₂SO) δ = 172.5, 172.5, 160.2 (d, ¹*J*_{CF} = 247 Hz), 143.9, 130.1, 130.1, 129.0, 127.5, 127.1, 127.0, 125.1, 125.0, 121.2, 121.1, 119.9, 119.9, 118.8 (d, ²*J*_{CF} = 24.1 Hz), 116.1, 116.1, 110.6, 71.1, 71.1, 68.3, 68.2, 65.7, 65.7, 52.0, 52.0, 51.7, 51.6, 48.0, 40.1, 38.4, 38.4, 31.4, 31.1, 31.0. HRMS (TOF, ES⁺) calculated for C₂₂H₂₄BrFN₂O₃ m/z: 462.0954; found, 462.0961.



1-((6-bromopyridin-3-yl)methyl)-N-((3*R*,4*S*)-3-hydroxytetrahydro-2*H*-pyran-4-yl)-1,2,3,4-tetrahydroquinoline-3-carboxamide

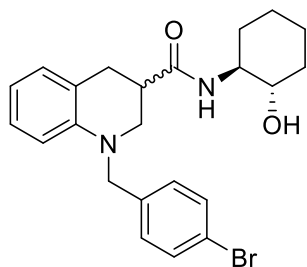
This compound was synthesized according to general procedure 2. Off-white solid (7% yield). ¹H NMR (400 MHz, MeOD) δ 7.35 (ddd, *J* = 9.8, 1.9, 1.1 Hz, 1H), 7.27 (ddd, *J* = 8.8, 1.7, 0.8 Hz, 1H), 7.18 (td, *J* = 8.1, 1.6 Hz, 1H), 7.00 (d, *J* = 7.5 Hz, 1H), 6.96 (t, *J* =

7.9 Hz, 1H), 6.58 (tt, $J = 7.4, 1.3$ Hz, 1H), 6.49 (dt, $J = 8.3, 1.4$ Hz, 1H), 4.63 – 4.45 (m, 2H), 4.08 – 3.73 (m, 2H), 3.58 – 3.38 (m, 4H), 3.15 (ddd, $J = 11.1, 9.7, 3.3$ Hz, 1H), 3.09 – 2.94 (m, 1H), 2.95 – 2.81 (m, 1H), 2.01 – 1.85 (m, 1H), 1.70 – 1.43 (m, 1H).



1-(4-bromobenzyl)-N-((3R,4S)-3-hydroxytetrahydro-2H-pyran-4-yl)-1,2,3,4-tetrahydroquinoline-3-carboxamide

This compound was synthesized according to general procedure 2. Off-white solid (89% yield) ^1H NMR (400 MHz, T₂MeOD) δ 7.44 (dd, $J = 8.5, 1.2$ Hz, 1H), 7.25 – 7.17 (m, 1H), 6.98 (d, $J = 7.5$ Hz, 1H), 6.93 (t, $J = 8.0$ Hz, 0H), 6.64 – 6.51 (m, 1H), 6.51 (d, $J = 8.2$ Hz, 0H), 4.56 – 4.39 (m, 1H), 4.02 – 3.69 (m, 1H), 3.51 – 3.35 (m, 2H), 3.13 (ddd, $J = 11.1, 9.7, 3.5$ Hz, 1H), 3.08 – 2.91 (m, 1H), 2.91 – 2.78 (m, 1H), 1.90 (tdd, $J = 11.2, 4.7, 2.3$ Hz, 0H), 1.67 – 1.39 (m, 1H).



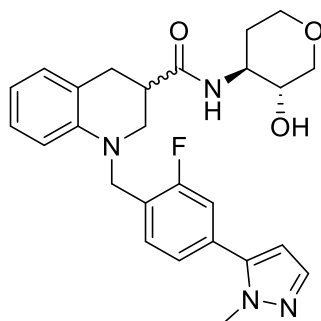
1-(4-bromobenzyl)-N-((1S,2S)-2-hydroxycyclohexyl)-1,2,3,4-tetrahydroquinoline-3-carboxamide

This compound was synthesized according to general procedure 2. White solid (73% yield). ^1H NMR (600 MHz, (CD₃)₂SO) δ 7.81 (d, $J = 7.9$ Hz, 1H), 7.51 (dd, $J = 8.5, 2.6$

Hz, 2H), 7.21 (dd, $J = 8.5, 2.1$ Hz, 2H), 6.95 (d, $J = 7.2$ Hz, 1H), 6.89 (t, $J = 7.7$ Hz, 1H), 6.50 (t, $J = 7.3$ Hz, 1H), 6.44 (d, $J = 8.3$ Hz, 1H), 4.57-4.51 (m, 2H), 4.40 (dd, $J = 17.1, 6.7$ Hz, 1H), 3.45-3.33 (m, 4H), 3.27-3.20 (m, 1H), 2.90-2.70 (m, 3H), 1.87-1.81 (m, 1H), 1.80-1.73 (m, 1H), 1.64-1.53 (m, 2H), 1.14-1.04 (m, 1H). ^{13}C NMR (150 MHz, $(\text{CD}_3)_2\text{SO}$) $\delta = 172.4, 172.3, 144.1, 144.1, 138.5, 131.3, 131.3, 128.9, 127.0, 126.9, 121.2, 121.0, 119.6, 115.8, 115.7, 110.7, 110.7, 71.2, 71.1, 54.2, 54.1, 53.6, 53.6, 51.9, 51.8, 38.5, 38.4, 34.0, 31.2, 31.0, 24.1, 24.1, 23.8$. HRMS (TOF, ES+) calculated for $\text{C}_{23}\text{H}_{27}\text{BrN}_2\text{O}_2$ m/z : 442.1256; found, 442.1257.

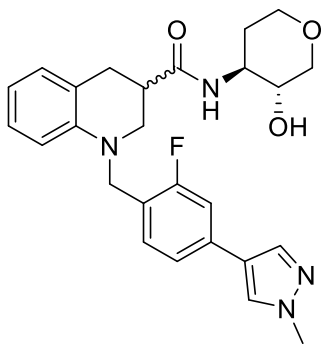
General procedure 3: Suzuki Synthesis

A degassed solution of Tetrakis(triphenylphosphine)palladium(0) (7 mol %), Cs_2CO_3 (2.0 eq), the appropriate aryl bromide (1.0 eq), and the appropriate boronic acid (1.1 eq) in 1,4-Dioxane/ H_2O (2:1, 0.2M) was heated to 100 °C and stirred for 16 h. Upon completion the reaction mixture was diluted with H_2O , extracted with DCM, passed through a phase separator, and concentrated. The crude material was purified via flash chromatography (Teledyne ISCO system, silica gel column, DCM:MeOH) provide a mixture of diastereomers.



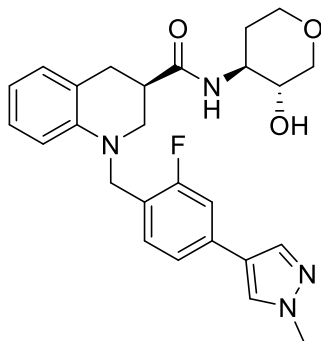
1-(2-fluoro-4-(1-methyl-1H-pyrazol-5-yl)benzyl)-N-((3R,4S)-3-hydroxytetrahydro-2H-pyran-4-yl)-1,2,3,4-tetrahydroquinoline-3-carboxamide

This compound was synthesized according to general procedure 3. Off-white solid (26.2% yield). ¹H NMR (400 MHz, (CD₃)₂SO) δ 8.01 (d, *J* = 7.9 Hz, 1H), 7.51 – 7.40 (m, 2H), 7.35 – 7.24 (m, 2H), 6.99 (d, *J* = 7.3 Hz, 1H), 6.94 (t, *J* = 7.8 Hz, 1H), 6.58 – 6.48 (m, 2H), 6.47 – 6.43 (m, 1H), 4.92 (dd, *J* = 11.0, 5.4 Hz, 1H), 4.67 (d, *J* = 17.5 Hz, 1H), 4.54 (dd, *J* = 17.3, 3.3 Hz, 1H), 3.86 (s, 3H), 3.76 (dq, *J* = 15.1, 6.3, 5.4 Hz, 2H), 3.62 (d, *J* = 8.4 Hz, 0H), 3.00 (ddd, *J* = 11.0, 9.6, 3.7 Hz, 1H), 2.93 – 2.75 (m, 2H), 1.78 (td, *J* = 7.1, 6.3, 3.2 Hz, 1H), 1.46 – 1.30 (m, 1H). ¹³C NMR (101 MHz, (CD₃)₂SO) δ 172.4, 161.3, 158.8, 143.9, 141.1, 137.8, 130.5, 128.9, 128.7, 127.0, 125.4, 125.2, 124.2, 121.0, 120.9, 115.9, 115.3, 115.0, 110.4, 106.1, 70.9, 68.1, 68.1, 65.6, 51.8, 51.6, 51.5, 48.0, 38.3, 37.5, 31.2, 31.0, 30.9. LC-MS (*m/z* + H) = 465.



1-[[2-fluoro-4-(1-methylpyrazol-4-yl)phenyl]methyl]-N-[(3R,4S)-3-hydroxytetrahydropyran-4-yl]-3,4-dihydro-2H-quinoline-3-carboxamide

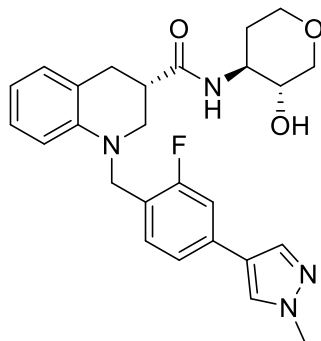
This compound was synthesized according to general procedure 3. White solid (53% yield).



(3S)-1-[[2-fluoro-4-(1-methylpyrazol-4-yl)phenyl]methyl]-N-[(3R,4S)-3-hydroxytetrahydropyran-4-yl]-3,4-dihydro-2H-quinoline-3-carboxamide

The mixture of diastereomers were separated via chiral chromatography to provide the a single diastereomer of unknown absolute stereochemistry. Peak 1. Off-white solid.

$[\alpha]_D^{23} +4.3$ ($c = 0.76$, DMSO). $^1\text{H NMR}$ (600 MHz, $(\text{CD}_3)_2\text{SO}$) δ 8.15 (s, 1H), 7.99 (d, $J = 7.9$ Hz, 1H), 7.88 (s, 1H), 7.43 (dd, $J = 11.8, 1.3$ Hz, 1H), 7.32 (dd, $J = 7.9, 1.4$ Hz, 1H), 7.17 (t, $J = 8.0$ Hz, 1H), 6.97 (d, $J = 7.5$ Hz, 1H), 6.93 (t, $J = 7.8$ Hz, 1H), 6.55-6.51 (m, 2H), 4.93 (d, $J = 5.5$ Hz, 1H), 4.58, 4.47 (ABq, $J_{AB} = 17.0$, 2H), 3.85 (s, 3H), 3.79 (dd, $J = 11.0, 4.7$ Hz, 2H), 3.76-3.72 (m, 1H), 3.66-3.59 (m, 1H), 3.43-3.30 (m, 3H), 3.28 (td, $J = 11.6, 2.1$ Hz, 1H), 3.01 (t, $J = 10.3$ Hz, 1H), 2.93-2.80 (m, 2H), 2.80-2.73 (m, 1H), 1.81-1.76 (m, 1H), 1.41-1.33 (m, 1H). $^{13}\text{C NMR}$ (150 MHz, $(\text{CD}_3)_2\text{SO}$) $\delta = 172.6, 160.8$ (d, $^1J_{CF} = 242$ Hz), 144.1, 136.3, 133.6 (d, $^3J_{CF} = 8.6$ Hz), 129.1 (d, $^4J_{CF} = 5.4$ Hz), 129.0, 128.2, 127.0, 122.4, 122.3, 121.2, 120.8, 120.7, 115.9, 111.7 (d, $^2J_{CF} = 22.4$ Hz), 110.7, 71.1, 68.3, 85.7, 52.0, 51.7, 48.1, 38.7, 38.5, 31.4, 31.1. HRMS (TOF, ES+) calculated for $\text{C}_{26}\text{H}_{29}\text{FN}_4\text{O}_3$ m/z : 464.2224; found, 464.2232.



(3R)-1-[[2-fluoro-4-(1-methylpyrazol-4-yl)phenyl]methyl]-N-[(3R,4S)-3-hydroxytetrahydropyran-4-yl]-3,4-dihydro-2H-quinoline-3-carboxamide

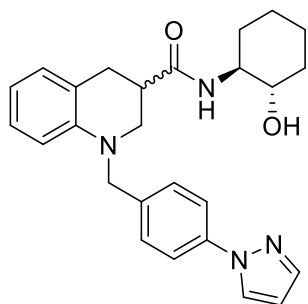
The mixture of diastereomers were separated via chiral chromatography to provide the a single diastereomer of unknown absolute stereochemistry. Peak 2. Off-white solid.

$[\alpha]_D^{23} +34.4$ ($c = 0.23$, DMSO). $^1\text{H NMR}$ (600 MHz, $(\text{CD}_3)_2\text{SO}$) δ 8.15 (s, 1H), 7.99 (d, $J = 7.9$ Hz, 1H), 7.87 (s, 1H), 7.43 (d, $J = 11.6$, 1H), 7.31 (d, $J = 7.9$, 1H), 7.16 (t, $J = 8.0$ Hz, 1H), 6.97 (d, $J = 7.2$ Hz, 1H), 6.93 (t, $J = 7.6$ Hz, 1H), 6.54-6.49 (m, 2H), 4.89 (d, $J = 5.4$ Hz, 1H), 4.57, 4.47 (ABq, $J_{AB} = 17.0$, 2H), 3.85 (s, 3H), 3.80-3.72 (m, 2H), 3.65-3.58 (m, 1H), 3.44-3.24 (m, 4H), 2.99 (t, $J = 10.3$ Hz, 1H), 2.90-2.71 (m, 3H), 1.82-1.77 (m, 1H), 1.42-1.34 (m, 1H). $^{13}\text{C NMR}$ (150 MHz, $(\text{CD}_3)_2\text{SO}$) $\delta = 172.6$, 160.8 (d, $^1J_{CF} = 242$ Hz), 144.1, 136.3, 133.6 (d, $^3J_{CF} = 8.7$ Hz), 129.1 (d, $^4J_{CF} = 5.3$ Hz), 129.0, 128.2, 127.1, 122.4, 122.3, 121.1, 120.7, 115.9, 111.7 (d, $^2J_{CF} = 22.4$ Hz), 110.7, 71.1, 68.3, 65.7, 52.0, 51.6, 48.1, 38.7, 38.5, 31.4, 31.2. HRMS (TOF, ES+) calculated for $\text{C}_{26}\text{H}_{29}\text{FN}_4\text{O}_3$ m/z : 464.2224; found, 464.2235.

General Procedure 4: Copper-Mediated Cross-Coupling Synthesis

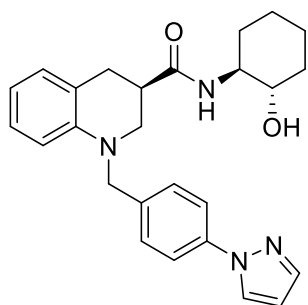
A degassed solution of pyrazole (1.1 eq), trans-N,N-dimethylcyclohexane-1,2-diamine (0.75 eq), cesium carbonate (1.5 eq), copper (i) iodide (0.75 eq), and 1-[(4-bromophenyl)methyl]-N-[(1S,2S)-2-hydroxycyclohexyl]-3,4-dihydro-2H-quinoline-3-

carboxamide in 1,4-dioxane (0.25M) was heated to 100 °C and stirred for 24 h. Upon completion the reaction mixture was diluted with H₂O, extracted with DCM, passed through a phase separator, and concentrated. The crude material was purified via flash chromatography (Teledyne ISCO system, silica gel column, DCM:MeOH) provide a mixture of diastereomers.



1-(4-(1H-pyrazol-1-yl)benzyl)-N-((1S,2S)-2-hydroxycyclohexyl)-1,2,3,4-tetrahydroquinoline-3-carboxamide

This compound was synthesized according to general procedure 4. Off-white solid (87% yield).

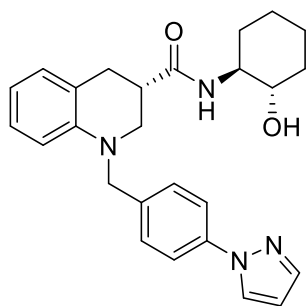


(R)-1-(4-(1H-pyrazol-1-yl)benzyl)-N-((1S,2S)-2-hydroxycyclohexyl)-1,2,3,4-tetrahydroquinoline-3-carboxamide

The mixture of diastereomers were separated via chiral chromatography to provide the a single diastereomer of unknown absolute stereochemistry. Peak 1. Off-white solid.

$[\alpha]_D^{23}$ -6.04 ($c = 1.15$, DMSO). ¹H NMR (600 MHz, (CD₃)₂SO) δ 8.43 (d, $J = 1.6$ Hz,

1H), 7.83 (d, $J = 5.3$ Hz, 1H), 7.77 (d, $J = 5.7$ Hz, 2H), 7.71 (d, $J = 1.0$ Hz, 1H), 7.36 (d, $J = 5.7$ Hz, 2H), 6.96 (d, $J = 4.9$ Hz, 1H), 6.90 (t, $J = 5.4, 4.9$ Hz, 1H), 6.53-6.48 (m, 3H), 4.61, 4.46 (ABq, $J_{AB} = 11.3$ Hz, 2H), 3.46-3.38 (m, 3H), 3.28-3.22 (m, 1H), 2.92-2.74 (m, 3H), 1.87-1.74 (m, 2H), 1.63-1.52 (m, 2H), 1.25-1.14 (m, 3H), 1.12-1.05 (m, 1H). ^{13}C NMR (150 MHz, $(\text{CD}_3)_2\text{SO}$) $\delta = 172.4, 144.3, 140.8, 138.5, 136.9, 128.9, 127.8, 127.6, 126.9, 121.2, 118.6, 115.8, 110.9, 107.7, 71.2, 54.2, 53.7, 52.0, 38.5, 34.1, 31.1, 31.0, 24.1, 23.8$. HRMS (TOF, ES+) calculated for $\text{C}_{26}\text{H}_{30}\text{N}_4\text{O}_2$ m/z : 430.2369; found, 430.2368.



(S)-1-(4-(1H-pyrazol-1-yl)benzyl)-N-((1S,2S)-2-hydroxycyclohexyl)-1,2,3,4-tetrahydroquinoline-3-carboxamide

The mixture of diastereomers were separated via chiral chromatography to provide the a single diastereomer of unknown absolute stereochemistry. Peak 2. Off-white solid. $[\alpha]_D^{23} +36.75$ ($c = 1.09$, DMSO). ^1H NMR (600 MHz, $(\text{CD}_3)_2\text{SO}$) δ 8.44 (d, $J = 1.6$ Hz, 1H), 7.83 (d, $J = 5.4$ Hz, 1H), 7.78 (d, $J = 5.7$ Hz, 2H), 7.72 (d, $J = 1.0$ Hz, 1H), 7.37 (d, $J = 5.7$ Hz, 2H), 6.97 (d, $J = 4.9$ Hz, 1H), 6.91 (t, $J = 5.4, 4.9$ Hz, 1H), 6.54-6.49 (m, 3H), 4.62, 4.48 (ABq, $J_{AB} = 11.3$ Hz, 2H), 3.47-3.40 (m, 3H), 3.27-3.21 (m, 1H), 2.91-2.74 (m, 3H), 1.87-1.76, (m, 2H), 1.64-1.56 (m, 2H), 1.25-1.16 (m, 3H), 1.15-1.08 (m, 1H). ^{13}C NMR (150 MHz, $(\text{CD}_3)_2\text{SO}$) $\delta = 172.4, 144.3, 140.8, 138.5, 136.9, 128.9, 127.8, 127.6, 127.0, 121.1, 118.6, 115.7, 110.8, 107.7, 71.2, 54.1, 53.7, 51.8, 38.5, 34.0, 31.3, 31.1,$

24.1, 23.8. HRMS (TOF, ES+) calculated for $C_{26}H_{30}N_4O_2$ m/z: 430.2369; found, 430.2368.

References for Chapter II

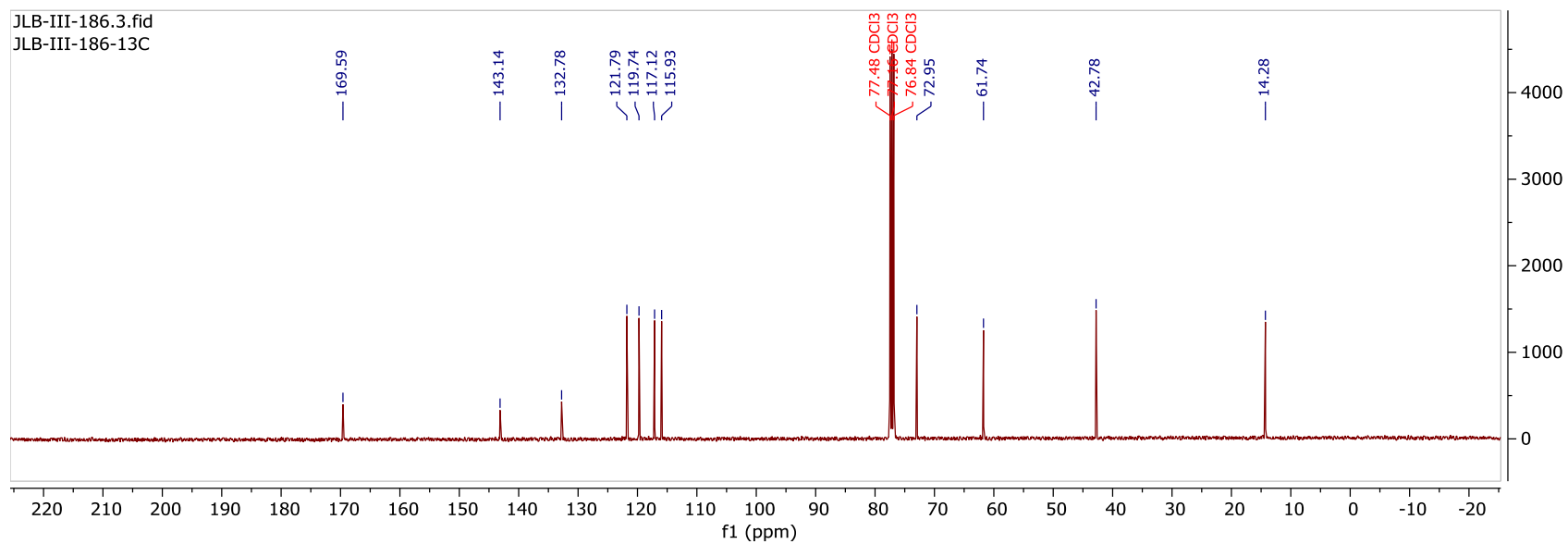
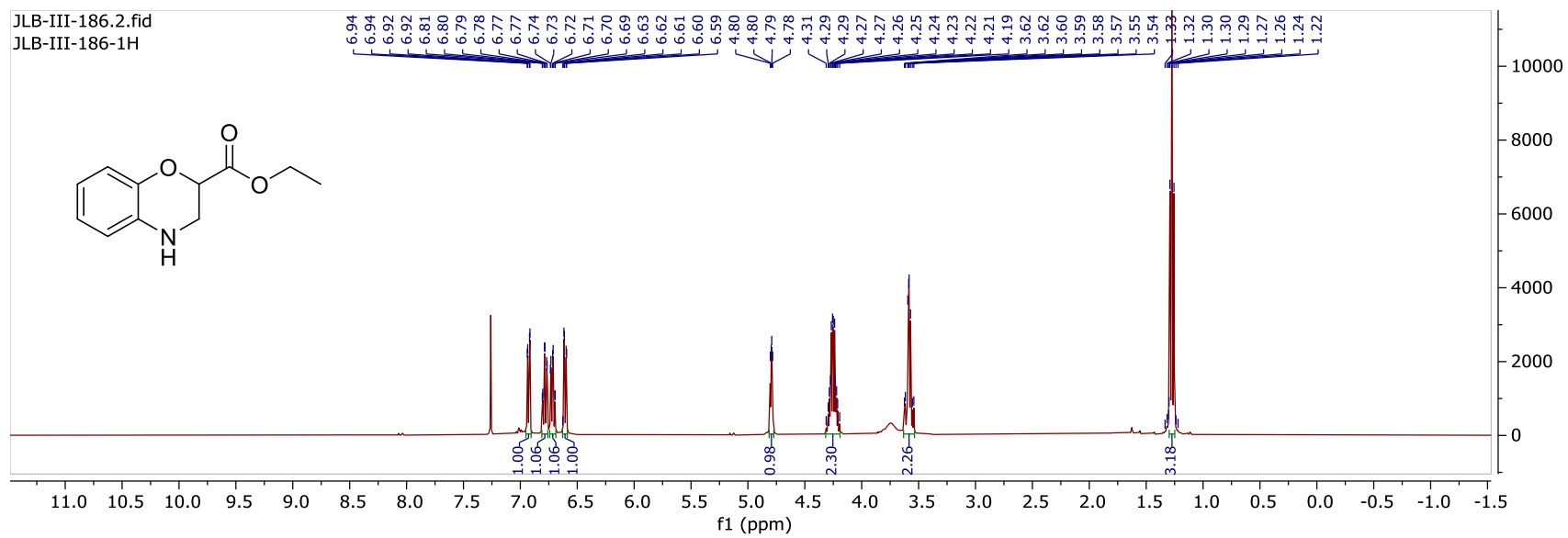
- 1) Vassilatis, D. K.; Hohmann, J. G.; Zeng, H.; Li, F.; Ranchalis, J. E.; Mortrud, M. T.; Brown, A.; Rodriguez, S. S.; Weller, J. R.; Wright, A. C.; Bergmann, J. E.; Gaitanaris, G. A. *Proceedings of the National Academy of Sciences of the United States of America* **2003**, *100*, 4903.
- 2) Kroeze, W. K.; Sheffler, D. J.; Roth, B. L. *Journal of cell science* **2003**, *116*, 4867.
- 3) Lv, X.; Liu, J.; Shi, Q.; Tan, Q.; Wu, D.; Skinner, J. J.; Walker, A. L.; Zhao, L.; Gu, X.; Chen, N.; Xue, L.; Si, P.; Zhang, L.; Wang, Z.; Katritch, V.; Liu, Z. J.; Stevens, R. C. *Protein & cell* **2016**, *7*, 325.
- 4) Rosenbaum, D. M.; Rasmussen, S. G.; Kobilka, B. K. *Nature* **2009**, *459*, 356.
- 5) Hilger, D.; Masureel, M.; Kobilka, B. K. *Nature structural & molecular biology* **2018**, *25*, 4.
- 6) Calebiro, D.; Koszegi, Z. *Molecular and cellular endocrinology* **2019**, *483*, 24.
- 7) Lim, W. K. *Recent patents on CNS drug discovery* **2007**, *2*, 107.
- 8) Lagerstrom, M. C.; Schioth, H. B. *Nature reviews. Drug discovery* **2008**, *7*, 339.
- 9) Felder, C. C.; Porter, A. C.; Skillman, T. L.; Zhang, L.; Bymaster, F. P.; Nathanson, N. M.; Hamilton, S. E.; Gomeza, J.; Wess, J.; McKinzie, D. L. *Life sciences* **2001**, *68*, 2605.
- 10) Levey, A. I.; Kitt, C. A.; Simonds, W. F.; Price, D. L.; Brann, M. R. *The Journal of neuroscience : the official journal of the Society for Neuroscience* **1991**, *11*, 3218.
- 11) Picciotto, M. R.; Higley, M. J.; Mineur, Y. S. *Neuron* **2012**, *76*, 116.
- 12) Bradley, S. J.; Tobin, A. B.; Prihandoko, R. *Neuropharmacology* **2018**, *136*, 361.
- 13) Dean, B.; Copolov, D.; Scarr, E. *Schizophrenia research* **2016**, *177*, 108.
- 14) Higley, M. J.; Picciotto, M. R. *Current opinion in neurobiology* **2014**, *29*, 88.
- 15) Levey, A. I. *Proceedings of the National Academy of Sciences of the United States of America* **1996**, *93*, 13541.
- 16) van der Zee, E. A.; Luiten, P. G. *Progress in neurobiology* **1999**, *58*, 409.
- 17) Zenko, D.; Hislop, J. N. *Neuropharmacology* **2018**, *136*, 374.
- 18) Caulfield, M. P. *Pharmacology & therapeutics* **1993**, *58*, 319.
- 19) Ishii, M.; Kurachi, Y. *Current pharmaceutical design* **2006**, *12*, 3573.
- 20) Mineur, Y. S.; Obayemi, A.; Wigstrand, M. B.; Fote, G. M.; Calarco, C. A.; Li, A. M.; Picciotto, M. R. *Proceedings of the National Academy of Sciences of the United States of America* **2013**, *110*, 3573.
- 21) The Alzheimer's Association. Facts and figures. **2020**. https://alz.org/alzheimers-dementia/facts-figures?_ga=2.245254533.1024911027.1583948912-797099381.1580325502.
- 22) The Alzheimer's Association. *What is Alzheimer's Disease?* **2020**. <https://www.alz.org/alzheimers-dementia/what-is-alzheimers>
- 23) Centers for Disease Control and Prevention. *Leading Causes of Death*. **2017**. <https://www.cdc.gov/nchs/fastats/leading-causes-of-death.htm>
- 24) Anagnostaras, S., Murphy, G., Hamilton, S. et al. *Nature neuroscience* **2003**, *6*, 51.
- 25) Scarr, E.; Udawela, M.; Thomas, E. A.; Dean, B. *Molecular psychiatry* **2018**, *23*, 295.
- 26) Atri, A. *Seminars in neurology* **2019**, *39*, 227.

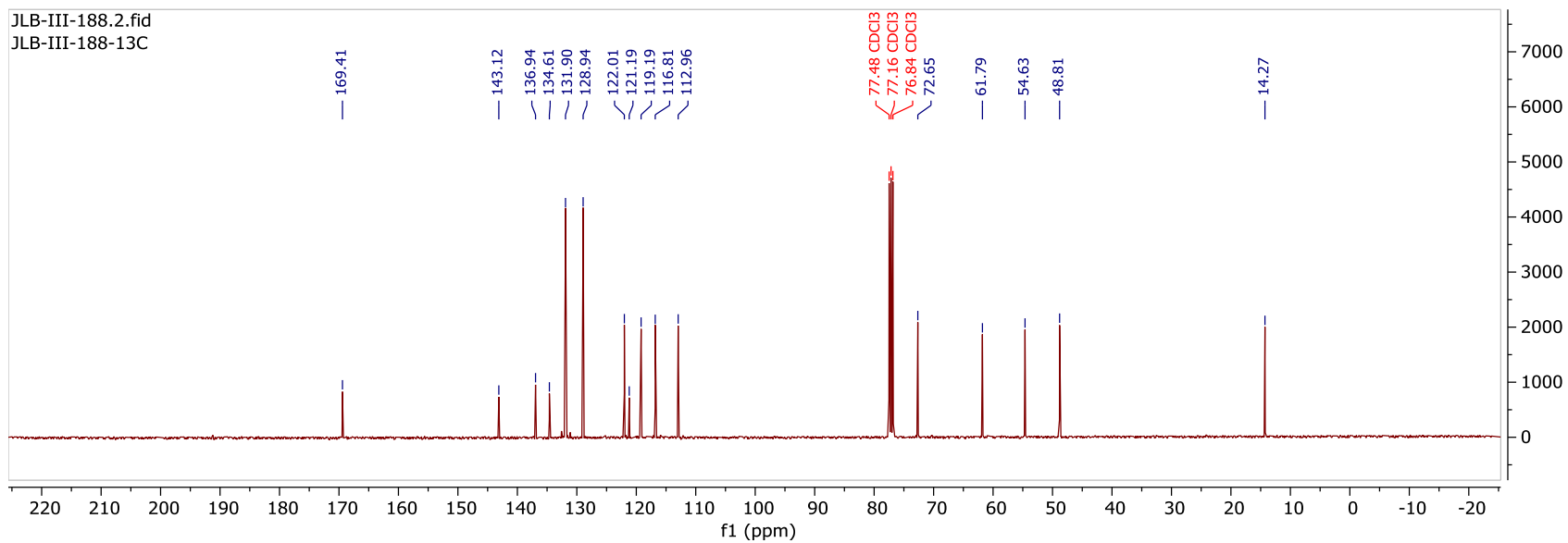
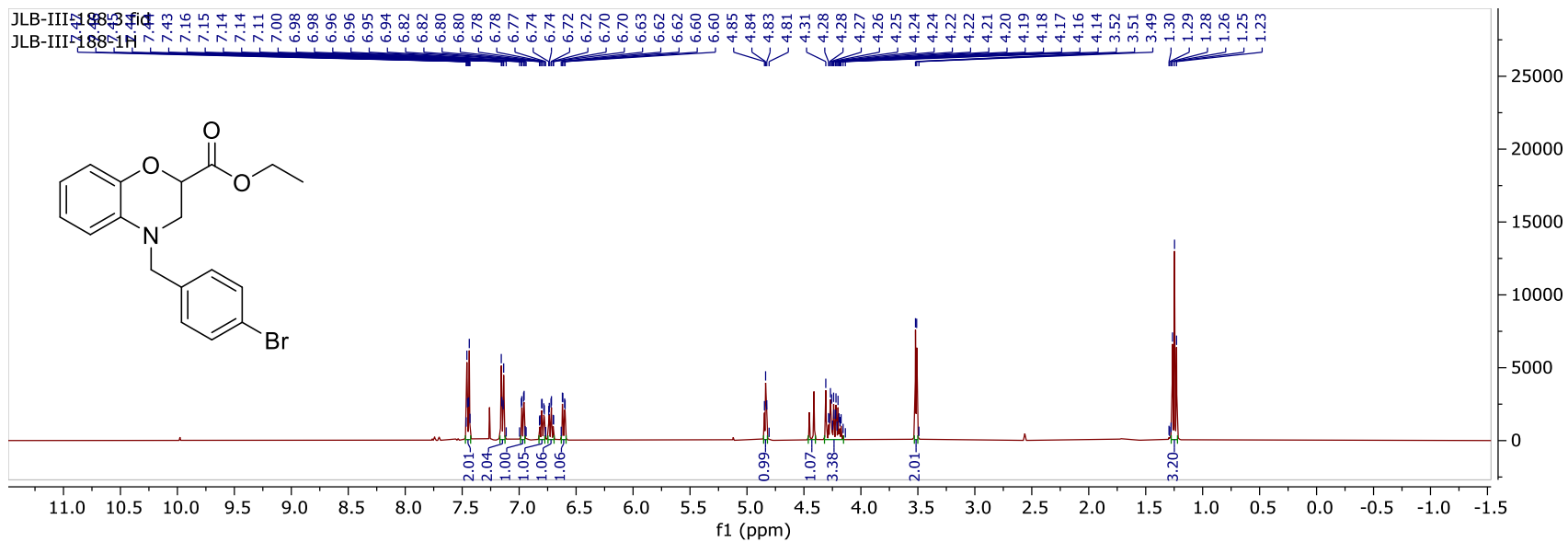
- 27) Bondi, M. W.; Edmonds, E. C.; Salmon, D. P. *Journal of the International Neuropsychological Society : JINS* **2017**, *23*, 818.
- 28) Gao, L. B.; Yu, X. F.; Chen, Q.; Zhou, D. *Minerva medica* **2016**, *107*, 108.
- 29) Medeiros, R.; Kitazawa, M.; Caccamo, A.; Baglietto-Vargas, D.; Estrada-Hernandez, T.; Cribbs, D. H.; Fisher, A.; LaFerla, F. M. *The American journal of pathology* **2011**, *179*, 980.
- 30) Woolley, M. L.; Carter, H. J.; Gartlon, J. E.; Watson, J. M.; Dawson, L. A. *European journal of pharmacology* **2009**, *603*, 147.
- 31) Bender, A. M.; Jones, C. K.; Lindsley, C. W. *ACS chemical neuroscience* **2017**, *8*, 435.
- 32) Shannon, H. E.; Bymaster, F. P.; Calligaro, D. O.; Greenwood, B.; Mitch, C. H.; Sawyer, B. D.; Ward, J. S.; Wong, D. T.; Olesen, P. H.; Sheardown, M. J.; Swedberg, M. D.; Suzdak, P. D.; Sauerberg, P. *The Journal of pharmacology and experimental therapeutics* **1994**, *269*, 271.
- 33) Lilly, E. **2016**.
- 34) Barak, S.; Weiner, I. *The international journal of neuropsychopharmacology* **2011**, *14*, 1233.
- 35) Bodick, N. C.; Offen, W. W.; Shannon, H. E.; Satterwhite, J.; Lucas, R.; van Lier, R.; Paul, S. M. *Alzheimer disease and associated disorders* **1997**, *11 Suppl 4*, S16.
- 36) Hamilton, S. E.; Nathanson, N. M. *The Journal of biological chemistry* **2001**, *276*, 15850.
- 37) Sum, C. S.; Murphy, B. J.; Li, Z.; Wang, T.; Zhang, L.; Cvijic, M. E. In *Assay Guidance Manual*; Sittampalam, G. S., Grossman, A., Brimacombe, K., Arkin, M., Auld, D., Austin, C. P., Baell, J., Bejcek, B., Caaveiro, J. M. M., Chung, T. D. Y., Coussens, N. P., Dahlin, J. L., Devanaryan, V., Foley, T. L., Glicksman, M., Hall, M. D., Haas, J. V., Hoare, S. R. J., Inglese, J., Iversen, P. W., Kahl, S. D., Kales, S. C., Kirshner, S., Lal-Nag, M., Li, Z., McGee, J., McManus, O., Riss, T., Saradjian, P., Trask, O. J., Jr., Weidner, J. R., Wildey, M. J., Xia, M., Xu, X., Eds. Bethesda MD, 2004.
- 38) Kenakin, T. *Molecular pharmacology* **2017**, *92*, 414.
- 39) Conn, P. J.; Christopoulos, A.; Lindsley, C. W. *Nature reviews. Drug discovery* **2009**, *8*, 41.
- 40) Conn, P. J.; Lindsley, C. W.; Meiler, J.; Niswender, C. M. *Nature reviews. Drug discovery* **2014**, *13*, 692.
- 41) Jiang, S.; Li, Y.; Zhang, C.; Zhao, Y.; Bu, G.; Xu, H.; Zhang, Y. W. *Neuroscience bulletin* **2014**, *30*, 295.
- 42) Foster, D. J.; Conn, P. J. *Neuron* **2017**, *94*, 431.
- 43) May, L. T.; Leach, K.; Sexton, P. M.; Christopoulos, A. *Annual review of pharmacology and toxicology* **2007**, *47*, 1.
- 44) Melancon, B. J.; Tarr, J. C.; Panarese, J. D.; Wood, M. R.; Lindsley, C. W. *Drug discovery today* **2013**, *18*, 1185.
- 45) Voss, T.; Li, J.; Cummings, J.; Farlow, M.; Assaid, C.; Froman, S.; Leibensperger, H.; Snow-Adami, L.; McMahon, K. B.; Egan, M.; Michelson, D. *Alzheimer's & dementia (New York, N. Y.)* **2018**, *4*, 173.
- 46) Ma, L.; Seager, M. A.; Wittmann, M.; Jacobson, M.; Bickel, D.; Burno, M.; Jones, K.; Graufelds, V. K.; Xu, G.; Pearson, M.; McCampbell, A.; Gaspar, R.; Shughrue, P.; Danziger, A.; Regan, C.; Flick, R.; Pascarella, D.; Garson, S.; Doran, S.; Kreatsoulas,

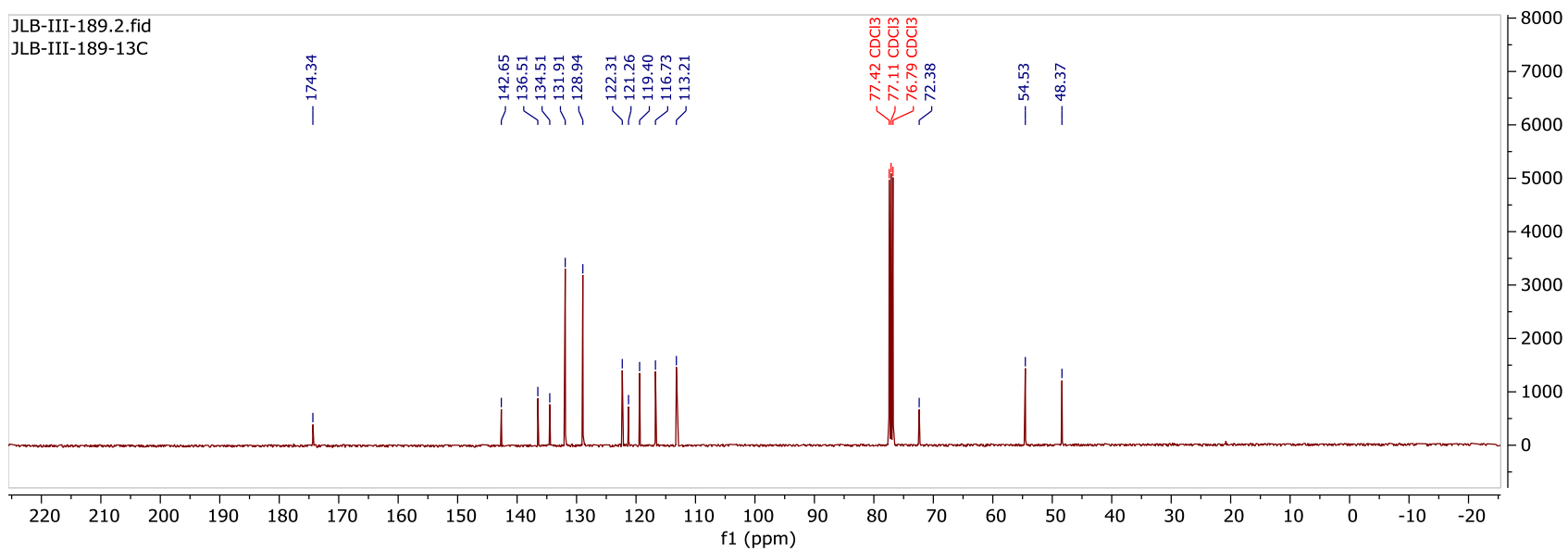
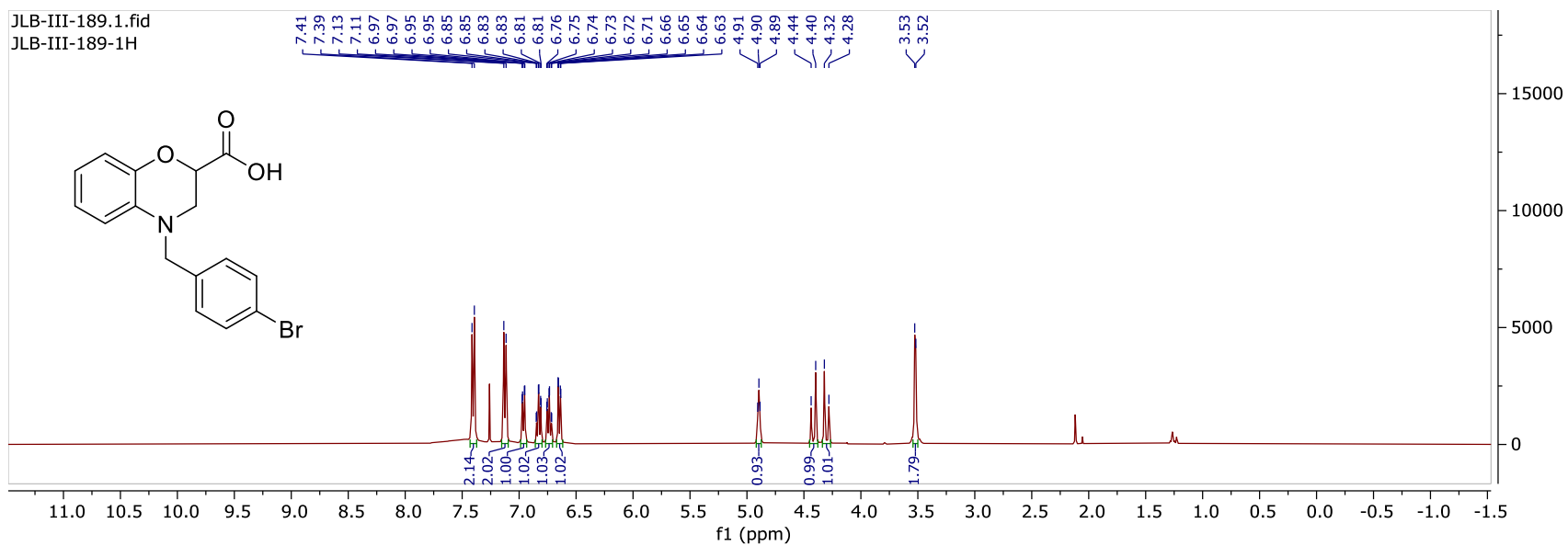
- C.; Veng, L.; Lindsley, C. W.; Shipe, W.; Kuduk, S.; Sur, C.; Kinney, G.; Seabrook, G. R.; Ray, W. J. *Proceedings of the National Academy of Sciences of the United States of America* **2009**, *106*, 15950.
- 47) Rook, J. M.; Abe, M.; Cho, H. P.; Nance, K. D.; Luscombe, V. B.; Adams, J. J.; Dickerson, J. W.; Remke, D. H.; Garcia-Barrantes, P. M.; Engers, D. W.; Engers, J. L.; Chang, S.; Foster, J. J.; Blobaum, A. L.; Niswender, C. M.; Jones, C. K.; Conn, P. J.; Lindsley, C. W. *ACS chemical neuroscience* **2017**, *8*, 866.
- 48) Moran, S. P.; Cho, H. P.; Maksymetz, J.; Remke, D. H.; Hanson, R. M.; Niswender, C. M.; Lindsley, C. W.; Rook, J. M.; Conn, P. J. *ACS chemical neuroscience* **2018**, *9*, 2218.
- 49) Moran, S. P.; Dickerson, J. W.; Cho, H. P.; Xiang, Z.; Maksymetz, J.; Remke, D. H.; Lv, X.; Doyle, C. A.; Rajan, D. H.; Niswender, C. M.; Engers, D. W.; Lindsley, C. W.; Rook, J. M.; Conn, P. J. *Neuropsychopharmacology : official publication of the American College of Neuropsychopharmacology* **2018**, *43*, 1763.
- 50) Panarese, J. D.; Cho, H. P.; Adams, J. J.; Nance, K. D.; Garcia-Barrantes, P. M.; Chang, S.; Morrison, R. D.; Blobaum, A. L.; Niswender, C. M.; Stauffer, S. R.; Conn, P. J.; Lindsley, C. W. *Bioorganic & medicinal chemistry letters* **2016**, *26*, 3822.
- 51) Khajehali, E.; Valant, C.; Jorg, M.; Tobin, A. B.; Conn, P. J.; Lindsley, C. W.; Sexton, P. M.; Scammells, P. J.; Christopoulos, A. *Biochemical pharmacology* **2018**, *154*, 243.
- 52) Engers, J. L.; Childress, E. S.; Long, M. F.; Capstick, R. A.; Luscombe, V. B.; Cho, H. P.; Dickerson, J. W.; Rook, J. M.; Blobaum, A. L.; Niswender, C. M.; Engers, D. W.; Conn, P. J.; Lindsley, C. W. *ACS medicinal chemistry letters* **2018**, *9*, 917.
- 53) Rook, J. M.; Bertron, J. L.; Cho, H. P.; Garcia-Barrantes, P. M.; Moran, S. P.; Maksymetz, J. T.; Nance, K. D.; Dickerson, J. W.; Remke, D. H.; Chang, S.; Harp, J. M.; Blobaum, A. L.; Niswender, C. M.; Jones, C. K.; Stauffer, S. R.; Conn, P. J.; Lindsley, C. W. *ACS chemical neuroscience* **2018**, *9*, 2274.
- 54) Davoren, J. E.; Lee, C. W.; Garnsey, M.; Brodney, M. A.; Cordes, J.; Dlugolenski, K.; Edgerton, J. R.; Harris, A. R.; Helal, C. J.; Jenkinson, S.; Kauffman, G. W.; Kenakin, T. P.; Lazzaro, J. T.; Lotarski, S. M.; Mao, Y.; Nason, D. M.; Northcott, C.; Nottebaum, L.; O'Neil, S. V.; Pettersen, B.; Popiolek, M.; Reinhart, V.; Salomon-Ferrer, R.; Steyn, S. J.; Webb, D.; Zhang, L.; Grimwood, S. *Journal of medicinal chemistry* **2016**, *59*, 6313.
- 55) Yang, Z. Q.; Shu, Y.; Ma, L.; Wittmann, M.; Ray, W. J.; Seager, M. A.; Koeplinger, K. A.; Thompson, C. D.; Hartman, G. D.; Bilodeau, M. T.; Kuduk, S. D. *ACS medicinal chemistry letters* **2014**, *5*, 604.
- 56) Boyd, J. W. J. *ACS J. Phys. Chem.* **1996**, *100*, 16141.
- 57) Bertron, J. L.; Cho, H. P.; Garcia-Barrantes, P. M.; Panarese, J. D.; Salovich, J. M.; Nance, K. D.; Engers, D. W.; Rook, J. M.; Blobaum, A. L.; Niswender, C. M.; Stauffer, S. R.; Conn, P. J.; Lindsley, C. W. *Bioorganic & medicinal chemistry letters* **2018**, *28*, 2175.

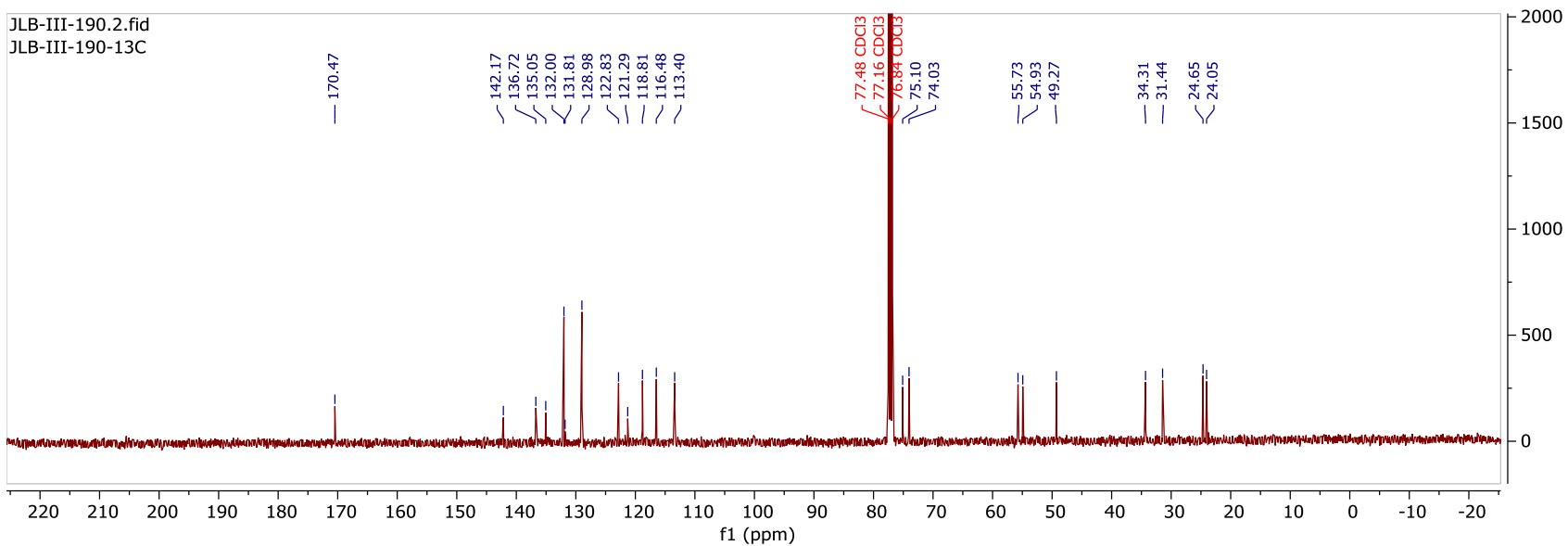
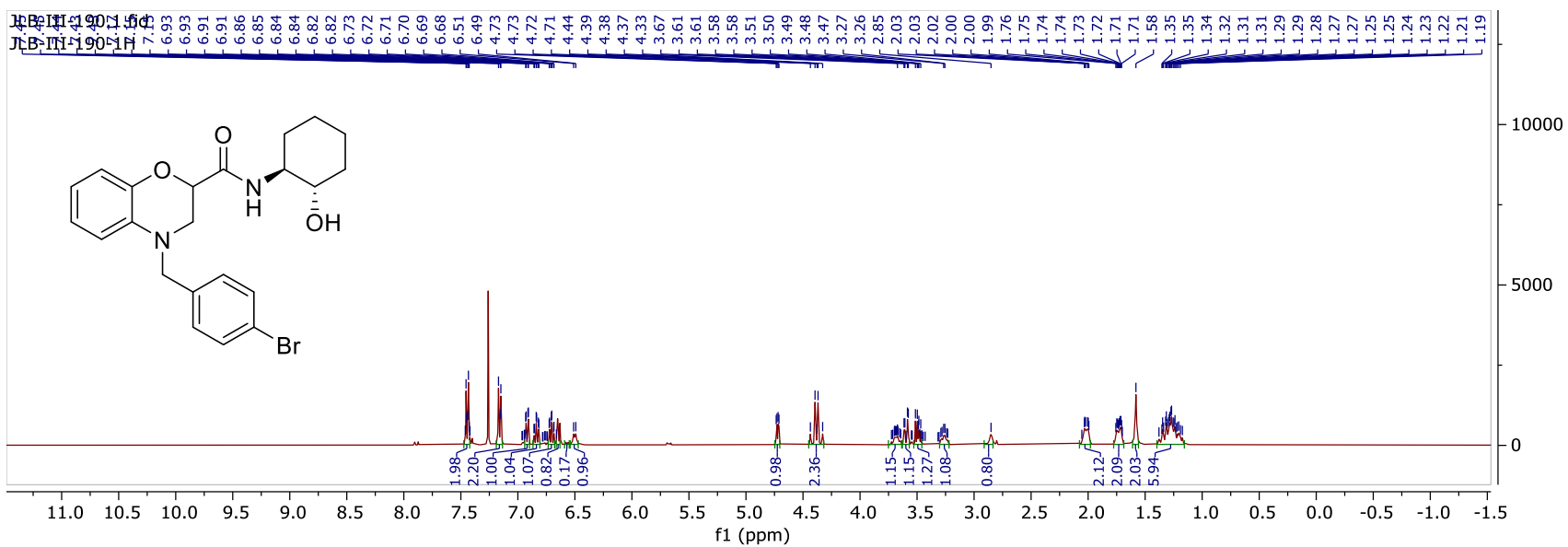
Appendix B

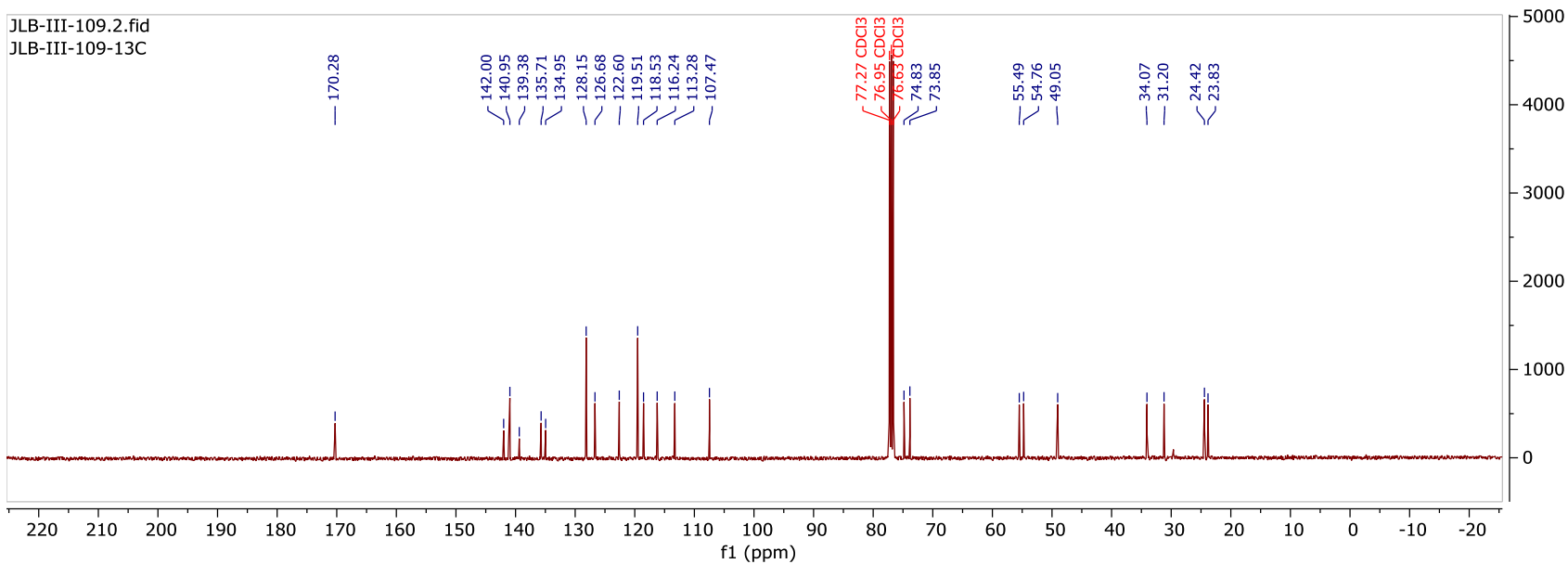
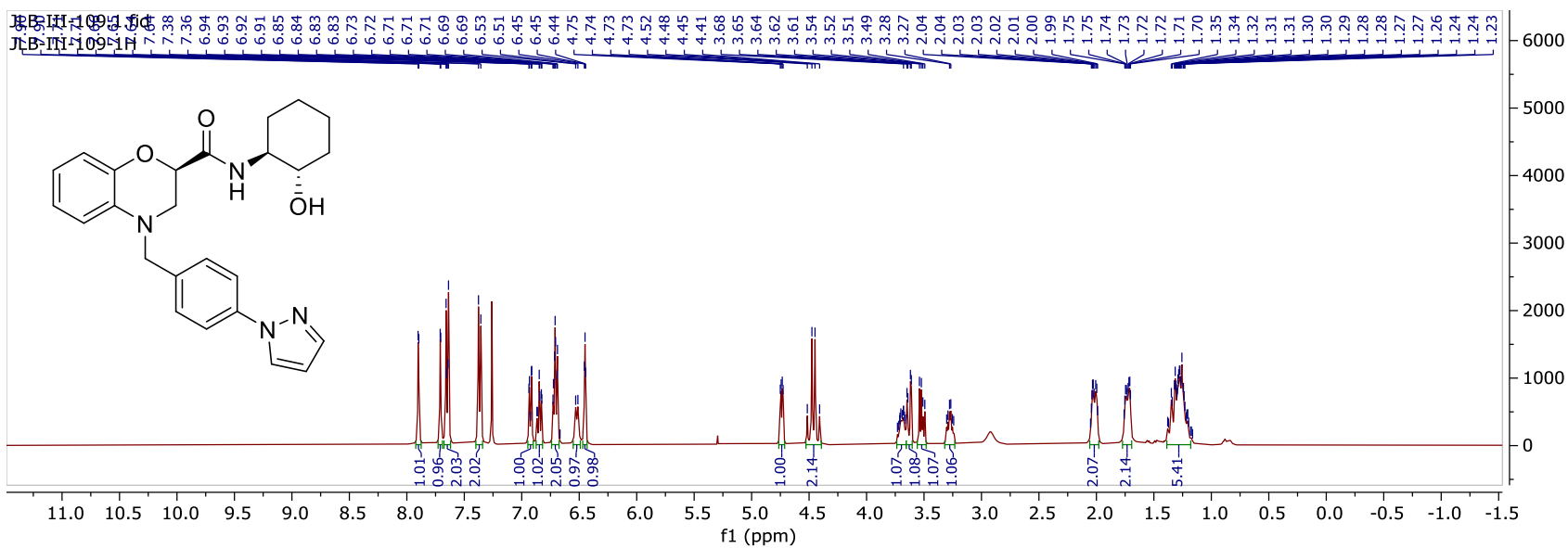
Relevant Spectra for Chapter II

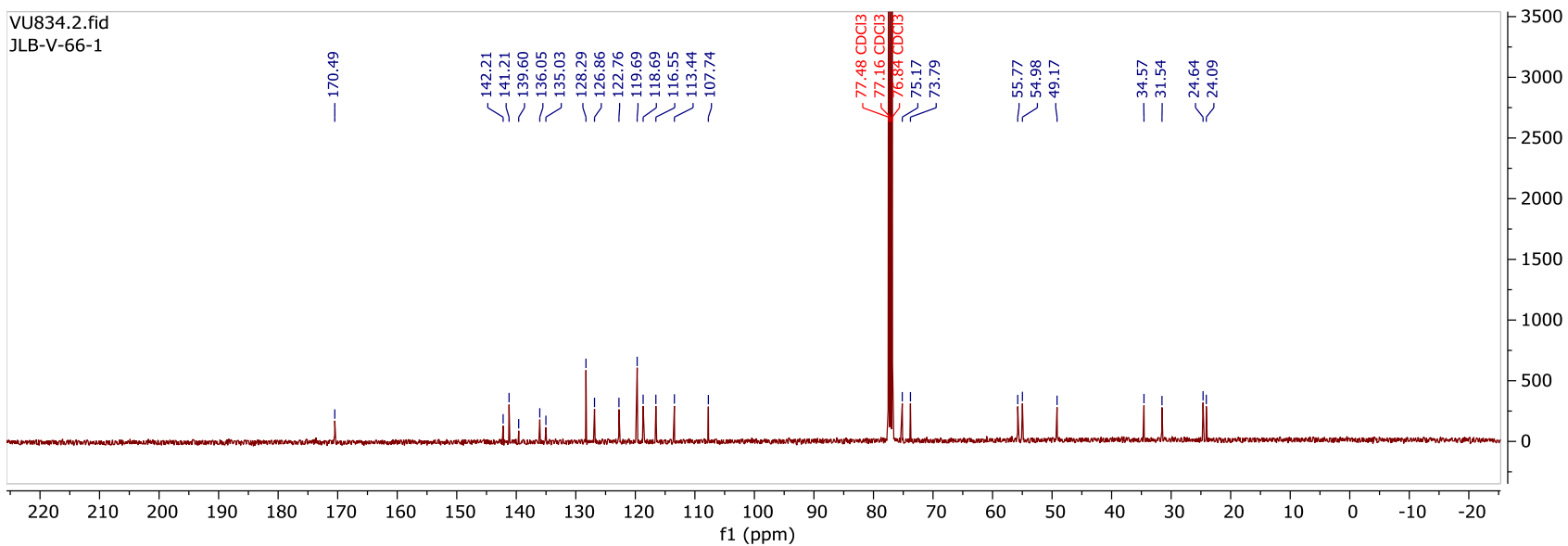
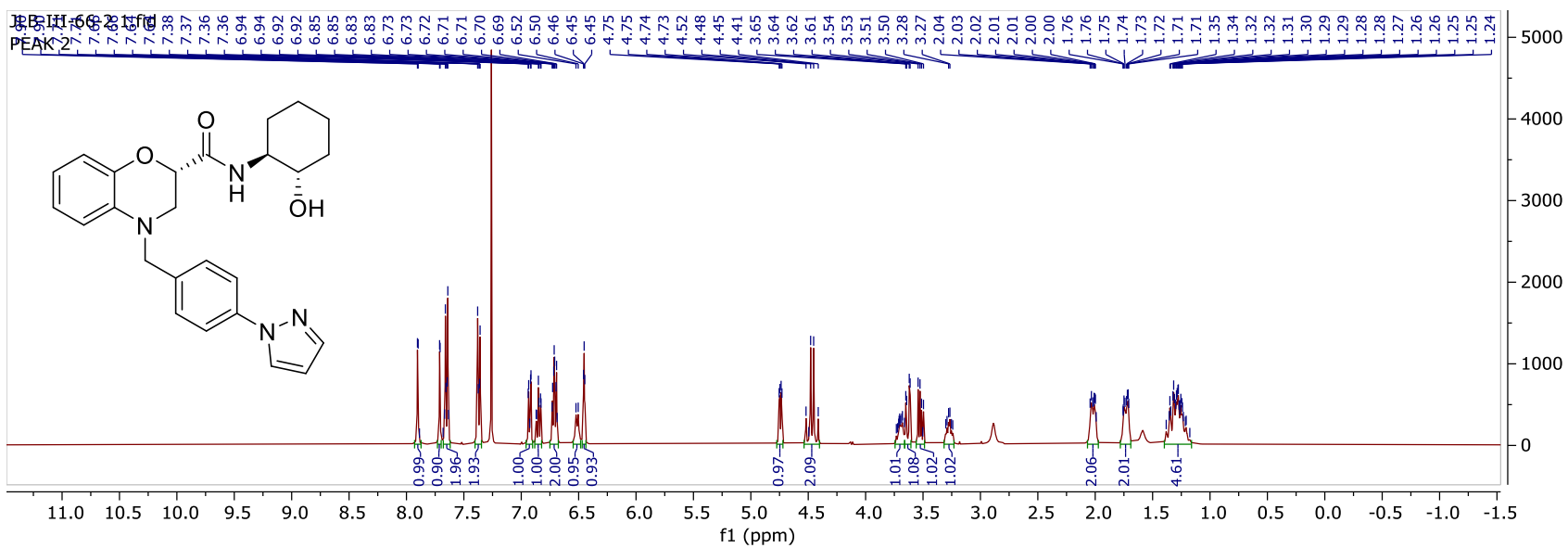


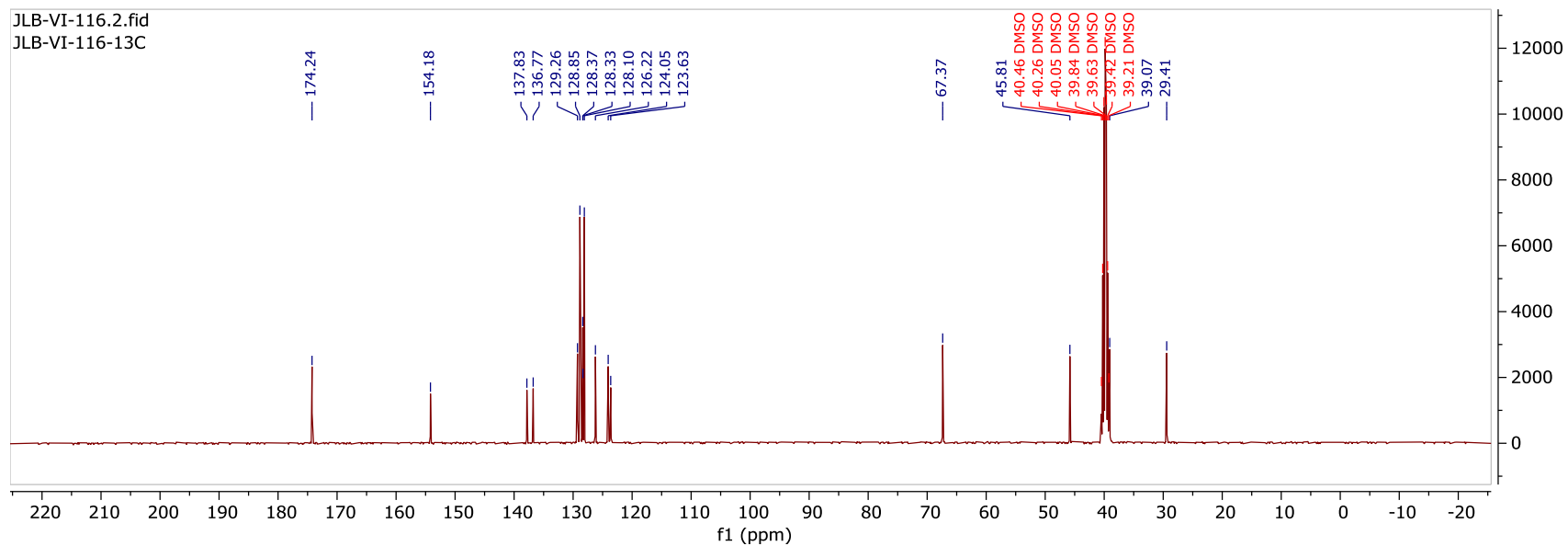
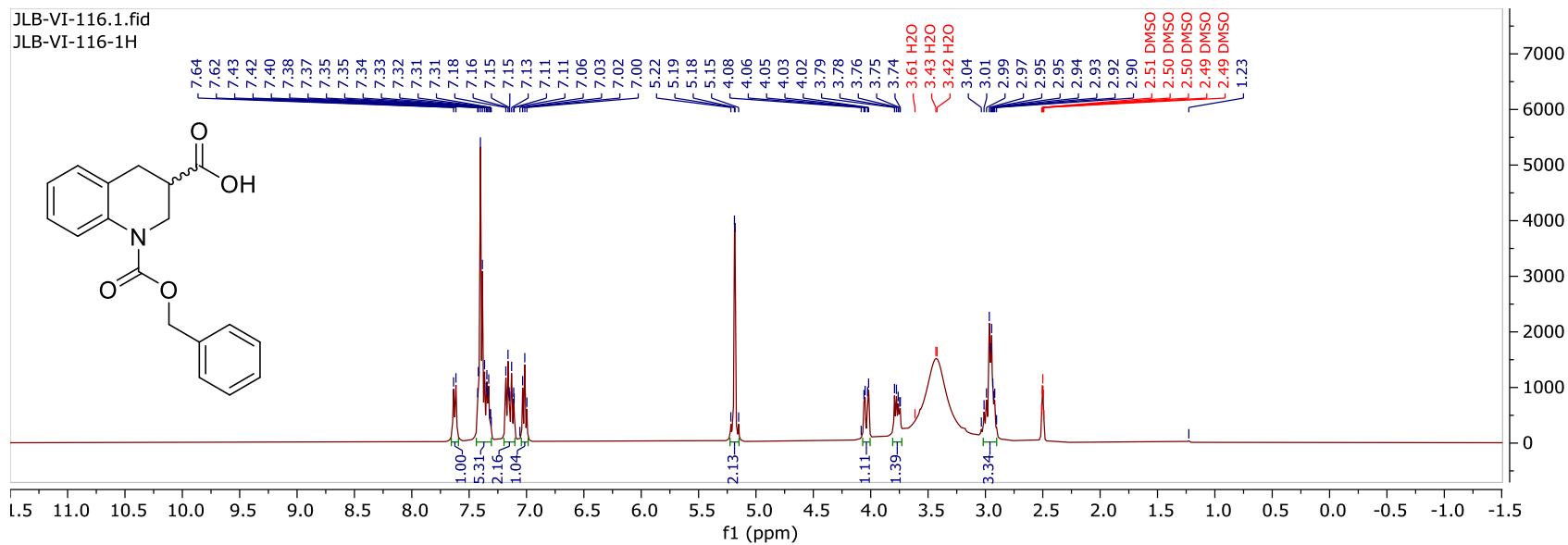


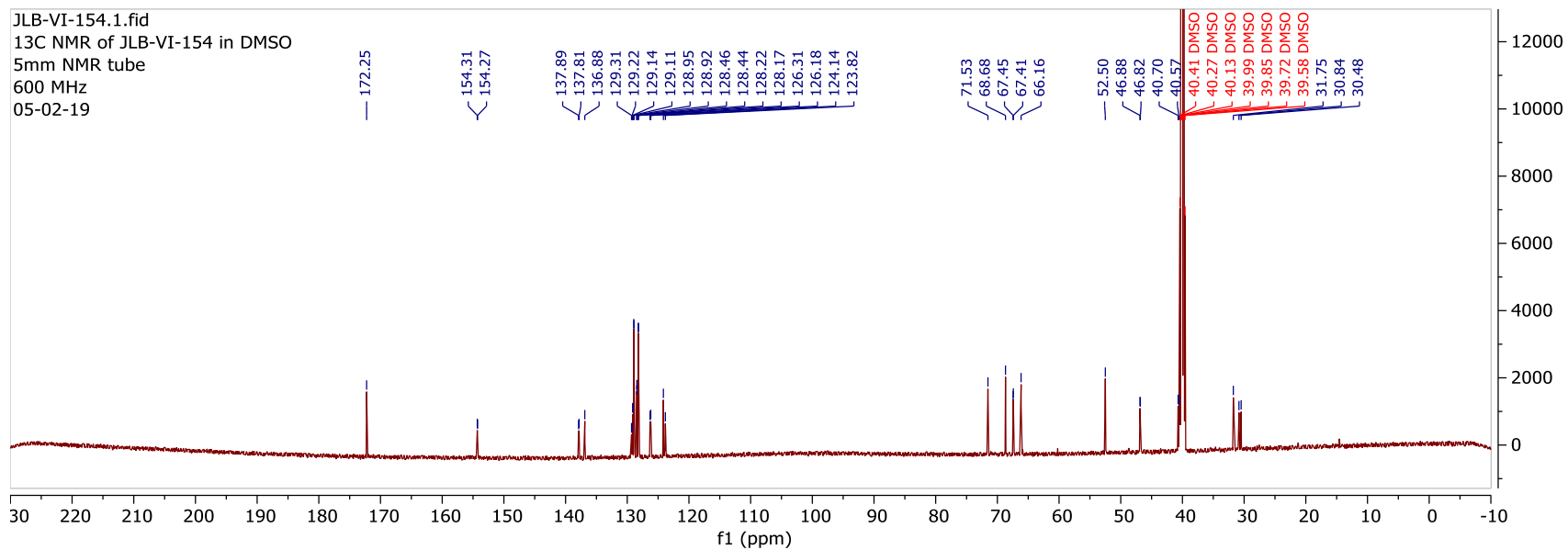
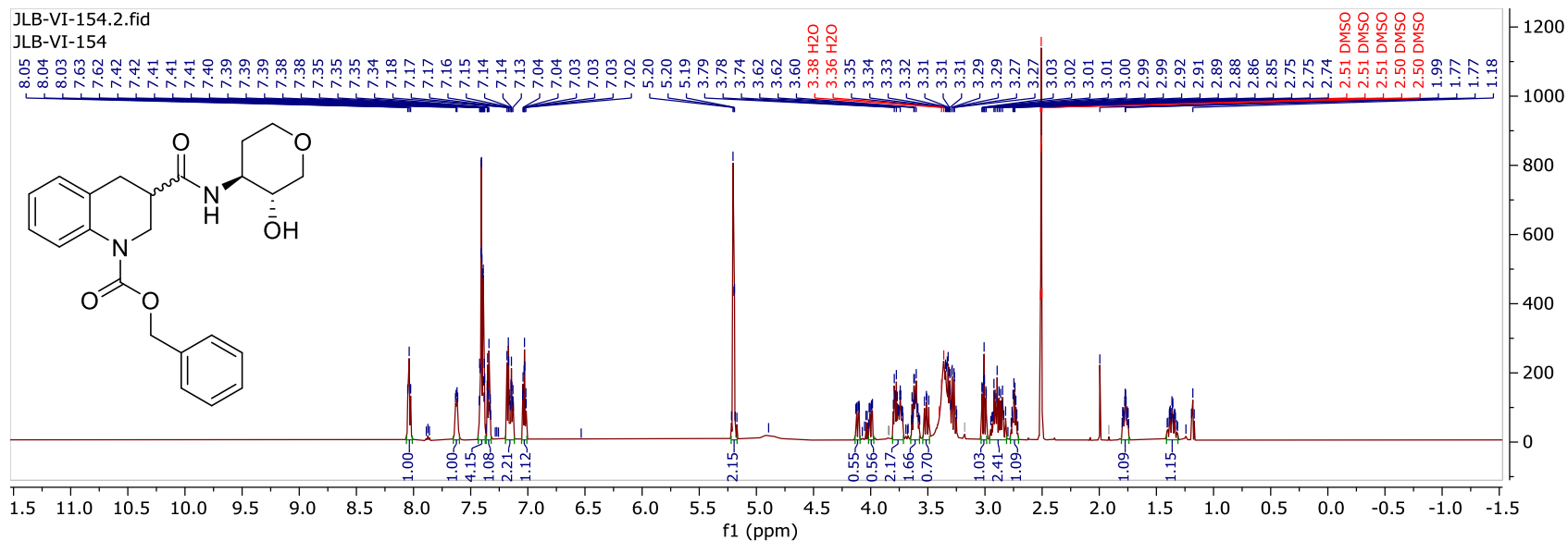


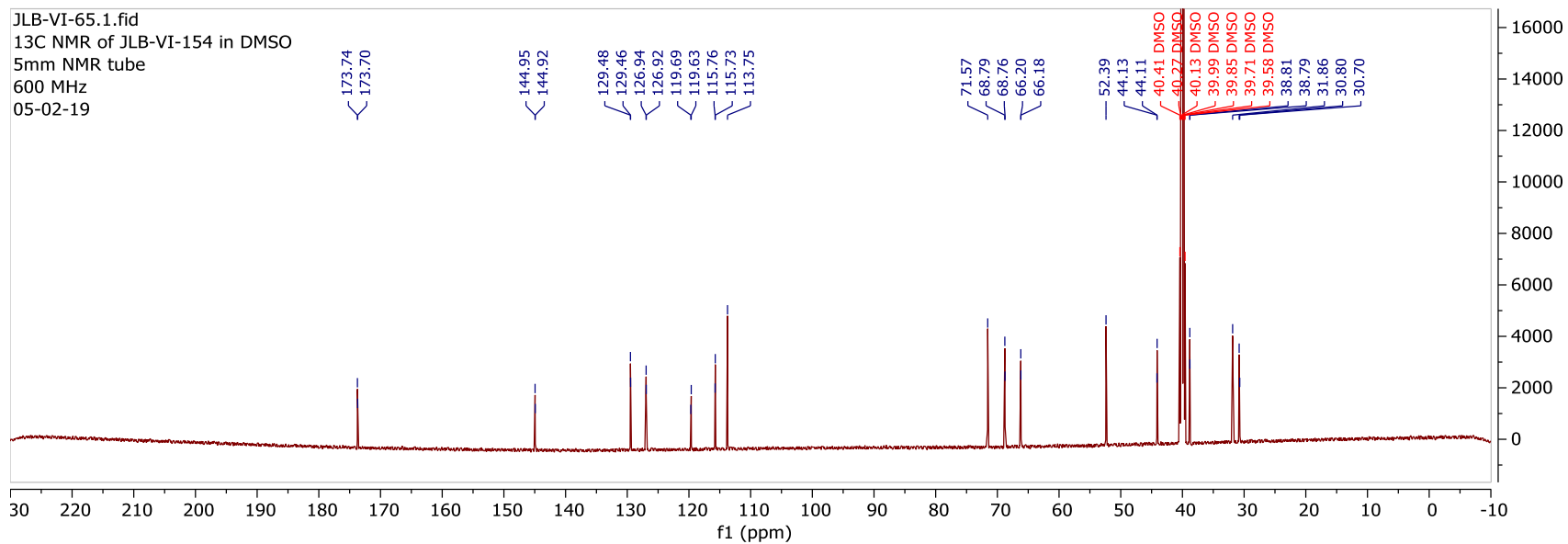
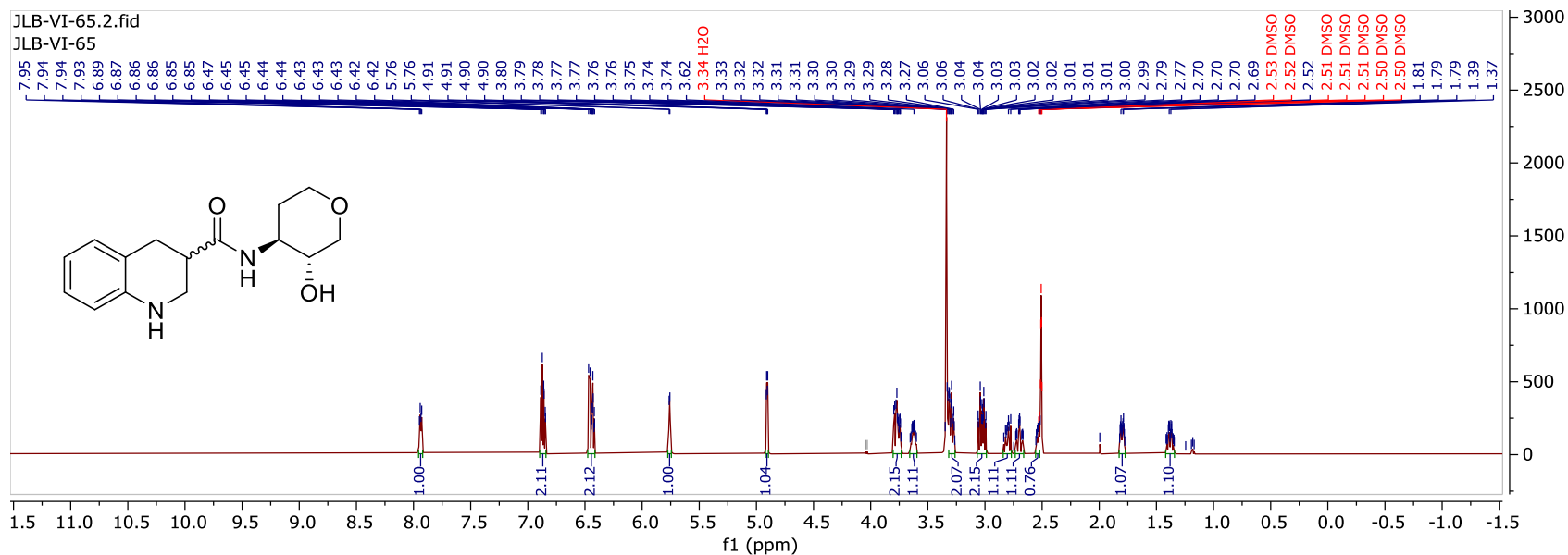


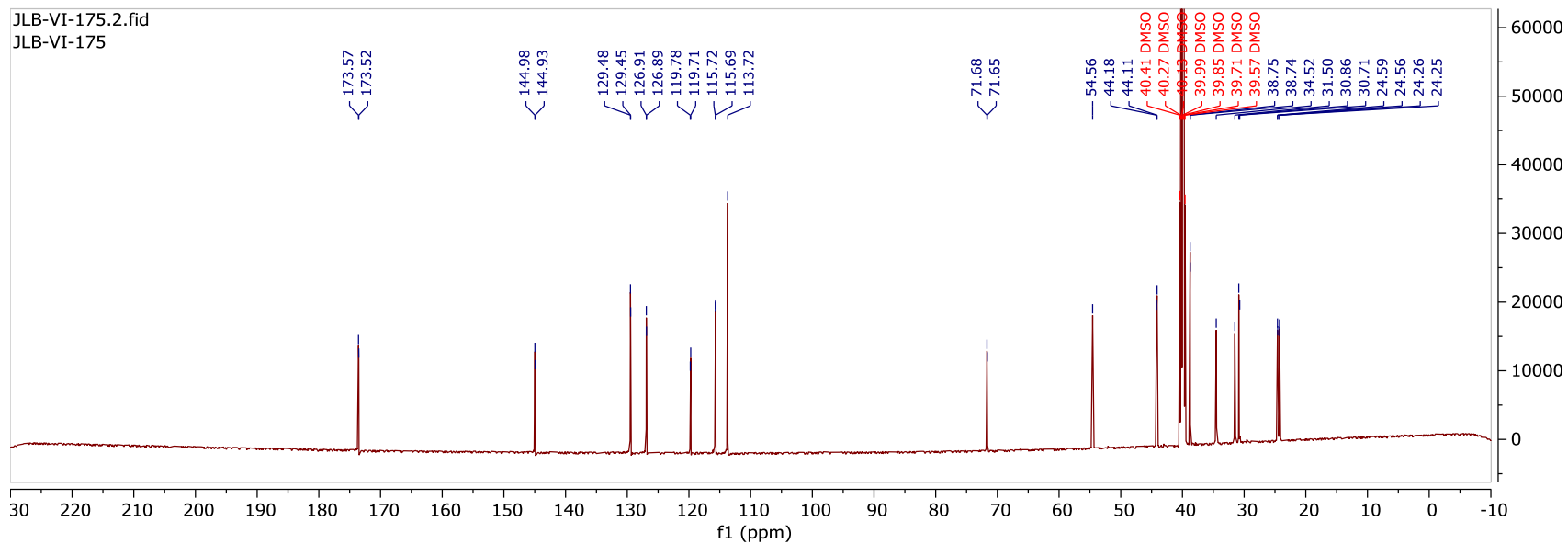
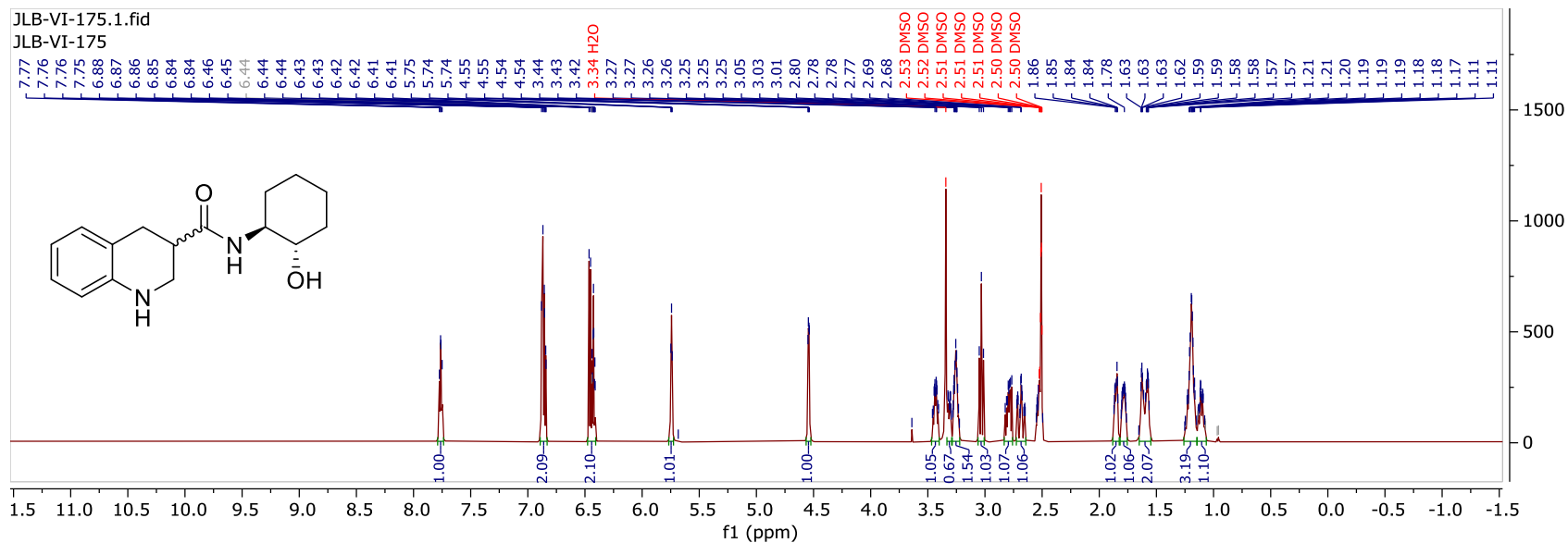


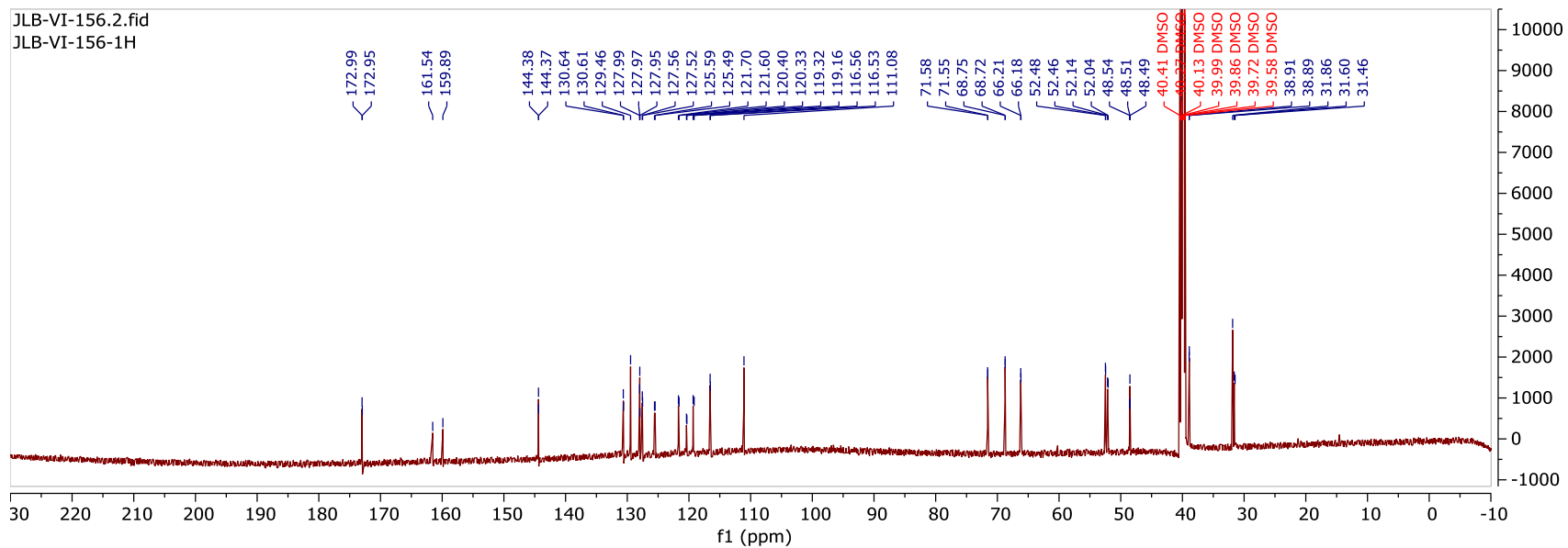
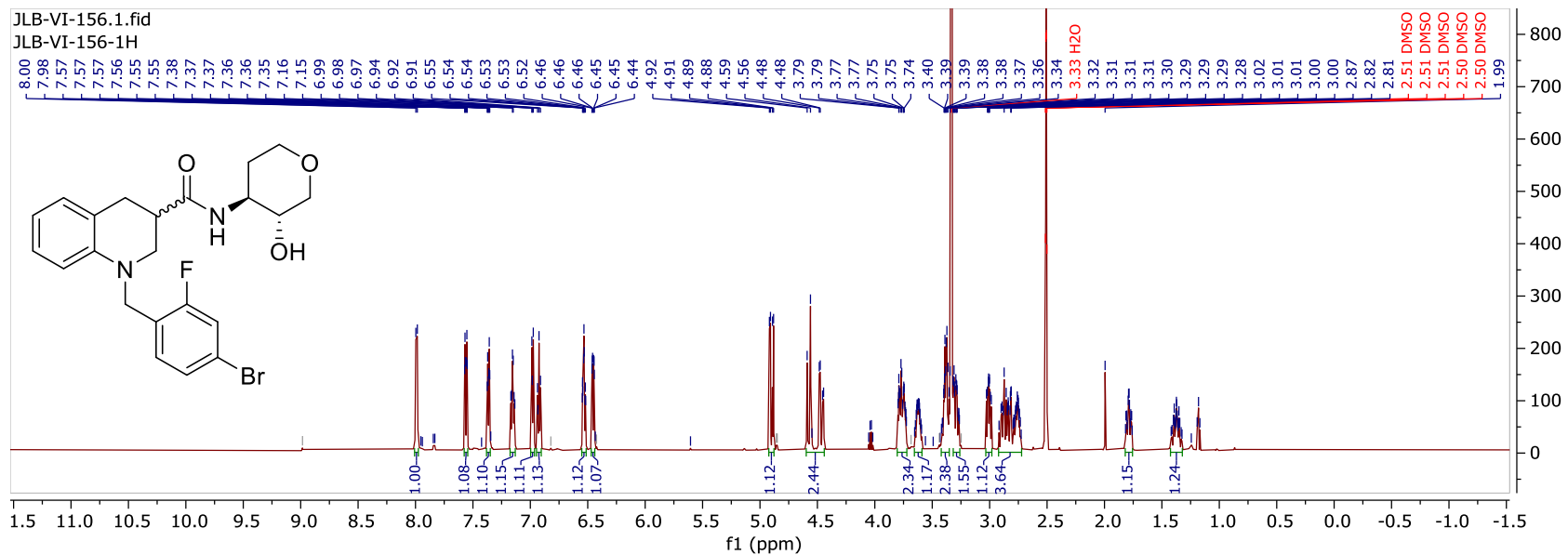


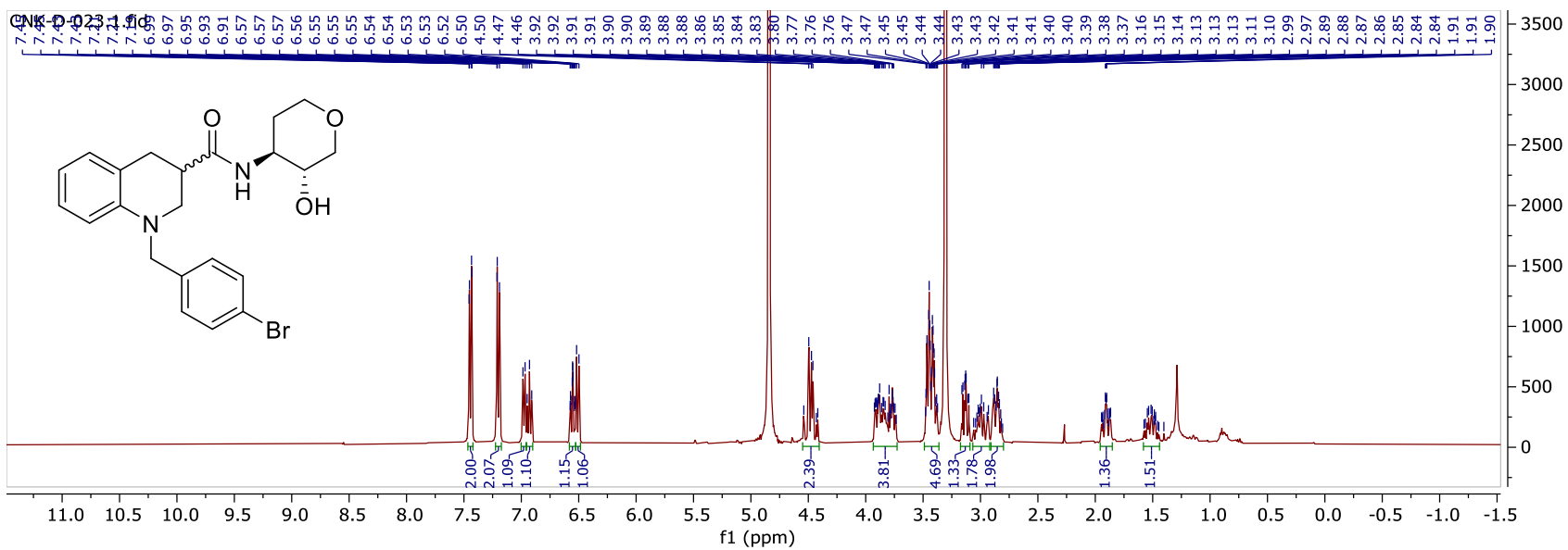


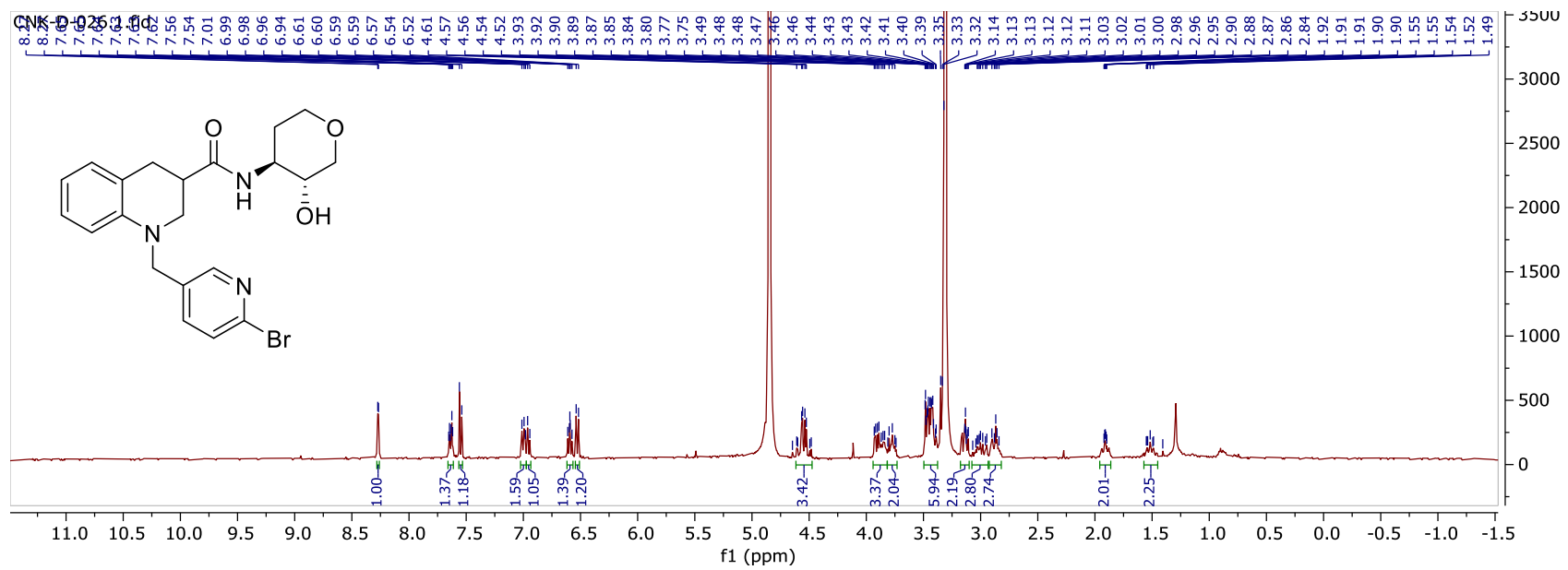


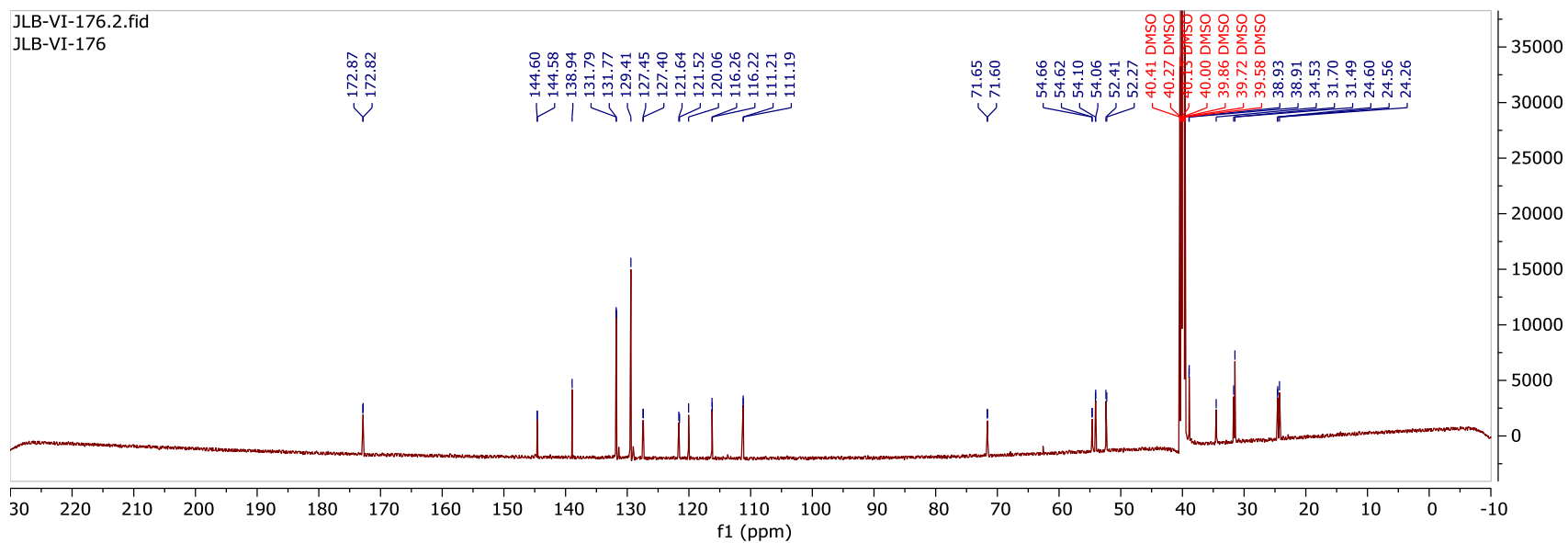
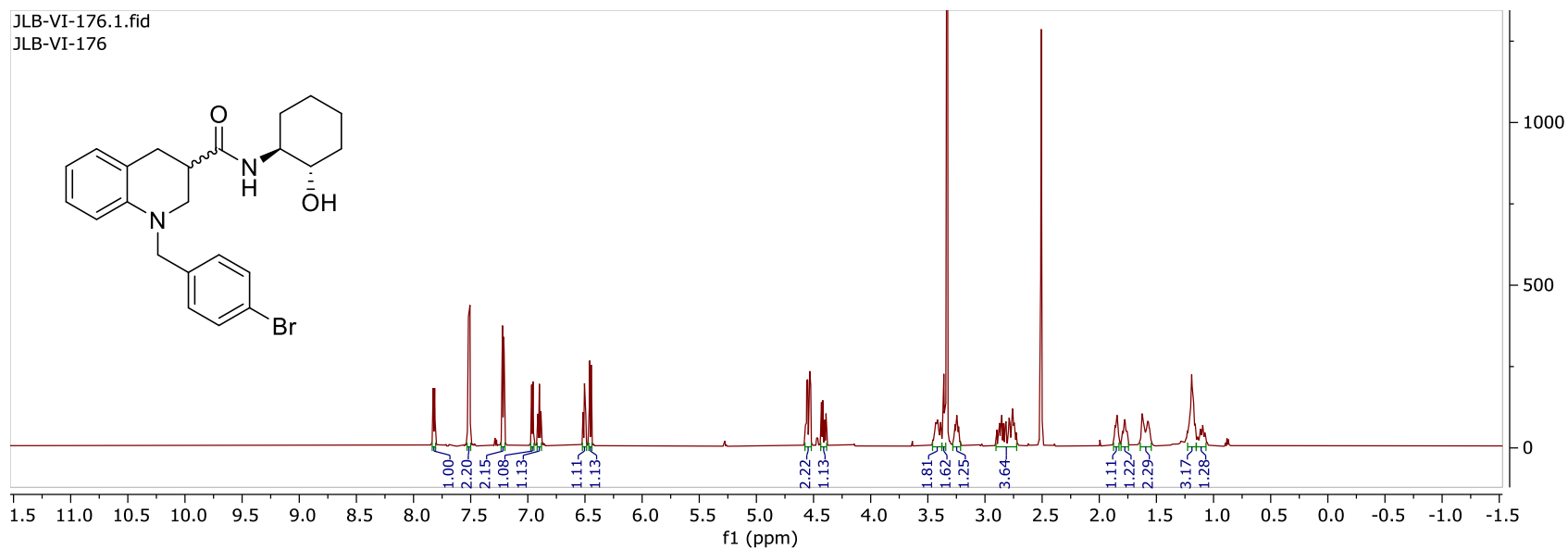


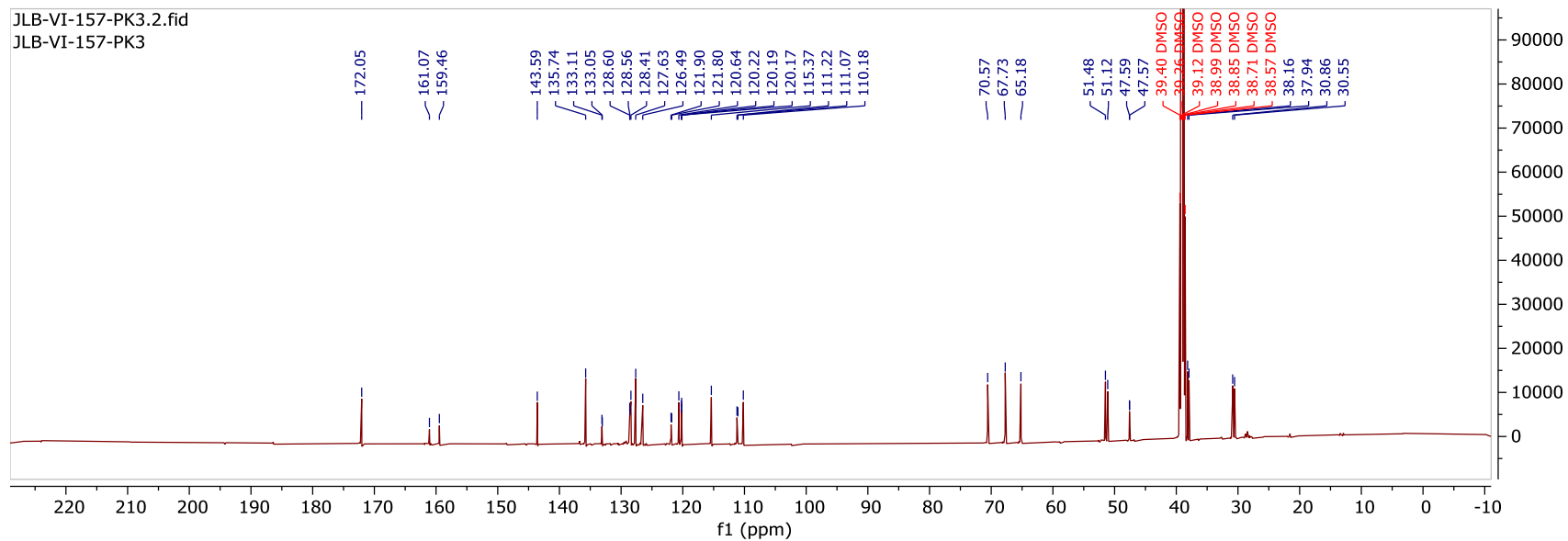
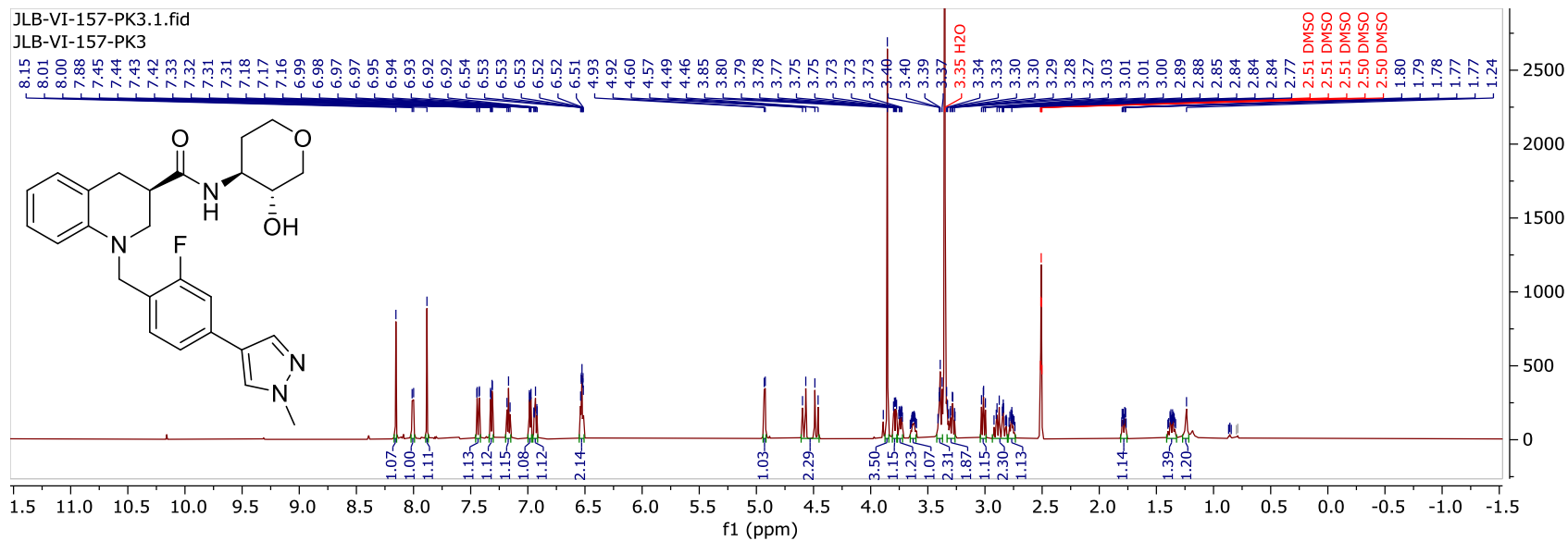


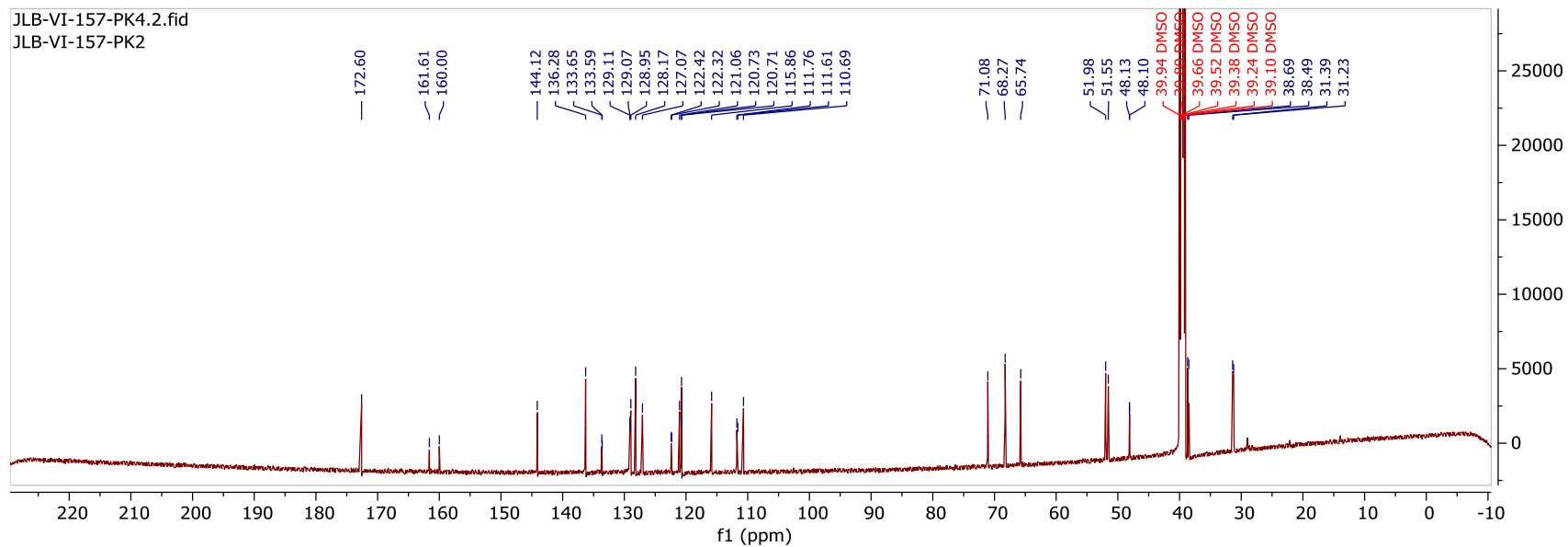
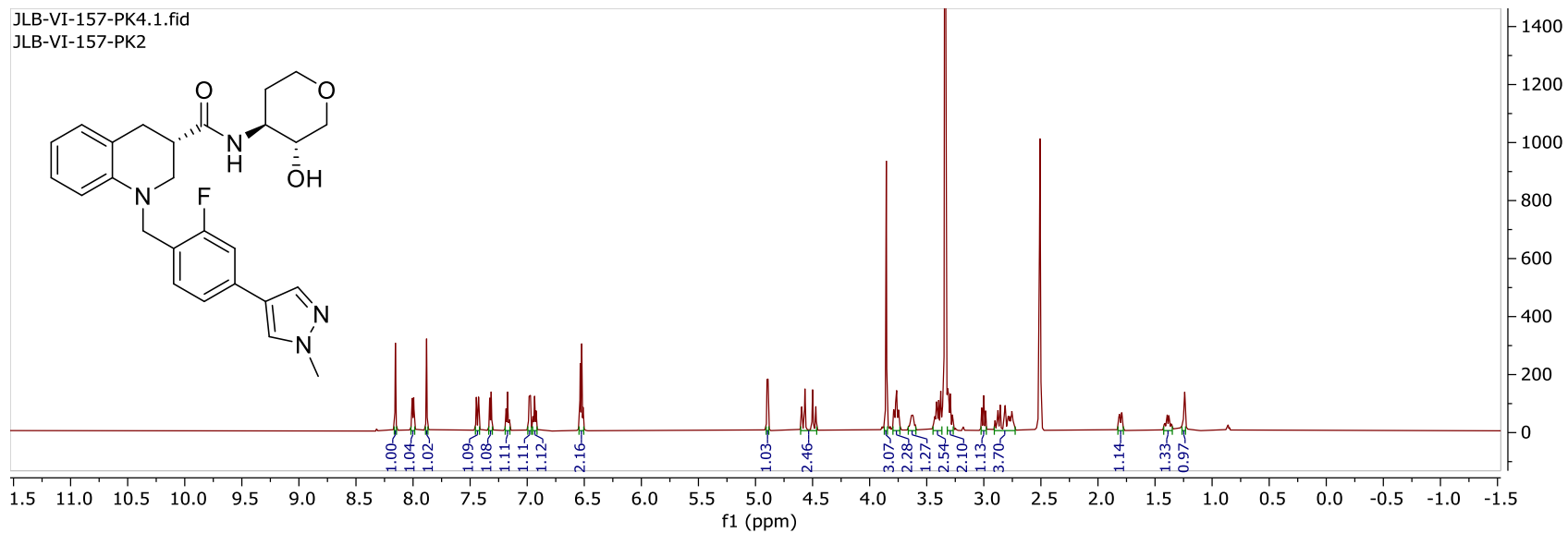


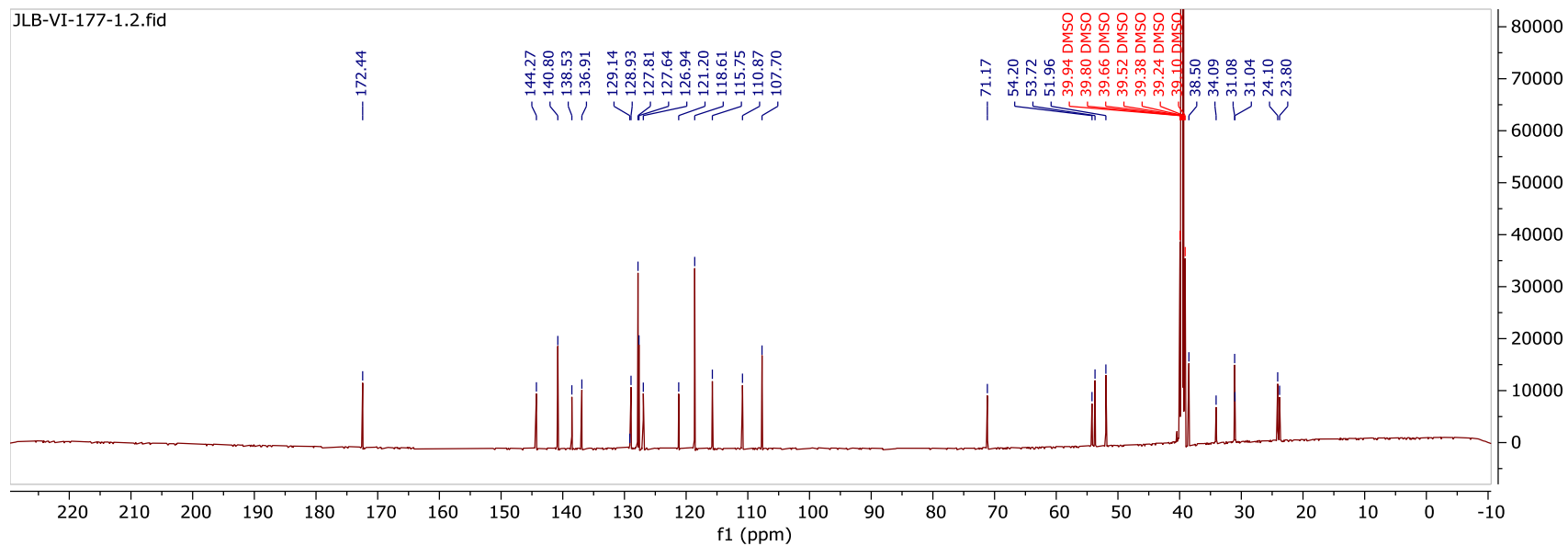
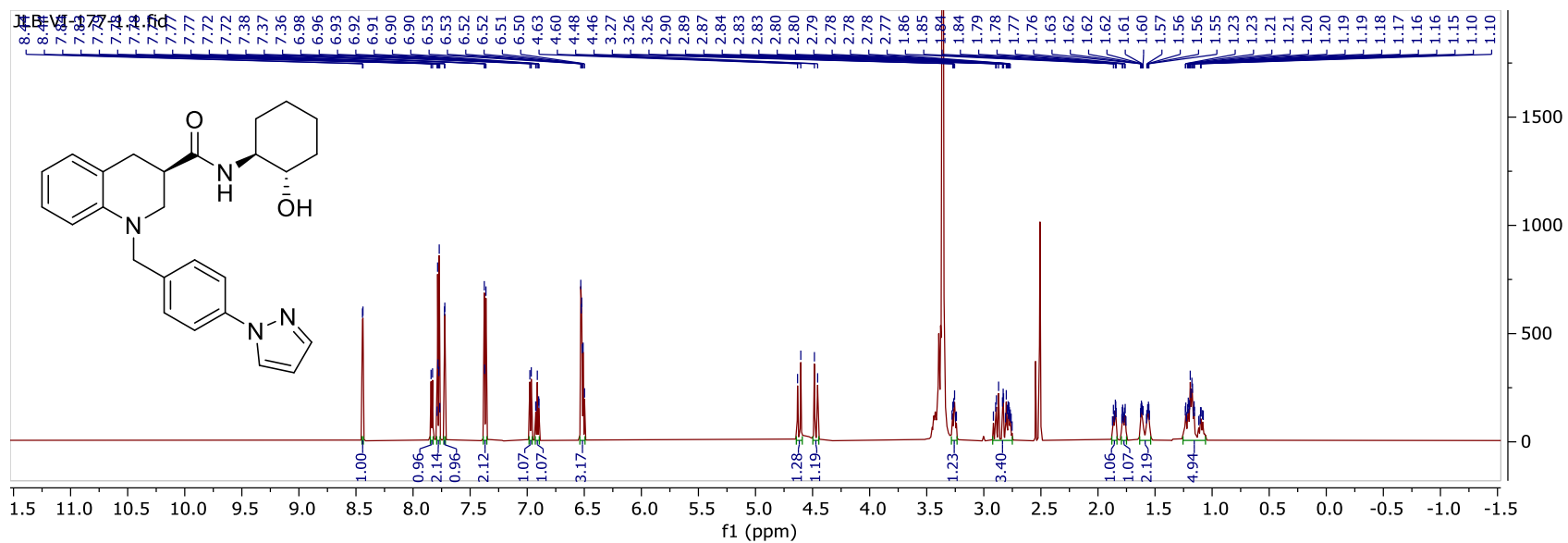


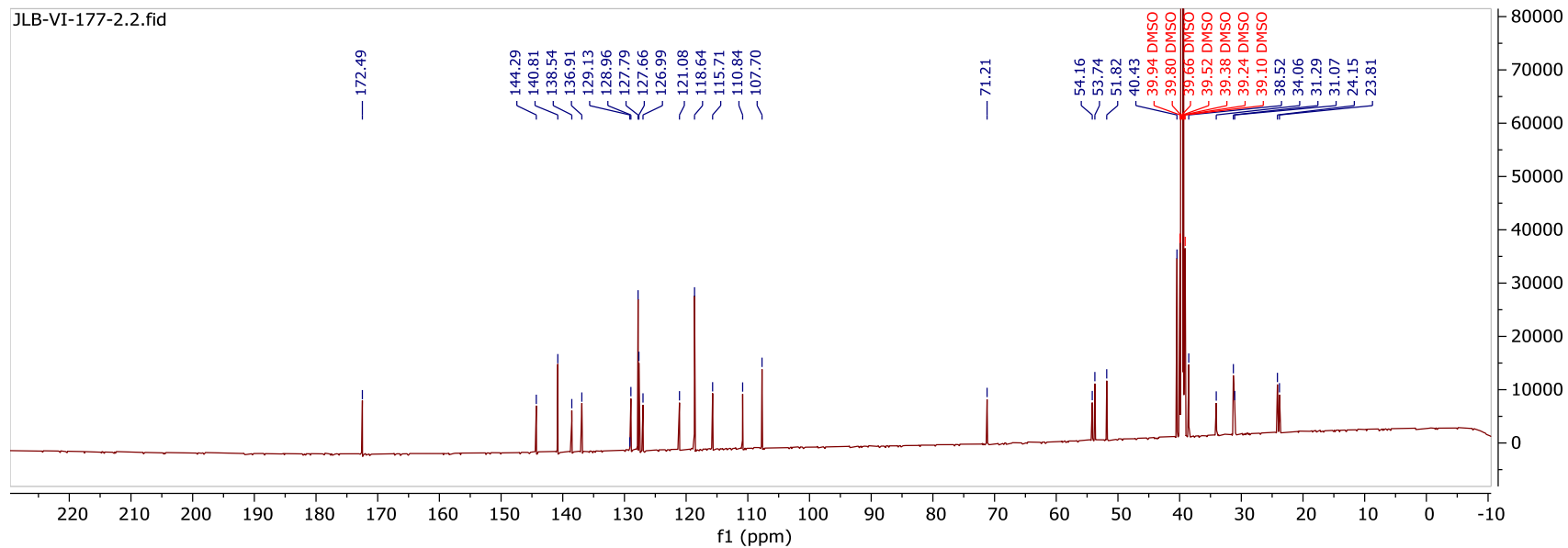
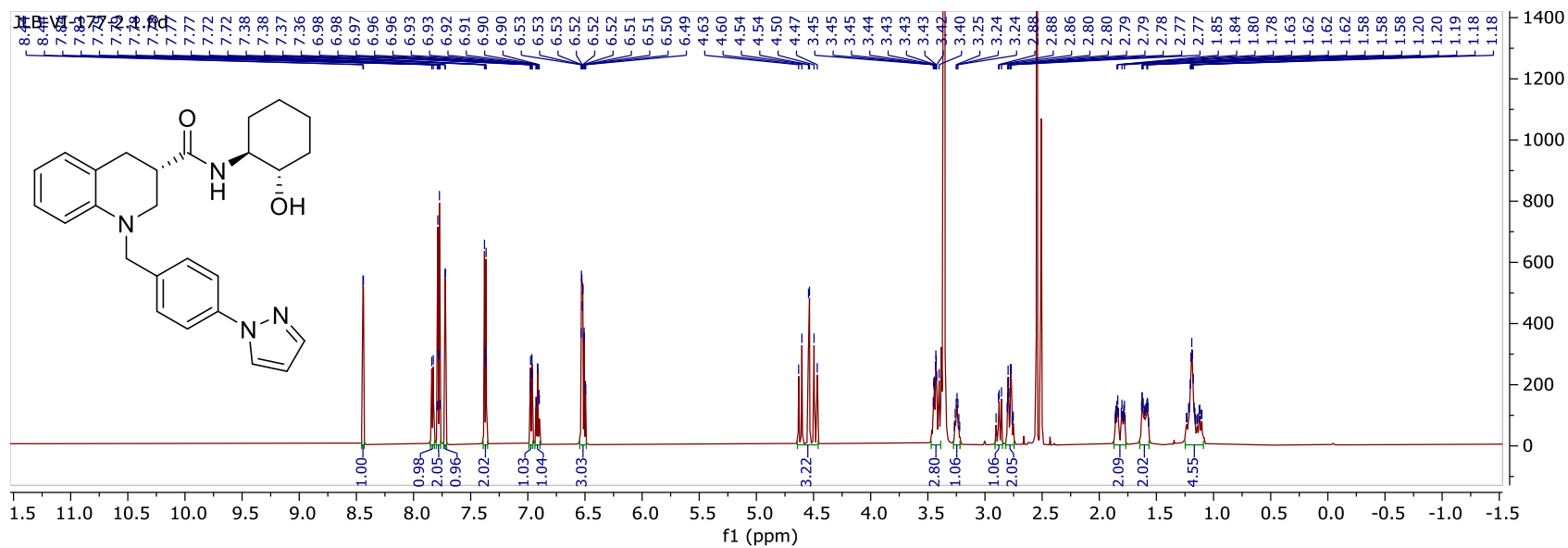












CHAPTER III

DEVELOPMENT OF NOVEL, BRAIN-PENETRANT, HUMAN AND MOUSE PAR4 ANTAGONISTS

Background and Introduction

G-Protein Coupled Receptors: Protease Activated Receptors

As previously mentioned in prior chapters, G-protein coupled receptors (GPCR) are among the most targeted receptors in drug discovery research due to their ubiquitous expression throughout the human body. GPCRs are the largest and most diverse collection of membrane receptors in eukaryotes.¹ The previous chapter focused on the muscarinic receptors, whereas this chapter will be focused on a unique and complex class of GPCRS, the protease activated receptors (PARs). Like the muscarinic receptors, the PARs are also a Family A, rhodopsin-like receptor, of which there are four subtypes (PAR1-4). PAR1, PAR3, and PAR4 are activated by serine protease thrombin, whereas PAR2 is instead activated by the serine protease, trypsin.² The uniqueness of this group of receptors lies in its activation. The PARs contain an extracellular peptide sequence that is tethered to its seven-transmembrane (7-TM) domain, which undergoes an irreversible proteolytic cleavage by their respective serine proteases to reveal a new N-terminus during activation. The new N-terminus remains tethered to the 7-TM during this process and serves as the native ligand, which binds intramolecularly to induce intracellular signaling (**Figure 3.1**).³ Immediately following

activation, the PARs are time-varyingly desensitized and internalized.⁴⁻⁹ However, the mechanism by which these processes occur is not well understood.

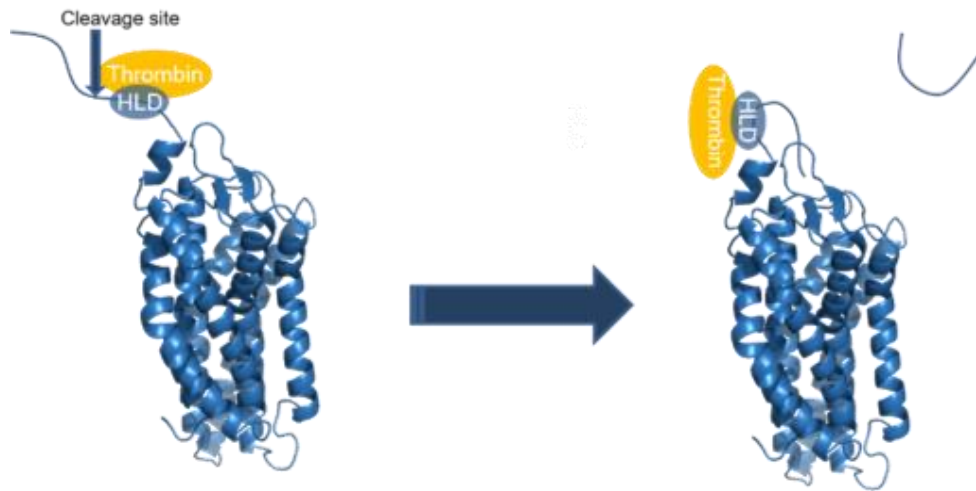


Figure 3.1 Cleavage and activation of PAR1 by serine protease, thrombin.

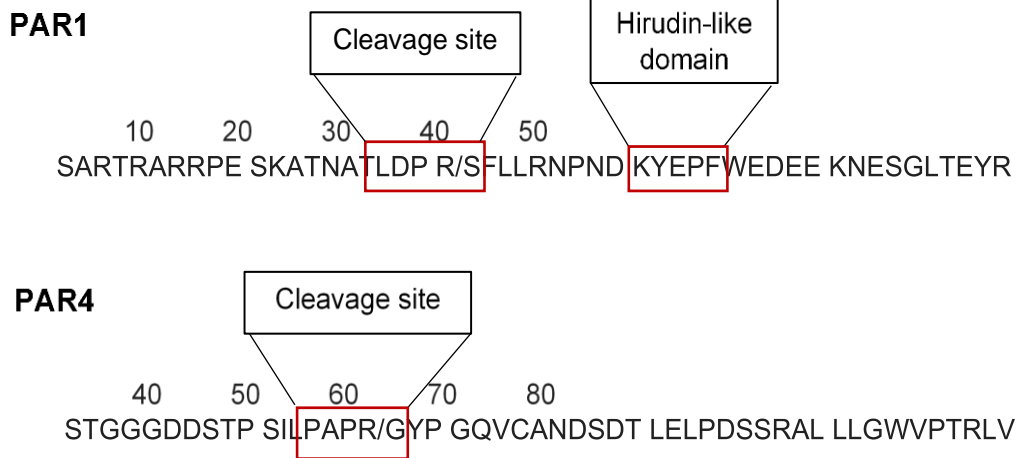
The PARs are primarily expressed in vascular, immune, and epithelial cells, as well as astrocytes and neurons. PAR regulation and expression levels have been observed to vary between species and tissue types. When activated, PAR1 and PAR2 induce $G\alpha_q$, $G\alpha_{i/o}$, and $G\alpha_{12/13}$ signal transduction pathways, while PAR4 signals through $G\alpha_q$ and $G\alpha_{12/13}$.⁴ The function of PAR3 has been a bit perplexing. Early studies reported that PAR3 was unable to transduce signals in rodents; rather, it functioned as a co-factor for PAR4 activation.^{10,11} Later studies reported that PAR3 may be able to induce intracellular calcium signals in human lung epithelial and astrocytoma cells, indicating different pharmacologies across different species.^{3,12,13} Human PAR1, PAR2, and PAR4 have typically been known to regulate hemostasis, thrombosis, and inflammation. PAR2 has been recognized for playing a role in modulating inflammation and pain.^{14,15} PAR1 and PAR4 have been known to form heterodimers, that act as a

dual receptor system in platelet activation.¹⁶ PAR1 and PAR4 are not the only dimer observed within this system. Other heterodimers as well as homodimers have also been detected, albeit little is known about their physiological roles.¹⁷⁻²¹ With several variations of homo and heterodimers, diverse cell expression levels, multiple heterotrimeric g-protein coupling partners, and physiological differing across species, the pharmacology of the PAR system is incredibly complex. To begin untangling and understanding the intricate pharmacology of the PARs, potent and selective tool compounds with acceptable drug metabolism and pharmacokinetic (DMPK) properties for *in vivo* testing must be developed.

PAR1 and PAR4 dual receptor system

As previously mentioned, PAR1 and PAR4 have been known to form heterodimers and act as a dual receptor system in the regulation of platelet activation. PAR1 contains a sequence of amino acids on its extracellular peptide chain known as the hirudin-like domain.²² The hirudin-like domain refers to the naturally occurring peptide, hirudin, found in the saliva of leeches. Hirudin serves as an anticoagulant by acting as a potent thrombin inhibitor binding to an anion-binding exosite, distinctly different from the active site.²³ This PAR1 hirudin-like domain also has a high affinity for thrombin, allowing for PAR1 activation at low circulating thrombin concentrations (**Figure 3.2A**).^{24,25} PAR4 lacks this region and therefore requires more than ten times the plasma concentration of thrombin for activation (**Figure 3.2B**).^{9,26} Because of this, it was once believed that PAR4 was a redundant receptor that acted as a fail-safe

A.



B.

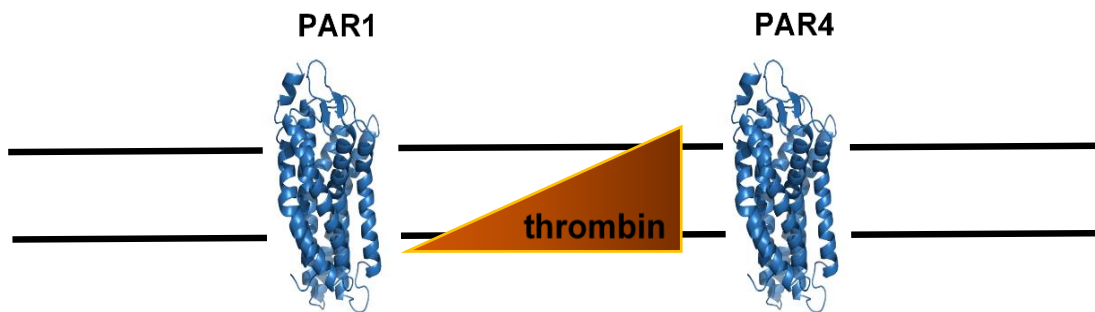


Figure 3.2 A) PAR1 and PAR4 cleavage sites, B) Activation of PAR1 at low plasma concentrations of thrombin and activation of PAR4 with increased plasma concentrations.

should PAR1 activation be perturbed. Studies have shown using monoclonal antibodies at the PAR1-thrombin interaction site that platelet coagulation can be blocked at low concentrations of thrombin. Platelet coagulation is restored at higher thrombin concentrations.^{27,28} In contrast, PAR4 monoclonal antibodies showed no effect on platelet activation by thrombin. When co-administering PAR1 and PAR4 antibodies however, a full suppression of platelet activation is observed.²⁹ These data suggest that while PAR1 and PAR4 typically function congruently, they can be activated

independently from one another. PAR1 and PAR4's ability to be independently activated is an important feature when considering the druggability of this system.

In addition, studies performed by the Hamm lab at Vanderbilt University and others have demonstrated that there is a noticeable difference in PAR1- and PAR4-initiated signaling pathways. Dunervay et al. and Falker et al. demonstrate that PAR1 signaling is transient. Contrarily, PAR4 exhibits a more robust and sustained signal that triggers irreversible platelet aggregation.^{30,31} These data imply that PAR1 plays a larger role in clotting initiation, while PAR4 plays a larger role in the propagation of clotting. Therefore, it was hypothesized that the inhibition of PAR4 activation will prevent the propagation or growth of clotting while still allowing for PAR1 initiation to form the initial hemostatic plug.

Vorapaxar (Zontivity)

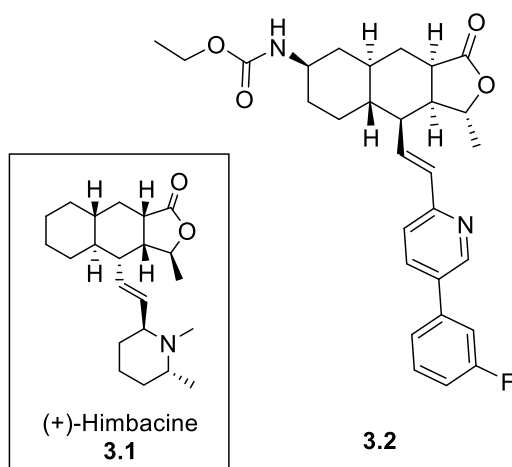


Figure 3.3 Structure of (+)-himbacine (3.1) and PAR1 antagonist, Vorapaxar (3.2).

Further supporting the hypothesis that PAR1 is crucial for platelet activation, a selective, PAR1 antagonist was developed by Merck & Co under trade name Zontivity

(Vorapaxar; **3.2**) to prevent thrombotic events in patients suffering from cardiovascular disease.³² Vorapaxar was derived from the natural product, himbacine (**3.1**) and became a first-in-class PAR1 antagonist (**Figure 3.3**).³³ It proved to be successful in preventing thrombosis. After two phase III clinical trials, the FDA issued a black box warning label stating that the use of Vorapaxar increases the risk of bleeding, including intracerebral hemorrhage and fatal bleeding.³⁴ The increased risk of bleeding with the use of Vorapaxar led to the hypothesis that PAR1 is likely crucial in platelet activation. Therefore, PAR1 is not a viable therapeutic target and scientists have turned to the exploration of PAR4 as a target for a safer therapeutic agent.

PAR4 and its therapeutic relevance

Neurodegenerative diseases affect millions of people nationwide and are known to cause immense suffering for both the patients and caregivers. Neurodegenerative disease is a general term for a large range of conditions associated with damage or death to neurons in the brain.³⁵ Disorders of this nature are quite debilitating and sadly incurable. The most common neurodegenerative diseases in the United States are Alzheimer's disease (AD) and Parkinson's disease (PD), with an estimated 5.8 million and nearly 1 million patients living with these diseases, respectfully. In addition, AD is the sixth largest cause of death in the U.S., which further attests to the prevalence and severity of the disease.^{35,36} With AD impacting close to 6 million people and costing the nation roughly \$277 billion annually, in direct and indirect costs, there is a great clinical demand for effective therapeutic agents in ameliorating the symptoms of the disease.³⁷

Several studies have demonstrated the involvement of PARs in hemostasis and inflammatory responses in the context of vascular injury and pain.^{16,27,28,38,39} However,

little attention has been focused on elucidating their physiological and pathological role in the central nervous system (CNS). All four PARs are widely expressed in the CNS on neuron, astrocyte, and microglial cells. In addition, neurons, astrocytes, and microglia also express serine proteases, such as thrombin, allowing for the activation of PARs in the CNS.⁴⁰⁻⁴² Increasing evidence indicates that thrombin-induced PAR receptor family activation contributes to both neuroprotection and neurodegeneration.

Thrombin is generated from the protein prothrombin, which is primarily synthesized in the liver. It was once believed that prothrombin was exclusively produced in the liver until experiments conducted by Monard and coworkers revealed that biosynthesis of prothrombin occurs, to a minimal extent, in the brain.⁴³ These data suggest that generally, physiological CNS concentrations of prothrombin are relatively low.⁴² When brain injury occurs, prothrombin is converted to thrombin, which cleaves and activates PAR1 and PAR4.^{40,43} Heterotrimeric protein $G\alpha_q$ then disassociates from PAR1 to activate phospholipase C (PLC), which cleaves phosphatidylinositol 4,5-bisphosphonate (PIP_2) to generate diacyl glycerol (DAG) and inositol 1,4,5-triphosphate (IP_3) (**Figure 3.4**). IP_3 diffuses away and binds to IP_3 receptors, causing an intracellular increase in calcium concentration. The mobilization of calcium into the cytosol results in downstream activation of the mitogen-activated protein kinase (MAPK) pathway, a signaling pathway well associated with microglia proliferation.⁴⁴⁻⁴⁶

Microglia are macrophage-like cells that serve as the primary immune effectors in the CNS. Under normal, physiological conditions, microglial cells exist in a “resting” state and become activated upon brain damage and/or neuronal death, presumably

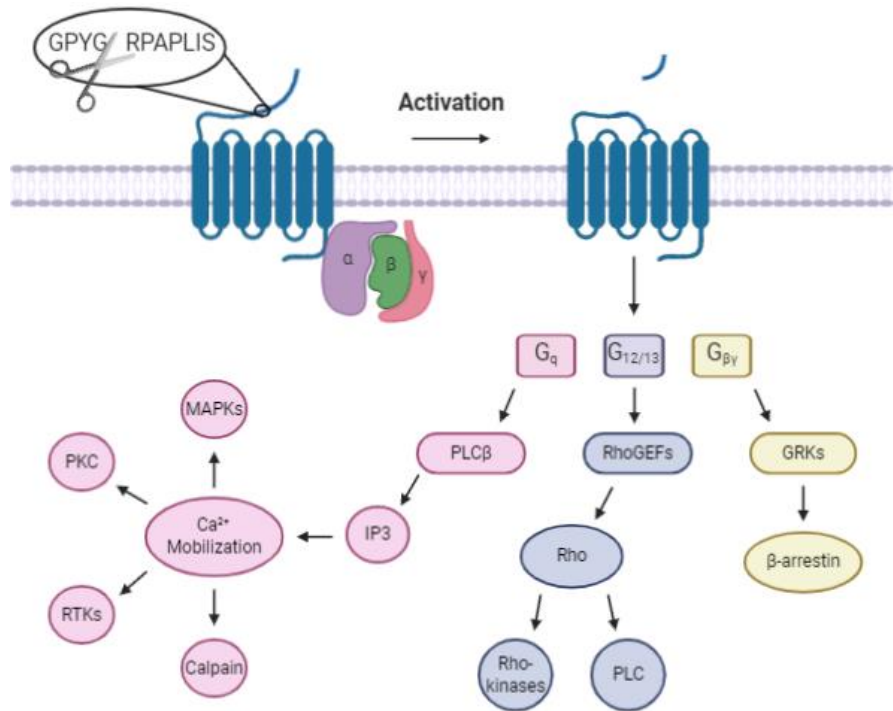


Figure 3.4 PAR4 signaling pathways when activated by thrombin.

through the aforementioned thrombin-induced signaling pathway⁴⁷⁻⁵⁰ Microglia proliferation and activation have been implicated in the pathology of hallmark characteristics tau protein aggregation and neurofibrillary degeneration in neurodegenerative tauopathies like AD, PD, and amyotrophic lateral sclerosis (ALS), therefore signifying that the thrombin-induced PAR family signaling pathway could be linked to neurodegeneration.⁵¹⁻⁵³ Thus, thrombin-induced PARs may be attractive therapeutic targets for the prevention and/or treatment of diseases such as AD, PD, and ALS.

Peptide agonists that mimic the activity of PAR1 and PAR4 native ligands post cleavage have been developed to probe their physiological function. Activation of PAR1 and PAR4 by their respective activating peptide mimics display the same

neurodegenerative responses observed as when induced by thrombin, further confirming their involvement in the signaling pathway.^{40,45,54} In addition, studies using PAR1- and PAR4-deficient mice revealed that the knockout (KO) mice exhibited less neuronal death and blood-brain barrier (BBB) damage than in wild type mice post brain damage.⁵⁵ These data confirm that PAR1 and PAR4 contribute to neurodegeneration therefore, making these protein receptors exciting, novel therapeutic targets for this particular disease state.

As mentioned previously, PAR1 and PAR4 are both expressed on astrocytes and microglial cells. At low concentrations of thrombin in the CNS, astrogliosis, BBB damage, and, to a minor extent, degeneration was observed.⁵¹ However, neurofibrillary degeneration was only observed at increased thrombin concentrations.^{45,54} We know from previous studies that PAR1 is activated at low circulating concentrations of thrombin and is rapidly phosphorylated and desensitized, while PAR4 is only activated once thrombin concentrations in the plasma reach a high enough concentration and maintains a persistent transducing signal. It is posited that post injury or disease induced brain damage, the activation of PAR1 and breakdown of the BBB allows for peripheral thrombin to enter the CNS, resulting in an increased concentration in the brain, allowing for the activation of PAR4 to induce neurodegeneration. Therefore, it was hypothesized that PAR4 can mediate neuronal signaling pathways responsible for neurodegeneration.

In addition, cerebral microbleeds (CMBs) are often observed in patients with PD and AD.⁵⁶⁻⁵⁹ CMBs are small, chronic hemorrhages located throughout the brain. Whether there is an association between CMBs, neurodegeneration, and cognition

remains elusive. Regardless, cardiovascular and neurodegenerative disease are frequently comorbid with increasing age.⁶⁰ Therefore, patients treated for neurodegenerative diseases are also often being treated concurrently with anticoagulant or antiplatelet agents. It is possible that these anticlotting therapeutics could potentially be associated with or contribute to the accumulation of CMBs in elderly patients presenting with AD or PD.^{57,59,61,62} Increasing evidence suggests that unlike traditional anticlotting agents, antagonizing PAR4 independently from PAR1 would prevent thrombosis while maintaining hemostasis.^{63,64} Thus, a PAR4 antagonist has the potential to mitigate neurodegeneration and cerebral bleeding. To investigate these potential disease states in addition to elucidating the complex pharmacology of the PARs in the CNS, a potent and selective, CNS penetrant, PAR4 tool molecule is necessary.

PAR4 Tool Compounds: Antagonists

To date, only a handful of low molecular weight, PAR4 antagonists have been described in the literature (**Figure 3.5**). Early PAR4 antagonists YD-3 (**3.3**), SEY-3 (**3.4**), and ML354 (**3.5**), although selective against PAR1, suffered from poor DMPK properties and lack of activity upon thrombin activation.⁶⁵ The instability of YD-3 and SEY-3 in liver microsomes and the toxicity liability associated with the nitro substituent of ML352 prevented these tool compounds from advancing *in vivo*. BMS-986120 (**3.6**), developed by pharmaceutical company Bristol-Myers Squibbs (BMS), was the first viable, *in vivo* tool compound with acceptable DMPK properties and activity against thrombin induced activation, and it served as a proof of concept in non-human primates. PAR4 antagonist BMS-986120 proved that by inhibiting PAR4, thrombotic

events can be prevented while maintaining hemostasis.^{63,64,66} While BMS-986120 is an effective PAR4 antagonist and selective against PAR1, its protein plasma binding (PPB > 99) combined with a CLogP of 5.5, it is likely that it is not CNS penetrant.²⁷

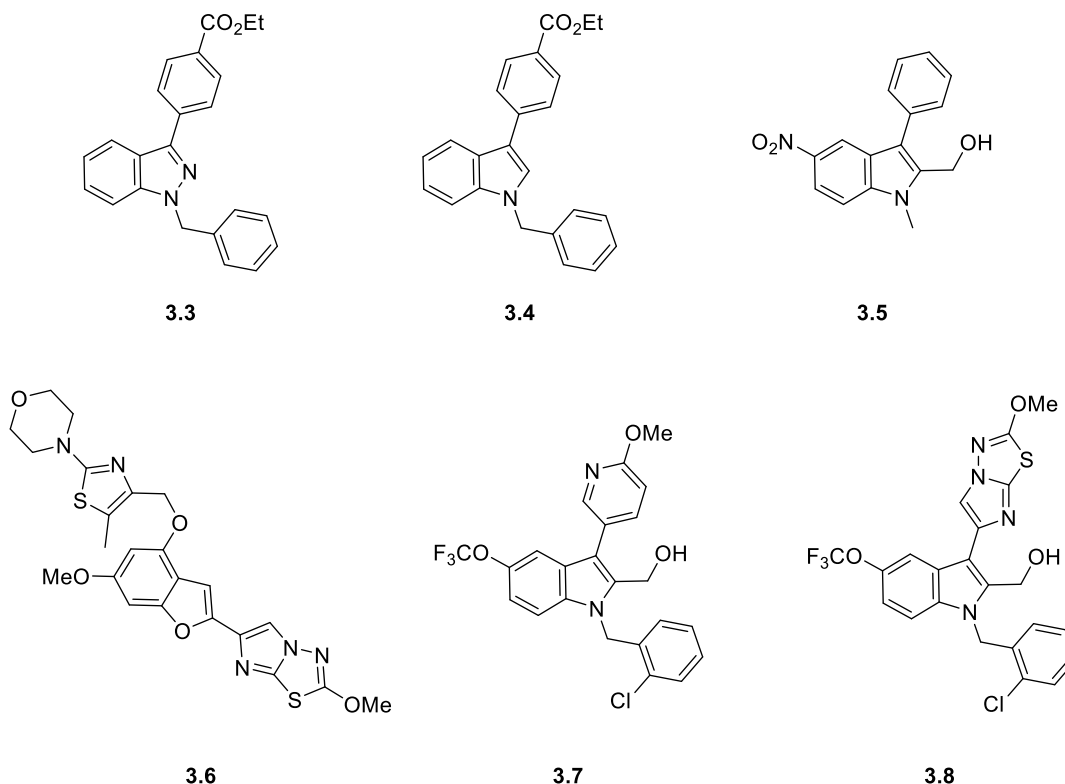


Figure 3.5 Known PAR4 antagonists **3.3-3.8**.

VU0488131 (**3.7**) and VU0661259 (**3.8**) were developed in-house by previous members of the Lindsley lab. **3.7** was derived from **3.5** and proved to be a potent and selective inhibitor against both PAR4-AP and thrombin induced activation⁶⁵. After conducting structure activity relationship (SAR) studies around BMS-986120, a minimum pharmacophore was identified and utilized along with **3.7** to generate the hybridized PAR4 antagonist **3.8**.⁶⁷ Compounds **3.7** and **3.8** exhibited significant inhibition against several CYP450 enzymes, in addition to displaying complex, mixed

modes of pharmacology, which is suboptimal for a tool molecule.⁶⁵ Therefore, there is still a need for the development of a potent, selective, brain penetrant PAR4 antagonist to further explore its role in mediating neurodegeneration.

Competitive vs. Non-competitive PAR4 Antagonist

BMS-986120 analog VU0652925 (**3.9**; originally developed by BMS), was resynthesized at Vanderbilt and tested in both our PAR4-AP assay and our thrombin mediated platelet activation assay (**Figure 3.6**). **3.9** was found to partially inhibit PAR4 thrombin induced activation and fully inhibit against PAR4-AP mediated activation. Schild analysis studies were conducted on **3.9**, which revealed that it functions via a non-competitive mode of inhibition. PAR4 antagonist VU0661224 (**3.10**) was derived from **3.9** and developed by the Lindsley lab at Vanderbilt University during minimum pharmacophore identification studies (**Figure 3.6**). **3.10** was found to be effective in inhibiting thrombin induced PAR4 activation at lower concentrations of thrombin. However, it was reversed with increasing thrombin concentrations, which is consistent with a competitive binding mode. Indeed, Schild analysis studies identified **3.10** as a competitive inhibitor.²⁷ To investigate the switch in binding modalities, studies were

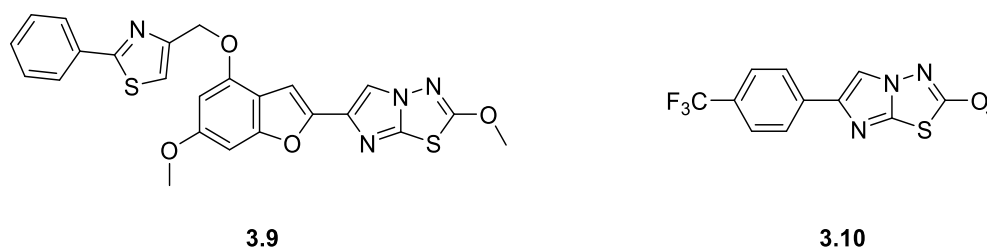


Figure 3.6 Structures of PAR4 antagonists VU0652925 (**3.9**) and VU0661224 (**3.10**).

conducted to identify a potential interaction responsible for the switch in the mechanism of inhibition.

A PAR4 homology model developed by the Meiler lab at Vanderbilt University based on the co-crystal structures of PAR1 and PAR2 (as there is currently not a crystal structure available for PAR4) was utilized in these studies.^{68,69} The PAR4 homology model docking studies indicate the removal of the phenyl thiazole moiety from **3.9** resulted in the binding mode switch from a non-competitive inhibitor to a competitive inhibitor. The homology model suggests that the phenyl thiazole portion of **3.9** extends deep into the transmembrane domain, while the extended fused ring system is situated up near the extracellular space (**Figure 3.7**). In addition, it has been reported that thrombin binds allosterically to clusters of electronegative aspartate residues on the second extracellular loop of the transmembrane domain and a second cluster in the *N*-terminal of the PAR4 receptor to facilitate the cleavage of the extracellular peptide sequence.⁷⁰ It has also been reported that following thrombin cleavage, the newly

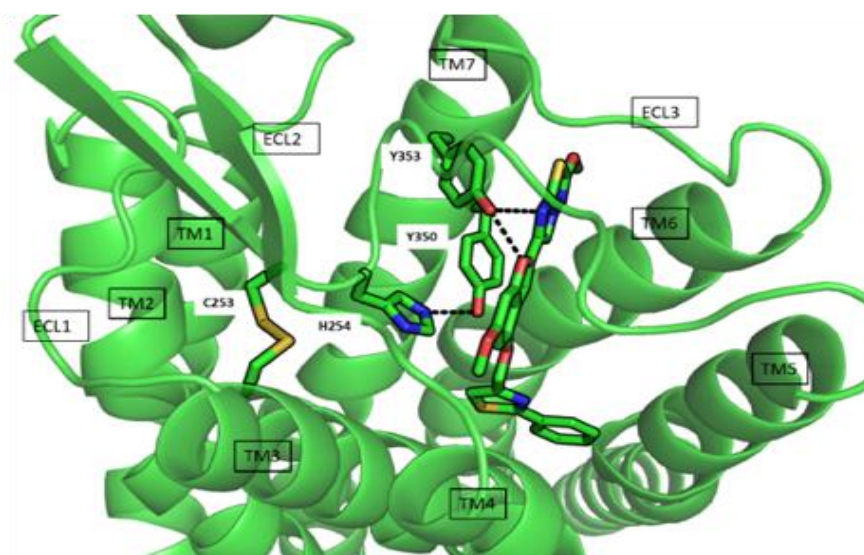


Figure 3.7 In silico docking studies of VU0652925 (**3.9**) in a PAR4 homology model. Image courtesy of Darwin Fu.

exposed tethered ligand also binds to the second extracellular loop.⁷¹ These data suggest that the orthosteric binding site for both thrombin and the tethered ligand are located at the surface of the receptor within the second extracellular loop region, further supporting our theory that **3.10** is likely binding at the surface of the receptor within this region and is out competed as thrombin plasma concentrations increase. Therefore, we believe that the mode of inhibition is dependent upon the molecules ability to generate binding interactions with amino acid residues located deep within the transmembrane domain. Because PAR4 is solely activated at high concentrations of thrombin, these data suggest that pursuing a non-competitive mode of inhibition would be more advantageous in developing an efficacious PAR4 antagonist.

PAR4 Pharmacogenomics – Single Nucleotide Polymorphisms

Pharmacogenomics is the study of how one's genome can affect their response to drugs. There have been several examples in the literature where single nucleotide polymorphisms (SNPs) in the genome cause discrepancies in the way the human body reacts to certain drugs.⁷²⁻⁷⁵ The gene that encodes the PAR4 receptor, *F2RL3*, has been revealed to harbor an A/G SNP (rs773902) that mediates a substitution of an alanine to threonine at residue 120. It has been noted that allelic frequencies of the A/G SNP are racially dimorphic, with residue Thr120 arising more commonly in black individuals (63%) than white individuals (19%).⁷² Bray and co-workers demonstrated a 3.7-fold increase in aggregation kinetics in those with the AA allele over those with GG. In addition, PAR4 receptors with the *F2RL3* AA genotype have been found to be resistant to desensitization post activation and require three-fold higher levels of PAR4-AP to induce receptor desensitization.⁷² These data suggest that the rs773902 SNP

genotype disparity in thrombin sensitivity is potentially mediated by receptor desensitization. Tool compounds have been utilized to further explore the pharmacology of these polymorphisms.

Unfortunately, there have been some discrepancies in the regulation of PAR4 function and inhibitory capacity of different PAR4 antagonist chemotypes. It has been reported that individuals homozygous for PAR4 Thr120 are resistant to YD-3 inhibition at concentrations up to 1 μ M, while BMS-986120 fully inhibits PAR4-AP aggregation in both genotypes at 400 nM. It is possible that the competitive nature of YD-3 prevents the activity necessary to induce platelet aggregation in the AA allele genotype and therefore, further evaluation is necessary.

Conclusions

Following a high-throughput screening (HTS) campaign, we will identify novel PAR4 antagonists that are primed for rapid and facile synthetic efforts to generate analogs for the optimization of a PAR4 tool compound. The PAR4 homology model will be utilized in addition to SAR, to drive our chemical approaches. Verified 'hit' compounds will be optimized through traditional medicinal chemistry efforts and iterative parallel synthesis. By developing a selective, brain penetrant non-competitive antagonist, we hope to achieve the necessary potency and efficacy necessary for *in vivo* validation and pharmacogenomic studies. The remainder of this chapter will describe our efforts towards the development of novel PAR4 antagonists.

Materials and Methods

General Synthetic Methods and Instrumentation

All NMR spectra were recorded on a 400 MHz AMX Bruker NMR spectrometer. ¹H and ¹³C chemical shifts are reported in δ values in ppm downfield with the deuterated solvent as the internal standard. Data are reported as follows: chemical shift, multiplicity (s = singlet, d = doublet, t = triplet, q = quartet, b = broad, m = multiplet), integration, coupling constant (Hz). Low resolution mass spectra were obtained on an Agilent 6120 or 6150 with ESI source. MS parameters were as follows: fragmentor: 70, capillary voltage: 3000 V, nebulizer pressure: 30 psig, drying gas flow: 13 L/min, drying gas temperature: 350 °C. Samples were introduced via an Agilent 1290 UHPLC comprised of a G4220A binary pump, G4226A ALS, G1316C TCC, and G4212A DAD with ULD flow cell. UV absorption was generally observed at 215 nm and 254 nm with a 4 nm bandwidth. Column: Waters Acquity BEH C18, 1.0 x 50 mm, 1.7 μm. Gradient conditions: 5% to 95% CH₃CN in H₂O (0.1% TFA) over 1.4 min, hold at 95% CH₃CN for 0.1 min, 0.5 mL/min, 55 °C. High resolution mass spectra were obtained on an Agilent 6540 UHD Q-TOF with ESI source. MS parameters were as follows: fragmentor: 150, capillary voltage: 3500 V, nebulizer pressure: 60 psig, drying gas flow: 13 L/min, drying gas temperature: 275 °C. Samples were introduced via an Agilent 1200 UHPLC comprised of a G4220A binary pump, G4226A ALS, G1316C TCC, and G4212A DAD with ULD flow cell. UV absorption was observed at 215 nm and 254 nm with a 4 nm bandwidth. Column: Agilent Zorbax Extend C18, 1.8 μm, 2.1 x 50 mm. Gradient conditions: 5% to 95% CH₃CN in H₂O (0.1% formic acid) over 1 min, hold at 95% CH₃CN for 0.1 min, 0.5 mL/min, 40 °C. For compounds that were purified on a Gilson

preparative reversed-phase HPLC, the system comprised of a 333 aqueous pump with solvent-selection valve, 334 organic pump, GX-271 or GX-281 liquid handler, two column switching valves, and a 155 UV detector. UV wavelength for fraction collection was user-defined, with absorbance at 254 nm always monitored. Method 1: Phenomenex Axia-packed Luna C18, 30 x 50 mm, 5 μ m column. Mobile phase: CH₃CN in H₂O (0.1% TFA). Gradient conditions: 0.75 min equilibration, followed by user defined gradient (starting organic percentage, ending organic percentage, duration), hold at 95% CH₃CN in H₂O (0.1% TFA) for 1 min, 50 mL/min, 23 °C. Method 2: Phenomenex Axia-packed Gemini C18, 50 x 250 mm, 10 μ m column. Mobile phase: CH₃CN in H₂O (0.1% TFA). Gradient conditions: 7 min equilibration, followed by user defined gradient (starting organic percentage, ending organic percentage, duration), hold at 95% CH₃CN in H₂O (0.1% TFA) for 7 min, 120 mL/min, 23 °C. All reagents were purchased from Aldrich Chemical Co. and were used without purification. All final compounds were >98% pure by LCMS (254 nm, 214 nM and ELSD). Following these purification protocols, final compounds were transferred to a barcode vial and diluted to a concentration of 10 μ M using molecular biology grade dimethylsulfoxide (DMSO). These compounds were registered into Dotmatics and assigned a VU identification number before being tested in the primary screening assay.

Blood collection and platelet isolation

Human platelets were obtained from healthy volunteers. The studies were approved by the Vanderbilt University Internal Review Board. Informed consent was S12 obtained from all individuals prior to the blood draw. Blood was collected into sodium citrate anticoagulant (final concentration 0.32%) through a 19 gauge needle.

Blood was centrifuged at 1100 rpm for 15 min at room temperature (Thermo forma 400 ML GP, Aerocarrier rotor 236). The platelet rich plasma layer was isolated, treated with acid citrate dextrose (0.25% citrate, 0.15% citric acid, 0.2% glucose final concentrations) for 10 min. Platelets are then pelleted by centrifugation at 2400 rpm and washed in Tyrode's buffer (15 mM HEPES, 0.33 mM NaH₂PO₄, pH7.4, 138 mM NaCl, 2.7 mM KCl, 1 mM MgCl₂, 5.5 mM dextrose, 0.1% BSA). Platelets were counted on a Coulter Counter, and diluted in Tyrode's to the indicated concentration.

Flow cytometry

Washed platelets were diluted to 1.5x10⁷ platelets/mL in Tyrode's buffer. Platelets were preincubated with compound or vehicle control and a combination of PE conjugated CD62p and FITC conjugated PAC1 (Becton Dickinson, Franklin Lakes, NJ) for 20 min. The reaction was stimulated with agonist for 10 min, then fixed with 1% paraformaldehyde (final concentration) for 20 min. PAR4-AP (AYPGKF) was from GL biochem (Shanghai, China). γ -thrombin was from Enzyme Research Laboratories (South bend, IN). γ -thrombin was treated for 20 min with 1 unit/ml hirudin (Sigma Aldrich, St. Louis, MO) to sequester residual α -thrombin within the preparation. Samples were analyzed on a BD LSR II. Compensation controls for dual color labeling (PE and FITC) were run each day of data collection. Data was analyzed using FlowJo (Ashland, OR). Mean fluorescence intensity (MFI) was determined by taking the geometric mean of the 20,000 fluorescence recordings within the platelet gate (forward versus side-scatter plot). MFI was normalized to internal vehicle treated control samples. Concentration response curves were generated by non-linear regression analysis in Prism (La Jolla, CA). IC₅₀ values with SEM were also calculated with Prism.

Schild Analysis Competition Binding Assay

Schild analysis and identification of competitive PAR4 antagonists. Progressive fold-shift experiments and accompanying Schild analysis with VU. Platelet activation was monitored by PAC1 binding. Platelets were pretreated with increasing concentrations of each antagonist for 20 minutes prior to activation with increasing concentrations of PAR4-AP. Each curve was constructed from at least three independent experiments. DRs were calculated from the EC_{50} s of each individual experiment ($\text{vehicle}EC_{50}/VU\#EC_{50}$) and plotted against the administered concentration of antagonist. A) Shown on the right are the means \pm 6 S.E.M. of log DR-1 ($n = 3$). In the graph insert, m is the slope from linear regression. DMSO, dimethylsulfoxide.

Drug Metabolism Methods: In vitro

Plasma protein binding: The protein binding of each compound was determined in plasma via equilibrium dialysis employing RED Plates (ThermoFisher Scientific, Rochester, NY). Plasma was added to the 96 well plate containing test compound and mixed thoroughly for a final concentration of 5 μ M. Subsequently, an aliquot of the plasma-compound mixture was transferred to the cis chamber (red) of the RED plate, with a phosphate buffer (25 mM, pH 7.4) in the trans chamber. The RED plate was sealed and incubated for 4 hours at 37°C with shaking. At completion, aliquots from each chamber were diluted 1:1 with either plasma (cis) or buffer (trans) and transferred to a new 96 well plate, at which time ice-cold acetonitrile containing internal standard (50 ng/mL carbamazepine) (2 volumes) was added to extract the matrices. The plate was centrifuged (3000 rcf, 10 min) and supernatants transferred and diluted 1:1 (supernatant: water) into a new 96 well plate, which was then sealed in preparation for

LC/MS/MS analysis. Each compound was assayed in triplicate within the same 96-well plate. Fraction unbound was determined using the following equation Intrinsic clearance: Human or rat hepatic microsomes (0.5 mg/mL) and 1 μ M test compound were incubated in 100 mM potassium phosphate pH 7.4 buffer with 3 mM MgCl₂ at 37°C with constant shaking. After a 5 min preincubation, the reaction was initiated by addition of NADPH (1 mM). At S13 selected time intervals (0, 3, 7, 15, 25, and 45 min), aliquots were taken and subsequently placed into a 96-well plate containing cold acetonitrile with internal standard (50 ng/mL carbamazepine). Plates were then centrifuged at 3000 rcf (4° C) for 10 min, and the supernatant was transferred to a separate 96-well plate and diluted 1:1 with water for LC/MS/MS analysis. The *in vitro* half-life (T_{1/2}, min, Eq. 1), intrinsic clearance (CL_{int}, mL/min/kg, Eq. 2) and subsequent predicted hepatic clearance (CL_{hep}, mL/min/kg, Eq. 3) was determined employing the following equations:

$$(1) \quad T_{1/2} = \frac{\text{Ln}(2)}{k}$$

where k represents the slope from linear regression analysis of the natural log percent remaining of test compound as a function of incubation time

$$(2) \quad CL_{\text{int}} = \frac{0.693}{\text{in vitro } T_{1/2}} \times \frac{\text{mL incubation}}{\text{mg microsomes}} \times \frac{45 \text{ mg microsomes}}{\text{gram liver}} \times \frac{45^a \text{ gram liver}}{\text{kg body wt}}$$

^a scale-up factor that is species specific

$$(3) \quad CL_{\text{hep}} = \frac{Q_h \cdot CL_{\text{int}}}{Q_h + CL_{\text{int}}}$$

where Q_h (hepatic blood flow) is species specific.

LC/MS/MS Bioanalysis of Samples from Plasma Protein Binding and Intrinsic Clearance Assays

Samples were analyzed on a Thermo Electron TSQ Quantum Ultra triple quad mass spectrometer (San Jose, CA) via electrospray ionization (ESI) with two Thermo Electron Accella pumps (San Jose, CA), and a Leap Technologies CTC PAL autosampler (Carrboro, NC). Analytes were separated by gradient elution on a dual column system with two Thermo Hypersil Gold (2.1 x 30 mm, 1.9 μ m) columns (San Jose, CA) thermostated at 40°C. HPLC mobile phase A was 0.1% formic acid in water and mobile phase B was 0.1% formic acid in acetonitrile. The gradient started at 10% B after a 0.2 min hold and was linearly increased to 95% B over 0.8 min; hold at 95% B for 0.2 min; returned to 10% B in 0.1 min. The total run time was 1.3 min and the HPLC flow rate was 0.8 mL/min. While pump 1 ran the gradient method, pump 2 equilibrated the alternate column isocratically at 10% B. Compound optimization, data collection and processing was performed using Thermo Electron's QuickQuan software (v2.3) and Xcalibur (v2.0.7 SP1).

Animal care and use

All animal study procedures were approved by the Institutional Animal Care and Use Committee and were conducted in accordance with the National Institutes of Health regulations of animal care covered in Principles of Laboratory Animal Care (National Institutes of Health). All animals were group housed under a 12-hour light/dark cycle with food and water available ad libitum. For behavioral studies, 8 – 10 week old male, C57Bl/6 were used.

Computational Modeling

Ligand docking into comparative models was done primarily using the Rosetta software based on protocols described in 1. The PAR4 structure for modeling was generated using the RosettaCM homology modeling protocol using experimentally-determined structures of PARs 1 and 2 (PDB ID: 3VW7 and 5NDD, respectively) as described in 2. Briefly, this protocol takes user-defined aligned sequences from proteins with high sequence similarity to the query sequence, superimposes residues accordingly, then undergoes residues insertion using both PDB-derived fragments and provided templates, followed by Monte Carlo-based backbone and sidechain perturbations and optimized using energy-based minimization. Clustering of the final models was used to obtain an "ensemble-like" representation to be carried forward into docking studies. Docking in Rosetta contains low-resolution sampling for initial pocket placement with coarse-grained sampling followed by high-resolution sampling of the ligand, protein sidechains and protein backbone based on Monte Carlo simulations with acceptance based on Metropolis criteria. This is followed by a final minimization to obtain a local minimum and report a final score for that protein-ligand conformation. Analysis of different conformations from docking was performed by looking at the score variation across a number of poses from different starting structures, clustering of these outputs, visual inspection using previous knowledge of known binders to PARs. Ligands were all prepared using the BCL for conformer generation and a provided script to obtain the appropriate Rosetta-readable ligand parameter files. RosettaCM, ligand preparation and docking were performed using the `run_rosettacm.sh`, `prep_ligands.sh` and `run_docking.sh` scripts provided. 1 Combs, S., DeLuca, S., DeLuca, S. et al. Small-

molecule ligand docking into comparative models with Rosetta. Nat Protoc 8, 1277–1298 (2013) doi:10.1038/nprot.2013.074. 2 Song, Yifan et al. “High-resolution comparative modeling with RosettaCM.” Structure (London, England : 1993) vol. 21,10 (2013): 1735-42. doi:10.1016/j.str.2013.08.005.

PAR4 structure preparation

Performed using RosettaCM using PAR1 and PAR2 crystal structures as templates.

/dors/meilerlab/home/fudy/Meiler-Save/Project-Folders/PAR-RosettaCM-Remodel/remodel/rosettacm/

run_rosettacm.sh

\$PATH_TO_ROSETTA/main/source/bin/rosetta_scripts.default.linuxgccrelease

@ flags

flags

i/o

-in:file:fasta rosettacm/par4.fasta

-parser:protocol rosettacm/rosetta_cm.xml

-restore_talaris_behavior

#membrane

-in:file:spanfile rosettacm/par4.span

-membrane:no_interpolate_Mpair

-membrane:Menv_penalties

-rg_reweight 0.1

relax options

-relax:minimize_bond_angles

-relax:minimize_bond_lengths

-relax:jump_move true

-default_max_cycles 200

-relax:min_type lbfgs_armijo_nonmonotone

-score:weights membrane_highres_Menv_smooth.wts

-use_bicubic_interpolation

-hybridize:stage1_probability 1.0

-sog_upper_bound 15

reduce memory footprint

-chemical:exclude_patches LowerDNA UpperDNA Cterm_amidation

SpecialRotamer VirtualBB ShoveBB VirtualDNAPhosphate VirtualNTerm

CTermConnect sc_orbitals pro_hydroxylated_case1 pro_hydroxylated_case2

ser_phosphorylated thr_phosphorylated tyr_phosphorylated tyr_sulfated

lys_dimethylated lys_monomethylated lys_trimethylated lys_acetylated

glu_carboxylated cys_acetylated tyr_diiodinated N_acetylated C_methylamidated

MethylatedProteinCterm

-linmem_ig 10

converted_alignment.fasta

```
## Apar4 Apar1_thread
#
scores_from_program: 0
0 ----DSSRALLLGWVPTLVPALYGLVLLVGLPANGLALWVLATQA-
PRLPSTMLLMNLAAADLLLALALPPRIAYHLRGQRWPFGEAACRLATAALYGHMYGS
VLLLA AVSLDRYLALVHPLRARALRGRRLALGLCMAAWLMAAALALPLTLQRQTFRLA
RSDRVLCHDALPLDAQASHWQPAFTCLALLGCFLPLLAMLLCYGATLHTLAASGR---
RYGHALRLTAVVLASAVAFFVPSNLLLLLHYSDPSP-
SAWGNLYGAYVPSLALSTLNSCVDPFIYYVSAEF-----
0 ----
DASGYLTSSWLTFLVPSVYTG VVVSLPLNIMAIVVFILKMKVKKPAVVYMLHLATADV
LFVSVLPFKISYYFSGSDWQFGSELCRFVTA AFYCNMYASILLMTVISIDRFLAVVYPM
RTLGRAS----
FTCLAIWALAIAGV VPLLLKEQTIQV PGLGITTCHDVLSETLLEGYYAYYFSAFSAVFFF
VPLIISTVCYVSIIRCLSSSAANRSKSRALFLSAAVFCIFIICFGPTNVLLIAHYSFLSHTS
TTEAAYFAYLLCVCVSSISCCIDPLIYYASSEC-----
--
## Apar4 Apar2_thread
#
scores_from_program: 0
0 ----DSSRALLLGWVPTLVPALYGLVLLVGLPANGLALWVLATQA-
PRLPSTMLLMNLAAADLLLALALPPRIAYHLRGQRWPFGEAACRLATAALYGHMYGS
VLLLA AVSLDRYLALVHPLRARALRGRRLALGLCMAAWLMAAALALPLTLQRQTFRLA
RSDRVLCHDALPLDAQASHWQPAFTCLALLGCFLPLLAMLLCYGATLHTLAASGR---
RYGHALRLTAVVLASAVAFFVPSNLLLLLHYSDPSP-
SAWGNLYGAYVPSLALSTLNSCVDPFIYYVSAEF-----
0
FSVDEFSASVLTGKLT TVFLPIVYTIVFVVALPSNGMALWVFLFR TKKKAPAVIYMANLA
LADLLSVIWFPLKIA YHIHGNNWIYGEALCNVLIGFFYANMYCSILFLTCLSVQRAW EIV
NPMGHSR-
KKANIAIGISLAIWLLILLVTIPLYVVKQTIFIPALQITTCHDVLPEQLLVGDMFNYFLSLAIG
VFLFPAFLTASAYVLMIRALENSEK---
KRKRAIKLAVTVAAMY LICFTPSNLLL VVHYFLIKS-
QGQSHVYALYIVALCLSTLN SCIDPFVYFVSHDFRDHAKNAL
```

Ligand Preparation

prep_ligands.sh

```
# This script uses an SDF of each ligand as the initial input

# Initial cleaning
bcl.exe molecule:Filter -add_h -neutralize -defined_atom_types -3d -input_filenames
${NAME}_ligand.sdf -output_matched ${NAME}_ligand.CLEANED.sdf -
output_unmatched ${NAME}_ligand.UNCLEANED.sdf -message_level Debug

# Generate conformers
```

```
bcl.exe molecule:ConformerGenerator -rotamer_library cod -top_models 100 -
ensemble_filenames ${NAME}_ligand.CLEANED.sdf -conformers_single_file
${NAME}_ligand.CLEANED.conf.sdf -conformation_comparer 'Dihedral(method=Max)'
30 -max_iterations 1000;
```

```
# Generate parameters file
python2.7 /programs/x86_64-
linux/rosetta/3.8/main/source/scripts/python/public/molfile_to_params.py -n ${NAME} -
p ${NAME} --mm-as-virt --long-names --conformers-in-one-file
${NAME}_ligand.CLEANED.conf.sdf --chain X
```

Ligand docking into PAR4

run_docking.sh

```
/dors/meilerlab/apps/rosetta/rosetta-
3.8/main/source/bin/rosetta_scripts.linuxgccrelease \
  @ /hd0/smithst/par4/scripts/flags_common \
  @ /dors/meilerlab/home/smithst/docking_benchmark/scripts/inputs/flags \
  -parser:protocol /hd0/smithst/par4/scripts/ligand_docking_hires.xml \
  -s "/hd0/smithst/par4/updates_from_matt/31Y9_for_matt_proteinonly.pdb
/hd0/smithst/par4/sets/8-8-18_JB_library/input_files/${LIG}.pdb " \
  -in:file:native
"/hd0/smithst/par4/updates_from_matt/31Y9_for_matt_proteinonly.pdb
/hd0/smithst/par4/sets/8-8-18_JB_library/input_files/${LIG}.pdb " \
  -extra_res_fa /hd0/smithst/par4/sets/8-8-18_JB_library/input_files/${LIG}.params \
  -out:file:silent /hd0/smithst/par4/sets/8-8-
18_JB_library/output_files/31Y9_template_${LIG}.out \
  -out:file:scorefile /hd0/smithst/par4/sets/8-8-
18_JB_library/output_files/31Y9_template_${LIG}.sc \
```

Development of Novel, Brain-penetrant, Human and Mouse PAR4

Antagonists

High-Throughput Screening Campaign: Identification of VU0543156

An HTS campaign was initiated on a $\geq 25,000$ membered library to identify effective PAR4 antagonists, often referred to as ‘hit’ compounds. Compounds were screened in a platelet flow cytometry assay using a soluble, PAR4 activating peptide mimic (PAR4-AP; AYPGKF) to determine potency and efficacy. ‘Hit’ compound

VU0543156 (**3.11**), was identified as a novel chemotype and although it is weakly active (PAR4-AP IC₅₀ = 3.42 μM), it inhibits PAR4-AP induced aggregation by nearly 95%, is selective against PAR1, and is primed for rapid synthesis and SAR (**Figure 3.8**). **Figure 3.8** also depicts our initial SAR strategies for the lead optimization of **3.11**.

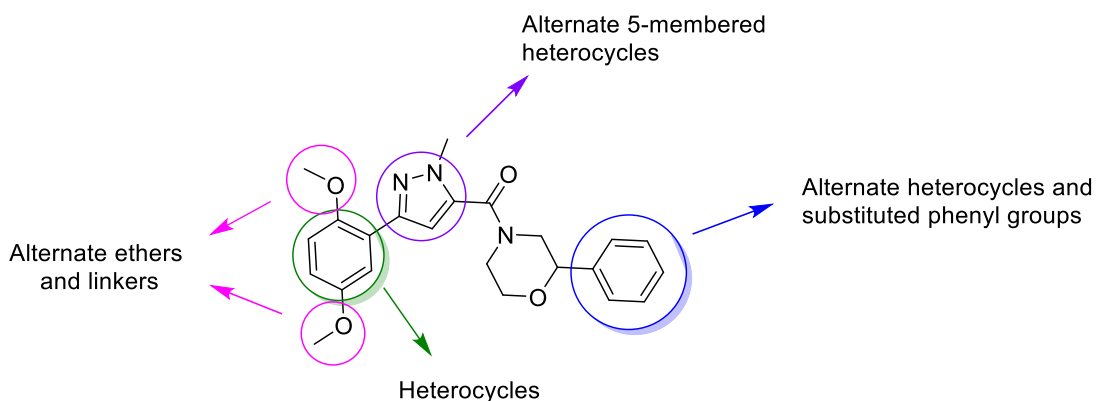
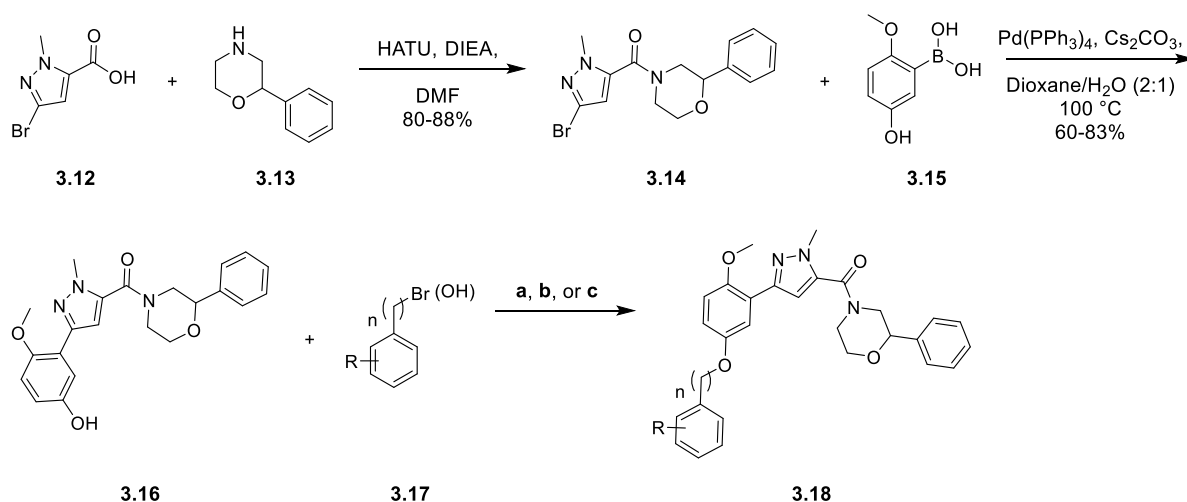


Figure 3.8 Structure of HTS hit VU0543156 (**3.11**) and proposed SAR strategy.

Initial SAR of Alternate Ethers: Analogs 3.19-3.62

We began our SAR efforts by focusing on the two methoxy substituents on the western aromatic ring of **3.11**. Specifically, we wanted to explore alternate ethers to probe the chemical space within the active site. Analogs of this nature were accessed



Scheme 3.1 Synthetic route to access ether analogs **3.19-3.62**, a) K₂CO₃, DMF, 60 °C; b) PPh₃, DtBAD, THF; c) CuI, Cs₂CO₃, *N,N*-dimethylcyclohexylamine, Dioxane, 100 °C. 50-72%.

via the representative example depicted in **Scheme 3.1**. Commercially available carboxylic acid **3.12** was reacted with either racemic or enantiomerically pure 2-phenylmorpholine (**3.13**) via a HATU mediated amide coupling to generate compound **3.14**. Next, compound **3.14** was subjected to Suzuki cross-coupling reaction conditions to install the western aromatic ring, followed by a S_N2 or Mitsunobu using the appropriate benzyl bromide or benzyl alcohol (**3.17**) to provide congeners of **3.18**. We commenced our SAR by appending a large, naked benzyl group to the northern or southern alcohol of the western aromatic ring to investigate the spatial limitations of the active pocket (**Figure 3.9**). The addition of the northern benzyl group (**3.19**) rendered the compound inactive, whereas the addition of the southern benzyl group (**3.20**)

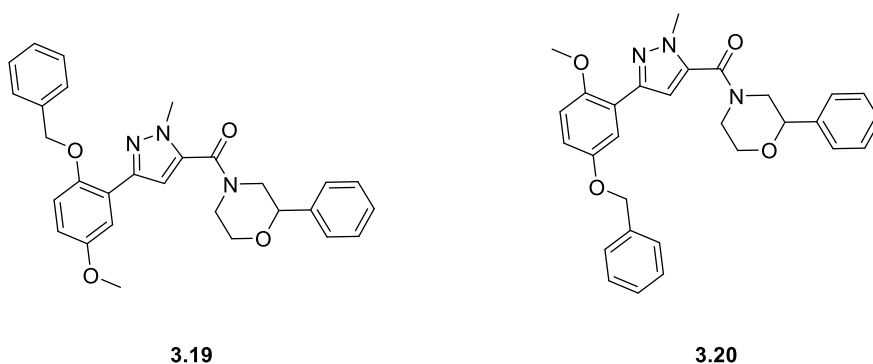
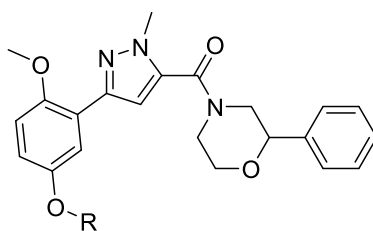


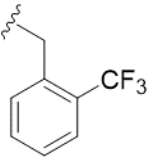
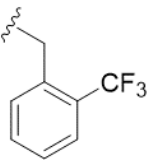
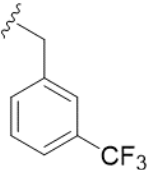
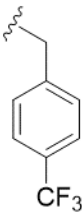
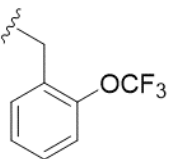
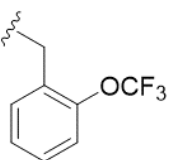
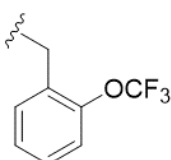
Figure 3.9 Structures of analogs VU6014723 (**3.19**) and VU6014232 (**3.20**).

resulted in a large improvement in potency from 3.42 μM to 363 nM. With a 10-fold improvement in potency, VU6014232 (**3.20**) became the new base scaffold for SAR (**Table 3.1**). We then incorporated a methyl group at the benzylic position in the hopes of generating a new chiral center. Unfortunately, the addition of the methyl group resulted in a loss in activity. A pyridine ‘walk’ revealed that a nitrogen in the meta (**3.23**) or para (**3.24**) position inhibited PAR4-AP induced activation >99%. Concurrently, a



3.21-3.62

Stereo-chemistry	R	Compound Number	VOID	PAC1 %Max	PAC1 IC ₅₀ (μM)	PAR1 %Max
racemic		3.21	VU6014722	6.81	1.7	83
racemic		3.22	VU6014721	3.91	1.6	99
racemic		3.23	VU6021737	0.75	0.35	88
racemic		3.24	VU6014718	0.89	0.47	98
racemic		3.25	VU6014616	4.79	1.2	84

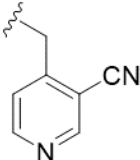
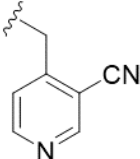
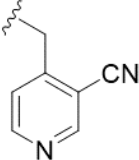
R		3.26	VU6015740	5.02	0.25	85
S		3.27	VU6015743	32.75	1.3	81
racemic		3.28	VU6014617	5.7	1.2	84
racemic		3.29	VU6014618	8.77	1.3	83
racemic		3.30	VU6014702	5.91	1.5	75
R		3.31	VU6015741	4.95	0.39	80
S		3.32	VU6015744	18.89	0.93	76

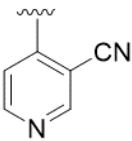
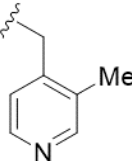
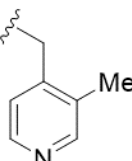
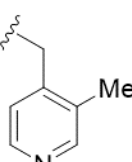
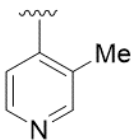
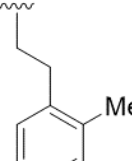
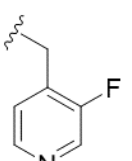
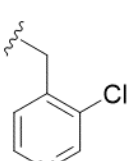
racemic		3.33	VU6014703	8.23	1.5	78
racemic		3.34	VU6014704	12.0	2.0	82
racemic		3.35	VU6017185	0.47	0.14	92
<i>R</i>		3.36	VU6015742	1.39	0.14	95
<i>S</i>		3.37	VU6015745	5.88	0.48	94
racemic		3.38	VU6017603	3.47	0.83	82
racemic		3.39	VU6017604	1.15	0.17	77
racemic		3.40	VU6017605	18.3	1.0	79

Table 3.1 Initial SAR of southern benzyl moiety – analogs **3.21-3.40**.

substituent ‘walk’ was done around the ring, where we deduced that substituents in the ortho position were the most conducive for activity as well. Cyano analog **3.35** emerged as the lead compound within this series, inhibiting PAR4-AP nearly 100%, with an IC₅₀ = 140 nM). In the attempt to drive down potency further, the enantiomers were resolved. The R-enantiomer (**3.36**) had a slight enantiomeric preference over the (S)-enantiomer (**3.37**). However, the (R)-enantiomer was equipotent to the racemate and did not give us the boost in potency that we had hoped for.

Our next attempt at improving potency was hybridizing PAR4 antagonists **3.24** and **3.25** to generate compound **3.41** depicted in **Table 3.2**. This modification resulted in an improvement in potency while maintaining efficacy and selectivity. Consistent with earlier observations, the R- (**3.42**) enantiomer was preferred over the S- (**3.43**) enantiomer, but again, did not improve potency over the parent (**3.41**). Moving forward, maintaining the 4-pyridine, we surveyed alternate substituents in place of the nitrile.

Stereo-chemistry	R	Compound Number	VOID	PAC1 %Max	PAC1 IC ₅₀ (μM)	PAR1 %Max
racemic		3.41	VU6017182	0.27	0.09	79
R		3.42	VU6019101	0.33	0.09	95
S		3.43	VU6025347	3.37	0.66	83

racemic		3.44	VU6024576	1.43	0.65	112
racemic		3.45	VU6019096	0.74	0.09	103
R		3.46	VU6019097	0.37	0.07	101
S		3.47	VU6022638	2.33	0.44	95
racemic		3.48	VU6020643	0.33	0.20	71
racemic		3.49	VU6021738	0.46	0.20	83
racemic		3.50	VU6019734	9.86	0.30	85
racemic		3.51	VU6019735	10.9	0.08	79

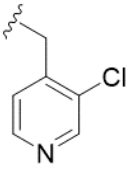
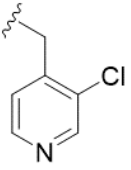
R		3.52	VU6021736	0.68	0.7	80
S		3.53	VU6022639	2.56	0.45	94

Table 3.2 SAR of 2-substituted benzylpyridines – analogs **2.41-2.53**.

Though methyl (**3.45**) and chloro (**3.51**) congeners were found to be equipotent, **3.45** displayed greater efficacy. (*R*)-enantiomers of methyl and chloro analogs, **3.46** and **3.52**, were discovered to have a minor improvement in activity over the racemates, giving rise to our new lead compounds. In addition, we extended and contracted the ether linker by a carbon linkage to further probe electronics and chemical space. Interestingly, while removing (**3.48**) or adding (**3.49**) a carbon to the ether-linkage maintained activity, a minor loss in potency was observed. This observation is consistent with compound moieties extending into extracellular space. Computational studies docking compound **3.46** in our PAR4 homology model using energy minimization constraints also indicated that the methylpyridine moiety was situated near the surface of the receptor, extending into extracellular space (**Figure 3.10**).

Next, we surveyed various saturated ring sizes to introduce more sp³ character into the molecule while simultaneously probing the electronics and chemical space of the active site (**Table 3.3**). In comparison to the planar benzyl analog **3.20**, the more three-dimensional cyclohexane congener **3.54** is comparable in potency. Potency

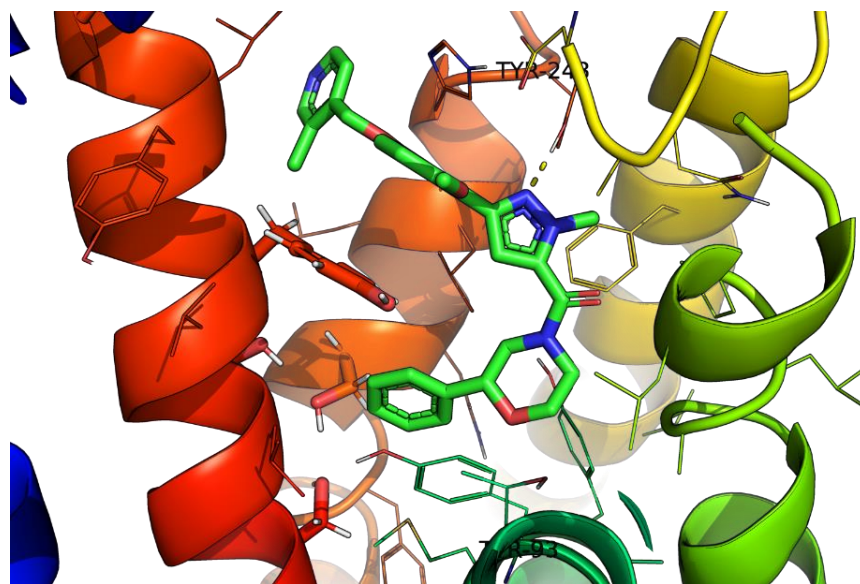
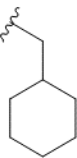
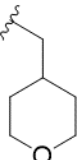


Figure 3.10 Structure of VU6019097 (**3.46**) docked in our PAR4 homology model. Image courtesy of Shannon T. Smith.

improves with the decrease in ring size to a cyclopentyl group (**3.57**) and improves further with the separation of enantiomers. (*R*)-cyclopentyl analog **3.57** improved potency even further to PAR4-AP IC₅₀ = 72 nM, which is on par with current lead compounds **3.46** (PAR4-AP IC₅₀ = 66 nM) and **3.52** (PAR4-AP IC₅₀ = 68 nM). However, potency diminishes as the ring size decreases further. Another strategy pursued to improve upon potency was incorporating a hydrogen bond accepting group within the

Stereo-chemistry	R	Compound Number	VOID	PAC1 %Max	PAC1 IC ₅₀ (μM)
racemic		3.54	VU6017606	3.36	0.27
racemic		3.55	VU6024574	0.30	0.22

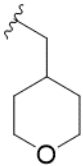
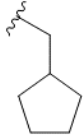
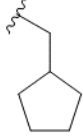
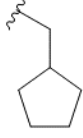
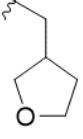


R		3.56	VU6024874	0.41	0.07
racemic		3.57	VU6017992	1.52	0.17
R		3.58	VU6020236	1.15	0.07
S		3.59	VU6022640	1.90	0.20
racemic		3.60	VU6024575	0.54	0.28
racemic		3.61	VU6020629	1.78	0.24
racemic		3.62	VU6020630	2.63	0.38

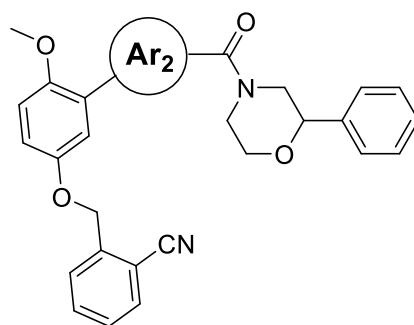
Table 3.3 SAR of methyl cycloalkyl ethers – analogs **2.54-2.62**.

cycloalkyl rings (**3.55** and **3.60**), mimicking the hydrogen bond accepting properties of the pyridine moiety in our other lead compounds (**3.46** and **3.52**). The (*R*)-enantiomer of the tetrahydropyran moiety (**3.55**) appeared to be equally as potent as our other lead compounds (PAR4-AP IC₅₀ = 71 nM). Hitting a potency plateau around PAR4-AP IC₅₀ =

70 nM, we elected to move away from the benzyl and methyl cycloalkyl ethers to explore a different portion of the molecule.

SAR around core pyrazole moiety: Analogs 3.63-3.76

Moving away from the ether linkers, we decided to explore alternate heterocycles for the pyrazole moiety (**Table 3.4**). These PAR4 antagonists were synthesized in a similar manner outlined in **Scheme 3.1**. Minor modifications were made, beginning with the exchange of the pyrazole for a pyrrole (**3.63**), which resulted in a complete loss in activity. Other minor alterations, such as incorporating diastereomer **3.64**, exploring a ring size increase (**3.65**), and walking the amide over one carbon (**3.66**), all led to a complete loss in activity. We quickly realized the vital importance of the pyrazole moiety within this scaffold and that any perturbations would likely result in a loss of activity. The homology model with analog **3.46** docked, also indicates that the nitrogen on the



3.63-3.66

R	VOID	Compound Number	PAC1 %Max	PAC1 IC ₅₀ (μM)
	VU6017766	3.63	109	N/A
	VU6017765	3.64	139	N/A

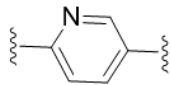
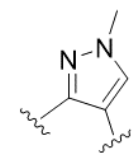
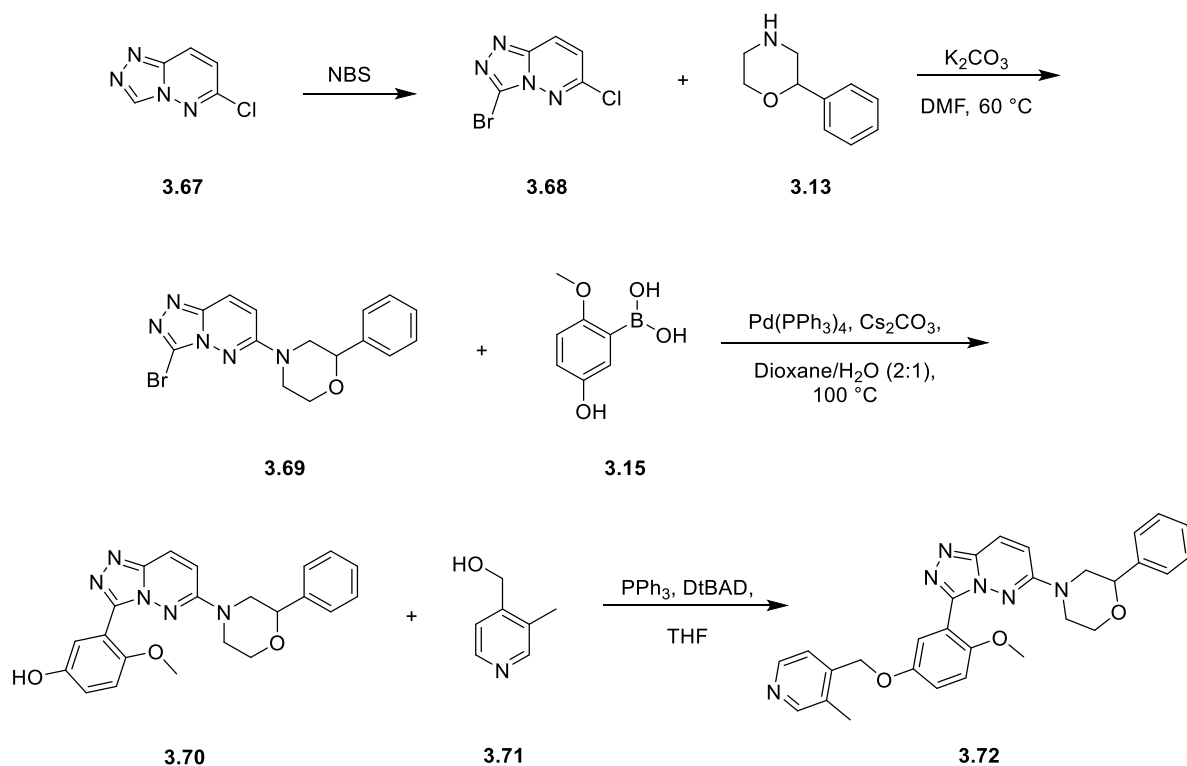
	VU6024872	3.65	80	N/A
	VU6024873	3.66	91	N/A

Table 3.4 SAR around pyrazole moiety – analogs **3.63-6.66**.

pyrazole makes a key hydrogen bonding interaction with residue TYR243. The empirical data collected from the deletion of said nitrogen (**3.63**), and resulting loss in activity, further supports the pose of our current lead compound in the PAR4 homology model.

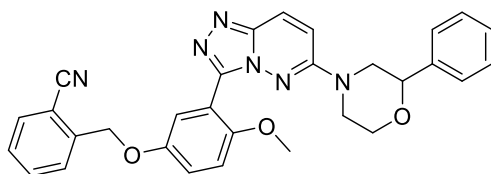
Our final effort concerning the pyrazole moiety, was to investigate the incorporation of a fused ring system. The fused ring analogs were synthesized via **Scheme 3.2**. Commercially available triazolopyridazine **3.67**, was selected, in part, to



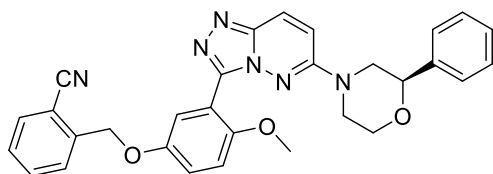
Scheme 3.2 Synthetic route to access triazolopyridazine analogs.

mimic the pyrazole moiety of the parent compound to attempt to keep electronics consistent, as we now know the pyrazole is crucial for activity. **3.67** was selectively brominated at the 3-position using NBS, followed by the regioselective addition of morpholine **3.13** utilizing S_NAr chemistry to provide compound **3.69**. From here, the synthesis proceeds in an identical fashion to previous analogs by reacting our aryl bromide with boronic acid **3.15** generating intermediate **3.70**, followed by a Mitsunobu with benzyl alcohol **3.71**, to provide congener **3.72**.

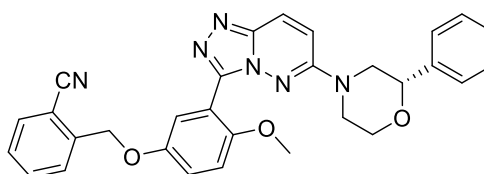
Interestingly, the pyrazole moiety is not only crucial for activity, but also selectivity. The introduction of the fused ring caused a selectivity switch to occur, where analog **3.72** now displays dual inhibition of PAR4 and PAR1, exhibiting a larger preference for the inhibition of PAR1 (**Figure 3.11**). Both enantiomers of **3.72** were synthesized and evaluated in our platelet flow cytometry assays. The (*S*)-enantiomer



VU6016706 (**3.72**)
 PAR4 PAC1 %Max = 61
 PAR1 PAC1 %Max = 18



VU602541 (**3.73**)
 PAR4 PAC1 %Max = 85
 PAR1 PAC1 %Max = 67



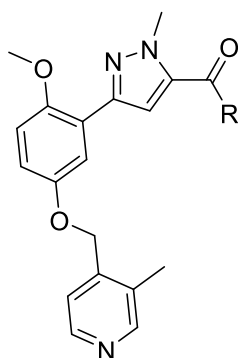
VU6016707 (**3.74**)
 PAR4 PAC1 %Max = 62
 PAR1 PAC1 %Max = 6

Figure 3.11 Structure and activities of analogs **3.72-3.74** in PAR1 and PAR4 human platelet assays.

(3.74) proved to be an even stronger PAR1 inhibitor, effectively inhibiting PAR1 up to 94%. Concentration response curves (CRCs) revealed that while **3.74** demonstrated PAR1 antagonist activity, it was only weakly potent, displaying a PAR4-AP IC₅₀ >10 μM. Although an interesting find, our efforts returned to the pyrazole containing, parent scaffold to conduct further SAR around the amide portion of the molecule.

SAR Around Amide Moiety – Analogs 3.77-3.97

Following the discovery that the pyrazole is imperative for both activity and selectivity, we began exploring alternate amide moieties (**Table 3.5**). From the docking pose of **3.64** in our PAR4 homology model, we noted a possible pi-stacking interaction



3.75-3.82

R	VOID	Compound Number	PAC1 %Max	PAC1 IC ₅₀ (μM)
	VU6026489	3.75	0.66	0.32
	VU6026490	3.76	5.13	2.4

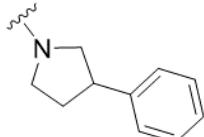
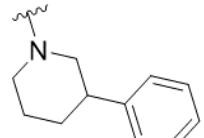
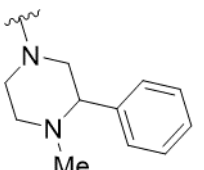
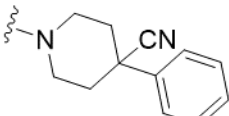
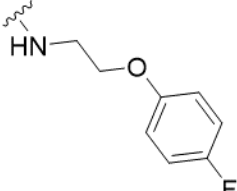
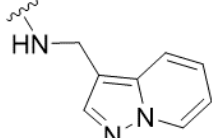
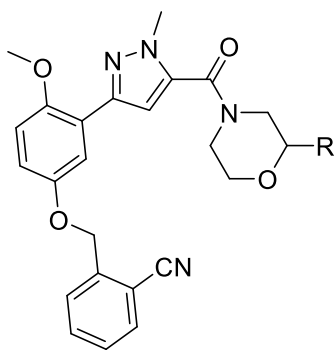
	VU6024176	3.77	-1.28	0.16
	VU6024871	3.78	1.3	0.63
	VU6016418	3.79	10.8	2.1
	VU6020628	3.80	0.32	0.24
	VU6019440	3.81	4.17	1.3
	VU6019439	3.82	2.84	1.2

Table 3.5 SAR around amide motif – analogs **3.75-3.82**.

between the phenyl substituent off the morpholine and tyrosine residue 93. To test this hypothesis, we replaced the phenyl group with a cyclohexyl moiety (**3.75**) to remove aromaticity, as well as removing the phenyl group all together (**3.76**). Both of these modifications resulted in a loss of potency and activity, further validating our homology model pose. Turning our attention to the morpholine, congeners **3.77-3.81** were synthesized to evaluate its importance within this scaffold. Our SAR focused on

maintaining the sp³ character of the morpholine ring to sustain the solubility of the scaffold. Pyrrolidine (**3.77**) and 4-cyanopiperidine (**3.80**) analogs only had a minor loss in potency, while piperidine (**3.78**), piperazine (**3.79**), and ‘open’ morpholine (**3.81**) analogs took a much larger hit. Lastly, we incorporated an amide moiety (**3.82**) found in another ‘hit’ compound. However, this alteration did not provide an increase in activity. Because these modifications were unfruitful, we returned to the morpholine amide and continued to probe SAR around the naked phenyl ring (**Table 3.6**).



3.83-3.95

Stereo-chemistry	R	Compound Number	VUID	PAC1 %Max	PAC1 IC ₅₀ (μM)
racemic		3.83	VU6019436	2.74	1.3
racemic		3.84	VU6019438	3.54	1.1
racemic		3.85	VU6019437	150	N/A

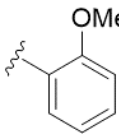
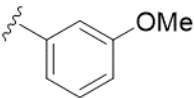
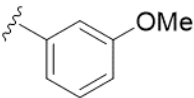
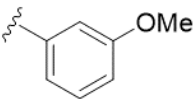
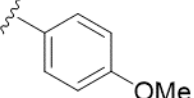
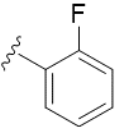
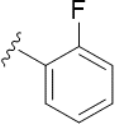
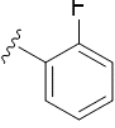
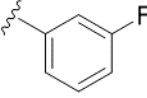
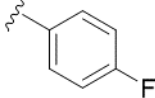
racemic		3.86	VU6018756	4.17	0.61
racemic		3.87	VU6018757	0.26	0.12
Enantiomer 1		3.88	VU6019736	12.13	0.11
Enantiomer 2		3.89	VU6019737	35.9	1.3
racemic		3.90	VU6018758	22.4	2.5
racemic		3.91	VU6018759	0.38	0.34
Enantiomer 1		3.92	VU6029456	0.45	0.21
Enantiomer 2		3.93	VU6029455	3.59	0.80
racemic		3.94	VU6018760	0.43	0.28
racemic		3.95	VU6024175	3.10	0.57

Table 3.6 SAR around eastern phenyl ring – analogs 3.83-3.95.

As can be seen in in **Table 3.6**, the pyridine ‘walk’ around the phenyl group (**3.82-3.85**) was not well tolerated. Next, we surveyed electron donating and electron withdrawing substituents around the ring. The racemic *meta*-OMe (**3.87**) and *ortho*-fluoro (**3.91**) analogs were resolved via super-critical fluid chromatography (SFC) to provide enantiomerically pure material of unknown absolute stereochemistry for *ex vivo* platelet assays. Single *meta*-OMe enantiomers **3.88** and **3.89** did not result in an improvement in potency. Rather, they both lost activity and therefore fell out of contention. While *ortho*-fluoro enantiomer **3.92** displayed a minor improvement in potency over the racemate, it did not surpass current lead compounds. Encountering steep SAR on this portion of the molecule we decided to move forward with further pharmacological studies.

Evaluating the Mode of Inhibition

With a sub-hundred nanomolar PAR4 antagonist in hand, we were able to evaluate the mode of action for PAR4 antagonist **3.46** in a competition binding assay (Schild analysis; **Figure 3.12**). The Schild analysis results are consistent with a

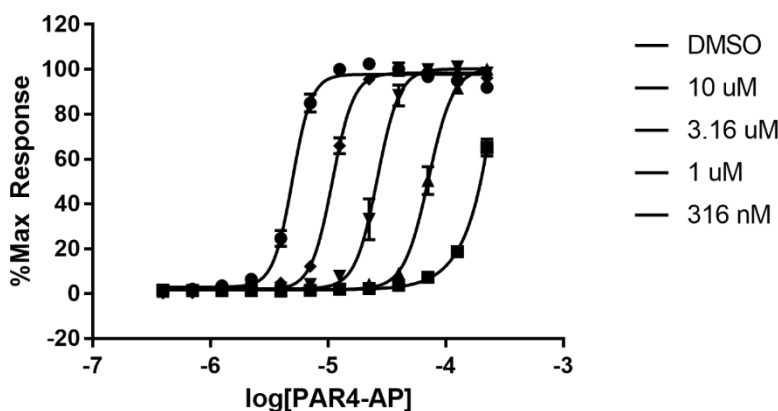


Figure 3.12 Schild analysis progressive fold shift is consistent with analog **3.12** competitively binding to PAR4.

competitive binding mode of inhibition, denoted by the leftward shift of the curve with increasing concentrations of PAR4-AP. Overlaying BMS-986120 with PAR4 antagonist **3.31** in our homology model, we noted the 2-phenylmorpholine of our series extends into the transmembrane domain in a different manner than BMS-986120 (**Figure 3.13**).

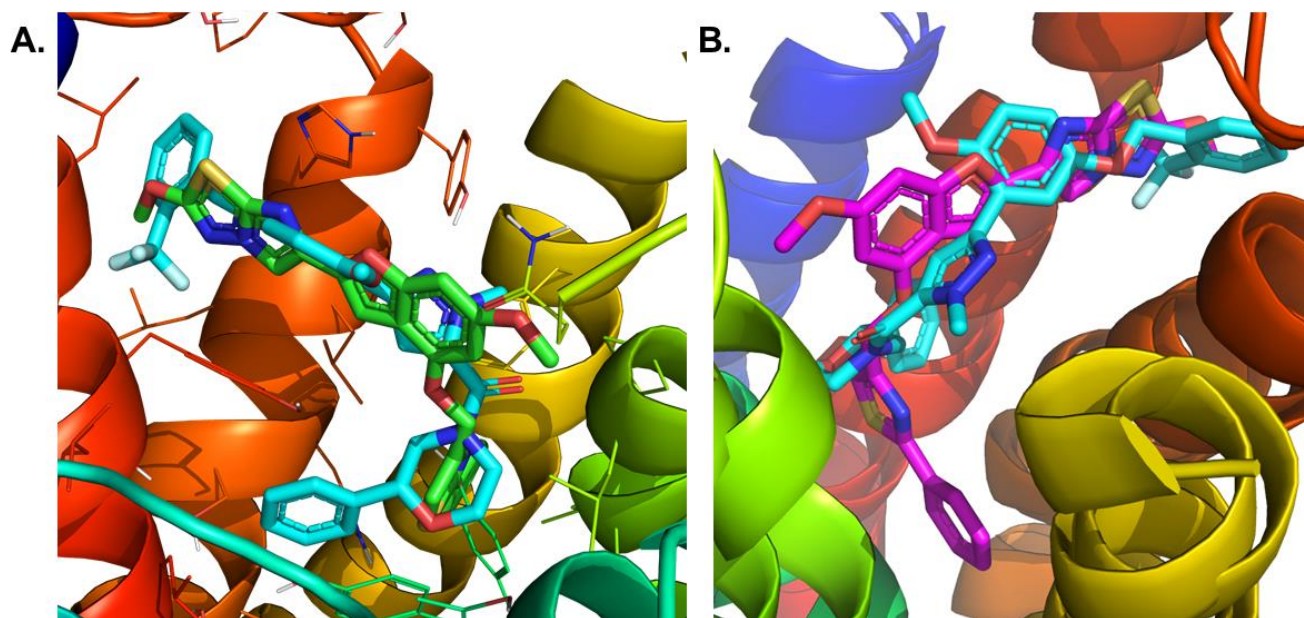
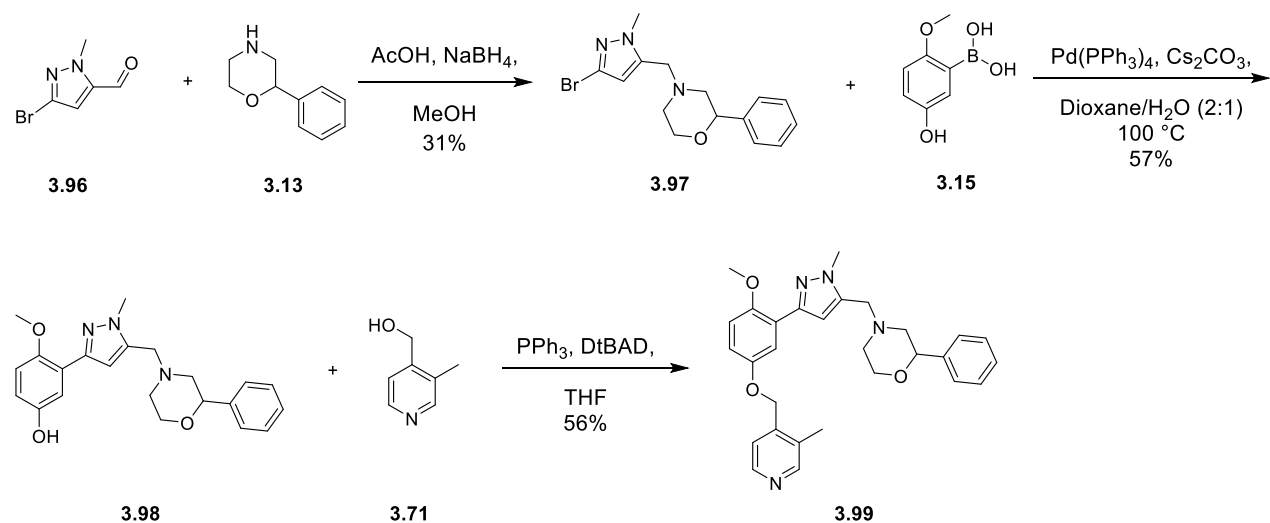


Figure 3.13 BMS-986120 overlaid with **3.31** in our PAR4 homology model from vantage points **A** and **B**.

Mentioned previously, minimum pharmacophore studies suggested that the phenylthiazole moiety of BMS-986120 is driving force for the non-competitive mode of inhibition. We hypothesized that by reducing the amide of congener **3.45** to the amine, we'd be introducing a more rotatable bond that would allow for the appropriate extension of the 2-phenylmorpholine down into the transmembrane domain, creating favorable interactions within the active site to engender a non-competitive mode of inhibition.



Scheme 3.3 Synthetic route to access analog **3.99**.

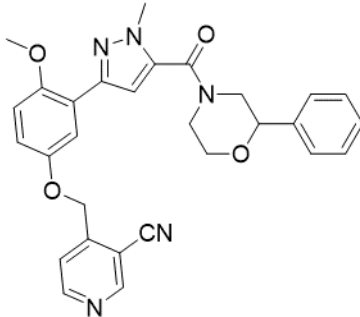
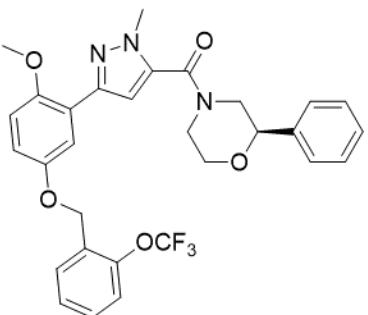
The synthetic route to access reduced amide analog **3.99** is outlined in **Scheme 3.3**.

Commercially available aldehyde **3.96** was reacted with 2-phenylmorpholine **3.13** using standard reductive amination conditions to provide intermediate **3.97**. Following the reductive amination, **3.97** was subjected to Suzuki conditions using aryl boronic acid **3.15** to provide alcohol **3.98**. Finally, a Mitsunobu reaction was performed, coupling intermediate **3.98** with benzyl alcohol **3.71** to generate PAR4 antagonist **3.99** for biological evaluation. Unfortunately, reducing the amide to the amine did not prompt the desired mode of inhibition switch. Instead, **3.99** resulted in a loss in activity (PAR4-AP PAC1 %Max = 32%), thus this avenue was not pursued further.

γ-thrombin Activity Screen

As mentioned previously, a soluble PAR4 peptide mimic (AYPGKF; PAR4-AP) has been used to activate PAR4 in *ex vivo* platelet screening assays, instead using native enzyme thrombin to induce activation. The utilization of PAR4-AP for initial SAR

has been a standard in the field, as it allows for the determination that our compounds are indeed inhibiting the PAR4 receptor, rather than inhibiting serine protease, γ -thrombin, and peptide cleavage. In addition, 30 μ M PAR4 peptide agonist AYPGKF, stimulates 72% of the maximal response to thrombin.⁷⁶ Because of the submaximal response, the assay utilizing PAR4-AP is able to detect PAR4 inhibitors that wouldn't normally be detected in the native, thrombin induced assay. Identifying PAR4 inhibitors at an early stage helps influence our strategies in approaching SAR. Of note, **Table 3.7** highlights compounds with inhibitory activity against PAR4-AP and, to an extent, against thrombin induced activation.

R	Compound Number	PAR4-AP PAC1 %Max	PAC1 IC ₅₀ (μ M)	γ -thrombin PAC1 %Max
	3.41	0.27	0.09	43.22
	3.31	4.95	389	54.62

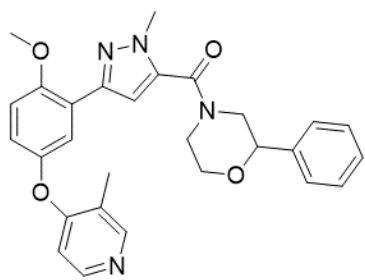
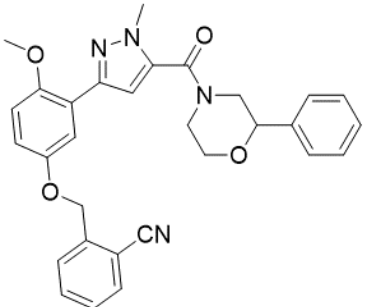
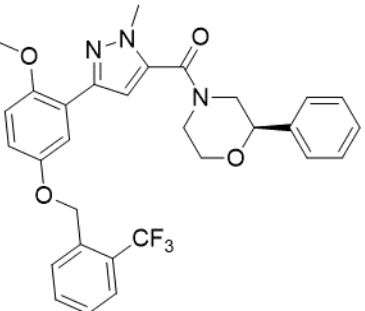
	3.48	0.33	0.20	64.02
	3.35	0.47	0.14	62.13
	3.27	5.02	249	65.02

Table 3.7 Congeners with activity against γ -thrombin induced platelet aggregation assay.

Five compounds inhibited thrombin induced activation by at least 35% while also having decent potency and efficacy. Cyanopyridine analog **3.41** emerged as the best PAR4 antagonist in this series overall in the context of human PAR4 (hPAR4), inhibiting γ -thrombin activation by nearly 60% and inhibiting PAR4-AP > 99% with an IC_{50} = 90 nM. While we've made significant progress, further optimization efforts are required to reach complete inhibition of thrombin induced platelet aggregation.

PAR4 Pharmacogenomic Profile

Not only are PAR4 antagonists YD-3, **3.46**, **3.52**, and **3.58** similar in potency, but Schild analysis deduced that, like YD-3, compound **3.46** is also a competitive antagonist. Also consistent with YD-3, PAR4 antagonists **3.46**, **3.52**, and **3.58** display a notable pharmacological difference between the GG and AA allele SNPs (**Figure 3.14**). Congeners **3.46**, **3.52**, and **3.58** all exhibit stronger activity against the GG allele over the AA allele. These data are consistent with the notion that individuals possessing the AA allele variation require nearly three times the concentration of PAR4-AP than individuals with the GG allele to induce receptor desensitization. These data are also consistent with our hypothesis that a non-competitive PAR4 antagonist would display no difference between SNP variants, while competitive antagonists would exhibit a distinct difference. Future efforts include making modifications within the series that will promote the development of a non-competitive PAR4 antagonist to assess its pharmacogenomic profile.

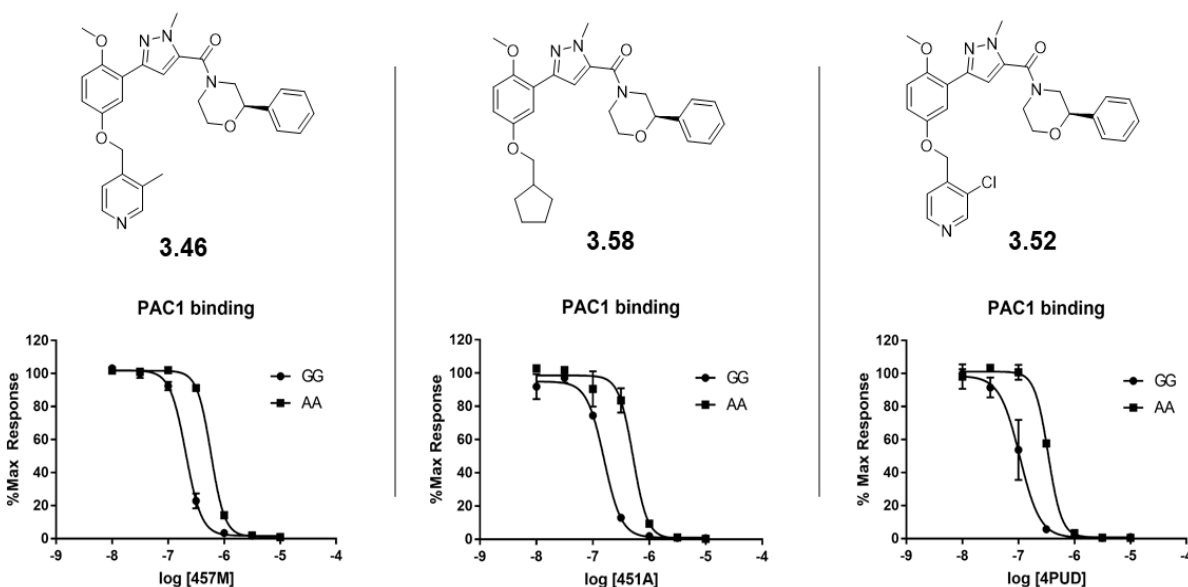


Figure 3.14 Pharmacogenomic differences between GG and AA alleles using compounds **3.46**, **3.58**, and **3.52**.

Human-Mouse PAR4 cross-over studies

At this stage, with our PAR4 antagonists reaching sub-hundred nanomolar potency against PAR4-AP and gaining traction against γ -thrombin inhibition, we screened our compounds in a single point platelet assay in mice platelets to determine their activity (**Figure 3.15**). Several analogs demonstrated activity in the mouse PAR4-AP platelet assay and were advanced further to obtain IC₅₀ values. PAR4 antagonists that display IC₅₀ values roughly 500 nM or less in the mouse PAR4-AP assay, along

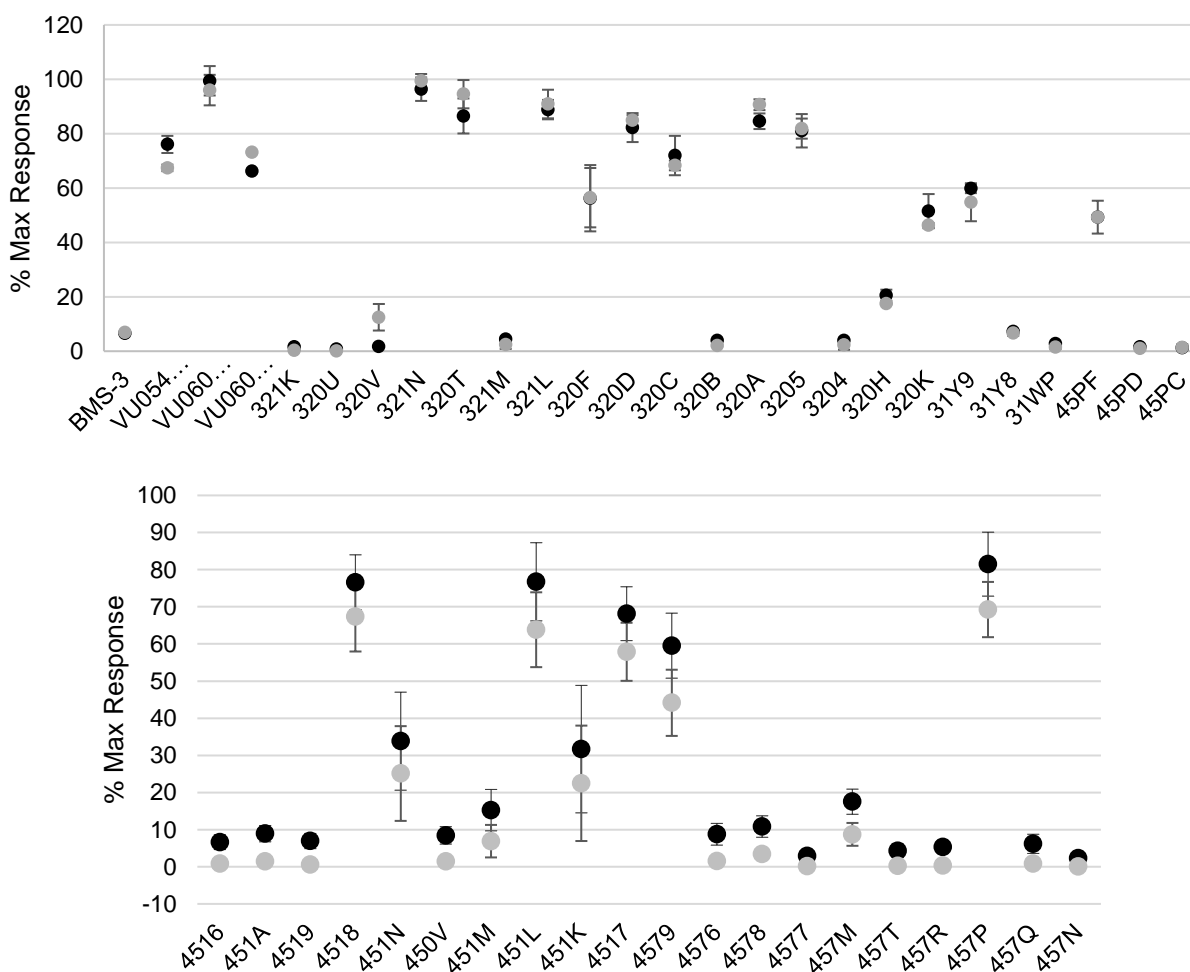
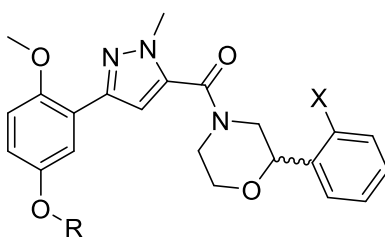
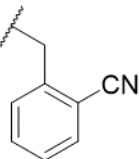
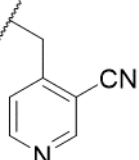
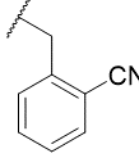


Figure 3.15 Single point assay with all active compounds to date in mouse platelets.

with their enantiomer and racemate, are highlighted in **Table 3.8**. Interestingly, the mouse PAR4 (mPAR4) receptor has an enantiopreference for the (*S*)-enantiomer, whereas with the hPAR4 receptor we've seen an enantiopreference the *R*-enantiomer. Analog **3.41** remains the most active chemotype within this series, with the (*S*)-enantiomer (**3.43**) being our most potent compound in mPAR4 and the ®-enantiomer



R	X	Compound Number	Stereo-chemistry	hPAR4-AP PAC-1 %Max	hPAR4-AP PAC-1	mPAR4-AP PAC-1
	F	3.91	racemic	0.38	0.34	0.31
	F	3.93	Single enantiomer ^a	3.63	0.80	0.37
	F	3.92	Single enantiomer ^a	0.63	0.21	0.49
	H	3.41	racemic	0.27	0.09	0.42
	H	3.43	<i>S</i>	3.37	0.62	0.30
	H	3.42	<i>R</i>	0.33	0.09	2.08
	H	3.35	racemic	0.47	0.14	0.37
	H	3.37	<i>S</i>	5.88	0.48	0.35
	H	3.36	<i>R</i>	1.93	0.14	2.1

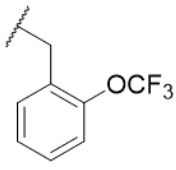
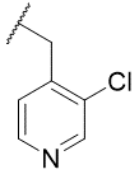
	H	3.30	racemic	5.91	1.49	0.70
	H	3.32	S	18.89	0.93	0.45
	H	3.31	R	4.95	0.39	1.05
	H	3.51	racemic	2.55	0.85	1.03
	H	3.53	S	2.51	0.44	0.53
	H	3.52	R	0.40	0.07	1.02

Table 3.8 Lead PAR4 antagonists in mouse platelet assay. ^aenantiomers of unknown absolute chemistry.

(**3.42**) the most potent in hPAR4. We believe the divergence in stereochemical activity between mouse and hPAR4 receptors could provide insight into the structural differences among the two active sites. After analyzing our human PAR4 homology model, we believe that the 2-phenylmorpholine in the *S*-conformation could possibly be clashing with HIS165, which causes it to lose its critical interaction with TYR243, in addition to losing the pi-stacking interaction with the *R*-conformation (**Figure 3.15A**).

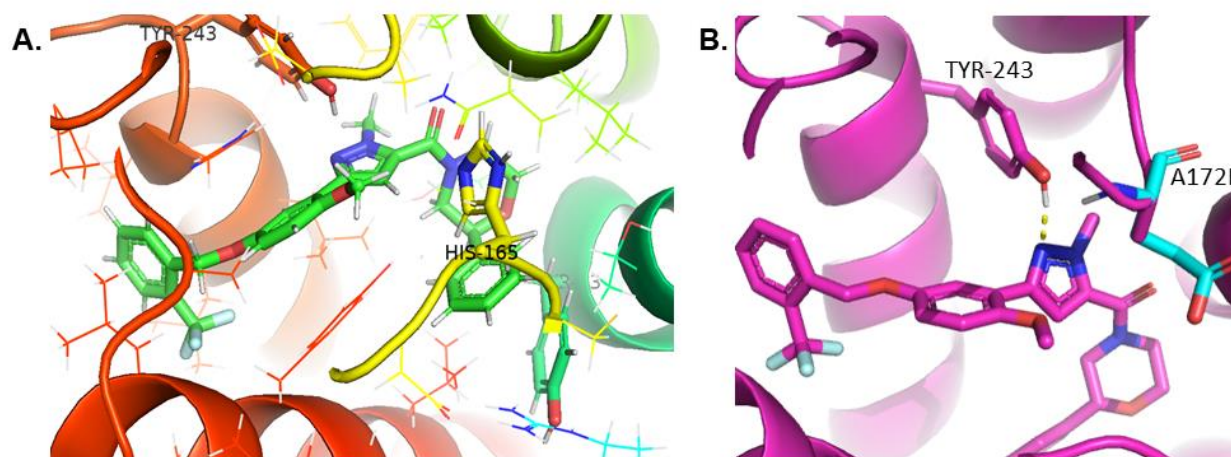


Figure 3.15 Congener **3.32** docked in hPAR4 homology model A) highlighting the histidine residue situated directly above the 2-phenylmorpholine, B) Depicting *in silico* mutation, A172E and its potential clashing interaction with TYR243. Images courtesy of Shannon T. Smith.

Based on our working hypothesis that Tyr243 is making a key hydrogen-bonding interaction with the nitrogen of the pyrazole, combined with mPAR4 and hPAR4 receptors having the opposite enantiopreference, we looked at *in silico* mutations in our hPAR4 homology model. With congener **3.31** docked in our hPAR4 homology model (magenta), native hPAR4 Ala172 residue was replaced with native mPAR4 Glu172 (cyan) (**Figure 3.15B**). Computational modeling studies suggest that the larger sidechain, glutamate, would likely sterically hinder the crucial hydrogen bonding interaction between Tyr243 and the central pyrazole, which could potentially explain the loss of activity in mouse platelets. To test this, mutation studies are under way to mutate mouse PAR4 Glu172 to alanine to observe whether affinity is rescued in the mouse platelet assays using *R*-analog, **3.31**.

DMPK Profiles of Lead Mouse PAR4 antagonists

DMPK profiles were obtained on the top five mouse PAR4 antagonists exhibiting roughly $IC_{50} \leq 500$ nM. Highlighted in **Table 3.9**, compounds with this chemotype generally displayed high clearance values apart from **3.32**, which exhibited a moderate *in vivo* clearance and the longest half-life in the series. These PAR4 antagonists were

Mouse IV Cassette PK					
Compound Number	Predicted CL _{Hep}	CL _p (mL/min/kg)	t _{1/2} (h)	V _{ss} (L/kg)	C _{max} (ng/mL)
3.32	79.7	58	0.70	2.2	153
3.53	88.1	268	0.18	3.8	58
3.37	87.1	111	0.71	5.3	45
3.43	87.6	230	0.29	4.9	43
3.92	87.9	109	0.45	5.2	56

Table 3.9 Pharmacokinetic data of mPAR4 lead compounds. Data courtesy of Frontage Laboratories.

also evaluated in a rat I.V plasma/brain level (PBL) cassette to determine their plasma protein binding (PPB) and CNS penetration (**Table 3.10**). Analog **3.32** exhibited the best

Rat IV Cassette PBL						
Compound Number	Rat PPB (f _u)	Rat BHB (f _u)	Plasma (ng/mL)	Brain (ng/g)	K _p	K _{p_{uu}}
3.32	0.001	0.001	30.9	16	0.52	0.52
3.53	0.017	0.004	10.9	46.1	4.23	1
3.37	0.004	0.002	15.7	37.8	2.41	1.2
3.43	0.022	0.005	9.21	20.4	2.22	0.5
3.92	0.002	0.001	15.5	31.2	2.02	1.01

Table 3.10 CNS exposure of mPAR4 lead compounds.

overall pharmacokinetic (PK) profile, with moderate mouse *in vivo* clearance (CL_p) and decent brain exposure (K_p) and was advanced for further DMPK studies. Male CD-1 mice were pre-treated with either pan-CYP450 inhibitor, 1-aminobenzotriazole (ABT) or vehicle two hours prior to a 10 mg/kg dose i.p of PAR4 antagonist **3.32**. Animals pre-treated with ABT displayed an improvement in t_{max}, C_{max}, and bioavailability (%F)(**Table 3.11**). In addition, plasma levels nearly double in the presence of ABT, which is similar

Mouse I.P. 3.32 PK					
Pre-treatment (2 hr)	t _{1/2} (h)	t _{max} (h)	C _{max} (ng/mL)	MRT _{inf} (h)	F (%)
Vehicle	8.66	0.50	225	10.0	40
ABT	5.72	1.25	844	7.12	116

Mouse I.P. 3.32 PBL				
Pre-treatment (2 hr)	Plasma (ng/mL)	Brain (ng/g)	K _p	K _{p_{uu}}
Vehicle	1245	65	0.05	0.14
ABT	2693	98	0.03	0.13

Table 3.11 Mouse pharmacokinetic and CNS exposure data of analog **3.32**, with and without pretreatment of ABT. a courtesy of Frontage Laboratories.

to what was observed in the mouse PK studies. To a minor extent, brain levels of **3.32** are also increased with the pre-treatment of ABT. Unfortunately, while DMPK properties were improved with the pre-treatment of ABT, the PK profile was still not sufficient enough to serve as an *in vivo* tool compound.

Addressing the Potential Metabolic Liabilities – Analogs 3.99-3.107

Assessing the structure of **3.35**, we hypothesized that the observed *in vivo* hepatic clearance could be as a result of two potential metabolic pathways: 1) Cytochrome P450-mediated dealkylation/oxidation sequence of the 1,4-dimethoxy aryl ring or 2) amide hydrolysis of the morpholine amide (**Figure 3.16**). As mentioned in

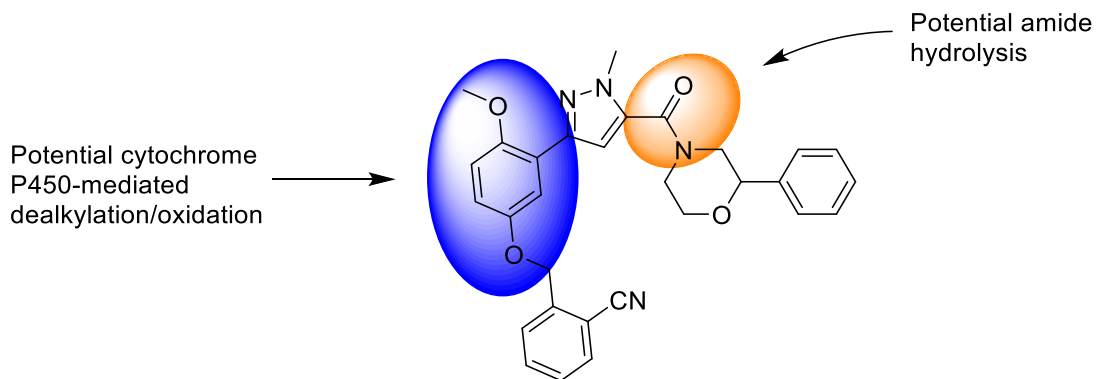
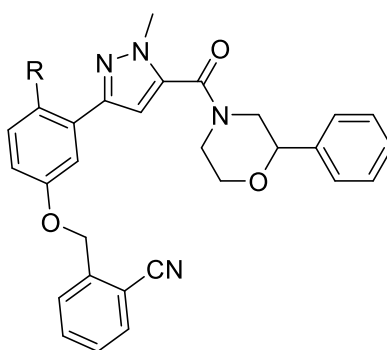


Figure 3.16 Potential metabolic liabilities within our scaffold – analog **3.35**.

previous sections, the amide moiety was reduced to the amine (**3.99**), which could potentially have improved clearance should it be mediated through amide hydrolysis. However, the modifications made to generate analog **3.99**, resulted in a loss in activity.

To address the potential cytochrome p450-mediated dealkylation/oxidation sequence on the western aryl ring, we began SAR around the northern methoxy group

(**Table 3.12**). Synthesis of these analogs were prepared in the same fashion outlined in **scheme 3.1** using the appropriate aryl boronic acid. SAR at this position proved to be steep, indicating that the methoxy group is crucial for activity. The deletion of the methoxy group (**3.100**) rendered the compound completely inactive. The incorporation of alternate hydrogen bonding acceptors (**3.101** and **3.102**) also resulted in complete inactivity. Finally, we attempted to alter the electronics of the methoxy group to potentially slow or halt potential demethylation by replacing the methoxy group with a trifluoromethoxy substituent. Unfortunately, the trifluoromethoxy modification also led to a complete loss of activity.

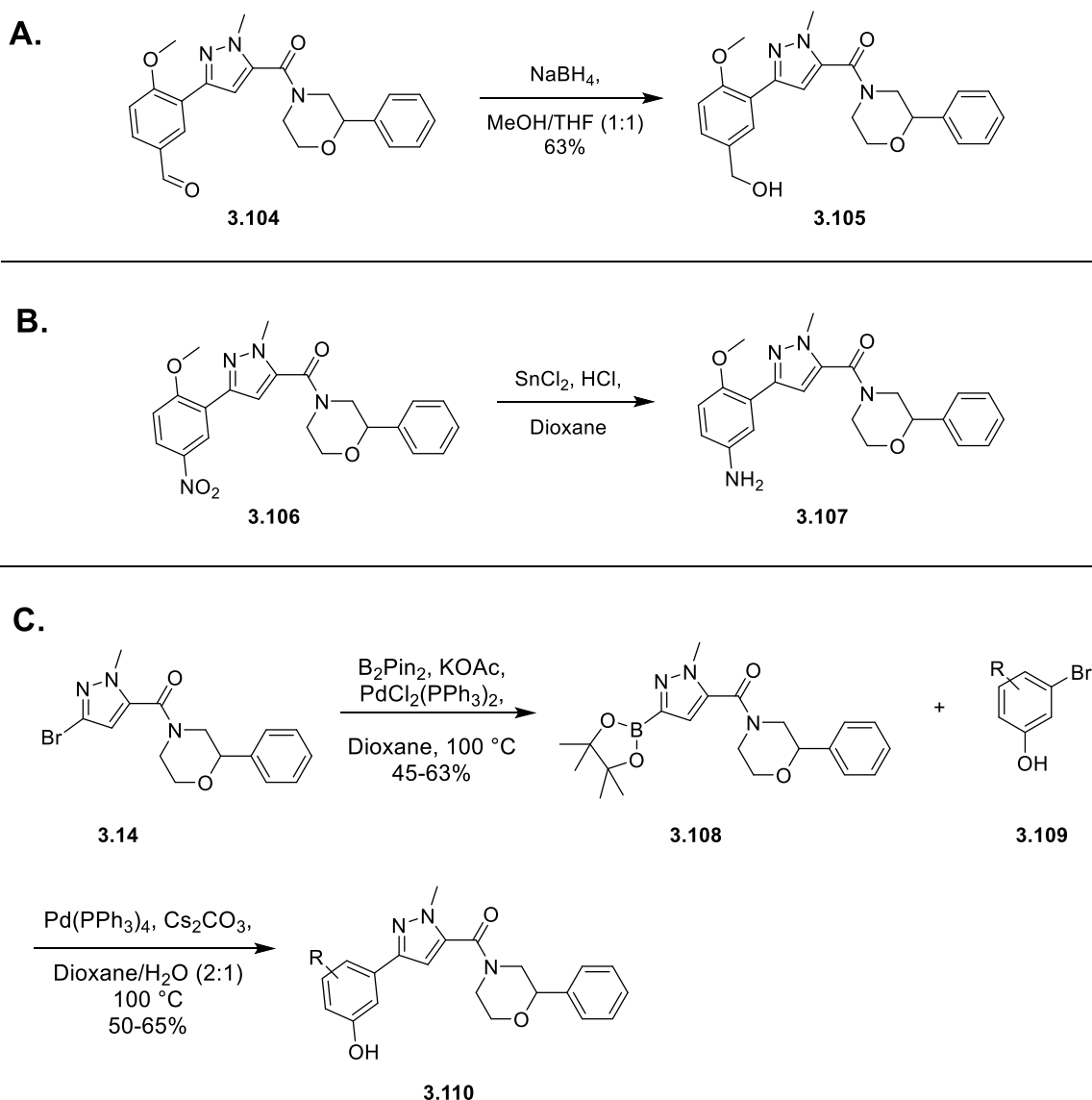


R	VOID	Compound Number	PAC1 %Max
H	VU6015739	3.100	111
F	VU6016416	3.101	98
CN	VU6016417	3.102	102
OCF ₃	VU6016707	3.103	119

Table 3.12 SAR around northern methoxy group.

Other strategies attempting to mitigate the potential dealkylation/oxidation metabolism sequence are highlighted in **Table 3.13**. Analogs **3.111-3.114** can be

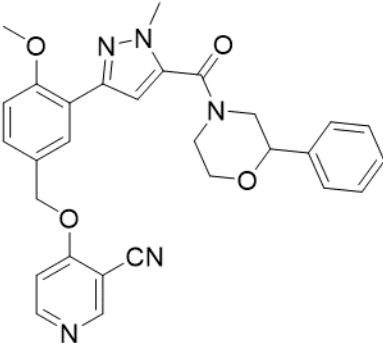
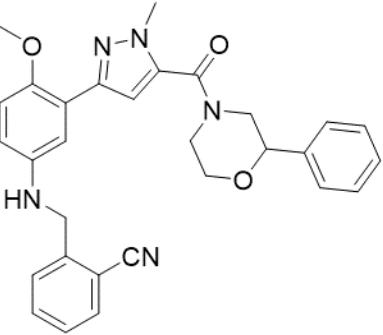
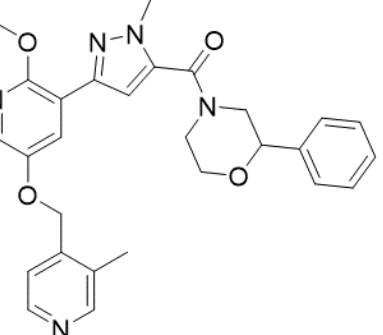
synthesized via the routes depicted in **Schemes 3.4A-3.4C**. The synthetic route to access intermediates **3.14**, **3.104**, and **3.106** is the same as is outlined in **Scheme 3.1**.



Scheme 3.4 Diverging routes from general **Scheme 3.1** to access analogs **3.111-3.114**.

Depicted in **Scheme 3.4A**, a sodium borohydride reduction is employed to reduce aldehyde **3.104** to alcohol **3.105**, which is then subjected to a subsequent Mitsunobu reaction using the appropriate phenol to generate ether **3.111**. In **Scheme 3.4B**, nitro phenol **3.106** was reduced to the aniline **3.107** using tin(II) chloride, followed by an $\text{S}_{\text{N}}2$

to provide **3.112**. Lastly, **Scheme 3.4C** highlights the synthetic route utilized to generate congeners **3.113** and **3.114**. A Miyaura borylation was employed to install the pinacolborane ester to react with the appropriate aryl bromides in a Suzuki reaction to provide analogs resembling **3.110**. Intermediates **3.110** are then coupled with 2-cyanobenzyl bromide to give PAR4 antagonists **3.113** and **3.114**.

Structure	VOID	Compound Number	PAC1 %Max	PAC1 IC ₅₀ (μM)
	VU6017767	3.111	22	3.8
	VU6018761	3.112	92	N/A
	VU6020634	3.113	5.3	1.3

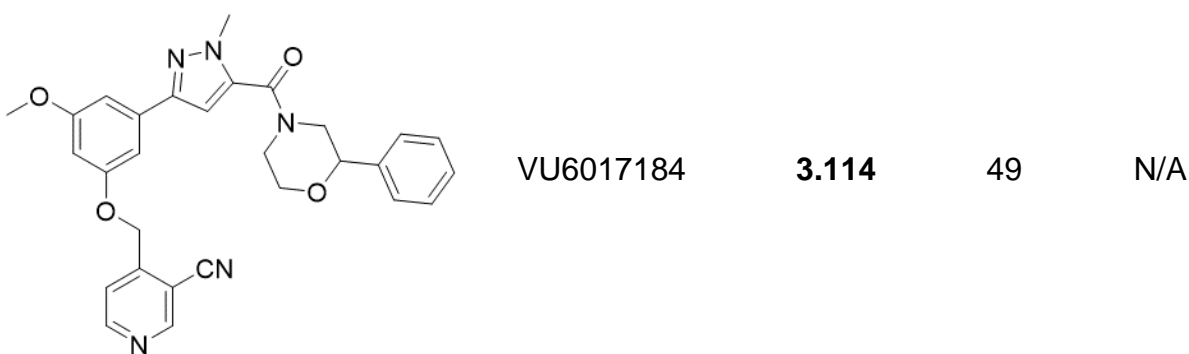


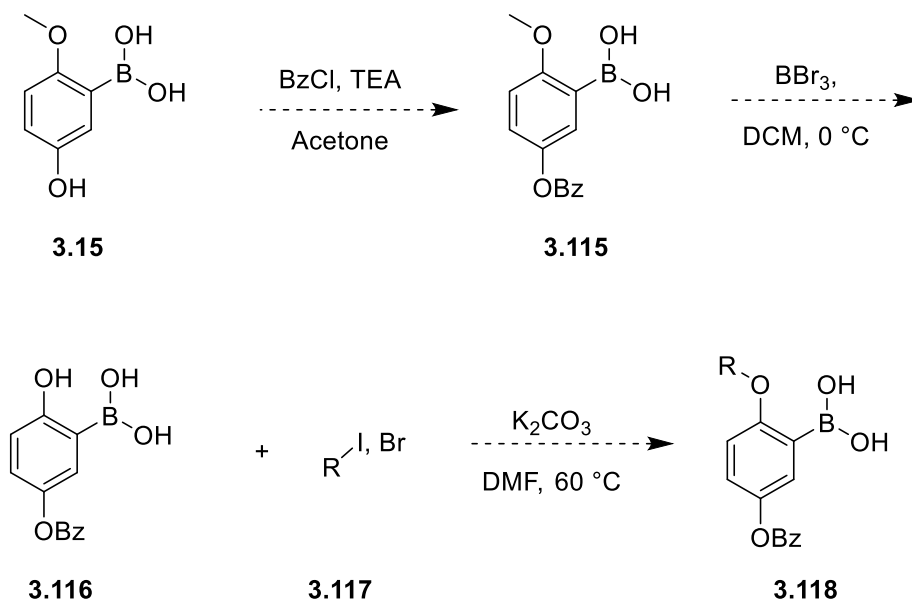
Table 3.13 SAR around the 1,4-dimethoxy phenyl motif.

Unfortunately, these approaches to improve DMPK also did not prove to be fruitful. Moving the oxygen of the ether linkage over one carbon (**3.111**) caused a loss of potency and efficacy. In addition, when the ether was replaced with an amine linker (**3.112**), it rendered the compound inactive, leading us to believe a hydrogen bonding acceptor was important at that location. We also attempted to incorporate a pyridine ring with the nitrogen alpha to the methoxy group (**3.113**), so in the event of demethylation, the metabolite would be halted at the pyridine. Congener **3.113**, while still relatively active, lost a great deal of potency with the incorporation of the pyridine. Lastly, we attempted to walk the methoxy substituent over one carbon to provide the 1,5-dimethoxy analog (**3.114**), which is far less susceptible to dealkylation/oxidation. Unfortunately, a diminution in activity was also seen with congener **3.114**. Therefore, the optimization campaign towards an acceptable *in vivo* tool compound will continue with attempts to improve the DMPK profile of this scaffold.

Future Directions and Conclusions

Future efforts in the development of a viable *in vivo* PAR4 antagonists include metabolic identification studies to determine the most metabolically labile site within our

scaffold. Concurrently, we will continue our efforts in blocking or slowing potential dealkylation/oxidation by employing the kinetic isotope effect or increasing the steric environment around the methoxy-motif utilizing the chemistry outlined in **Scheme 3.5**.



Scheme 3.5 Future synthetic route to access alkyl ether analogs.

In addition to ameliorating the DMPK profile deficits of this series, we will make synthetic efforts to promote a non-competitive mode of inhibition. We hypothesize that a non-competitive PAR4 antagonist will improve activity in our thrombin induced platelet assay, elucidate the pharmacogenomic profile of the rs773902 SNP variations, and promote efficacy in rodent models of cognition. Mutation studies are also under way to potentially elucidate structural differences between mouse and human PAR4 while simultaneously validating our homology model.

To summarize, we report a chiral series of selective, highly brain-penetrant PAR4 antagonists with cross-over activity in mouse and human and the potential to mediate

neurodegenerative pathways. We identified a diverging, fused, heterocyclic scaffold to pursue PAR1 antagonists. In addition, we improved human PAR4 potency from hPAR4-AP $IC_{50} = 3.4 \mu\text{M}$ to sub-hundred nanomolar, as well as improved mouse PAR4 potency from mPAR4-AP $IC_{50} > 10 \mu\text{M}$ to roughly 350 nM. Furthermore, we've managed to inhibit activity against thrombin induced human platelet aggregation by nearly 60%. Finally, we've made headway in confirming the validity of our PAR4 homology model based off the PAR1 and PAR2 x-ray crystallography structures.

Experimental Methods

General Synthetic Methods and Instrumentation

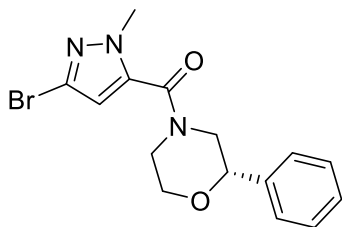
Unless otherwise stated, all reactions were conducted in flame-dried or oven-dried glassware under inert atmospheres of argon. All commercially available reagents and reaction solvents were used as received, unless otherwise noted. Reactions were conducted at room temperature (rt, approximately 23 °C) unless otherwise noted. All ^1H NMR and ^{13}C NMR spectra were recorded on a Bruker AV-400 (400 MHz) or Bruker AV-NMR (600 MHz) instrument. Chemical shifts are reported in ppm relative to residual solvent peaks as an internal standard set to δH 7.26 or δC 77.0 (CDCl_3) and δH 3.31 or δC 49.0 (CD_3OD). Data are reported as follows: chemical shift, multiplicity (s = singlet, d = doublet, t = triplet, q = quartet, br = broad, m = multiplet), integration, and coupling constant (Hz). IR spectra were recorded as thin films and are reported in wavenumbers (cm^{-1}). Low resolution mass spectra were obtained on an Agilent 1200 LCMS with electrospray ionization. High resolution mass spectra were recorded on a Waters Qtof-

API-US plus Acquity system. The value Δ is the error in the measurement (in ppm) given by the equation $\Delta = [(ME - MT)/MT] \times 106$, where ME is the experimental mass and MT is the theoretical mass. The HRMS results were obtained with ES as the ion source and leucine enkephalin as the reference. Optical rotations were measured on a PerkinElmer-341 polarimeter. Analytical thin layer chromatography was performed on 250 μ M silica gel 60 F254 plates. Visualization was accomplished with UV light, and/or the use of ninhydrin, anisaldehyde and ceric ammonium molybdate solutions followed by charring on a hot-plate. Chromatography on silica gel was performed using Silica Gel 60 (230–400 mesh) from Sorbent Technologies. Analytical HPLC was performed on an Agilent 1200 analytical LCMS with UV detection at 214 and 254 nm along with ELSD detection. Solvents for extraction, washing, and chromatography were HPLC grade. All reagents were purchased from Aldrich Chemical Co. and were used without purification. All polymer-supported reagents were purchased from Biotage, Inc. Flame-dried (under vacuum) glassware was used for all reactions. All reagents and solvents were commercial grade and purified prior to use when necessary. High-resolution mass spectrometry (HRMS) data were obtained using a Micromass Q-ToF API-US mass spectrometer.

General Procedure 1: Synthesis of Amides

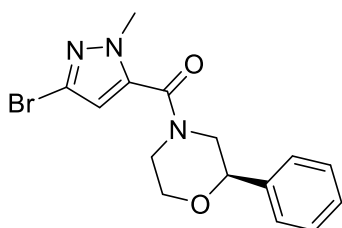
A solution of HATU (1.1 eq), *N,N*-Diisopropylethylamine (3.0 eq), 3-Bromo-1-Methylpyrazole-5-carboxylic acid (1.0 eq) in DMF (0.25M) was stirred at room temperature for 20 min to which the appropriate amine (1.1 eq) was then added. The reaction mixture was stirred at room temperature for 1 h. Upon completion, the reaction mixture was diluted in H₂O and extracted with EtOAc (3x). The combined organic layers

were washed with brine, dried over MgSO₄, filtered, concentrated, and purified via flash chromatography (Teledyne ISCO system, silica gel column, hexanes:EtOAc) to provide the desired product.



Synthesis of (5-bromo-2-methyl-pyrazol-3-yl)-[(2S)-2-phenylmorpholin-4-yl]methanone

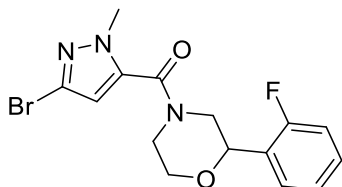
This compound was synthesized according to general procedure 1. White solid (80% yield). $[\alpha]^{25}_D = \text{Error! Bookmark not defined.}$ -52.9 (c = 2.37, MeOH). ¹H NMR (400 MHz, CDCl₃) δ 7.38-7.32 (m, 5H), 6.32 (s, 1H), 4.68-4.48 (m, 2H), 4.16-3.87 (m, 5H), 3.71 (bs, 1H), 3.43-2.89 (m, 2H). ¹³C NMR (100 MHz, CDCl₃) δ = 159.7, 138.5, 136.7, 128.8, 126.2, 124.3, 109.2, 78.2, 66.9, 53.7, 48.4, 47.4, 42.2, 38.7. HRMS (TOF, ES+) calc'd for C₁₅H₁₆BrN₃O₂ 349.0426; found, 349.0431.



Synthesis of (5-bromo-2-methyl-pyrazol-3-yl)-[(2R)-2-phenylmorpholin-4-yl]methanone

This compound was synthesized according to general procedure 1. White solid. (70% yield). $[\alpha]^{24}_D = +58.9$ (c = 1.33, MeOH). ¹H NMR (400 MHz, CDCl₃) δ 7.38-7.32 (m, 5H), 6.32 (s, 1H), 4.68-4.48 (m, 2H), 4.16-3.87 (m, 5H), 3.71 (bs, 1H), 3.43-2.89 (m, 2H). ¹³C

NMR (100 MHz, CDCl₃) δ = 159.7, 138.5, 136.7, 128.8, 126.2, 124.3, 109.2, 78.2, 66.9, 53.7, 48.4, 47.4, 42.2, 38.7. HRMS (TOF, ES+) calc'd for C₁₅H₁₆BrN₃O₂, 349.0426; found, 349.0431.



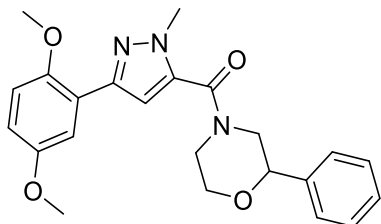
Synthesis of (3-bromo-1-methyl-1H-pyrazol-5-yl)(2-(2-fluorophenyl)morpholino)methanone

This compound was synthesized according to general procedure 1. White Solid (80% yield). ¹H NMR (400 MHz, CDCl₃) δ 7.43 (t, *J* = 7.0 Hz, 1H), 7.25-7.19 (m, 1H), 7.11 (t, *J* = 7.4 Hz, 1H), 6.98 (t, *J* = 9.2 Hz, 1H), 6.29 (s, 1H), 4.69 (d, *J* = 9.4 Hz, 1H), 4.49 (bs, 1H), 4.23-3.97 (m, 2H), 3.89 (s, 3H), 3.68 (bs, 1H), 3.45-2.72 (bm, 2H). ¹³C NMR (100 MHz, CDCl₃) δ = 159.6, 159.5 (¹*J*_{CF} = 242 Hz), 136.6, 130.0 (³*J*_{CF} = 8.3 Hz), 127.4, 125.4, 124.6, 124.2, 115.4 (²*J*_{CF} = 21.3 Hz), 109.3, 72.5, 67.0, 42.2, 38.7. HRMS (TOF, ES+) calc'd for C₁₅H₁₅ BrFN₃O₂, 367.0332; found, 367.0339.

General Procedure 2: Synthesis of Phenols

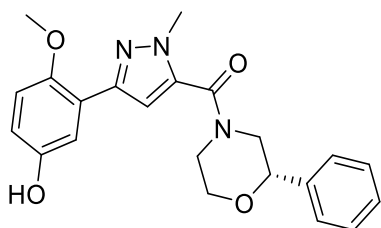
A degassed solution of tetrakis(triphenylphosphine)palladium(0) (5 mol%), cesium carbonate (1.5 eq), the appropriate (5-bromo-2-methyl-pyrazol-3-yl)-[2-phenylmorpholin-4-yl]methanone (1.0 eq), and 5-hydroxy-2-methoxyphenylboronic acid (1.1 eq) in 1,4-Dioxane: H₂O (2:1)(0.2M) was heated to 100°C and let stir for 16 h. The reaction mixture was then cooled, diluted with H₂O, and extracted with DCM (3x). The combined organics were passed through a phase separator, concentrated, and purified

via flash chromatography (Teledyne ISCO system, silica gel column, hexanes:EtOAc) to provide the desired product.



Synthesis of (3-(2,5-dimethoxyphenyl)-1-methyl-1H-pyrazol-5-yl)(2-phenylmorpholino)methanone

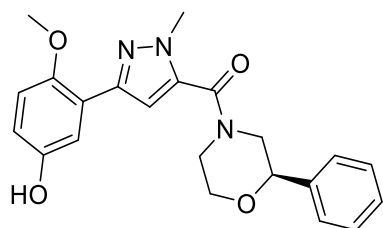
This compound was synthesized according to general procedure 2. White solid (88% yield). $^1\text{H NMR}$ (400 MHz, CDCl_3) δ 7.53 (d, $J = 3.1$ Hz, 1H), 7.35 (d, $J = 19.3$ Hz, 7H), 6.90 (d, $J = 6.5$ Hz, 2H), 6.85 (dd, $J = 8.9, 3.1$ Hz, 1H), 4.56 – 4.49 (m, 1H), 4.06 (s, 3H), 3.82 (d, $J = 7.2$ Hz, 6H), 3.21 (t, $J = 102.4$ Hz, 2H). $^{13}\text{C NMR}$ (100 MHz, CDCl_3) δ 161.23, 153.99, 151.17, 146.61, 128.72, 128.49, 126.12, 122.30, 115.07, 113.14, 113.13, 108.46, 78.30, 77.48, 77.16, 76.84, 67.00, 56.36, 55.97, 38.48. LC-MS [$m/z + \text{H}$] = 332.0.



Synthesis of [5-(5-hydroxy-2-methoxy-phenyl)-2-methyl-pyrazol-3-yl]-[(2S)-2-phenylmorpholin-4-yl]methanone

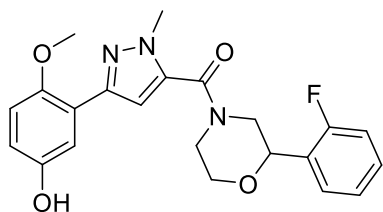
This compound was synthesized according to general procedure 2. White solid (88% yield). $[\alpha]_D^{25} = \text{Error! Bookmark not defined.}$ -50.7 ($c = 1.34$, MeOH). $^1\text{H NMR}$ (400 MHz, CDCl_3) δ 7.69-7.52 (m, 1H), 7.49-7.29 (m, 5H), 6.89-6.77 (m, 3H), 4.82-4.42 (m,

2H), 4.36-3.93 (bs, 5H), 3.91-3.62 (bs, 4H), 3.58-2.85 (m, 2H). ^{13}C NMR (100 MHz, CDCl_3) δ = 161.2, 151.0, 150.0, 146.5, 132.3, 132.2, 132.1, 132.0, 128.7, 128.6, 128.5, 126.1, 122.1, 115.8, 115.1, 113.3, 108.4, 78.2, 77.4, 67.0, 56.3, 38.4. HRMS (TOF, ES+) calc'd for $\text{C}_{22}\text{H}_{23}\text{N}_3\text{O}_4$, 393.1689; found, 393.1700.



Synthesis of [5-(5-hydroxy-2-methoxy-phenyl)-2-methyl-pyrazol-3-yl]-[(2R)-2-phenylmorpholin-4-yl]methanone

This compound was synthesized according to general procedure 2. White solid (78% yield). $[\alpha]_D^{24} = +67.3$ ($c = 1.22$, MeOH). ^1H NMR (400 MHz, CDCl_3) δ 7.69-7.52 (m, 1H), 7.49-7.29 (m, 5H), 6.89-6.77 (m, 3H), 4.82-4.42 (m, 2H), 4.36-3.93 (bs, 5H), 3.91-3.62 (bs, 4H), 3.58-2.85 (m, 2H). ^{13}C NMR (100 MHz, CDCl_3) δ = 161.2, 151.0, 150.0, 146.5, 132.3, 132.2, 132.1, 132.0, 128.7, 128.6, 128.5, 126.1, 122.1, 115.8, 115.1, 113.3, 108.4, 78.2, 77.4, 67.0, 56.3, 38.4. HRMS (TOF, ES+) calc'd for $\text{C}_{22}\text{H}_{23}\text{N}_3\text{O}_4$, 393.1689; found, 393.1700.

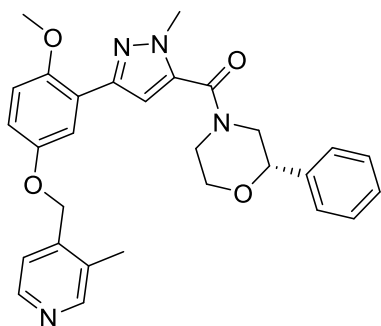


Synthesis of (2-(2-fluorophenyl)morpholino)(3-(5-hydroxy-2-methoxyphenyl)-1-methyl-1H-pyrazol-5-yl)methanone

This compound was synthesized according to general procedure 2. White solid (71% yield). ^1H NMR (400 MHz, CDCl_3) δ 7.52 (m, 2H), 7.30-7.20 (bs, 1H), 7.14 (t, $J = 7.4$ Hz, 1H), 7.07-6.84 (m, 2H), 6.80-6.72 (m, 2H), 4.82 (dd, $J = 10.4, 1.7$ Hz, 1H), 4.67-4.25 (m, 1H), 4.21-3.93 (bs, 5H), 3.75 (s, 4H), 3.51-2.85 (m, 2H). ^{13}C NMR (100 MHz, CDCl_3) $\delta =$ 161.3, 159.4 ($^1J_{\text{CF}} = 249$ Hz), 150.6, 150.4, 146.7, 134.9, 130.0 ($^3J_{\text{CF}} = 8.2$ Hz), 127.5, 125.6, 124.5, 121.7, 116.0, 115.4, 115.2, 113.1, 108.4, 72.4, 66.9, 56.0, 52.8, 42.2, 38.1. HRMS (TOF, ES+) calc'd for $\text{C}_{22}\text{H}_{22}\text{FN}_3\text{O}_4$, 411.1594; found, 411.1599.

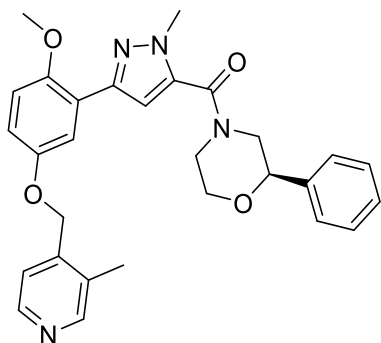
General Procedure 3: Synthesis of benzyl ethers

A solution of the appropriate [5-(5-hydroxy-2-methoxy-phenyl)-2-methyl-pyrazol-3-yl]-(2-phenylmorpholin-4-yl)methanone (1.0 eq), Di-tert-butyl azodicarboxylate (1.5 eq), triphenylphosphine (1.3 eq), and the appropriate benzyl alcohol (1.1 eq) in THF (0.2M) was allowed to stir at room temperature for 16 h. The reaction mixture was concentrated, re-dissolved in MeOH, loaded onto a pre-wetted SCX cartridge, washed with 6 column volumes of MeOH, eluted with 1 column volume 7N NH_3/MeOH , and concentrated to remove triphenylphosphine oxide. The crude material was then purified using a Gilson HPLC system (30 x 50 mm column; H_2O with 0.1% TFA:acetonitrile). Fractions containing the desired product were quenched with saturated NaHCO_3 , extracted with DCM, and concentrated to liberate the product as the free base.



Synthesis of [5-[2-methoxy-5-[(3-methyl-4-pyridyl)methoxy]phenyl]-2-methylpyrazol-3-yl]-((2S)-2-phenylmorpholin-4-yl)methanone

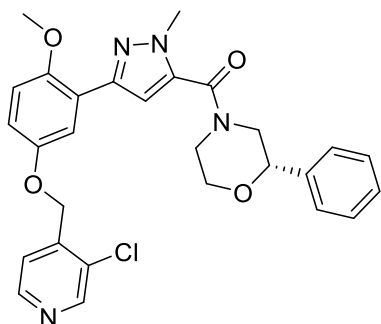
This compound was synthesized according to general procedure 3. Clear oil (47% yield). $[\alpha]_D^{25} = \text{Error! Bookmark not defined.}$ -59.4 ($c = 1.18$, MeOH). $^1\text{H NMR}$ (400 MHz, CDCl_3) δ 8.45 (d, $J = 11.5$ Hz, 2H), 7.64 (s, 1H), 7.47 (d, $J = 4.8$ Hz, 1H), 7.44-7.29 (bs, 5H), 6.92 (s, 3H), 5.07 (s, 2H), 4.84-4.42 (m, 2H), 4.07 (bs, 5H), 3.84 (bs, 4H), 3.60-2.85 (m, 2H). $^{13}\text{C NMR}$ (100 MHz, CDCl_3) $\delta = 161.2, 152.7, 151.7, 150.8, 148.0, 146.4, 144.4, 138.7, 135.2, 130.8, 128.8, 128.5, 126.1, 122.5, 121.7, 115.7, 114.4, 113.0, 108.5, 78.3, 67.5, 67.0, 56.3, 54.0, 48.4, 47.6, 42.1, 38.5, 15.8$. HRMS (TOF, ES+) calc'd for $\text{C}_{29}\text{H}_{30}\text{N}_4\text{O}_4$, 498.2267; found, 498.2277.



Synthesis of [5-[2-methoxy-5-[(3-methyl-4-pyridyl)methoxy]phenyl]-2-methylpyrazol-3-yl]-((2R)-2-phenylmorpholin-4-yl)methanone

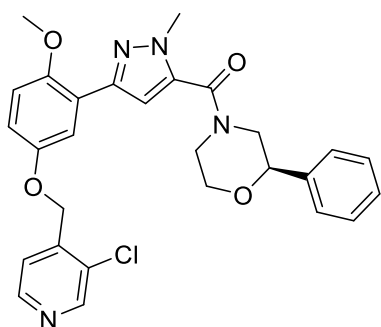
This compound was synthesized according to general procedure 3. Clear oil (32% yield). $[\alpha]_D^{24} = \text{Error! Bookmark not defined.}$ +51.2 ($c = 2.07$, MeOH). $^1\text{H NMR}$ (400 MHz, CDCl_3) δ 8.45 (d, $J = 11.5$ Hz, 2H), 7.64 (s, 1H), 7.47 (d, $J = 4.8$ Hz, 1H), 7.44-7.29 (bs, 5H), 6.92 (s, 3H), 5.07 (s, 2H), 4.84-4.42 (m, 2H), 4.07 (bs, 5H), 3.84 (bs, 4H), 3.60-2.85 (m, 2H). $^{13}\text{C NMR}$ (100 MHz, CDCl_3) $\delta = 161.2, 152.7, 151.7, 150.8, 148.0,$

146.4, 144.4, 138.7, 135.2, 130.8, 128.8, 128.5, 126.1, 122.5, 121.7, 115.7, 114.4, 113.0, 108.5, 78.3, 67.5, 67.0, 56.3, 38.5, 15.8. HRMS (TOF, ES+) calc'd for $C_{29}H_{30}N_4O_4$, 498.2267; found, 498.2277.



Synthesis of [5-[5-[(3-chloro-4-pyridyl)methoxy]-2-methoxy-phenyl]-2-methyl-pyrazol-3-yl]-[(2S)-2-phenylmorpholin-4-yl]methanone

This compound was synthesized according to general procedure 3. Orange oil (78% yield). $[\alpha]^{24}_D = -37.8$ ($c = 2.58$, MeOH). 1H NMR (400 MHz, $CDCl_3$) δ 8.57 (s, 1H), 8.50 (d, $J = 4.9$ Hz, 1H), 7.65 (s, 1H), 7.59 (d, $J = 4.9$ Hz, 1H), 7.49-7.28 (bs, 5H), 6.91 (s, 3H), 5.17 (s, 2H), 4.84-4.42 (m, 2H), 4.07 (bs, 5H), 3.83 (bs, 4H), 3.60-2.82 (m, 2H). ^{13}C NMR (100 MHz, $CDCl_3$) $\delta = 161.2, 154.3, 152.2, 151.9, 149.1, 148.2, 146.3, 144.4, 132.3, 132.2, 132.0, 129.7, 128.7, 128.5, 126.1, 122.7, 122.4, 115.3, 114.8, 112.9, 108.5, 78.3, 67.0, 66.5, 56.3, 38.5, 28.3, 28.0$. HRMS (TOF, ES+) calc'd for $C_{28}H_{27}ClN_4O_4$, 518.1733; found, 518.1721.

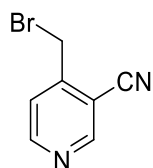


Synthesis of 5-[5-[(3-chloro-4-pyridyl)methoxy]-2-methoxy-phenyl]-2-methyl-pyrazol-3-yl]-[(2*R*)-2-phenylmorpholin-4-yl]methanone

This compound was synthesized according to general procedure 3. Orange oil (76% yield). $[\alpha]_D^{24} = \text{Error! Bookmark not defined.} +39.6$ ($c = 2.51$, MeOH). $^1\text{H NMR}$ (400 MHz, CDCl_3) δ 8.57 (s, 1H), 8.50 (d, $J = 4.9$ Hz, 1H), 7.65 (s, 1H), 7.59 (d, $J = 4.9$ Hz, 1H), 7.49-7.28 (bs, 5H), 6.91 (s, 3H), 5.17 (s, 2H), 4.84-4.42 (m, 2H), 4.07 (bs, 5H), 3.83 (bs, 4H), 3.60-2.82 (m, 2H). $^{13}\text{C NMR}$ (100 MHz, CDCl_3) $\delta = 161.2, 154.3, 152.2, 151.9, 149.1, 148.2, 146.3, 144.4, 132.3, 132.2, 132.0, 129.7, 128.7, 128.5, 126.1, 122.7, 122.4, 115.3, 114.8, 112.9, 108.5, 78.3, 67.0, 66.5, 56.3, 38.5, 28.3, 28.0$. HRMS (TOF, ES+) calc'd for $\text{C}_{28}\text{H}_{27}\text{ClN}_4\text{O}_4$, 518.1733; found, 518.1721.

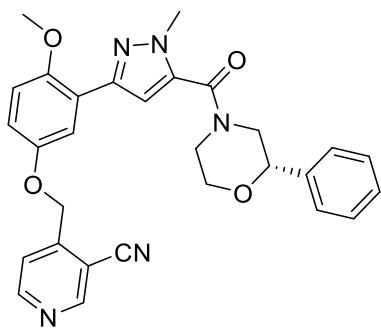
General Procedure 4: Synthesis of benzyl ethers

A solution of [5-(5-hydroxy-2-methoxy-phenyl)-2-methyl-pyrazol-3-yl]-[(2*S*)-2-phenylmorpholin-4-yl]methanone (1.0 eq), potassium carbonate (1.5 eq), and the appropriate benzyl bromide (1.1 eq) in DMF (0.15M) was heated to 60 °C and stirred for 3 h. The reaction mixture was passed through a syringe filter and the crude material was purified using a Gilson HPLC (30 x 50 mm column, H_2O with 0.1% TFA:acetonitrile). Fractions containing the desired product were quenched with saturated NaHCO_3 , extracted with DCM, and concentrated to liberate the product as the free base.



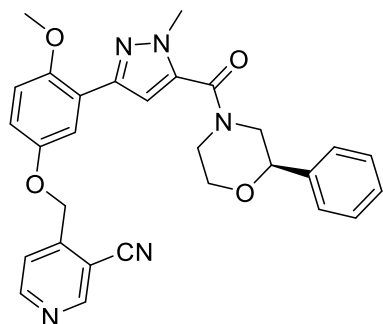
Synthesis of 4-(bromomethyl)pyridine-3-carbonitrile

3-Cyano-4-methylpyridine (1.0 eq), *N*-Bromosuccinimide (1.5 eq), and 2,2'-azobis(2-methylpropionitrile) (0.47 eq) were suspended in carbon tetrachloride (0.5M) and the reaction mixture was heated to reflux for 3.5 h. The reaction mixture was cooled to room temperature and concentrated by half the volume *in vacuo*. The resulting solution was filtered over a pad of celite. The solution was then concentrated to dryness and the material was taken forward without further purification. Assumed quantitative yield.



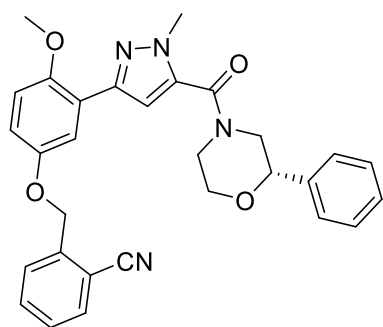
Synthesis of 4-[[4-methoxy-3-[1-methyl-5-[(2S)-2-phenylmorpholine-4-carbonyl]pyrazol-3-yl]phenoxy]methyl]pyridine-3-carbonitrile

This compound was synthesized according to general procedure 4. Clear oil (4-25% yield). $[\alpha]^{23}_D = \text{Error! Bookmark not defined.} -32.5$ ($c = 0.82$, MeOH). $^1\text{H NMR}$ (400 MHz, CDCl_3) δ 8.88 (s, 1H), 8.81 (d, $J = 5.2$ Hz, 1H), 7.72 (d, $J = 5.1$ Hz, 1H), 7.66 (s, 1H), 7.47-7.29 (bs, 5H), 6.92 (d, $J = 5.1$ Hz, 3H), 5.29 (s, 2H), 4.82-4.42 (m, 2H), 4.06 (bs, 5H), 3.83 (bs, 4H), 3.58-2.87 (m, 2H). $^{13}\text{C NMR}$ (100 MHz, CDCl_3) $\delta = 166.9, 161.2, 153.4, 152.9, 152.1, 151.9, 150.3, 146.2, 128.8, 128.5, 126.2, 122.8, 121.9, 115.5, 115.1, 114.8, 113.0, 108.5, 108.0, 78.3, 67.1, 67.0, 56.3, 55.7, 38.5, 32.0, 29.8, 25.0, 17.2$. HRMS (TOF, ES⁺) calc'd for $\text{C}_{29}\text{H}_{27}\text{N}_5\text{O}_4$, 509.2063; found, 509.2068.



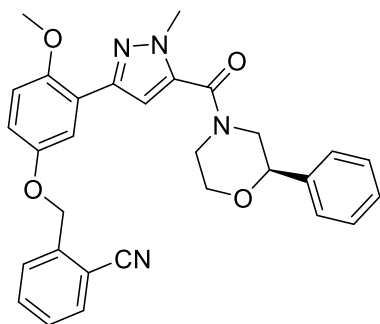
Synthesis of 4-[[4-methoxy-3-[1-methyl-5-[(2R)-2-phenylmorpholine-4-carbonyl]pyrazol-3-yl]phenoxy]methyl]pyridine-3-carbonitrile

This compound was synthesized according to general procedure 4. Clear oil (6-28% yield). $[\alpha]_D^{23} = \text{Error! Bookmark not defined.} +29.4$ ($c = 0.92$, MeOH). $^1\text{H NMR}$ (400 MHz, CDCl_3) δ 8.88 (s, 1H), 8.81 (d, $J = 5.2$ Hz, 1H), 7.72 (d, $J = 5.1$ Hz, 1H), 7.66 (s, 1H), 7.47-7.29 (bs, 5H), 6.92 (d, $J = 5.1$ Hz, 3H), 5.29 (s, 2H), 4.82-4.42 (m, 2H), 4.06 (bs, 5H), 3.83 (bs, 4H), 3.58-2.87 (m, 2H). $^{13}\text{C NMR}$ (100 MHz, CDCl_3) $\delta = 166.9, 161.2, 153.4, 152.9, 152.1, 151.9, 150.3, 146.2, 128.8, 128.5, 126.2, 122.8, 121.9, 115.5, 115.1, 114.8, 113.0, 108.5, 108.0, 78.3, 67.1, 67.0, 56.3, 55.7, 38.5, 32.0, 29.8, 25.0, 17.2$. HRMS (TOF, ES+) calc'd for $\text{C}_{29}\text{H}_{27}\text{N}_5\text{O}_4$, 509.2063; found, 509.2068.



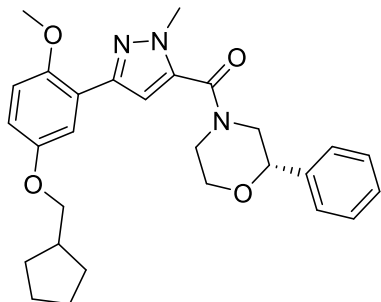
Synthesis of 2-[[4-methoxy-3-[1-methyl-5-[(2S)-2-phenylmorpholine-4-carbonyl]pyrazol-3-yl]phenoxy]methyl]benzonitrile

This compound was synthesized according to general procedure 4. Orange Oil (60% yield). $[\alpha]_D^{25} = -46.1$ ($c = 1.95$, CHCl_3). $^1\text{H NMR}$ (400 MHz, CDCl_3) δ 7.73-7.68 (m, 3H), 7.62 (td, $J = 7.6$ Hz, 1.1 Hz, 1H), 7.44-7.29 (m, 6H), 6.97-6.90 (m, 3H), 5.28 (s, 2H), 4.88-4.43 (m, 2H), 4.07 (bs, 5H), 3.83 (bs, 4H), 3.60-2.86 (m, 2H). $^{13}\text{C NMR}$ (100 MHz, CDCl_3) $\delta = 161.2, 152.5, 151.8, 146.4, 141.1, 138.6, 135.1, 133.1, 132.9, 128.7, 128.6, 128.5, 128.4, 126.1, 122.5, 117.3, 115.6, 114.9, 112.9, 111.2, 108.5, 78.3, 68.4, 67.0, 56.3, 54.0, 48.4, 42.1, 38.5$. HRMS (TOF, ES+) calc'd for $\text{C}_{30}\text{H}_{28}\text{N}_4\text{O}_4$, 508.2111; found, 508.2116.



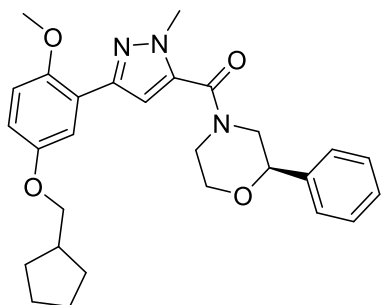
2-[[4-methoxy-3-[1-methyl-5-[(2R)-2-phenylmorpholine-4-carbonyl]pyrazol-3-yl]phenoxy]methyl]benzonitrile

This compound was synthesized according to general procedure 4. Orange Oil (80% yield). $[\alpha]_D^{25} = +54.5$ ($c = 2.57$, CHCl_3). $^1\text{H NMR}$ (400 MHz, CDCl_3) δ 7.73-7.68 (m, 3H), 7.62 (td, $J = 7.6$ Hz, 1.1 Hz, 1H), 7.44-7.29 (m, 6H), 6.97-6.90 (m, 3H), 5.28 (s, 2H), 4.88-4.43 (m, 2H), 4.07 (bs, 5H), 3.83 (bs, 4H), 3.60-2.86 (m, 2H). $^{13}\text{C NMR}$ (100 MHz, CDCl_3) $\delta = 161.2, 152.5, 151.8, 146.4, 141.1, 138.6, 135.1, 133.1, 132.9, 128.7, 128.6, 128.5, 128.4, 126.1, 122.5, 117.3, 115.6, 114.9, 112.9, 111.2, 108.5, 78.3, 68.4, 67.0, 56.3, 54.0, 48.4, 42.1, 38.5$. HRMS (TOF, ES+) calc'd for $\text{C}_{30}\text{H}_{28}\text{N}_4\text{O}_4$, 508.2111; found, 508.2116.



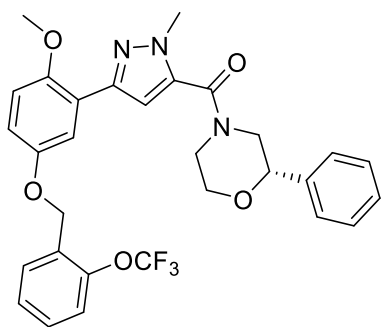
Synthesis of [5-[5-(cyclopentylmethoxy)-2-methoxy-phenyl]-2-methyl-pyrazol-3-yl]-[(2S)-2-phenylmorpholin-4-yl]methanone

This compound was synthesized according to general procedure 4. Clear oil (50% yield). $[\alpha]_D^{25} = \text{Error! Bookmark not defined.} -54.6$ ($c = 1.51$, MeOH). $^1\text{H NMR}$ (400 MHz, CDCl_3) δ 7.52 (d, $J = 2.7$ Hz, 1H), 7.47-7.29 (bs, 5H), 6.92-6.83 (m, 3H), 4.85-4.43 (m, 2H), 4.06 (bs, 5H), 3.85 (d, $J = 7.0$ Hz, 2H), 3.84-3.67 (bs, 4H), 3.58-2.85 (m, 2H), 2.35 (sep, $J = 4.4$ Hz, 1H), 1.88-1.78 (m, 2H), 1.69-1.53 (m, 4H), 1.42-1.32 (m, 2H). $^{13}\text{C NMR}$ (100 MHz, CDCl_3) $\delta = 161.2, 153.7, 151.1, 146.7, 138.7, 135.1, 128.7, 128.5, 126.1, 122.3, 115.6, 114.5, 113.1, 108.5, 78.4, 73.1, 67.0, 56.4, 54.0, 48.4, 47.6, 42.2, 39.3, 38.5, 31.0, 30.0, 29.6, 25.6$. HRMS (TOF, ES+) calc'd for $\text{C}_{28}\text{H}_{33}\text{N}_3\text{O}_4$, 475.2471; found, 475.2481.



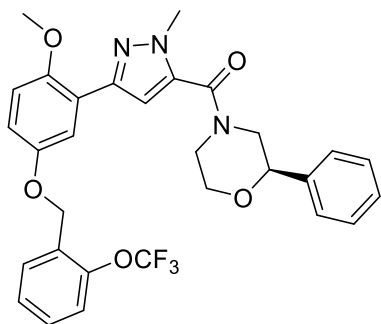
Synthesis of [5-[5-(cyclopentylmethoxy)-2-methoxy-phenyl]-2-methyl-pyrazol-3-yl]-[(2R)-2-phenylmorpholin-4-yl]methanone

This compound was synthesized according to general procedure 4. Clear oil (47% yield). $[\alpha]^{25}_D = +69.7$ ($c = 1.42$, MeOH). $^1\text{H NMR}$ (400 MHz, CDCl_3) δ 7.52 (d, $J = 2.7$ Hz, 1H), 7.47-7.29 (bs, 5H), 6.92-6.83 (m, 3H), 4.85-4.43 (m, 2H), 4.06 (bs, 5H), 3.85 (d, $J = 7.0$ Hz, 2H), 3.84-3.67 (bs, 4H), 3.58-2.85 (m, 2H), 2.35 (sep, $J = 4.4$ Hz, 1H), 1.88-1.78 (m, 2H), 1.69-1.53 (m, 4H), 1.42-1.32 (m, 2H). $^{13}\text{C NMR}$ (100 MHz, CDCl_3) $\delta = 161.2, 153.7, 151.1, 146.7, 138.7, 135.1, 128.7, 128.5, 126.1, 122.3, 115.6, 114.5, 113.1, 108.5, 78.4, 73.1, 67.0, 56.4, 54.0, 48.4, 47.6, 42.2, 39.3, 38.5, 31.0, 30.0, 29.6, 25.6$. HRMS (TOF, ES+) calc'd for $\text{C}_{28}\text{H}_{33}\text{N}_3\text{O}_4$, 475.2471; found, 475.2481.



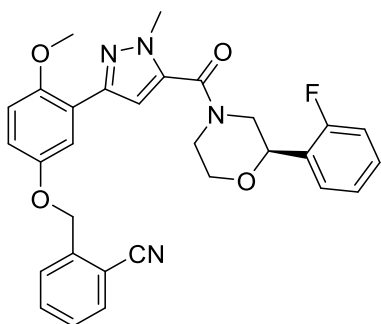
Synthesis of [5-[2-methoxy-5-[[2-(trifluoromethoxy)phenyl]methoxy]phenyl]-2-methyl-pyrazol-3-yl]-[(2S)-2-phenylmorpholin-4-yl]methanone

This compound was synthesized according to general procedure 4. Orange oil (62% yield). $[\alpha]^{25}_D = \text{Error! Bookmark not defined.}$ -47.6 ($c = 2.23$, MeOH). $^1\text{H NMR}$ (400 MHz, CDCl_3) δ 7.64 (dd, $J = 7.5, 1.52$ Hz, 2H) 7.51-7.26 (m, 8H), 6.91 (d, $J = 2.5$ Hz, 3H), 5.17 (s, 2H), 4.85-4.42 (m, 2H), 4.07 (bs, 5H), 3.83 (bs, 4H), 3.6-2.85 (m, 2H). $^{13}\text{C NMR}$ (100 MHz, CDCl_3) $\delta = 161.2, 152.8, 151.6, 146.8, 146.5, 135.1, 130.4, 130.3, 130.2, 129.6, 129.2, 128.7, 128.5, 127.1, 127.0, 126.1, 122.5, 120.7$ (q, $J_{CF} = 256$ Hz), 120.6, 120.5, 115.5, 114.9, 112.9, 108.5, 78.2, 67.0, 65.1, 64.4, 56.3, 38.5. HRMS (TOF, ES+) calc'd for $\text{C}_{30}\text{H}_{28}\text{F}_3\text{N}_3\text{O}_5$, 567.1981; found, 567.1989.



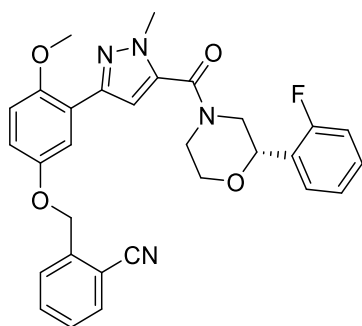
Synthesis of [5-[2-methoxy-5-[[2-(trifluoromethoxy)phenyl]methoxy]phenyl]-2-methyl-pyrazol-3-yl]-[(2R)-2-phenylmorpholin-4-yl]methanone

This compound was synthesized according to general procedure 4. Orange oil (62% yield). $[\alpha]_D^{25} = +46.7$ ($c = 2.24$, MeOH). $^1\text{H NMR}$ (400 MHz, CDCl_3) δ 7.64 (dd, $J = 7.5$, 1.5 Hz, 2H) 7.51-7.26 (m, 8H), 6.91 (d, $J = 2.5$ Hz, 3H), 5.17 (s, 2H), 4.85-4.42 (m, 2H), 4.07 (bs, 5H), 3.83 (bs, 4H), 3.6-2.85 (m, 2H). $^{13}\text{C NMR}$ (100 MHz, CDCl_3) $\delta = 161.2$, 152.8, 151.6, 146.8, 146.5, 135.1, 130.4, 130.3, 130.2, 129.6, 129.2, 128.7, 128.5, 127.1, 127.0, 126.1, 122.5, 120.7 (q, $J_{\text{CF}} = 256$ Hz), 120.6, 120.5, 115.5, 114.9, 112.9, 108.5, 78.2, 67.0, 65.1, 64.4, 56.3, 38.5. HRMS (TOF, ES+) calc'd for $\text{C}_{30}\text{H}_{28}\text{F}_3\text{N}_3\text{O}_5$, 567.1981; found, 567.1989.



Synthesis of 2-((3-(5-(2-(2-fluorophenyl)morpholine-4-carbonyl)-1-methyl-1H-pyrazol-3-yl)-4-methoxyphenoxy)methyl)benzonitrile

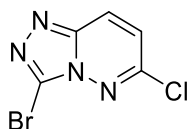
This compound was synthesized according to general procedure 4. Racemic material separated via Supercritical Fluid, chiral chromatography. Single enantiomer of unknown stereochemistry. $[\alpha]^{24}_D = +68.3$ ($c = 1.08$, CHCl_3). White solid. $^1\text{H NMR}$ (400 MHz, CDCl_3) δ 7.74-7.67 (m, 3H), 7.63 (t, $J = 7.2, 8.0$ Hz, 1H), 7.52 (t, $J = 6.8$ Hz, 1H), 7.42 (t, $J = 7.4$ Hz, 1H), 7.34-7.27 (bs, 1H), 7.18 (t, $J = 7.2$ Hz, 1H), 7.11-6.99 (bs, 1H), 6.99-6.89 (m, 3H), 5.28 (s, 2H), 4.85 (dd, $J = 10.5, 2.2$ Hz, 1H), 4.82-4.10 (m, 3H), 4.07 (s, 3H), 3.85 (bs, 4H), 3.58-2.86 (m, 2H). $^{13}\text{C NMR}$ (100 MHz, CDCl_3) $\delta = 161.3, 159.6$ ($^1J_{\text{CF}} = 244$ Hz), 152.5, 151.8, 146.3, 141.1, 135.1, 133.1, 133.0, 130.0, 129.9, 128.6, 128.34, 127.6, 125.8, 124.6, 122.6, 117.3, 115.6, 114.9, 112.9, 111.2, 108.5, 72.5, 68.4, 67.2, 56.2, 42.2, 38.5, 29.8. HRMS (TOF, ES+) calc'd for $\text{C}_{30}\text{H}_{27}\text{FN}_4\text{O}_4$, 526.2016; found, 56526.2013.



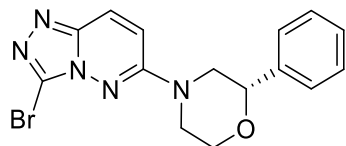
2-((3-(5-(2-(2-fluorophenyl)morpholine-4-carbonyl)-1-methyl-1H-pyrazol-3-yl)-4-methoxyphenoxy)methyl)benzonitrile

This compound was synthesized according to general procedure 4. Racemic material separated via Supercritical Fluid, chiral chromatography. Single enantiomer of unknown stereochemistry. White solid. $[\alpha]^{24}_D = -62.9$ ($c = 1.03$, CHCl_3) $^1\text{H NMR}$ (400 MHz, CDCl_3) δ 7.74-7.67 (m, 3H), 7.63 (t, $J = 7.2, 8.0$ Hz, 1H), 7.52 (t, $J = 6.8$ Hz, 1H), 7.42 (t,

$J = 7.4$ Hz, 1H), 7.34-7.27 (bs, 1H), 7.18 (t, $J = 7.2$ Hz, 1H), 7.11-6.99 (bs, 1H), 6.99-6.89 (m, 3H), 5.28 (s, 2H), 4.85 (dd, $J = 10.5, 2.2$ Hz, 1H), 4.82-4.10 (m, 3H), 4.07 (s, 3H), 3.85 (bs, 4H), 3.58-2.86 (m, 2H). ^{13}C NMR (100 MHz, CDCl_3) $\delta = 161.3, 159.6$ ($^1J_{\text{CF}} = 244$ Hz), 152.5, 151.8, 146.3, 141.1, 135.1, 133.1, 133.0, 130.0, 129.9, 128.6, 128.34, 127.6, 125.8, 124.6, 122.6, 117.3, 115.6, 114.9, 112.9, 111.2, 108.5, 72.5, 68.4, 67.2, 56.2, 42.2, 38.5, 29.8. HRMS (TOF, ES+) calc'd for $\text{C}_{30}\text{H}_{27}\text{FN}_4\text{O}_4$, 526.2016; found, 56526.2013.

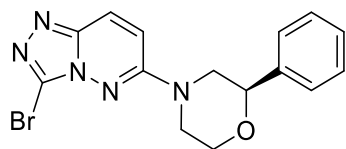


3-bromo-6-chloro-[1,2,4]triazolo[4,3-b]pyridazine: A solution of 6-chloro-[1,2,4]triazolo[4,3-B]pyridazine (1.0 eq), *N*-Bromosuccinimide (1.1 eq) in DMF (0.25M) was heated to reflux and was stirred for 16 h. The reaction mixture was then cooled to room temperature. While stirring, an aqueous solution of saturated sodium bicarbonate was added drop wise. The layers were separated and the aqueous layer was extracted with EtOAc (3x). The combined organics were dried over MgSO_4 , filtered, concentrated and purified via flash chromatography (Teledyne ISCO system, silica gel column, hexanes:EtOAc) to provide the desired product as a white solid (62-72% yield). ^1H NMR (400 MHz, CDCl_3) δ 8.09 (d, $J = 9.6$ Hz, 1H), 7.20 (d, $J = 9.6$ Hz, 1H). ^{13}C NMR (100 MHz, CDCl_3) $\delta = 150.8, 144.6, 126.5, 125.0, 123.3$. HRMS (TOF, ES+) calc'd for $\text{C}_5\text{H}_2\text{BrClN}_4$, 231.9151; found, 231.9151.



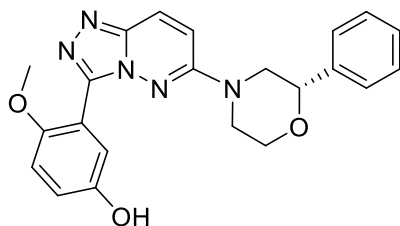
Synthesis of (2S)-4-(3-bromo-[1,2,4]triazolo[4,3-b]pyridazin-6-yl)-2-phenylmorpholine

A solution of potassium carbonate (1.5 eq), 2S-phenylmorpholine (1.1 eq), and 3-bromo-6-chloro-[1,2,4]triazolo[4,3-b]pyridazine (1.0 eq) in DMF (0.1M) was heated to 60 °C and stirred for 4 h. The reaction mixture was then diluted in H₂O, extracted with CHCl₃/IPA (3:1), passed through a phase separator, and concentrated. The crude material was purified via flash chromatography (Teledyne ISCO system, silica gel column, hexanes:EtOAc) to provide the titled compound as a white solid (72% yield). ¹H NMR (400 MHz, CDCl₃) δ 7.86 (d, *J* = 10.1 Hz, 1H), 7.47-7.33 (m, 5H), 6.99 (d, *J* = 10.1 Hz, 1H), 4.65 (dd, *J* = 10.6, 2.5 Hz, 1H), 4.26-4.14 (m, 2H), 4.09 (d, *J* = 13.5 Hz, 1H), 3.92 (td, *J* = 11.8, 2.7 Hz, 1H), 3.35 (dt, *J* = 12.6, 3.5 Hz, 1H), 3.11 (dd, *J* = 13.1, 10.7 Hz, 1H). ¹³C NMR (100 MHz, CDCl₃) δ = 155.4, 144.3, 138.9, 128.8, 128.6, 126.4, 125.1, 125.0, 124.2, 114.0, 113.8, 77.8, 66.4, 52.3, 45.7. HRMS (TOF, ES⁺) calc'd for C₁₅H₁₄BrN₅O, 359.0382; found, 259.0385.



Synthesis of (2R)-4-(3-bromo-[1,2,4]triazolo[4,3-b]pyridazin-6-yl)-2-phenylmorpholine

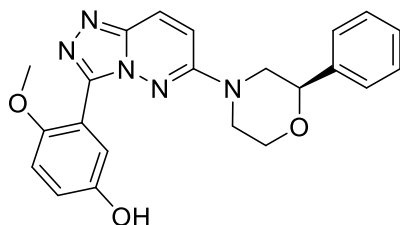
A solution of potassium carbonate (1.5 eq), 2*R*-phenylmorpholine (1.1 eq), and 3-bromo-6-chloro-[1,2,4]triazolo[4,3-*b*]pyridazine (1.0 eq) in DMF (0.1M) was heated to 60 °C and stirred for 4 h. The reaction mixture was diluted in H₂O, extracted with CHCl₃/IPA (3:1), passed through a phase separator, and concentrated. The crude material was purified via flash chromatography (Teledyne ISCO system, silica gel column, hexanes:EtOAc) to provide the desired product as a white solid (68% yield). ¹H NMR (400 MHz, CDCl₃) δ 7.86 (d, *J* = 10.1 Hz, 1H), 7.47-7.33 (m, 5H), 6.99 (d, *J* = 10.1 Hz, 1H), 4.65 (dd, *J* = 10.6, 2.5 Hz, 1H), 4.26-4.14 (m, 2H), 4.09 (d, *J* = 13.5 Hz, 1H), 3.92 (td, *J* = 11.8, 2.7 Hz, 1H), 3.35 (dt, *J* = 12.6, 3.5 Hz, 1H), 3.11 (dd, *J* = 13.1, 10.7 Hz, 1H). ¹³C NMR (100 MHz, CDCl₃) δ = 155.4, 144.3, 138.9, 128.8, 128.6, 126.4, 125.1, 125.0, 124.2, 114.0, 113.8, 77.8, 66.4, 52.3, 45.7. HRMS (TOF, ES+) calc'd for C₁₅H₁₄BrN₅O, 359.0382; found, 259.0385.



Synthesis of 4-methoxy-3-[6-[(2*S*)-2-phenylmorpholin-4-yl]-[1,2,4]triazolo[4,3-*b*]pyridazin-3-yl]phenol

A degassed solution of tetrakis(triphenylphosphine)palladium(0) (7 mol%), cesium carbonate (1.5 eq), 5-hydroxy-2-methoxyphenylboronic acid (1.1 eq), and (2*S*)-4-(3-bromo-[1,2,4]triazolo[4,3-*b*]pyridazin-6-yl)-2-phenyl-morpholine (1.0 eq) in 1,4-Dioxane/H₂O (2:1, 0.1M) was heated to 100°C and let stir for 5 h. The reaction mixture was diluted with H₂O and extracted with DCM (3x). The combined organics were then

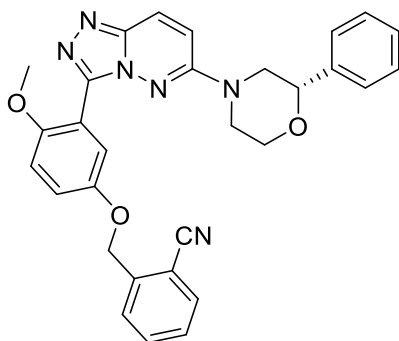
passed through a phase separator and concentrated. The crude material was purified via flash chromatography (Teledyne ISCO system, silica gel column, DCM:MeOH) to provide the desired product as a white solid (54% yield). $[\alpha]_D^{24} = \text{Error! Bookmark not defined.} +27.7$ ($c = 1.01$, MeOH). $^1\text{H NMR}$ (400 MHz, CDCl_3) δ 7.84 (d, $J = 10.0$ Hz, 1H), 7.63 (d, $J = 2.8$ Hz, 1H), 7.38-7.27 (m, 6H), 7.02 (dd, $J = 8.9, 2.8$ Hz, 1H), 6.94 (d, $J = 10.1$ Hz, 1H), 6.84 (d, $J = 8.9$ Hz, 1H), 4.55 (dd, $J = 10.5, 1.9$ Hz, 1H), 4.12-3.99 (m, 2H), 3.92 (d, $J = 13.1$ Hz, 1H), 3.78 (td, $J = 11.7, 2.0$ Hz, 1H), 3.67 (s, 3H), 3.18 (td, $J = 12.5, 3.3$ Hz, 1H), 2.94 (dd, $J = 12.8, 10.7$ Hz, 1H). $^{13}\text{C NMR}$ (100 MHz, CDCl_3) $\delta = 154.7, 151.5, 151.1, 147.8, 142.9, 139.1, 128.7, 128.4, 126.2, 124.4, 119.6, 118.9, 115.4, 114.0, 112.7, 77.3, 66.4, 56.2, 52.7, 45.9$. HRMS (TOF, ES+) calc'd for $\text{C}_{22}\text{H}_{21}\text{N}_5\text{O}_3$, 403.1644; found, 403.1648.



Synthesis of 4-methoxy-3-[6-[(2R)-2-phenylmorpholin-4-yl]-[1,2,4]triazolo[4,3-b]pyridazin-3-yl]phenol

A degassed solution of tetrakis(triphenylphosphine)palladium(0) (7 mol%), cesium carbonate (1.5 eq), 5-hydroxy-2-methoxyphenylboronic acid (1.1 eq), and (2R)-4-(3-bromo-[1,2,4]triazolo[4,3-b]pyridazin-6-yl)-2-phenyl-morpholine (1.0 eq) in 1,4-Dioxane/ H_2O (2:1, 0.1M) was heated to 100°C and let stir for 5 h. The reaction mixture was diluted with H_2O and extracted with DCM (3x). The combined organics were then passed through a phase separator and concentrated. The crude material was purified

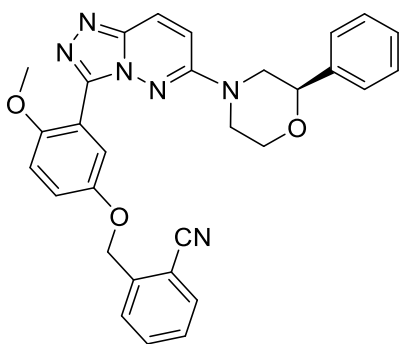
via flash chromatography (Teledyne ISCO system, silica gel column, DCM:MeOH) to provide the desired product as a white solid (53% yield). $[\alpha]^{24}_D = \text{Error! Bookmark not defined}$. -26.3 ($c = 0.565$, MeOH). $^1\text{H NMR}$ (400 MHz, CDCl_3) δ 7.84 (d, $J = 10.0$ Hz, 1H), 7.63 (d, $J = 2.8$ Hz, 1H), 7.38-7.27 (m, 6H), 7.02 (dd, $J = 8.9, 2.8$ Hz, 1H), 6.94 (d, $J = 10.1$ Hz, 1H), 6.84 (d, $J = 8.9$ Hz, 1H), 4.55 (dd, $J = 10.5, 1.9$ Hz, 1H), 4.12-3.99 (m, 2H), 3.92 (d, $J = 13.1$ Hz, 1H), 3.78 (td, $J = 11.7, 2.0$ Hz, 1H), 3.67 (s, 3H), 3.18 (td, $J = 12.5, 3.3$ Hz, 1H), 2.94 (dd, $J = 12.8, 10.7$ Hz, 1H). $^{13}\text{C NMR}$ (100 MHz, CDCl_3) $\delta = 154.7, 151.5, 151.1, 147.8, 142.9, 139.1, 128.7, 128.4, 126.2, 124.4, 119.6, 118.9, 115.4, 114.0, 112.7, 77.3, 66.4, 56.2, 52.7, 45.9$. HRMS (TOF, ES+) calc'd for $\text{C}_{22}\text{H}_{21}\text{N}_5\text{O}_3$, 403.1644; found, 403.1648.



Synthesis of 2-[[4-methoxy-3-[6-[(2S)-2-phenylmorpholin-4-yl]-[1,2,4]triazolo[4,3-b]pyridazin-3-yl]phenoxy]methyl]benzonitrile

A solution of potassium carbonate (1.5 eq), 2-cyanobenzyl bromide (1.1 eq), 4-methoxy-3-[6-[(2S)-2-phenylmorpholin-4-yl]-[1,2,4]triazolo[4,3-b]pyridazin-3-yl]phenol (1 eq), in DMF (0.2M) was heated to 65 °C and stirred for 16 h. The reaction mixture was passed through a syringe filter and crude material was then purified using a Gilson HPLC system (30 x 50 mm column; H_2O with 0.1% TFA:acetonitrile). Fractions containing the desired product were quenched with saturated NaHCO_3 , extracted with

DCM, and concentrated to liberate the product as the free base (40% yield). $[\alpha]^{24}_D = +19.7$ ($c = 3.6$, MeOH). $^1\text{H NMR}$ (400 MHz, CDCl_3) δ 7.97 (d, $J = 10.4$ Hz, 1H), 7.71-7.60 (m, 3H), 7.45 (dd, $J = 7.3, 1.6$ Hz, 1H), 7.41 (d, $J = 3.1$ Hz, 1H), 7.39-7.28 (m, 5H), 7.17 (dd, $J = 9.0, 3.1$ Hz, 1H), 6.99 (t, $J = 10.1$ Hz, 2H), 5.22 (s, 2H), 4.62 (dd, $J = 10.6, 2.6$ Hz, 1H), 4.16 (dd, $J = 11.5, 2.2$ Hz, 1H), 4.07 (dt, $J = 14.0, 2.0$ Hz, 1H), 3.96 (d, $J = 13.3$ Hz, 1H), 3.86 (td, $J = 11.9, 2.7$ Hz, 1H), 3.79 (s, 3H), 3.24 (td, $J = 12.5, 3.6$ Hz, 1H), 3.23 (dd, $J = 10.6, 2.4$ Hz, 1H). $^{13}\text{C NMR}$ (100 MHz, CDCl_3) $\delta = 154.8, 153.2, 151.9, 146.8, 143.1, 140.7, 139.1, 133.2, 133.0, 128.7, 128.7, 128.6, 128.4, 126.2, 125.1, 118.4, 118.4, 117.2, 116.6, 113.3, 112.7, 111.4, 77.6, 77.4, 68.7, 66.5, 56.4, 52.7, 46.0$. HRMS (TOF, ES+) calc'd for $\text{C}_{30}\text{H}_{26}\text{N}_6\text{O}_3$, 518.2066; found, 518.2076.



Synthesis of 2-[[4-methoxy-3-[6-[(2R)-2-phenylmorpholin-4-yl]-[1,2,4]triazolo[4,3-b]pyridazin-3-yl]phenoxy]methyl]benzonitrile

A solution of potassium carbonate (1.5 eq), 2-cyanobenzyl bromide (1.1 eq), 4-methoxy-3-[6-[(2R)-2-phenylmorpholin-4-yl]-[1,2,4]triazolo[4,3-b]pyridazin-3-yl]phenol (30.mg, 0.07000mmol) in DMF (0.2M) was heated to 65 °C and stirred for 16 h. The reaction mixture was passed through a syringe filter and crude material was then purified using a Gilson HPLC system (30 x 50 mm column; H_2O with 0.1% TFA:acetonitrile). Fractions containing the desired product were quenched with

saturated NaHCO₃, extracted with DCM, and concentrated to liberate the product as the free base (35% yield). $[\alpha]_D^{24} = \text{Error! Bookmark not defined.} -15.5$ ($c = 0.47$, MeOH). ¹H NMR (400 MHz, CDCl₃) δ 7.97 (d, $J = 10.4$ Hz, 1H), 7.71-7.60 (m, 3H), 7.45 (dd, $J = 7.3, 1.6$ Hz, 1H), 7.41 (d, $J = 3.1$ Hz, 1H), 7.39-7.28 (m, 5H), 7.17 (dd, $J = 9.0, 3.1$ Hz, 1H), 6.99 (t, $J = 10.1$ Hz, 2H), 5.22 (s, 2H), 4.62 (dd, $J = 10.6, 2.6$ Hz, 1H), 4.16 (dd, $J = 11.5, 2.2$ Hz, 1H), 4.07 (dt, $J = 14.0, 2.0$ Hz, 1H), 3.96 (d, $J = 13.3$ Hz, 1H), 3.86 (td, $J = 11.9, 2.7$ Hz, 1H), 3.79 (s, 3H), 3.24 (td, $J = 12.5, 3.6$ Hz, 1H), 3.23 (dd, $J = 10.6, 2.4$ Hz, 1H). ¹³C NMR (100 MHz, CDCl₃) $\delta = 154.8, 153.2, 151.9, 146.8, 143.1, 140.7, 139.1, 133.2, 133.0, 128.7, 128.7, 128.6, 128.4, 126.2, 125.1, 118.4, 118.4, 117.2, 116.6, 113.3, 112.7, 111.4, 77.6, 77.4, 68.7, 66.5, 56.4, 52.7, 46.0$. HRMS (TOF, ES+) calc'd for C₃₀H₂₆N₆O₃, 518.2066; found, 518.2076.

References for Chapter III

- (1) Lagerstrom, M. C.; Schioth, H. B. *Nature reviews. Drug discovery* **2008**, *7*, 339.
- (2) Ramachandran, R.; Noorbakhsh, F.; Defea, K.; Hollenberg, M. D. *Nature reviews. Drug discovery* **2012**, *11*, 69.
- (3) Adams, M. N.; Ramachandran, R.; Yau, M. K.; Suen, J. Y.; Fairlie, D. P.; Hollenberg, M. D.; Hooper, J. D. *Pharmacology & therapeutics* **2011**, *130*, 248.
- (4) Soh, U. J.; Dores, M. R.; Chen, B.; Trejo, J. *British journal of pharmacology* **2010**, *160*, 191.
- (5) Paing, M. M.; Stutts, A. B.; Kohout, T. A.; Lefkowitz, R. J.; Trejo, J. *The Journal of biological chemistry* **2002**, *277*, 1292.
- (6) Sidhu, T. S.; French, S. L.; Hamilton, J. R. *International journal of molecular sciences* **2014**, *15*, 6169.
- (7) Heuberger, D. M.; Schuepbach, R. A. *Thrombosis journal* **2019**, *17*, 4.
- (8) Ricks, T. K.; Trejo, J. *The Journal of biological chemistry* **2009**, *284*, 34444.
- (9) French, S. L.; Hamilton, J. R. *British journal of pharmacology* **2016**, *173*, 2952.
- (10) Nakanishi-Matsui, M.; Zheng, Y. W.; Sulciner, D. J.; Weiss, E. J.; Ludeman, M. J.; Coughlin, S. R. *Nature* **2000**, *404*, 609.
- (11) Cumashi, A.; Ansuini, H.; Celli, N.; De Blasi, A.; O'Brien, P. J.; Brass, L. F.; Molino, M. *Thrombosis and haemostasis* **2001**, *85*, 533.
- (12) Bretschneider, E.; Spanbroek, R.; Lotzer, K.; Habenicht, A. J.; Schror, K. *Thrombosis and haemostasis* **2003**, *90*, 704.
- (13) Ostrowska, E.; Reiser, G. *Cellular and molecular life sciences : CMLS* **2008**, *65*, 970.
- (14) Bao, Y.; Hou, W.; Hua, B. *Expert opinion on therapeutic targets* **2014**, *18*, 15.
- (15) Rothmeier, A. S.; Ruf, W. *Seminars in immunopathology* **2012**, *34*, 133.
- (16) Kahn, M. L.; Nakanishi-Matsui, M.; Shapiro, M. J.; Ishihara, H.; Coughlin, S. R. *The Journal of clinical investigation* **1999**, *103*, 879.
- (17) Arachiche, A.; Mumaw, M. M.; de la Fuente, M.; Nieman, M. T. *The Journal of biological chemistry* **2013**, *288*, 32553.
- (18) McLaughlin, J. N.; Patterson, M. M.; Malik, A. B. *Proceedings of the National Academy of Sciences of the United States of America* **2007**, *104*, 5662.
- (19) Smith, T. H.; Li, J. G.; Dores, M. R.; Trejo, J. *The Journal of biological chemistry* **2017**, *292*, 13867.
- (20) Lin, H.; Liu, A. P.; Smith, T. H.; Trejo, J. *Pharmacological reviews* **2013**, *65*, 1198.
- (21) de la Fuente, M.; Noble, D. N.; Verma, S.; Nieman, M. T. *The Journal of biological chemistry* **2012**, *287*, 10414.

- (22) Ludeman, M. J.; Kataoka, H.; Srinivasan, Y.; Esmon, N. L.; Esmon, C. T.; Coughlin, S. R. *The Journal of biological chemistry* **2005**, *280*, 13122.
- (23) Fenton, J. W., 2nd; Villanueva, G. B.; Ofosu, F. A.; Maraganore, J. M. *Haemostasis* **1991**, *21 Suppl 1*, 27.
- (24) Fenton, J. W., 2nd *Seminars in thrombosis and hemostasis* **1989**, *15*, 265.
- (25) Rydel, T. J.; Tulinsky, A.; Bode, W.; Huber, R. *Journal of molecular biology* **1991**, *221*, 583.
- (26) Nieman, M. T.; Schmaier, A. H. *Biochemistry* **2007**, *46*, 8603.
- (27) Duvernay, M. T.; Temple, K. J.; Maeng, J. G.; Blobaum, A. L.; Stauffer, S. R.; Lindsley, C. W.; Hamm, H. E. *Molecular pharmacology* **2017**, *91*, 39.
- (28) Nieman, M. T. *Blood* **2016**, *128*, 169.
- (29) Brass, L. F.; Vassallo, R. R., Jr.; Belmonte, E.; Ahuja, M.; Cichowski, K.; Hoxie, J. A. *The Journal of biological chemistry* **1992**, *267*, 13795.
- (30) Falker, K.; Haglund, L.; Gunnarsson, P.; Nylander, M.; Lindahl, T. L.; Grenegard, M. *The Biochemical journal* **2011**, *436*, 469.
- (31) Duvernay, M.; Young, S.; Gailani, D.; Schoenecker, J.; Hamm, H. E. *Molecular pharmacology* **2013**, *83*, 781.
- (32) Gryka, R. J.; Buckley, L. F.; Anderson, S. M. *Drugs in R&D* **2017**, *17*, 65.
- (33) Chelliah, M. V.; Eagen, K.; Guo, Z.; Chackalamannil, S.; Xia, Y.; Tsai, H.; Greenlee, W. J.; Ahn, H. S.; Kurowski, S.; Boykow, G.; Hsieh, Y.; Chintala, M. *ACS medicinal chemistry letters* **2014**, *5*, 561.
- (34) Administration, F. D. **2014**.
- (35) (JPND), J. P. N. D. R.
- (36) Association, T. A. s. **2020**.
- (37) Association, A. s. **2017**.
- (38) Coughlin, S. R. *Journal of thrombosis and haemostasis : JTH* **2005**, *3*, 1800.
- (39) Kataoka, H.; Hamilton, J. R.; McKemy, D. D.; Camerer, E.; Zheng, Y. W.; Cheng, A.; Griffin, C.; Coughlin, S. R. *Blood* **2003**, *102*, 3224.
- (40) Sokolova, E.; Reiser, G. *Thrombosis and haemostasis* **2008**, *100*, 576.
- (41) Luo, W.; Wang, Y.; Reiser, G. *Brain research reviews* **2007**, *56*, 331.
- (42) Rohatgi, T.; Sedehizade, F.; Reymann, K. G.; Reiser, G. *The Neuroscientist : a review journal bringing neurobiology, neurology and psychiatry* **2004**, *10*, 501.
- (43) Dihanich, M.; Kaser, M.; Reinhard, E.; Cunningham, D.; Monard, D. *Neuron* **1991**, *6*, 575.
- (44) Bao, Y.; Gao, Y.; Yang, L.; Kong, X.; Zheng, H.; Hou, W.; Hua, B. *Channels (Austin, Tex.)* **2015**, *9*, 5.
- (45) Suo, Z.; Wu, M.; Citron, B. A.; Gao, C.; Festoff, B. W. *The Journal of biological chemistry* **2003**, *278*, 31177.
- (46) Bhatia, H. S.; Roelofs, N.; Munoz, E.; Fiebich, B. L. *Scientific reports* **2017**, *7*, 116.
- (47) Hickman, S.; Izzy, S.; Sen, P.; Morsett, L.; El Khoury, J. *Nature neuroscience* **2018**, *21*, 1359.
- (48) Moller, T.; Hanisch, U. K.; Ransom, B. R. *Journal of neurochemistry* **2000**, *75*, 1539.

- (49) Wu, J.; Yang, S.; Xi, G.; Fu, G.; Keep, R. F.; Hua, Y. *Neurological research* **2009**, *31*, 183.
- (50) Wu, J.; Yang, S.; Xi, G.; Song, S.; Fu, G.; Keep, R. F.; Hua, Y. *Acta neurochirurgica. Supplement* **2008**, *105*, 59.
- (51) Suo, Z.; Wu, M.; Citron, B. A.; Palazzo, R. E.; Festoff, B. W. *The Journal of biological chemistry* **2003**, *278*, 37681.
- (52) Lee, V. M.; Goedert, M.; Trojanowski, J. Q. *Annual review of neuroscience* **2001**, *24*, 1121.
- (53) Tolnay, M.; Probst, A. *IUBMB life* **2003**, *55*, 299.
- (54) Suo, Z.; Wu, M.; Ameenuddin, S.; Anderson, H. E.; Zoloty, J. E.; Citron, B. A.; Andrade-Gordon, P.; Festoff, B. W. *Journal of neurochemistry* **2002**, *80*, 655.
- (55) Mao, Y.; Zhang, M.; Tuma, R. F.; Kunapuli, S. P. *Journal of cerebral blood flow and metabolism : official journal of the International Society of Cerebral Blood Flow and Metabolism* **2010**, *30*, 1044.
- (56) Hatada, Y.; Hashimoto, M.; Shiraishi, S.; Ishikawa, T.; Fukuhara, R.; Yuki, S.; Tanaka, H.; Miyagawa, Y.; Kitajima, M.; Uetani, H.; Tsunoda, N.; Koyama, A.; Ikeda, M. *Journal of Alzheimer's disease : JAD* **2019**, *71*, 273.
- (57) Daida, K.; Tanaka, R.; Yamashiro, K.; Ogawa, T.; Oyama, G.; Nishioka, K.; Shimo, Y.; Umemura, A.; Hattori, N. *Journal of the neurological sciences* **2018**, *393*, 39.
- (58) Ham, J. H.; Yi, H.; Sunwoo, M. K.; Hong, J. Y.; Sohn, Y. H.; Lee, P. H. *Journal of neurology* **2014**, *261*, 1628.
- (59) Poliakova, T.; Levin, O.; Arablinskiy, A.; Vasenina, E.; Zerr, I. *Journal of neurology* **2016**, *263*, 1961.
- (60) Lee, J.; Sohn, E. H.; Oh, E.; Lee, A. Y. *Dementia and neurocognitive disorders* **2018**, *17*, 73.
- (61) Charidimou, A.; Werring, D. J. *Journal of the neurological sciences* **2012**, *322*, 50.
- (62) Gorelick, P. B.; Farooq, M. U. *JAMA neurology* **2016**, *73*, 908.
- (63) Han, X.; Nieman, M. T. *Arteriosclerosis, thrombosis, and vascular biology* **2018**, *38*, 287.
- (64) Wong, P. C.; Seiffert, D.; Bird, J. E.; Watson, C. A.; Bostwick, J. S.; Giancarli, M.; Allegretto, N.; Hua, J.; Harden, D.; Guay, J.; Callejo, M.; Miller, M. M.; Lawrence, R. M.; Banville, J.; Guy, J.; Maxwell, B. D.; Priestley, E. S.; Marinier, A.; Wexler, R. R.; Bouvier, M.; Gordon, D. A.; Schumacher, W. A.; Yang, J. *Science translational medicine* **2017**, *9*.
- (65) Temple, K. J.; Duvernay, M. T.; Young, S. E.; Wen, W.; Wu, W.; Maeng, J. G.; Blobaum, A. L.; Stauffer, S. R.; Hamm, H. E.; Lindsley, C. W. *Journal of medicinal chemistry* **2016**, *59*, 7690.
- (66) Chen, P.; Ren, S.; Song, H.; Chen, C.; Chen, F.; Xu, Q.; Kong, Y.; Sun, H. *Bioorganic & medicinal chemistry* **2019**, *27*, 116.
- (67) Temple, K. J.; Duvernay, M. T.; Maeng, J. G.; Blobaum, A. L.; Stauffer, S. R.; Hamm, H. E.; Lindsley, C. W. *Bioorganic & medicinal chemistry letters* **2016**, *26*, 5481.

- (68) Zhang, C.; Srinivasan, Y.; Arlow, D. H.; Fung, J. J.; Palmer, D.; Zheng, Y.; Green, H. F.; Pandey, A.; Dror, R. O.; Shaw, D. E.; Weis, W. I.; Coughlin, S. R.; Kobilka, B. K. *Nature* **2012**, *492*, 387.
- (69) Cheng, R. K. Y.; Fiez-Vandal, C.; Schlenker, O.; Edman, K.; Aggeler, B.; Brown, D. G.; Brown, G. A.; Cooke, R. M.; Dumelin, C. E.; Dore, A. S.; Geschwindner, S.; Grebner, C.; Hermansson, N. O.; Jazayeri, A.; Johansson, P.; Leong, L.; Prihandoko, R.; Rappas, M.; Soutter, H.; Snijder, A.; Sundstrom, L.; Tehan, B.; Thornton, P.; Troast, D.; Wiggin, G.; Zhukov, A.; Marshall, F. H.; Dekker, N. *Nature* **2017**, *545*, 112.
- (70) Sanchez Centellas, D.; Gudlur, S.; Vicente-Carrillo, A.; Ramstrom, S.; Lindahl, T. L. *Thrombosis research* **2017**, *154*, 84.
- (71) Boknas, N.; Faxalv, L.; Sanchez Centellas, D.; Wallstedt, M.; Ramstrom, S.; Grenegard, M.; Lindahl, T. L. *Thrombosis and haemostasis* **2014**, *112*, 558.
- (72) Edelstein, L. C.; Simon, L. M.; Lindsay, C. R.; Kong, X.; Teruel-Montoya, R.; Tourdot, B. E.; Chen, E. S.; Ma, L.; Coughlin, S.; Nieman, M.; Holinstat, M.; Shaw, C. A.; Bray, P. F. *Blood* **2014**, *124*, 3450.
- (73) Tourdot, B. E.; Stoveken, H.; Trumbo, D.; Yeung, J.; Kanthi, Y.; Edelstein, L. C.; Bray, P. F.; Tall, G. G.; Holinstat, M. *Arteriosclerosis, thrombosis, and vascular biology* **2018**, *38*, 1632.
- (74) Morikawa, Y.; Kato, H.; Kashiwagi, H.; Nishiura, N.; Akuta, K.; Honda, S.; Kanakura, Y.; Tomiyama, Y. *Thrombosis research* **2018**, *162*, 44.
- (75) Heenkenda, M. K.; Lindahl, T. L.; Osman, A. *Blood* **2018**, *132*, 2103.
- (76) Faruqi, T. R.; Weiss, E. J.; Shapiro, M. J.; Huang, W.; Coughlin, S. R. *The Journal of biological chemistry* **2000**, *275*, 19728.

Appendix C

Spectra Relevant to Chapter III

